



energies

Advanced Signal Processing Techniques Applied to Power Systems Control and Analysis

Edited by

Zbigniew Leonowicz, Sanjeevikumar Padmanaban,
Antonio Bracale, Alessandro Burgio,
Tomasz Sikorski and Przemyslaw Janik

Printed Edition of the Special Issue Published in *Energies*

Advanced Signal Processing Techniques Applied to Power Systems Control and Analysis

Advanced Signal Processing Techniques Applied to Power Systems Control and Analysis

Special Issue Editors

Zbigniew Leonowicz

Sanjeevikumar Padmanaban

Antonio Bracale

Alessandro Burgio

Tomasz Sikorski

Przemysław Janik

MDPI • Basel • Beijing • Wuhan • Barcelona • Belgrade • Manchester • Tokyo • Cluj • Tianjin



Special Issue Editors

Zbigniew Leonowicz
Wroclaw University of Science
and Technology
Poland

Sanjeevikumar Padmanaban
Aalborg University
Denmark

Antonio Bracale
University of Naples Parthenope
Italy

Alessandro Burgio
Independent Researcher
Italy

Tomasz Sikorski
Wroclaw University of Science
and Technology
Poland

Przemyslaw Janik
Wroclaw University of Science
and Technology
Poland

Editorial Office

MDPI
St. Alban-Anlage 66
4052 Basel, Switzerland

This is a reprint of articles from the Special Issue published online in the open access journal *Energies* (ISSN 1996-1073) (available at: https://www.mdpi.com/journal/energies/special_issues/ASPTA.PSCA).

For citation purposes, cite each article independently as indicated on the article page online and as indicated below:

LastName, A.A.; LastName, B.B.; LastName, C.C. Article Title. <i>Journal Name</i> Year , Article Number, Page Range.

ISBN 978-3-03936-186-1 (Hbk)

ISBN 978-3-03936-187-8 (PDF)

© 2020 by the authors. Articles in this book are Open Access and distributed under the Creative Commons Attribution (CC BY) license, which allows users to download, copy and build upon published articles, as long as the author and publisher are properly credited, which ensures maximum dissemination and a wider impact of our publications.

The book as a whole is distributed by MDPI under the terms and conditions of the Creative Commons license CC BY-NC-ND.

Contents

About the Special Issue Editors	vii
Preface to "Advanced Signal Processing Techniques Applied to Power Systems Control and Analysis"	ix
Michał Jasiński, Tomasz Sikorski, Paweł Kostyła, Dominika Kaczorowska, Zbigniew Leonowicz, Jacek Rezmer, Jarosław Szymańda, Przemysław Janik, Daniel Bejmer, Marek Rybiański and Elżbieta Jasińska Influence of Measurement Aggregation Algorithms on Power Quality Assessment and Correlation Analysis in Electrical Power Network with PV Power Plant Reprinted from: <i>Energies</i> 2019 , <i>12</i> , 3547, doi:10.3390/en12183547	1
Gopinath Subramani, Vigna K. Ramachandaramurthy, P. Sanjeevikumar, Jens Bo Holm-Nielsen, Frede Blaabjerg, Leonowicz Zbigniew and Paweł Kostyła Techno-Economic Optimization of Grid-Connected Photovoltaic (PV) and Battery Systems Based on Maximum Demand Reduction (MDRed) Modelling in Malaysia Reprinted from: <i>Energies</i> 2019 , <i>12</i> , 3531, doi:10.3390/en12183531	19
Sivapragash C., Sanjeevikumar Padmanaban, Hossain Eklas, Jens Bo Holm-Nielsen and R. Hemalatha Location-Based Optimized Service Selection for Data Management with Cloud Computing in Smart Grids Reprinted from: <i>Energies</i> 2019 , <i>12</i> , 4517, doi:10.3390/en12234517	41
Stefano Lodetti, Jorge Bruna, Julio J. Melero and José F. Sanz Wavelet Packet Decomposition for IEC Compliant Assessment of Harmonics under Stationary and Fluctuating Conditions Reprinted from: <i>Energies</i> 2019 , <i>12</i> , 4389, doi:10.3390/en12224389	57
Asghar Sabati, Ramazan Bayindir, Sanjeevikumar Padmanaban, Eklas Hossain and Mehmet Rida Tur Small Signal Stability with the Householder Method in Power Systems Reprinted from: <i>Energies</i> 2019 , <i>12</i> , 3412, doi:10.3390/en12183412	73
Umashankar Subramaniam, Sagar Mahajan Bhaskar, Dhafer J. Almkhles, Sanjeevikumar Padmanaban and Zbigniew Leonowicz Investigations on EMI Mitigation Techniques: Intent to Reduce Grid-Tied PV Inverter Common Mode Current and Voltage Reprinted from: <i>Energies</i> 2019 , <i>12</i> , 3395, doi:10.3390/en12173395	89
Karunakaran Venkatesan, Uma Govindarajan, Padmanathan Kasinathan, Sanjeevikumar Padmanaban, Jens Bo Holm-Nielsen and Zbigniew Leonowicz Economic Analysis of HRES Systems with Energy Storage During Grid Interruptions and Curtailment in Tamil Nadu, India: A Hybrid RBFNOEHO Technique Reprinted from: <i>Energies</i> 2019 , <i>12</i> , 3047, doi:10.3390/en12163047	107
Padmini Sankaramurthy, Bharatiraja Chokkalingam, Sanjeevikumar Padmanaban, Zbigniew Leonowicz and Yusuff Adedayo Rescheduling of Generators with Pumped Hydro Storage Units to Relieve Congestion Incorporating Flower Pollination Optimization Reprinted from: <i>Energies</i> 2019 , <i>12</i> , 1477, doi:10.3390/en12081477	133

Ramesh Ananthavijayan, Prabhakar Karthikeyan Shanmugam, Sanjeevikumar Padmanaban, Jens Bo Holm-Nielsen, Frede Blaabjerg and Viliam Fedak Software Architectures for Smart Grid System—A Bibliographical Survey Reprinted from: <i>Energies</i> 2019 , <i>12</i> , 1183, doi:10.3390/en12061183	153
Tohid Harighi, Sanjeevikumar Padmanaban, Ramazan Bayindir, Eklas Hossain and Jens Bo Holm-Nielsen Electric Vehicle Charge Stations Location Analysis and Determination—Ankara (Turkey) Case Study Reprinted from: <i>Energies</i> 2019 , <i>12</i> , 3472, doi:10.3390/en12183472	171
B. Kavya Santhoshi, K. Mohana Sundaram, Sanjeevikumar Padmanaban, Jens Bo Holm-Nielsen and Prabhakaran K. K. Critical Review of PV Grid-Tied Inverters Reprinted from: <i>Energies</i> 2019 , <i>12</i> , 1921, doi:10.3390/en12101921	193
Somashree Pathy, C. Subramani, R. Sridhar, T. M. Thamizh Thentral and Sanjeevikumar Padmanaban Nature-Inspired MPPT Algorithms for Partially Shaded PV Systems: A Comparative Study Reprinted from: <i>Energies</i> 2019 , <i>12</i> , 1451, doi:10.3390/en12081451	219

About the Special Issue Editors

Zbigniew Leonowicz, Professor (full), is a graduate of the Electrical Department of Wrocław University of Technology, where he obtained his doctorate in 2001 and habilitation in 2012 before being appointed as University Professor in 2016. In 2019, he received his Full Professor nomination both in Poland and the Czech Republic. His main areas of scientific interest include signal analysis, renewable energy, quality of energy, and ecology. Has has been awarded multiple times as Best Reviewer by numerous international journals and Publons. <http://weny.pwr.edu.pl/en/employees/zbigniew-leonowicz>.

Sanjeevikumar Padmanaban (Member '12, Senior Member '15, IEEE) completed his bachelor's degree in Electrical Engineering at the University of Madras, India, in 2002; master's degree (Hons.) in Electrical Engineering at Pondicherry University, India, in 2006; and Ph.D. degree in Electrical Engineering at the University of Bologna, Italy, in 2012. He served as Associate Professor with VIT University from 2012 to 2013. In 2013, he joined the National Institute of Technology, India, as a Faculty Member. In 2014, he was invited as a visiting researcher at the Department of Electrical Engineering, Qatar University, Qatar, funded by the Qatar National Research Foundation (Government of Qatar). He continued his research activities at the Dublin Institute of Technology, Ireland, in 2014. He was an Associate Professor with the Department of Electrical and Electronics Engineering, University of Johannesburg, South Africa, from 2016 to 2018. Since 2018, he has been a Faculty Member of the Department of Energy Technology, Aalborg University, Esbjerg, Denmark. He has authored 350 plus scientific papers and has received the Best Paper cum Most Excellence Research Paper Award from IET-SEISCON'13, IET-CEAT'16, and five best paper awards from ETAEERE'16 and sponsored a Lecture note in Electrical Engineering, Springer book series. He is a fellow of the Institution of Engineers, FIE, India; Institution of Telecommunication and Electronics Engineers, FIETE, India; and Institution of Engineering and Technology, IET, UK. He serves as an Editor/Associate Editor/Editorial Board member of numerous refereed journal, most notably, *IEEE Systems*, *IEEE Access*, *IET Power Electronics*, and *Journal of Power Electronics* (Korea), and is the subject editor of *IET Renewable Power Generation*, *IET Generation, Transmission and Distribution*, and *FACTS Journal*, Canada.

Antonio Bracale received his degree in Telecommunication Engineering from the University of Naples "Federico II" (Italy) in 2002 and the Ph.D. degree in electrical energy conversion from the Second University of Naples, in 2005. Since 2008, he has been with the Department of Engineering, University of Naples "Parthenope", (Italy), where he is currently an associate professor. His research interest concerns power quality, energy forecasting and power systems analysis. He is an IEEE Senior Member.

Alessandro Burgio (1973, Italy) is a consultant with over 20 years of experience in the field of electric power systems, energy efficiency and reliability, and design and prototyping of electronic devices for electric power measurement and conditioning. Since 2019, he has been serving with the Italian company Evolvere SpA as designer and analyst of distributed energy storage systems in a national energy community framework. He is also the executive director of a consortium of about 25 municipalities for the collective purchase of electricity in the deregulated Italian market.

Before assuming his current duties, Dr. Burgio has been the project leader of a National Operating Programme Project financed by the Italian Minister of Economic Development; he also served as research fellow and lecturer.

Dr. Burgio's research activities have resulted in more than 60 papers, published in indexed scientific journals and discussed at international conferences; these research activities have also resulted in a patent of a micro cogenerator for net-zero-power dwelling based on a free-piston Stirling engine.

Dr. Burgio is a member of various programs and scientific and technical committees of esteemed journals and conferences. He holds a master's degree in Management Engineering and a Ph.D. in Computer and System Engineering from the University of Calabria, Italy.

Tomasz Sikorski (University Professor) received his Ph.D. degree in application of time-frequency analysis in electrical power systems from Wroclaw University of Technology, Poland, in 2005. In 2006, he was postdoctoral research in Laboratory of Brian Science in RIKEN Institute Tokyo. During 2006–2010, he led the postdoc project founded by Polish Ministry of Higher Education and Science dedicated to the application of novel signal processing methods in the analysis of power quality disturbances in power systems with distributed generation. The project was realized in cooperation with Institute of Power Systems Automation Research Center, Poland. He also participated in a project based on agreements between the governments of Poland and Spain focused on wind energy. He received his habilitation in 2014 and became University Professor in 2016. He cooperates with industry and power system operators regarding the monitoring, detection, and analysis of conducted disturbances and time-varying phenomena in power systems. He has published more than 120 papers and holds an international patent with ABB.

Przemyslaw Janik, Ph.D., D.Sc., Associated Professor, A graduate of the Electrical Department of the Wroclaw University of Technology. In 2005 obtained the doctorate and in 2018 the habilitation degree, in 2019 became a university professor. Area of scientific interest: signal analysis, neural networks, renewable energy, power quality.

Preface to "Advanced Signal Processing Techniques Applied to Power Systems Control and Analysis"

This monograph showcases the results of the latest research aimed at facilitating the development of modern electric power systems, grids and devices, smart grids, and protection devices, as well as for developing tools for more accurate and efficient power system analysis. Conventional signal processing is not more effective for extracting all of the relevant information from distorted signals through filtering, estimation, and detection in order to facilitate decision-making and to control actions. Machine learning algorithms, optimization techniques, and efficient numerical algorithms, distributed signal processing, and statistical signal detection and estimation may help in solving contemporary challenges in modern power systems. The increased use of digital information and control technology can improve the grid's reliability, security, and efficiency; dynamic optimization of grid operations; demand response; incorporation of demand-side resources and integration of energy-efficient resources; distribution automation; and integration of smart appliances and consumer devices. Signal processing offers the tools needed to convert measurement data to information and to transform information into actionable intelligence.

**Zbigniew Leonowicz, Sanjeevikumar Padmanaban, Antonio Bracale, Alessandro Burgio,
Tomasz Sikorski, Przemyslaw Janik**
Special Issue Editors

Article

Influence of Measurement Aggregation Algorithms on Power Quality Assessment and Correlation Analysis in Electrical Power Network with PV Power Plant

Michał Jasiński ^{1,*}, Tomasz Sikorski ^{1,*}, Paweł Kostyła ¹, Dominika Kaczorowska ¹, Zbigniew Leonowicz ¹, Jacek Rezmer ¹, Jarosław Szymańda ¹, Przemysław Janik ², Daniel Bejmert ², Marek Rybiański ³ and Elżbieta Jasińska ⁴

¹ Department of Electrical Engineering Fundamentals, Faculty of Electrical Engineering, Wrocław University of Science and Technology, 50-370 Wrocław, Poland; pawel.kostyla@pwr.edu.pl (P.K.); dominika.kaczorowska@pwr.edu.pl (D.K.); zbigniew.leonowicz@pwr.edu.pl (Z.L.);

jacek.rezmer@pwr.edu.pl (J.R.); jaroslaw.szymanda@pwr.edu.pl (J.S.)

² TAURON Ekoenergia Ltd., 58-500 Jelenia Góra, Poland; przemyslaw.janik@tauron-ekoenergia.pl (P.J.); daniel.bejmert@tauron-ekoenergia.pl (D.B.)

³ Center of Energy Technology, 58-100 Świdnica, Poland; m.rybianski@fea.pl

⁴ Association of Polish Power Engineers—Branch in Lubin, 59-300 Lubin, Poland; jasinel@poczta.onet.pl

* Correspondence: michal.jasinski@pwr.edu.pl (M.J.); tomasz.sikorski@pwr.edu.pl (T.S.)

Received: 21 August 2019; Accepted: 10 September 2019; Published: 16 September 2019

Abstract: Recently a number of changes were introduced in amendment to standard EN 50160 related to power quality (PQ) including 1 min aggregation intervals and the obligation to consider 100% of measured data taken for the assessment of voltage variation in a low voltage (LV) supply terminal. Classical power quality assessment can be extended using a correlation analysis so that relations between power quality parameters and external indices such as weather conditions or power demand can be revealed. This paper presents the results of a comparative investigation of the application of 1 and 10 min aggregation times in power quality assessment as well as in the correlation analysis of power quality parameters and weather conditions and the energy production of a 100 kW photovoltaic (PV) power plant connected to a LV network. The influence of the 1 min aggregation time on the result of the PQ assessment as well as the correlation matrix in comparison with the 10 min aggregation algorithm is presented and discussed.

Keywords: power quality; voltage variations; PV system; aggregation times; correlation analysis

1. Introduction

The most often used standards related to power quality (PQ) are EN 50160:2010 [1] with further amendment EN 50160:2015 [2] as well as IEC 61000-4-30 [3] and IEEE 1159 [4]. The classical method of assessing power quality is based on choosing a representative period of time, normally 1 week, which should represent normal operating conditions of the observed electrical power network (EPN). The parameters which are taken into consideration in PQ assessment are as follows: frequency variation (f), voltage variation (U), flicker represented by long-term flicker severity (P_{lt}) and short-term flicker severity (P_{st}), asymmetry (k_{u2}), total harmonic distortion in voltage ($THDu$), content of harmonic from 2nd to 50th. In the methodology of power quality assessment, the measurement time interval and aggregation time interval have to be distinguished. The basic measurement time interval for the parameter magnitudes (supply voltage, harmonics, interharmonics and unbalance) is a 10-cycle time interval for a 50 Hz power system or a 12-cycle time interval for a 60 Hz power system. Then, the measurement time intervals are aggregated over a 150/180-cycle interval (150 cycles for 50 Hz nominal or 180 cycles for 60 Hz nominal), 10 min interval and 2 h interval.

The review of present literature indicates that there is some discussion related to the assessment of power quality in terms of the influence of the aggregation time interval on the effect of the assessment. This issue has a significant meaning in terms of the assessment of power quality at the point of the common coupling (PCC) of the distributed generation (DG), especially when the observed DG is characterized by high variations of the energy production. Common examples are PV installations with their inherent relation of generated energy with cloud effect. The discussed aspect has already been reflected in the amendment to standard EN 50160:2015 where a 1 min aggregation interval is suggested for the assessment of voltage variation in low voltage (LV) power systems. Selected issues related to aggregation interval influence can be found in the below works:

- Article [5] looks at the time varying nature of the PQ distortion level caused by different working conditions of the load demand as well as energy production delivered to the mining electrical power network by distributed generation.
- Article [6] presents and discusses the behavior of the voltage in the Algerian Low-Voltage distribution network and the influence of the PV generation. The assessment is based on PQ analysis according to EN 50160 and IEC 61000-2-2 standards. The standard EN 50160:2011 was used.
- Paper [7] presents a photovoltaic (PV) system with an uninterruptible power supply (UPS), equipped with energy storage (25 kWh) and a system for monitoring and management of energy flow. It contains the analysis of energy quality measurements carried out at a point where the PV system is connected to the power grid. The assessment is based on PQ analysis according to EN 50160 and country regulation—Instructions for Distribution Network Traffic and Exploitation applicable since 1 January, 2014, TAURON Dystrybucja S.A. The standard EN 50160:2011 was used.
- Article [8] describes possible adverse effects of the source on the power network parameters while meeting the conditions contained in the applicable standards and regulations. The presented documents are EN 50160:2011, VDE-AR-N-4105, EN 61000-2-2, Polish Regulation of the Minister of Economy of 2007-05-01, Polish Instructions of traffic and operation in distribution networks (network code).
- Article [9] contains the investigation of the effects of a high-power installed photovoltaic on a rural LV grid. Additionally, the paper presents the comparison of different measures from a technical perspective. The article analysis is based on EN 50160:2011.
- Article [10] describes a study of the rapid voltage change. It is realized by modelling the moving cloud shadow and compares the hosting capacity (HC) from the perspective of both dynamic and static characteristics. The article indicates the requirements for a static characteristic based on 10 min on the basis of EN 50160:2011.
- Article [11] presents a model of a selected part of a distribution network. The model was created in Matlab/Simulink, based on real data, and the impact of PV power plants on voltage amplitude in accordance with EN 50160:2011. The measurement data are based on 1 week in summer.
- Article [12] deals with impact of two PV plants with equal characteristics. The first is strongly connected (urban area) and second one is weakly connected (rural area) to the distribution grid at the PCC. The PQ demands are based on EN 50160:2011.
- Paper [13] contains research on the impact of the aggregation interval (1 min, 10 min, 30 min), aggregation method (mean, max) and assessment quantiles (95%, 99%) on voltage quality parameters. The considered parameters are voltage magnitude, selected harmonics, total harmonic distortion index and unbalance. The research is based on a database of measurements performed in public low voltage grids. The article conclusion indicates that a higher aggregation interval usually results in a less dynamic time series with a smaller variation range, however for the investigated measurement data no significant influence of the calculation parameters on the results could be identified. Some negligible maximum absolute deviation has been observed for different aggregation intervals. Similar analysis of the aggregation impact is presented in paper [14] and the

obtained results are similar. However, both papers have recommended a further verification of the results for grids with a significantly different structure. This recommendation was a motivation for the presented paper. That is why this paper is focused on the investigation of the possible impact of the aggregation interval on power quality assessment in a particular case of the point of common coupling of a photovoltaic plant when the variability of the parameters is more expected.

The presented state of the art supports the need for further verification of the influence of the aggregation interval on power quality assessment for power grids with different structures. Nowadays the widely discussed issue is the integration of distributed energy resources with a power system and its impact on power quality. One of the main contributions of this work compared to previous research dedicated to the investigation of the influence of the aggregation interval on power quality assessment is to expand research into a real measurement case of a 100 kW photovoltaic plant directly connected to a low voltage power network. The investigated case is interesting due to the variability of power quality parameters associated with variable nature of energy production affected by weather conditions. Additionally, this work explores an additional aspect of the possible impact of the aggregation interval which is its influence on the correlation analysis between weather conditions and power quality parameters. The presented results highlight some differences between the correlation coefficient obtained using 10 min and 1 min aggregation intervals.

Taking into consideration the effects of the quoted discussion, the aim of this paper is to present a comparative investigation of the application of 1 and 10 min aggregation times in power quality assessment. The selected times are based on the demands of PQ assessment in accordance with the amendment to the standard EN 50160 where both 1 min and 10 min aggregation intervals are considered [1,2]. The observed object is the 100 kW PV power plant connected directly to LV power network. Additionally, the paper extends the discussion of using different aggregation intervals in the context of correlation analysis of the PQ parameters and weather conditions. The obtained results highlight the impact of PV energy production on PQ level at the PCC when different aggregation times are used.

2. Comparative Study of Recent Developments in Power Quality Requirements

The permissible levels of power quality parameters used for the assessment of public distribution networks is based on standard EN 50160. This standard was changed significantly in 2015. The comparison of demand levels for standard EN 50160:2010 [1] and standard EN 50160:2015 [2] were involved in Table 1.

Studying contents of Table 1 it can be noticed that the most significant difference is the extended requirement for the time period when the parameters should preserve the permissible levels. The acceptance level for parameters are similar for both [1] and [2] but the time to maintain the parameter at a given level is required at 100% of the observations in [2] while the previous version of the standard [1] generally uses 95% for the time of observation. This indicates that the trend is toward continuous maintenance of power quality parameters (f , U , P_{lt} , k_{u2} , $THDu$, harmonic 2nd to 50th) for the acceptance level.

A significant change is noted for frequency. For the systems with a synchronous connection, the requirements for the 50 Hz systems is setup to $50 \text{ Hz} \pm 0.1 \text{ Hz}$ for 100% of the time. The acceptance level corresponding to 100% of measurement data was restricted from 47 Hz to 49.9 Hz. The frequency is a grid parameter and local changes generally have no significant influence on frequency but the formulated requirement might be a very restrictive demand for distribution system operators.

The next difference between the documents is the mentioned aggregation time for voltage variations. In [1], the 10 min aggregation was used. In [2], the 1 min aggregation is proposed for a LV power network. The reduction of aggregation time as well as the demand for 100% of the data to be in the permissible range creates a serious question for the sensitivity of the assessment when a single aggregated 1 min value can cause a negative assessment of voltage variation.

The next difference is the introduction of the requirement for short-term flicker severity which uses 10 min aggregation interval. Until 2015, long-term flicker severity was used, where 2 h aggregation is applied. It creates the next question about the sensitivity of the assessment when rapid changes of power demand or power generation might be considered.

Standard [2] introduced the requirement level for harmonic from 26th to 50th. Additionally, the mean value of $THDu$ measured data was defined. It indicates that when the $THDu$ level is high (higher than 5%) for a long period of time it may lead to a negative assessment [15]

Table 1. Comparison of permissible levels of power quality parameters in EN 50160:2010 [1] and EN 50160:2015 [2] for a 50 Hz system.

Parameter	Symbol	Resolution	Acceptance Level	
			Standard EN 50160:2010 [1]	Standard EN 50160:2015 [2]
Frequency variation	f	10 s	49.5 to 50.5 Hz for 99.5% of measurement data set, 47 to 52 Hz for 100% of measurement data set	49.9 to 50.1 Hz for 100% of measurement data set
Voltage variation	U	10 min	90 to 110% U_{ref} for 95% of measurement data set, 85 to 110% U_{ref} for 100% of measurement data set	Not defined
		1 min	Not defined	90 to 110% U_{ref} for 100% of measurement data set
Flicker	P_{st}	10 min	Not defined	1.2 for 95% of measurement data set
	P_{It}	2 h	1 for 95% of measurement data set	1 for 100% of measurement data set
Asymmetry	k_{u2}	10 min	2% for 95% of measurement data set, 3% in special localization	2% for 100% of measurement data set
Total harmonic distortion in voltage	$THDu$	10 min	8% for 95% of measurement data set	8% for 100% of measurement data set, Mean value from all period of time lower than 5%
Harmonic h2–h50	h2–h50	10 min	for 95% of measurement data set: 6.0% for h5; 5.0% for h3, h7; 3.5% for h11; 3.0% for h13; 2.0% for h2, h17; 1.5% for h9, h19, h23, h25; 1.0% for h4,	for 100% measurement data set: 6.0% for h5; 5.0% for h3, h7; 3.5% for h11; 3.0% for h13; 2.0% for h2, h17; 1.5% for h9, h19, h23, h25; 1.0% for h4, h29, h31, h35, h37, h41, h43, h47, h49;
			0.5% for h6, h8, h10, h12, h14, h15, h16, h18, h20, h21, h22, h24.	0.5% for h6, h8, h10, h12, h14, h15, h16, h18, h20, h21, h22, h24, h26, h27, h28, h30, h32, h33, h34, h36, h38, h39, h40, h42, h44, h45, h46, h48, h50.

3. Description of Investigated PV Power Plant

The investigated photovoltaic power plant (PVPP) consists of numerous of small photovoltaic systems. The range of installed power of the PV systems are: 3 kWp, 5 kWp, 17 kWp, 25 kWp, 30 kWp with a total power of 132.37 kWp, however referring to an agreement with the local distribution system operator, the generated power is limited to 100 kW. Thus, technically one of the 30 kWp system works in the regulatory mode in order to keep maximum of generated power to 100 kW. The diagram with the assignment of specific PV technologies and range of installed power is shown in Figure 1. PV modules are made on the basis of different technologies which have been marked in in Figure 1 with given colors:

- First generation—silicon cells, from crystalline silicon:

- Monocrystalline (sc-Si) (yellow),
- Multicrystalline (mc-Si) (orange),
- Second generation—thin-film cells:
 - Cadmium telluride cells (CdTe) (pink),
 - Burns from CuInGaSe2 copper-indium selenide (Copper-Indium-Gallium-Diselenide—CIGS) (green).

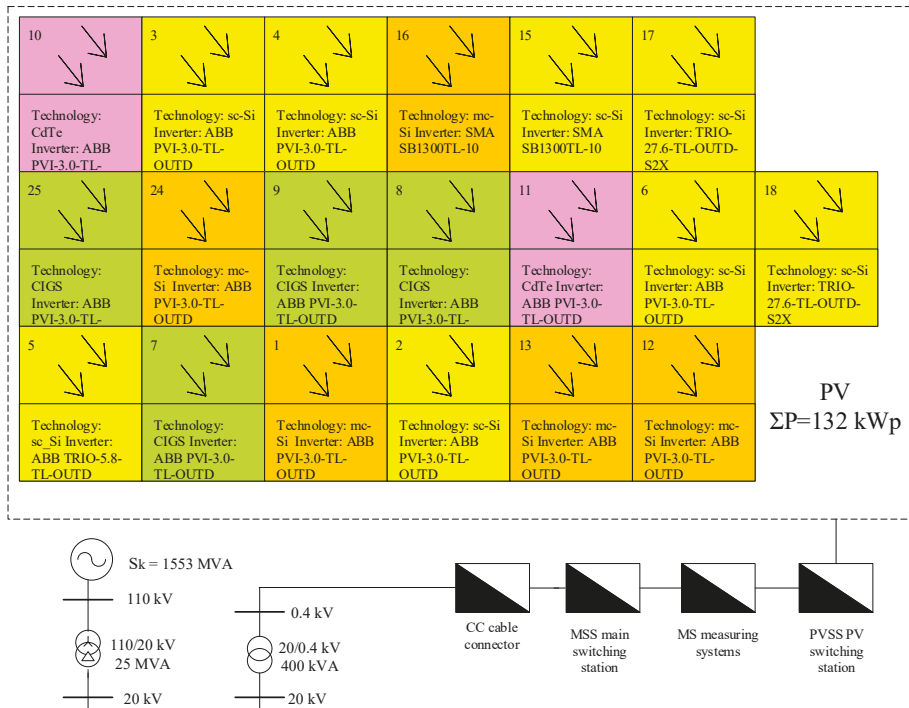


Figure 1. The diagram of investigated photovoltaic power plant with the assignment of rated power and photovoltaic (PV) technologies related to particular PV systems. Note: sc-Si—monocrystalline, mc-Si—multicrystalline, CdTe—Cadmium telluride cells, CIGS—Copper-Indium-Gallium-Diselenide, CC—connector cable, MSS—main switching station, MS—measuring system, PVSS—photovoltaic switching station.

The PV power plant (PVPP) is located in the south-western part of Poland. The angle of the PV panel position is $\beta = 31^\circ$.

The database of measurements consists of electric and non-electrical quantities associated with individual PV installations. The elements of non-electrical quantities are irradiance, temperature of the panels and wind. Electrical quantities come from the particular PV inverters on the AC and DC sides. Additionally, power quality parameters are measured at the point of common coupling of the PV power plant, noted as MS (measuring systems). The energy production is also measured by energy meters.

Additionally, the weather data are collected by a separate weather station including:

- Air pressure, $AtmP$
- Ambient temperature, Ta

- Relative humidity, RH
- Wind speed, WS
- Global horizontal irradiance, Gh
- Diffuse horizontal irradiance, Gd

In order to investigate the influence of the aggregation time interval, PQ parameters and weather condition measurements were conducted from selected period of 12 July, 2018 to 18 July, 2018. This period of observation can be treated as a representative week of measurement data consisting of high and low irradiance levels and different weather conditions. Methods of the measurement and aggregation times were conducted in accordance with class A of standard [3]. The PQ recorder was set up so that the 1 min and 10 min aggregations were collected simultaneously. In order to demonstrate the PV power plant behavior in the selected period of observation in Figure 2, the active power generation in the week for both 1 min and 10 min aggregation is shown. Negative active power during the night is caused by the energy consumption of the plant, mainly related to supplying the database server and cooling the technical container. The application of a 1 min aggregation interval in comparison to a 10 min interval allows the real changeability or power generation to be expressed better, especially in view of extremum values caused by the cloud effect.

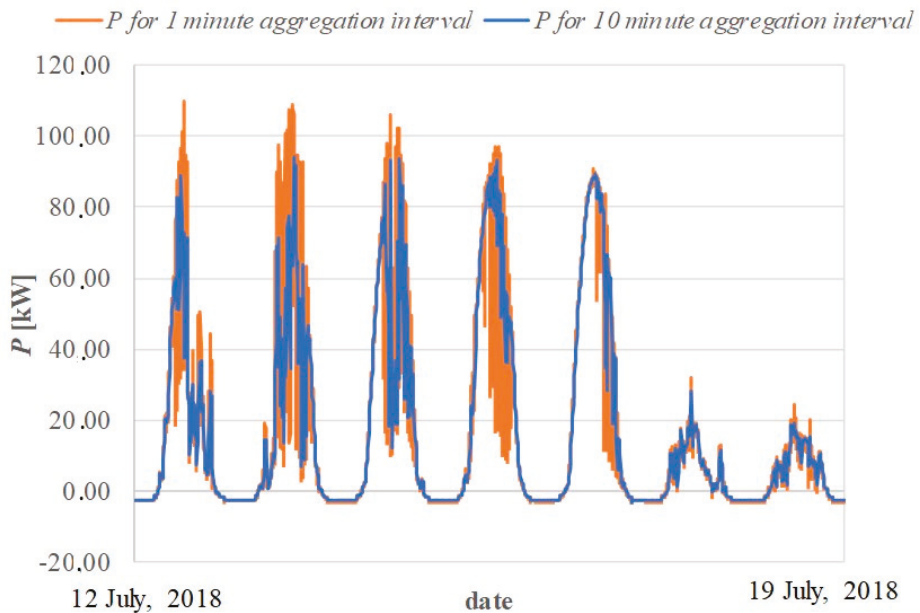


Figure 2. Active power generation of observed PV power plant during selected week using 1 min and 10 min aggregation intervals.

To demonstrate the variation of the weather conditions, the changes of ambient temperature, global horizontal irradiance and diffuse horizontal irradiance is presented in Figure 3 using a 10 min aggregation interval and in Figure 4 using a 1 min aggregation interval. Comparison of the application of 1 min and 10 min of data indicates the higher changeability and extremum values of observed measurements.

4. Results of the PQ Assessment and Correlation Analysis for Different Aggregation Time Intervals

4.1. General Comparison of the PQ Assessment Results Using Requirements of EN 50160:2010 and EN 50160:2015

The results of the PQ assessment for both EN 50160:2010 [1] and EN 50160:2015 [2] are presented in Table 2. The analysis indicates that PQ assessment in accordance with [1,2] gives different results of the assessment. The differences appear mainly when the assessment considers 100% of the measurement data set.

Table 2. Comparison of general results of the power quality assessment obtained using 50160:2010 [1] and 50160:2015 [2].

Parameter	EN 50160:2010 [1]	EN 50160:2015 [2]	Comments
f	✓	✗	Maximum frequency value 50.103 Hz
U	✓	✓	-
P_{st}	-	✓	Single values exceeded but for less than 95% of the time
P_{lt}	✓	✓	-
k_{u2}	✓	✓	-
$THDu$	✓	✓	-
$h2-h14$	✓	✓	-
$h15$	✓	✗	$h15$ maximum value for L3 is 0.51 %
$h16-h25$	✓	✓	-
$h26-h50$	-	✓	-

4.2. Voltage Variation Analysis Using 1 Min and 10 Min Aggregation Intervals

The standard EN 50160:2015 [2] has introduced the analysis of voltage variation in 1 min aggregation time. Previously, referring to EN 50160:2010 [1], the analysis was based on a 10 min aggregation interval. Table 3 presents the obtained values of minimal, mean, maximal, variance, standard deviation and median values of voltage variations aggregated in 1 min and 10 min. The analysis indicates that:

- the mean value is the same for 1 min and 10 min aggregation intervals;
- extreme values are higher for the 1 min aggregation interval;
- variation and standard deviation are higher for the 1 min aggregation interval;
- the median value is very similar for both the 1 min and 10 min aggregation intervals.

Using 1 min or 10 min aggregation intervals has preserved the general character of the investigated connection point. For example, using 1 min and 10 min aggregations indicate some asymmetry in the voltage in the connection point of the observed PV power plant. The differences between values of voltage in particular phases are the effect of the structure of the investigated PV power plant. The PV power plant consists of a number of one-phase PV installations which are connected to different phases and can bring some differences in voltages in particular phases. Generally, it can be concluded that application of a 1 min aggregation interval in comparison to a 10 min interval introduces better observability of variations of voltage that exhibits itself by the higher level of extreme values and standard deviation. Table 3 shows that the voltage variation parameters including minimal and maximal values or standard deviations better express the variability of the observed parameters when 1 min aggregation is used. Generally, it can be concluded that the application of a 1 min aggregation

interval in comparison to 10 min introduces better observability of variations of voltage that exhibits itself by a higher level of extreme values and standard deviation.

Table 3. Comparison of voltage variation parameters of 1 min and 10 min aggregation intervals.

Voltage Variations Parameters	1 Min Aggregation			10 Min Aggregation		
	L1	L2	L3	L1	L2	L3
Mean value	240.12	238.83	239.63	240.12	238.83	239.63
Minimal value	232.83	230.01	231.38	234.00	230.81	232.73
Maximal value	248.44	249.90	248.30	246.10	246.53	247.31
Variation	5.81	8.98	8.10	5.54	8.58	7.67
Standard deviation	2.41	3.00	2.85	2.35	2.93	2.77
Median value	239.86	238.88	239.60	239.85	238.85	239.61

In order to highlight the impact of the aggregation interval on the assessment of PQ parameters at the point of the connection of the PV power plant, Figure 5 presents the analysis of voltage variations in classic term (10 min), short term (1 min) and very short term (200 ms extreme minimum and maximum values of each 10 min aggregated data) for two opposite weather conditions:

- high level of irradiance (12 July, 2018 12:00) $G_h = 759 \text{ W/m}^2$
- low level of irradiance (17 July, 2018 12:00) $G_h = 172 \text{ W/m}^2$

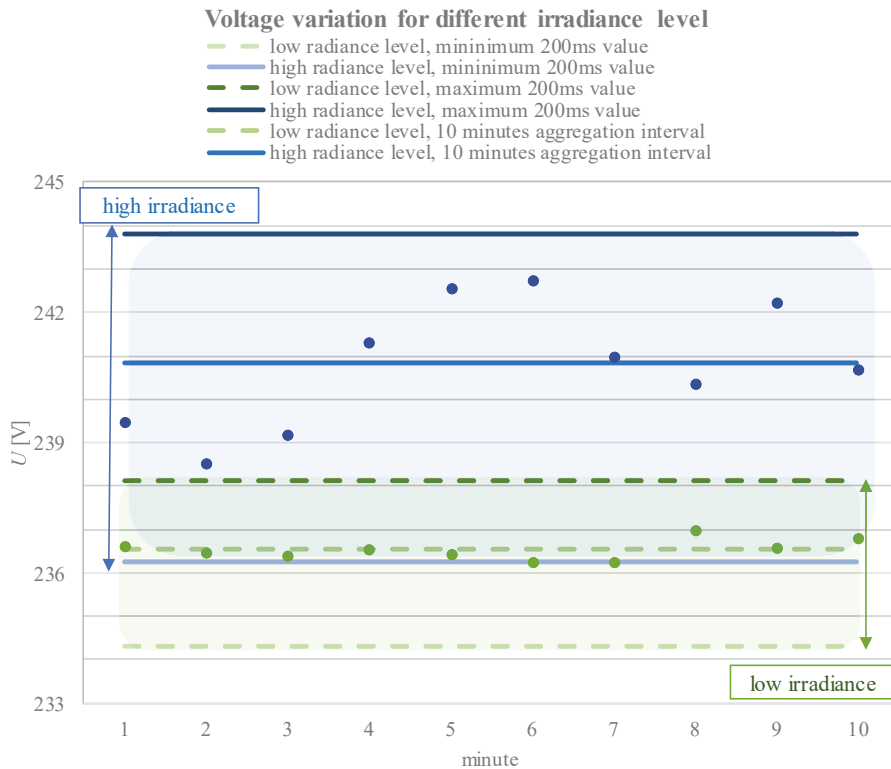


Figure 5. Observability of voltage variations of the selected phase for different aggregation intervals at different solar irradiance levels.

The results are presented for one representative phase. In order to minimize the impact of the network operating condition, the comparison was performed for similar working conditions i.e., working day and working hour (12:00), but the selected days represent different conditions of solar irradiance. Using both 10 min and 1 min aggregation intervals, an expected relationship between solar irradiance and the voltage is represented. The high solar irradiance level directly indicates the higher level of active power generation that naturally increases voltage in the connection point. However, using 1 min aggregation data additional observations and conclusions can be done. From having 1 min data it can be seen that the envelope of voltage variation is wider for the higher irradiance level than for the smaller solar irradiance. It can be stated that using a 1 min aggregation interval the cloud effect on voltage variation is better represented than when a 10 min aggregation is applied. It can be concluded generally that a shorter aggregation interval allows the variable nature of observed parameter to be expressed better. Instead of one mean 10 min value, a time series of 1 min values is considered.

4.3. Correlation Analysis Using 1 Min and 10 Min Aggregation Intervals

The next issue concerns the possible impact of the aggregation interval that can be considered in terms of the effect on the result of the correlation analysis of selected power quality parameters and weather condition. The correlation was calculated for 1 min and 10 min aggregation time respectively. Correlation analysis was performed using the Statistica software. A correlation matrix function was used, which is based on determining the linear correlation of the straight line (r-Pearson). It defines the degree of proportional relations of the values of two variables. Correlation analysis was performed between pairs of parameters representing power quality, weather condition, level of active power production. No preliminary data standardization was performed. Correlation levels were determined on the basis of the r_{xy} correlation coefficient defined as [16]:

$$r_{xy} = \frac{\sum_{i=1}^N (x_i - \bar{x})(y_i - \bar{y})}{\sqrt{\sum_{i=1}^N (x_i - \bar{x})^2 \sum_{i=1}^N (y_i - \bar{y})^2}} \quad (1)$$

The interpretation of the correlation level based on the determined r_{xy} coefficient is presented in Table 4.

Table 4. Correlation level description [17].

Positive Correlation	Negative Correlation	Correlation Level Description
$r_{xy} = 0$	$r_{xy} = 0$	No correlation
$0 < r_{xy} \leq 0.1$	$-0.1 \leq r_{xy} < 0$	Slight correlation
$0.1 < r_{xy} \leq 0.4$	$-0.4 \leq r_{xy} < -0.1$	Poor correlation
$0.4 < r_{xy} \leq 0.7$	$-0.7 \leq r_{xy} < -0.4$	Noticeable correlation
$0.7 < r_{xy} \leq 0.9$	$-0.9 \leq r_{xy} < -0.7$	High correlation
$0.9 < r_{xy}$	$r_{xy} < -0.9$	Strong correlation

The prepared matrix of correlation is an extended matrix which consists of PQ parameters and weather condition measurements together so that the analysis of the correlation coefficient can be performed simultaneously between particular power quality themselves, for example between voltage level and harmonic contents, as well as between power quality parameters and weather condition, for example between horizontal irradiance and voltage level. The results of the correlation coefficients using 10 min aggregated data is presented in Table 5. Comparative results obtained 1 min aggregated data is collected in Table 6. Additionally, the correlation diagrams of all pairs of parameters is shown in Figure 6 for the 10 min data and in Figure 7 for the 1 min data.

Table 5. Correlation matrix of power quality (PQ) and weather parameters for 10 min aggregated data.

	1	2	3	4	5	6	7	8	9	10	11	12	13	14	15	16	17	18	19
1	1.00																		
2	-0.0	1.00																	
3	-0.2	-0.8	1.00																
4	-0.0	0.01	0.00	1.00															
5	0.21	0.63	-0.6	0.00	1.00														
6	0.12	0.40	-0.3	0.00	0.71	1.00													
7	0.29	0.62	-0.6	-0.0	0.46	0.27	1.00												
8	0.35	0.48	-0.5	-0.0	0.34	0.10	0.95	1.00											
9	0.37	0.43	-0.4	-0.0	0.32	0.05	0.90	0.96	1.00										
10	-0.2	0.14	-0.0	0.01	0.30	0.44	-0.2	-0.4	-0.4	1.00									
11	-0.2	0.14	-0.0	0.01	0.28	0.41	-0.2	-0.4	-0.4	0.98	1.00								
12	-0.2	0.11	-0.0	0.03	0.27	0.41	-0.2	-0.3	-0.4	0.93	0.89	1.00							
13	-0.2	-0.1	0.27	-0.0	-0.0	0.06	-0.3	-0.5	-0.4	0.20	0.21	0.16	1.00						
14	-0.0	-0.5	0.44	-0.0	-0.5	-0.5	-0.3	-0.2	-0.1	-0.4	-0.3	-0.3	0.24	1.00					
15	-0.0	-0.5	0.42	-0.0	-0.5	-0.5	-0.2	-0.1	-0.0	-0.4	-0.4	-0.4	0.16	0.93	1.00				
16	-0.0	-0.5	0.45	-0.0	-0.5	-0.5	-0.3	-0.2	-0.1	-0.4	-0.4	-0.4	0.22	0.91	0.95	1.00			
17	0.20	0.63	-0.6	0.00	0.99	0.70	0.48	0.35	0.34	0.29	0.27	0.26	-0.0	-0.5	-0.5	-0.5	1.00		
18	0.20	0.62	-0.5	0.01	0.99	0.72	0.47	0.34	0.32	0.31	0.29	0.28	-0.0	-0.5	-0.5	-0.5	1.00	1.00	
19	0.20	0.62	-0.6	0.00	0.99	0.70	0.48	0.36	0.34	0.28	0.26	0.25	-0.0	-0.5	-0.5	-0.5	1.00	1.00	1.00

Note: 1—*AtmP* (air pressure), 2—*Ta* (ambient temperature), 3—*RH* (relative humidity), 4—*WS* (wind speed), 5—*Gh* (global horizontal irradiance), 6—*Gd* (diffuse horizontal irradiance), 7—*UL1* (voltage variation L1), 8—*UL2* (voltage variation L2), 9—*UL3* (voltage variation L3), 10—*P_{stL1}* (short-term flicker severity L1), 11—*P_{stL2}* (short-term flicker severity L2), 12—*P_{stL3}* (short-term flicker severity L3), 13—*k_{u2}* (asymmetry), 14—*THDu_{L1}* (total harmonic distortion L1), 15—*THDu_{L2}* (total harmonic distortion L2), 16—*THDu_{L3}* (total harmonic distortion L3), 17—*P_{L1}* (active power change L1), 18—*P_{L2}* (active power change L2), 19—*P_{L3}* (active power change L3).

Table 6. Correlation matrix of PQ and weather parameters for 1 min aggregated data.

	1	2	3	4	5	6	7	8	9	10	11	12	13	14	15	16	17	18	19
1	1.00																		
2	-0.0	1.00																	
3	-0.2	-0.8	1.00																
4	-0.0	0.01	0.00	1.00															
5	0.20	0.60	-0.5	0.00	1.00														
6	0.12	0.39	-0.3	0.00	0.69	1.00													
7	0.28	0.60	-0.5	-0.0	0.46	0.27	1.00												
8	0.35	0.47	-0.5	-0.0	0.35	0.11	0.95	1.00											
9	0.36	0.41	-0.4	-0.0	0.33	0.06	0.90	0.96	1.00										
10	-0.1	0.10	-0.0	0.02	0.23	0.34	-0.2	-0.3	-0.3	1.00									
11	-0.1	0.09	-0.0	0.02	0.21	0.32	-0.2	-0.3	-0.3	0.98	1.00								
12	-0.1	0.09	-0.0	0.02	0.23	0.34	-0.2	-0.3	-0.3	0.95	0.94	1.00							
13	-0.2	-0.1	0.25	-0.0	-0.0	0.04	-0.3	-0.4	-0.3	0.11	0.13	0.12	1.00						
14	-0.0	-0.5	0.41	-0.0	-0.5	-0.4	-0.3	-0.1	-0.1	-0.2	-0.2	-0.2	0.21	1.00					
15	-0.0	-0.5	0.40	-0.0	-0.5	-0.5	-0.2	-0.1	-0.0	-0.3	-0.3	-0.3	0.14	0.91	1.00				
16	-0.0	-0.5	0.43	-0.0	-0.5	-0.5	-0.3	-0.1	-0.1	-0.3	-0.3	-0.3	0.20	0.88	0.93	1.00			
17	0.20	0.60	-0.5	0.00	0.97	0.69	0.48	0.37	0.35	0.22	0.21	0.22	-0.0	-0.4	-0.5	-0.4	1.00		
18	0.19	0.60	-0.5	0.00	0.97	0.70	0.48	0.36	0.34	0.24	0.22	0.23	-0.0	-0.5	-0.5	-0.5	1.00	1.00	
19	0.20	0.60	-0.5	0.00	0.97	0.69	0.49	0.37	0.36	0.22	0.20	0.22	-0.0	-0.4	-0.5	-0.4	1.00	1.00	1.00

Note: 1—*AtmP* (air pressure), 2—*Ta* (ambient temperature), 3—*RH* (relative humidity), 4—*WS* (wind speed), 5—*Gh* (global horizontal irradiance), 6—*Gd* (diffuse horizontal irradiance), 7—*UL1* (voltage variation L1), 8—*UL2* (voltage variation L2), 9—*UL3* (voltage variation L3), 10—*P_{stL1}* (short-term flicker severity L1), 11—*P_{stL2}* (short-term flicker severity L2), 12—*P_{stL3}* (short-term flicker severity L3), 13—*k_{u2}* (asymmetry), 14—*THDu_{L1}* (total harmonic distortion L1), 15—*THDu_{L2}* (total harmonic distortion L2), 16—*THDu_{L3}* (total harmonic distortion L3), 17—*P_{L1}* (active power change L1), 18—*P_{L2}* (active power change L2), 19—*P_{L3}* (active power change L3).

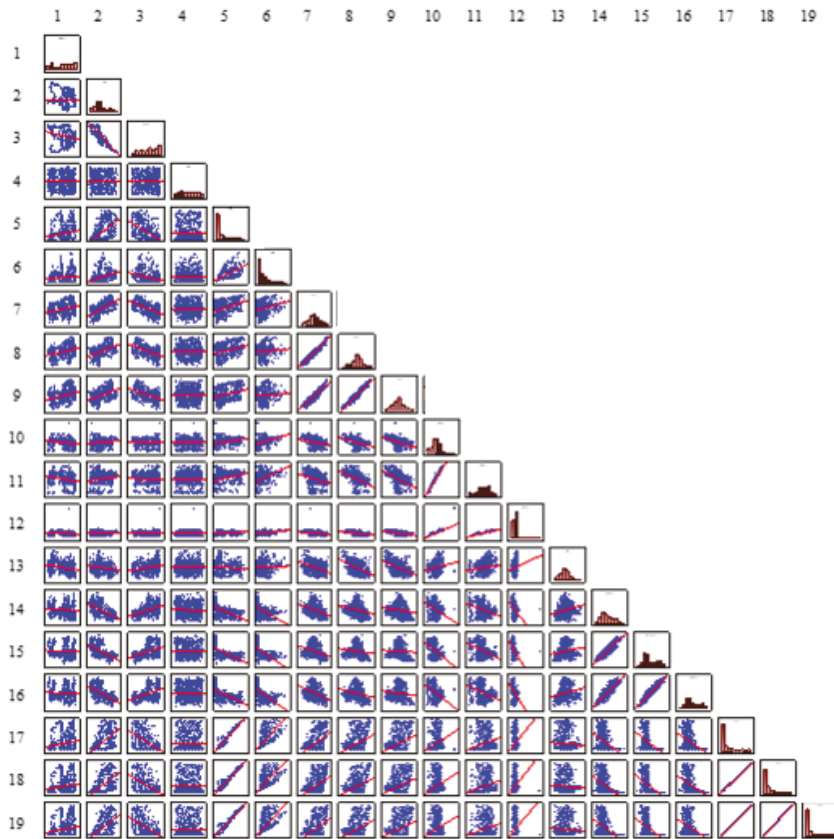


Figure 6. Correlation diagrams for all pairs of parameters (PQ and weather) when 10 min aggregation interval is used. Note: 1—*AtmP* (air pressure), 2—*Ta* (ambient temperature), 3—*RH* (relative humidity), 4—*WS* (wind speed), 5—*Gh* (global horizontal irradiance), 6—*Gd* (diffuse horizontal irradiance), 7—*UL1* (voltage variation L1), 8—*UL2* (voltage variation L2), 9—*UL3* (voltage variation L3), 10—*P_{stL1}* (short-term flicker severity L1), 11—*P_{stL2}* (short-term flicker severity L2), 12—*P_{stL3}* (short-term flicker severity L3), 13—*k_{u2}* (asymmetry), 14—*THDu_{L1}* (total harmonic distortion L1), 15—*THDu_{L2}* (total harmonic distortion L2), 16—*THDu_{L3}* (total harmonic distortion L3), 17—*P_{L1}* (active power change L1), 18—*P_{L2}* (active power change L2), 19—*P_{L3}* (active power change L3).

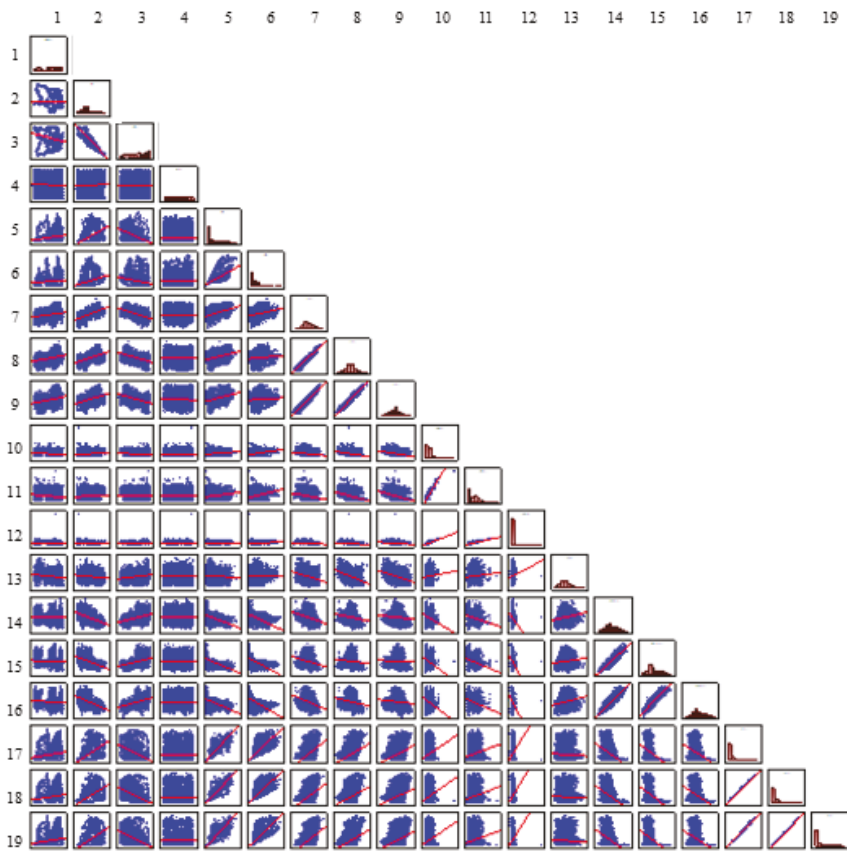


Figure 7. Correlation diagrams for all pairs of parameters (PQ and weather) when 1 min aggregation interval is used. Note: 1—*AtmP* (air pressure), 2—*Ta* (ambient temperature), 3—*RH* (relative humidity), 4—*WS* (wind speed), 5—*Gh* (global horizontal irradiance), 6—*Gd* (diffuse horizontal irradiance), 7—*UL1* (voltage variation L1), 8—*UL2* (voltage variation L2), 9—*UL3* (voltage variation L3), 10—*P_{stL1}* (short-term flicker severity L1), 11—*P_{stL2}* (short-term flicker severity L2), 12—*P_{stL3}* (short-term flicker severity L3), 13—*k_{u2}* (asymmetry), 14—*THDu_{L1}* (total harmonic distortion L1), 15—*THDu_{L2}* (total harmonic distortion L2), 16—*THDu_{L3}* (total harmonic distortion L3), 17—*P_{L1}* (active power change L1), 18—*P_{L2}* (active power change L2), 19—*P_{L3}* (active power change L3).

The analysis of the correlation matrix of PQ parameters and weather conditions using a 10 min aggregation interval, presented in Table 4 and Figure 6, indicates that there is:

- strong correlation between global horizontal irradiance intensity (*Gh*) and active power (*P*) with an extremal value equal to 0.99;
- high correlation between intensity of the diffuse horizontal irradiance component (*Gd*) and active power (*P*) with an extremal value equal to 0.72;
- noticeable correlation between ambient temperature (*Ta*) and voltage variation (*U*) with an extremal value equal to 0.62, total harmonic distortion in voltage (*THDu*) with an extremal value equal to -0.55 and active power (*P*) with an extremal value equal to 0.63;
- noticeable correlation between relative humidity (*RH*) and voltage variation (*U*) with an extremal value equal to -0.60 , total harmonic distortion in voltage (*THDu*) with an extremal value equal to 0.45, active power (*P*) with an extremal value equal to -0.60 ;

- noticeable correlation between global horizontal irradiance intensity (Gh) and total harmonic distortion in voltage ($THDu$) with an extremal value equal to -0.58 ;
- noticeable correlation between intensity of the diffuse horizontal irradiance component (Gd) and short-term flicker severity (P_{st}) with an extremal value equal to 0.44 ;
- strong correlation between the line-to-line values of three-phase parameters ($U, P_{st}, THDu, P$) with a minimal value equal to 0.90 ;
- noticeable correlation between L1 voltage variations (U) and L1, L2, L3 active power (P) with an extremal value equal to 0.48 ;
- noticeable correlation between L2 and L3 voltages variations (U) and L2 and L3 short-term flicker severities (P_{st}) with an extremal value equal to -0.47 ;
- noticeable correlation between short-term flicker severities (P_{st}) and total harmonic distortion in voltage ($THDu$) with an extremal value equal to -0.49 ;
- noticeable correlation between total harmonic distortion in voltage ($THDu$) and active power (P) with an extremal value equal to -0.59 ;
- other correlations are too low to be noticeable.

Using both 10 min and 1 min aggregation intervals, an expected relationship between solar irradiance and the active power production as well as voltage level is represented by the high level of correlation coefficients. The higher solar irradiance level, the higher level of active power generation is observed that naturally has an influence on voltage level in the connection point. The correlation analysis is sensitive enough to show small differences between phases which can be explained by the structure of the investigated PV power plant. The PV power plant consists of many small individual PV installations including one-phase installations thus the active power or voltage level may differ slightly in particular phases. It has resulted in a correlation coefficient related to the phases.

Analyzing the correlation matrix of PQ parameters and weather conditions for the 1 min aggregation interval, presented in Table 6 and Figure 7, confirms generally the same correlation results as for the 10 min interval. However, in order to highlight the impact of the aggregation interval on the results of the correlation analysis, a separate matrix of differences was prepared and presented in Table 7. The matrix consists of differences calculated between the absolute value of adequate correlation coefficients obtained using 10 min and 1 min aggregation intervals. A positive value of the difference denotes that the correlation coefficient calculated using the 10 min aggregation is higher than that calculated using the 1 min aggregation. The obtained result of the investigated differences indicates that the correlation results using 10 min and 1 min aggregation are characterized by comparative level of correlation coefficient for all measured parameters. The comparative means that the maximal difference is slight and less than 0.1. The exception of this result is the correlation between flicker severity (P_{st}) and voltage level (U) and total harmonic distortion in voltage ($THDu$). For these parameters, the maximal value of difference is 0.15. Generally, it can be concluded that using a 10 min aggregation interval in comparison to a 1 min aggregation results in a slightly higher level of correlation coefficients. The sign of the coefficients remains the same. In other words, it can be concluded generally that the application of different aggregation time intervals does not change the direction of the correlation but has an influence on the absolute value of the correlation coefficient. Shorter aggregation time intervals assure sharper observability of the process but exhibit a higher level of standard deviation and wider envelope of parameter variation. Compared to the 1 min time series, the 10 min data are more "monotonous" than the 1 min data due to the averaging process over the 10 min interval. Thus, the correlation analysis performed using 10 min data, which are more smoothed, results in higher values of correlation coefficient.

Table 7. Matrix of differences between correlation coefficients obtained using 1 and 10 min aggregation intervals.

	1	2	3	4	5	6	7	8	9	10	11	12	13	14	15	16	17	18	19
1	0.00																		
2	0.00	0.00																	
3	0.00	0.00	0.00																
4	0.00	0.00	0.00	0.00															
5	0.01	0.02	0.02	0.00	0.00														
6	0.00	0.00	0.00	0.00	0.02	0.00													
7	0.01	0.02	0.02	0.00	0.00	0.00	0.00												
8	0.01	0.01	0.01	0.00	-0.01	0.00	0.00	0.00											
9	0.01	0.01	0.02	0.00	-0.01	-0.01	0.00	0.01	0.00										
10	0.06	0.04	0.01	0.00	0.07	0.10	0.05	0.10	0.12	0.00									
11	0.06	0.05	0.02	0.00	0.07	0.09	0.04	0.09	0.12	0.00	0.00								
12	0.03	0.02	0.00	0.01	0.04	0.07	0.03	0.06	0.08	-0.0	-0.05	0.00							
13	0.03	0.01	0.02	0.01	0.00	0.02	0.06	0.06	0.07	0.09	0.08	0.04	0.00						
14	0.00	0.03	0.02	0.00	0.05	0.03	0.04	0.03	0.02	0.11	0.12	0.09	0.03	0.00					
15	0.00	0.02	0.01	0.01	0.04	0.03	0.02	0.02	0.01	0.15	0.15	0.11	0.02	0.02	0.00				
16	0.00	0.01	0.01	0.00	0.04	0.02	0.02	0.01	0.01	0.12	0.12	0.08	0.02	0.03	0.02	0.00			
17	0.01	0.02	0.02	0.00	0.02	0.02	-0.01	-0.01	-0.0	0.06	0.06	0.04	0.01	0.04	0.03	0.03	0.00		
18	0.01	0.02	0.02	0.00	0.02	0.02	-0.01	-0.02	-0.0	0.07	0.07	0.05	0.01	0.04	0.04	0.03	0.00	0.00	
19	0.01	0.02	0.02	0.00	0.02	0.02	-0.01	-0.01	-0.0	0.06	0.06	0.04	0.01	0.04	0.03	0.03	0.00	0.00	0.00

Note: 1—*AtmP* (air pressure), 2—*Ta* (ambient temperature), 3—*RH* (relative humidity), 4—*WS* (wind speed), 5—*Gh* (global horizontal irradiance), 6—*Gd* (diffuse horizontal irradiance), 7—*UL1* (voltage variation L1), 8—*UL2* (voltage variation L2), 9—*UL3* (voltage variation L3), 10—*P_{sIL1}* (short-term flicker severity L1), 11—*P_{sHL2}* (short-term flicker severity L2), 12—*P_{sHL3}* (short-term flicker severity L3), 13—*k_{u2}* (asymmetry), 14—*THDuL1* (total harmonic distortion L1), 15—*THDuL2* (total harmonic distortion L2), 16—*THDuL3* (total harmonic distortion L3), 17—*P_{L1}* (active power change L1), 18—*P_{L2}* (active power change L2), 19—*P_{L3}* (active power change L3).

5. Discussions

The investigations presented in this paper correspond to the recent amendment to the PQ standard EN 50160:2015 [2] in comparison to the previous version EN 50160:2010 [1]. The main issues in relation to the development of the mentioned standard are the influence of the requirement for the assessed PQ parameters to preserve the limits 100% of the observed time in comparison to the previous requirement of 95% of the time of observation, as well as influence of the suggestion to use a 1 min aggregation time interval in the case of a LV power system in comparison to the classical 10 min aggregation. Additionally, the issue of the aggregation interval is extended in the paper for the analysis of the influence of the aggregation interval on correlation analysis between PQ parameters and weather conditions. The formulated problems can have a meaning in analysis of the integration of distributed energy resources with a power system in the light of increasing requirements for power quality parameters and increasing concentration of distributed generation in power systems.

In order to highlight mentioned issues, the results of the investigation of a real measurement of a 100 kW photovoltaic power plant directly connected to a LV power system is presented. In relation to the requirement for the assessed PQ parameters to preserve the limits 100% of the observed time, it can be concluded that such requirement can be hard to obtain in selected cases. For example, the investigated 15th harmonic in voltage in the PCC of the investigated 100 kW PV power plant does not preserve the requirement for 100% of the observed time, but has a positive assessment for the requirement of 95% of the observed time. It should be emphasized that the flagging concept was implemented, and the investigated measurement data are free of events which might have affected the assessment by extremal values. A similar conclusion can be formulated in the case of a variation in frequency demand. A more restricted limit for the permissible level of frequency variation and demand for 100% of the observed time causes the assessment to be negative when the requirements

related to the amendment to the standard EN 50160:2015 [2] is applied, but would be positive according to requirements of the previous version EN 50160:2010 [1].

Novel power quality analysis is not only concentrated on PQ parameters but also finds a relation between external components and their impact on power quality. In the case of integration of distributed generation with a power system, a prominent example is the influence of weather conditions on power quality. A tool used for the assessment can be a correlation analysis. Thus, an additional aim of the paper is to investigate the influence of the aggregation time interval on the correlation analysis. Generally, it can be concluded that the obtained result of the investigated differences indicates that the correlation analysis using 10 min and 1 min aggregation intervals are characterized by comparative level of correlation coefficient. The application of different aggregation time intervals does not change the direction of the correlation but has an influence on the absolute value of the correlation coefficient. The 10 min data are more smoothed than the 1 min time series due to the averaging process over the 10 min and correlation coefficients obtained using 10 min aggregation are slightly higher. Only in case of flicker severity, expressed by parameter P_{st} , which is sensitive even for single voltage fluctuations, is the difference of the correlation coefficient noticeable.

The obtained results indicate the need for further investigation of the sensitivity of the assessment when new requirements for power quality limits are created or a shorter aggregation time interval is considered. The advantage of the application of a shorter aggregation time interval is the enhancement of the observability of the investigated objects. However, it has an impact on extended requirements for the measurement devices and increases the time and computational power required for analysis due to the extended size of the power quality database.

6. Conclusions

The presented results indicate that general outcomes of the analysis for both 1 min and 10 min aggregation are similar. However where the requirements for the parameters are forced to be fulfilled during 100% of the observation time, the 1 min aggregation makes the observability of the object more restricted. This allows us to formulate general conclusion that the results of power quality assessment using the 1 min aggregation can be dependent on cooperation of the observed object with the power systems, the used regulation and integration systems, as well as the condition of the power system at the connection point. Furthermore, the obtained results show some potential in using variations of observed power quality parameters in the development of power quality analysis when a 1 min aggregation is used. It was shown that the voltage variation parameters including minimal and maximal values or standard deviations better express the variability of the observed parameters when 1 min aggregation is used. It was also shown that the assessment of power quality parameters at the connection point of a PV power plant, when the cloud effect or variable operating condition of the low voltage network are considered, is characterized by slightly higher values in the variation of the observed power quality parameters when a 1 min aggregation interval is applied than in case of 10 min aggregation. This allows us to conclude that using 1 min aggregation increases the sensitivity of power quality assessment that might be desirable in future when power grids with a high concentration of distributed energy resources, microgrids or grids working in the islanding condition are considered.

Author Contributions: Conceptualization, M.J. and T.S.; methodology, M.J., T.S. and P.K.; software, J.S., M.J. and T.S.; validation, T.S., J.R. and Z.L.; formal analysis, M.J. and T.S.; investigation, M.J., T.S. and P.K.; resources, M.J., T.S., P.K., P.J., D.B., M.R., J.S.; writing—M.J. and T.S.; writing—review and editing, M.J., T.S., E.J., D.K.; visualization, M.J., E.J.; supervision, T.S.; project administration, T.S.; funding acquisition, M.J. and T.S.

Funding: This research was funded by Polish Ministry of Science and Higher Education under the grants for young researchers 049M/0004/19 as well as under the project “Developing a platform for aggregating generation and regulatory potential of dispersed renewable energy sources, power retention devices and selected categories of controllable load” supported by European Union Operational Program Smart Growth 2014-2020, Priority Axis I: Supporting R&D carried out by enterprises, Measure 1.2: Sectoral R&D Programs, POIR.01.02.00-00-0221/16, performed by TAURON Ekoenergia Ltd. under Polish Sectoral Program PBSE coordinated by The National Centre of Research and Development in Poland.

Acknowledgments: This work uses weather condition data provided by the Center of Energy Technology in Świdnica, Poland.

Conflicts of Interest: The authors declare no conflict of interest.

Abbreviations

AC	alternative current
AtmP	air pressure
CC	connector cable
CdTe	Cadmium telluride cells
CIGS	Copper-Indium-Gallium-Diselenide
DC	direct current
EN	European Standard
f	frequency variation
G_d	intensity of the scattered radiation component
G_h	total horizontal radiation intensity
HC	host capacity
IEC	International Electrotechnical Commission
IEEE	Institute of Electrical and Electronics Engineers
k_{u2}	asymmetry
mc-Si	multicrystalline
MS	measuring system
MSS	main switching station
P	active power change
P_{lt}	long-term flicker severity
P_{st}	short-term flicker severity
PVFS	PV Solar Farm
PVSS	photovoltaic switching station
RES	renewable energy sources
RH	relative humidity
sc-Si	monocrystalline
T_a	ambient temperature
THD	total harmonic distortion
U	voltage variation
VDE	Verband der Elektrotechnik, Elektronik und Informationstechnik
WS	wind speed

References

1. EN 50160: *Voltage Characteristics of Electricity Supplied by Public Distribution Network*; PKN: Warszawa, Polska, 2010.
2. EN 50160: *Voltage Characteristics of Electricity Supplied by Public Distribution Network*; PKN: Warszawa, Polska, 2015.
3. IEC 61000 4–30 *Electromagnetic Compatibility (EMC)—Part 4–30: Testing and Measurement Techniques—Power Quality Measurement Methods*; PKN: Warszawa, Polska, 2015.
4. IEEE. *Monitoring and Definition of Electric Power Quality*; IEEE: Piscataway Township, NJ, USA, 2009.
5. Jasiński, M.; Sikorski, T.; Borkowski, K. Clustering as a tool to support the assessment of power quality in electrical power networks with distributed generation in the mining industry. *Electr. Power Syst. Res.* **2019**, *166*, 52–60. [[CrossRef](#)]
6. Bouchakour, S.; Arab, A.H.; Abdeladim, K.; Amrouche, S.O.; Semaoui, S.; Taghezouit, B.; Boulahchiche, S.; Razagui, A. Investigation of the voltage quality at PCC of grid connected PV system. *Energy Procedia* **2017**, *141*, 66–70. [[CrossRef](#)]
7. Gała, M.; Jąderko, A. Assessment of the impact of photovoltaic system on the power quality in the distribution network. *Prz. Elektrotech.* **2018**, *94*, 162–165. [[CrossRef](#)]

8. Grycan, W.; Brusilowicz, B.; Kupaj, M. Photovoltaic farm impact on parameters of power quality and the current legislation. *Sol. Energy* **2018**, *165*, 189–198. [CrossRef]
9. Bogenrieder, J.; Glass, O.; Luchscheider, P.; Stegner, C.; Weller, J. Technical comparison of measures for voltage regulation in low-voltage grids. In Proceedings of the 24th International Conference on Electricity Distribution, Glasgow, UK, 12–15 June 2017; pp. 1–5.
10. Divshali, P.H.; Soder, L. Improving PV hosting capacity of distribution grids considering dynamic voltage characteristic. In Proceedings of the Power Systems Computation Conference (PSCC), Dublin, Ireland, 11–15 June 2018.
11. Vojtek, M.; Kolcun, M.; Špes, M. Utilization of energy storages in low voltage grids with high penetration of photovoltaics—Addressing voltage issues. In Proceedings of the 2018 19th International Scientific Conference on Electric Power Engineering (EPE), Brno, Czech Republic, 16–18 May 2018.
12. Ramljak, I.; Ramljak, I. PV plant connection in urban and rural LV grid: Comparison of voltage quality results. In *Advanced Technologies, Systems, and Applications III*; Springer: Berlin, Germany, 2018; pp. 271–278.
13. Meyer, J.; Domagk, M.; Darda, T.; Eberl, G. Influence of aggregation intervals on power quality assessment according to EN 50160. In Proceedings of the 22nd International Conference and Exhibition on Electricity Distribution (CIRED 2013), Institution of Engineering and Technology, Stockholm, Sweden, 10–13 June 2013; p. 1174.
14. Elphick, S.; Gosbell, V.; Perera, S. The effect of data aggregation interval on voltage results. In Proceedings of the 2007 Australasian Universities Power Engineering Conference, Perth, Australia, 9–12 December 2007; pp. 1–7.
15. Jasiński, M.; Rezmer, J.; Sikorski, T.; Szymańda, J. Integration Monitoring of On-Grid Photovoltaic System: Case Study. *Period. Polytech. Electr. Eng. Comput. Sci.* **2019**, *63*, 99–105. [CrossRef]
16. Statsoft Polska StatSoft Electronic Statistic Textbook. Available online: <http://www.statsoft.pl/textbook/stathome.html> (accessed on 15 February 2019).
17. Sikorski, T. *Monitoring i Ocena Jakości Energii w Sieciach Elektroenergetycznych z Udziałem Generacji Rozproszonej*; Oficyna Wydawnicza Politechniki Wrocławskiej: Wrocław, Poland, 2013. (In Polish)



© 2019 by the authors. Licensee MDPI, Basel, Switzerland. This article is an open access article distributed under the terms and conditions of the Creative Commons Attribution (CC BY) license (<http://creativecommons.org/licenses/by/4.0/>).

Article

Techno-Economic Optimization of Grid-Connected Photovoltaic (PV) and Battery Systems Based on Maximum Demand Reduction (MDRed) Modelling in Malaysia

Gopinath Subramani ¹, Vigna K. Ramachandaramurthy ^{2,*}, P. Sanjeevikumar ³,
Jens Bo Holm-Nielsen ³, Frede Blaabjerg ⁴, Leonowicz Zbigniew ⁵ and Pawel Kostyla ⁵

¹ Centre of Advanced Electrical and Electronic Systems (CAEES), Faculty of Engineering & the Built Environment, Segi University, Kota Damansara, Petaling Jaya 47810, Malaysia; sgopinath@segi.edu.my

² Institute of Power Engineering, Department of Electrical Power Engineering, College of Engineering, Universiti Tenaga Nasional, Kajang 43000, Malaysia

³ Center for Bioenergy and Green Engineering, Department of Energy Technology, Aalborg University, 6700 Esbjerg, Denmark; san@et.aau.dk (P.S.); jhn@et.aau.dk (J.B.H.-N.)

⁴ Center of Reliable Power Electronics (CORPE), Department of Energy Technology, Aalborg University, 9220 Esbjerg, Denmark; fbl@et.aau.dk

⁵ Faculty of Electrical Engineering, Wroclaw University of Science and Technology, Wyb. Wyspianskiego 27, 50370 Wroclaw, Poland; zbigniew.leonowicz@pwr.edu.pl (L.Z.); pawel.kostyla@pwr.edu.pl (P.K.)

* Correspondence: vigna@uniten.edu.my

Received: 11 July 2019; Accepted: 9 September 2019; Published: 13 September 2019

Abstract: Under the present electricity tariff structure in Malaysia, electricity billing on a monthly basis for commercial and industrial consumers includes the net consumption charges together with maximum demand (MD) charges. The use of batteries in combination with photovoltaic (PV) systems is projected to become a viable solution for energy management, in terms of peak load shaving. Based on the latest studies, maximum demand (MD) reduction can be accomplished via a solar PV-battery system based on a few measures such as load pattern, techno-economic traits, and electricity scheme. Based on these measures, the Maximum Demand Reduction (MDRed) Model is developed as an optimization tool for the solar PV-battery system. This paper shows that energy savings on net consumption and maximum demand can be maximized via optimal sizing of the solar PV-battery system using the MATLAB genetic algorithm (GA) tool. GA optimization results revealed that the optimal sizing of solar PV-battery system gives monthly energy savings of up to 20% of net consumption via solar PV self-consumption, 3% of maximum demand (MD) via MD shaving and 2% of surplus power supplied to grid via net energy metering (NEM) in regards to Malaysian electricity tariff scheme and cost of the overall system.

Keywords: maximum demand (MD); solar PV; battery energy storage system (BESS); net energy metering (NEM); maximum demand reduction (MDRed) model

1. Introduction

The release of greenhouse gases, especially CO₂, by utilities using coal and gas reduces the ozone layer and creates more pollution. Energy demand in developing countries is projected to rise about 65% by 2040, reflecting the growing prosperity and the accelerating economies. The global energy demand will increase by about 35% due to the world's population growth [1]. The high penetration level of solar photovoltaic (PV) in the utility sector decreases the greenhouse gases emissions and promotes the use of renewable energy compared to conventional energy resources. Solar PV systems are able to deliver an alternative solution to reduce the peaking load throughout the day.

However, the intermittent supply of solar PV system during bad weather condition reduces the ability to supply power during peak hours [2]. Solar PV system in combination with energy storage is expected to be the optimum solution to accommodate the peak load.

In the modern era, energy storage technology has been widely applied for peak load reduction. Energy storage devices such as batteries, thermal storage, and supercapacitors offer similar functionality to peaking power plants. Nevertheless, each of these technologies has economic and technical barriers to be solved [3]. Sustainable Energy Development Authority (SEDA) Malaysia has promoted clean energy use by authorizing the implementation of renewable energy tariff mechanisms under the Renewable Energy Act 2011. In November 2016, the Net Energy Metering (NEM) scheme was implemented to encourage the use of renewable energy (RE), especially solar PV in the grid. NEM permits the self-consumption of generated power by the RE while exporting the surplus power to the utilities at a fixed rate. Under the NEM scheme, the surplus generation rate has been set at MYR 0.31 (USD 0.07)/kWh and MYR 0.238 (USD 0.05)/kWh for low voltage and medium voltage interconnection facilities, respectively [4].

Nevertheless, the low energy rate will reduce the excess energy profit compared to the current Time-of-Use (ToU) pricing scheme of Malaysian electricity tariff [5]. This has driven the focus on optimization of the solar PV-battery system to capitalize on the energy-saving profits associated with the electricity price variances between ToU and NEM scheme. Under the ToU scheme, maximum demand (MD) is measured by recording the peak load over the timeframe of successive 30 min intervals from 8.00 a.m. until 10.00 p.m. every day in a month. Table 1 displays the Malaysian electricity tariff rate for different categories of utility customers. As per Table 1, for industrial and commercial sectors, electricity tariff scheme is effective from 1st January 2014 and supersedes the previous tariff schedule which was effective from 1st June 2011 according to Tenaga Nasional Berhad (TNB), the Malaysian electricity company and only electric utility company in Peninsular Malaysia. Based on the Malaysian electricity scheme under TNB, commercial and industrial sectors are categorized based on different tariff rates. C1 and E1 customers incur flat rate charges for MD and net consumption. For C2 and E2 categories, net consumption will be charged based on peak and off-peak periods together with MD charges. The peak period timeframe is from 8.00 a.m. until 10.00 p.m. and the off-peak period is from 10.00 p.m. until 8.00 a.m., respectively [6]. For these reasons, the commercial and industrial customers are encouraged to manage their load consumption according to their respective electricity tariff scheme by focusing on peak and off-peak period rates. Implementation of renewable energy (RE) projects is expected to reduce the maximum demand and will contribute significantly to the overall generation mix in Malaysia.

Table 1. Malaysia electricity tariff categories (Medium Voltage level).

Tariff	Unit	C1 ^a	C2 ^b	E1 ^c	E2 ^d
Peak	RM (USD)/kWh	0.0	0.365 (0.08)	0.0	0.365 (0.08)
Off-peak	RM (USD)/kWh	0.0	0.224 (0.05)	0.0	0.219 (0.05)
Net consumption	RM (USD)/kWh	0.365 (0.08)	0.0	0.337 (0.08)	0.0
Maximum Demand (MD)	RM (USD)/kW	30.3 (6.82)	45.1 (10.2)	29.6 (6.7)	37.0 (8.3)

C1^a represents the commercial sector (general) [6]. C2^b represents the commercial sector (peak and off-peak) [6].

E1^c represents the industrial sector (general) [6]. E2^d represents the industrial sector (peak and off-peak) [6].

Adding solar photovoltaic generation to commercial or industrial loads reduces utility energy (kWh) charges, but often has little effect on maximum demand (kW) charges. As per Figure 1, peak demands or maximum demand often occur early in the morning during the beginning of office hours when the solar PV generation is slowly increased. Commercial customers with PV generation may have the same high peak (kW) demand but with a lower average (kW) demand. Since they have a higher maximum demand, they will generally benefit more from maximum demand reduction using a battery energy storage system. Peak shaving or maximum demand reduction is the process of reducing the amount of energy purchased from the utility sector during peak hours. A couple of the options

include reducing consumption by turning off non-essential equipment during peak hours. Apart from that, installing solar PV-battery systems that can assist with reducing maximum demand, since much of the peak demand occurs during times when this system would be effective.

However, variation in solar irradiance pattern especially during peak hours may lead to a minimal reduction of MD since electricity billing for MD charges are captured on any day with peaking load throughout the month. Therefore, a new approach called Maximum Demand Reduction (MDRed) scheme has been developed to optimally size the solar PV-battery system with respect to Time-of-Use (ToU) pricing scheme of Malaysian electricity tariff and cost of the overall system corresponding to Return on Investment (ROI). Apart from that, this approach will solve the challenges faced due to intermittency of solar PV generation for reliable operation of maximum demand reduction during peak hours with the support of battery energy storage system.

2. Concept of Maximum Demand Reduction (MDRed) Model

Recently, a lot of studies and models have been developed using solar PV-battery systems. Braam et al. [7] have developed a novel forecast-based control system for photovoltaic-battery systems. It estimates the photovoltaic excess power and develops a charging plan for the battery to store the energy from the photovoltaic peak-production. Wang et al. [8] have developed a state-space based model for BESS and implement a modest yet effective method for peak load reduction by considering device limitations. Pimm et al. [9] have developed a demand model to produce high-resolution domestic load profiles to determine how much peak shaving could be achieved with battery storage. An efficient technique of finding the prospective peak shaving using electricity storage is developed for this purpose. It shows that adequate levels of storage capacity can provide significant peak demand reductions if properly coordinated. Ru et al. [10] have studied the minimization of the cost associated with purchasing from (or selling back to) the utility grid and the battery capacity loss while at the same time sustaining the load and decreasing the peak demand purchased from the grid.

Apart from that, Linssen et al. [11] have developed the Battery-Photovoltaic-Simulation (BaPSi) model to conduct techno-economic analyses of PV-battery systems. The model reflects the variation in the environment to determine the solar PV sizing and battery storage capacity. For each system, the mixture of the total costs of electric supply as well as associated technical and economic output parameters are calculated. Kleissl et al. [12] have developed an operational battery dispatch control system using linear programming for a solar PV-battery storage system that practices load and solar prediction to alleviate peak load. Moghim et al. [13] developed the battery energy storage system (BESS) control algorithm to concurrently overcome the outage issue and shave the peak demand considering the BESS sizing and degradation, microgrid system cost reduction, as well as microgrid scheduling. Liu et al. [14] studied the energy management with battery energy storage system (BESS) optimisation by bearing in mind the cost of distributed generations, cost of battery system, and bi-directional energy trading. Dongol et al. [15] developed the Model Predictive Control (MPC) scheme that could be applied to an existing grid linked household with PV-battery system such that the use of battery is maximized and at the same time, peaks in PV power and load demand are reduced.

Optimal sizing of the solar PV-battery system needs to be based on the effectiveness of self-consumption and MD reduction with respect to return on investment. As stated by Subramani, et al. [16], based on Figures 1 and 2, the optimal solar PV-battery sizing depends on important elements such as load pattern, techno-economic traits, and electricity billing scheme to meet high maximum demand reduction. In regard to load profile, the load consumption data of one (1) or two (2) years will be adequate to show the load steadiness mainly on MD level and load consumption pattern during the peak period. Since the MD charges are very high, the energy savings through optimal sizing of the PV and battery system will be able to maximize the electricity bill savings mainly due to peak load reduction for commercial and industrial customers. Battery efficiency in terms of the state of charge (SOC) and depth of discharge (DOD) together with solar irradiance and PV inverter efficiency will be key for optimal sizing. The total cost of the solar PV-battery system will be very critical in

response to the total energy savings, to have a good return on investment to undertake the project. As the core battery technology matures and unit pricing declines, bi-directional battery converters providing both battery charging (AC to DC) and battery inverting (DC to AC) will emerge as a rapidly growing new market for power converters. The Maximum Demand Reduction (MDRed) model is proposed and developed as an optimization tool for the solar PV-battery system. It focuses on peak load shaving and maximization of self-consumption via PV generation and battery system with respect to MD limits. The MDRed model consist of a solar PV array, PV inverter, lithium-ion battery and bi-directional converter. The MDRed model is developed by considering the technical and economic perspective. Firstly, a technical model is formulated which focuses on the battery storage and solar PV capacity to reduce the net load consumption and maximize the MD shaving for a given load pattern. Secondly, the economic model focuses on the cost associated with the system components compared with the energy savings through net consumption and maximum demand to cater for the highest Return on Investment. A flowchart describing the proposed MDRed model is shown in Figure 2. The required input parameters for MDRed model calculation include the consumer load data, solar PV-battery system specification data, and general economic parameters. In MDRed Model, the electricity supply chain is based on the energy balance between the supply and the demand side with respect to MD limitations.

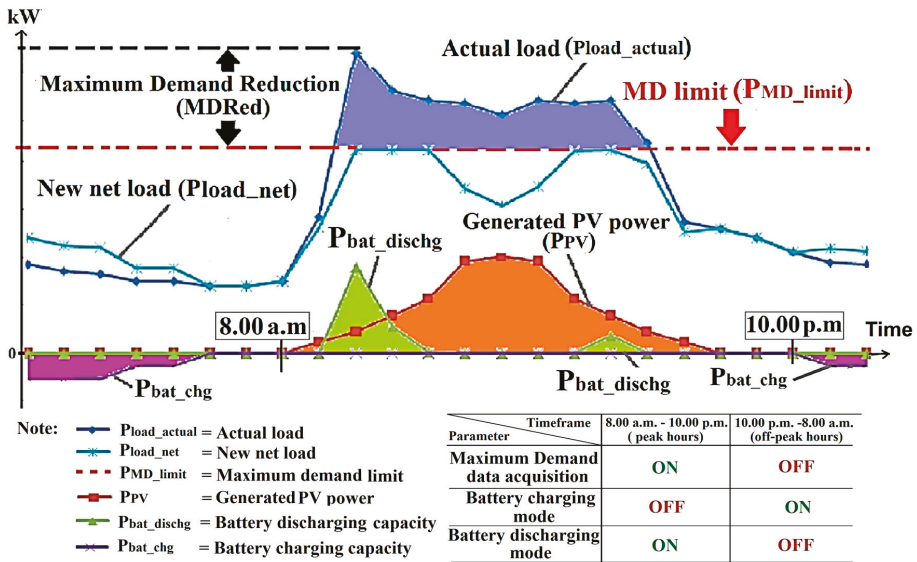


Figure 1. Peak or maximum demand shaving concept using solar PV-battery system [13].

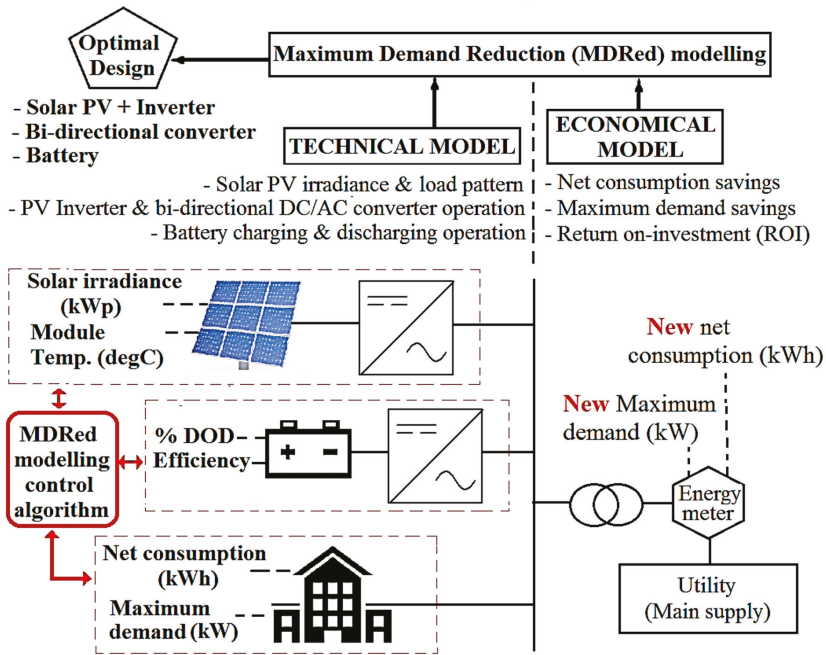


Figure 2. Maximum demand reduction (MDRed) modeling approach.

3. MATLAB Genetic Algorithm (GA) for MDRed Optimization Model

Based on Table 2, optimization techniques such as Genetic Algorithm (GA), Harmony Search (HS), Particle Swarm Optimization (PSO) and Hybrid Optimization are the most prominent algorithms to size the solar PV-battery system.

Table 2. Comparison of optimization techniques.

Technique	Highlights	Strength	Weakness	Ref.
Genetic Algorithm (GA)	Mimics processes of natural evolution, like inheritance, mutation, selection, and crossover	Can solve problems with multiple solutions; easily transferable to existing simulations and models	Convergence speed is slower than other stochastic algorithms	[17,18]
Particle swarm optimization (PSO)	Mimics bird and fish movement behavior	The speed of their searching is fast; calculation in PSO is simple in comparison to other methods	Cannot work out the problems of non-coordinate system	[17,18]
Bee-inspired algorithms	Based on the intelligent foraging behavior of honey bee	The algorithm has local search and global search ability; implemented with several optimization problems; easy to use	Random initialization; algorithm has several parameters	[19]
Harmony search	Based on improvisation process of jazz musicians	Can handle discrete variables as well as continuous variables; ability to perform a global and local search	Complex solving process	[20]
Biogeography-based optimization (BBO)	Behavior studies of species in nature	Fast computation time; good convergence accuracy	Poor in exploiting the solutions; no provision for selecting the best members of each generation	[21]
Hybrid optimization technique	Developed by using two or more algorithms	Better accuracy in results; takes less computational time(in some cases)	Increased complexity; difficult to code	[22]

Also, these techniques can deal with the random probability distribution or generate a pattern of renewable energy sources [23]. In this paper, the GA programming is developed for the optimization of optimal solar PV-battery sizing in regard to peak load shaving. GA has several advantages such as problem-solving with numerous solutions, easy to understand and can directly be transferred to existing simulations and models [24]. Therefore, several modeling equations and approaches for designing a solar PV-battery system via GA have been developed to ensure the optimum sizing of the overall system.

The proposed MDRed model using GA coding was developed to solve the optimal capacity of solar PV and battery system to maximize the energy savings via self-consumption and MD shavings. Input data includes hourly solar irradiation in Watts-peak (Wp) and multiple patterns of monthly load power consumption in kilowatts (kW). Besides that, battery charging and discharging shall be operated based on Time of Use (ToU) under Malaysian electricity tariff for commercial and industrial sector. MDRed modelling scheme is made of mathematical formulation which includes the electricity tariff model, solar PV model and battery energy storage system model. Apart from that, the economical model mainly focuses on cost of the solar PV and battery system and Return on Investment (ROI).

3.1. Financial Model

3.1.1. Electricity Tariff Model

Most electricity tariff categories for commercial and industrial sectors are designed to encourage customers to control their electricity demand at daytime peaks since MD charges are very high. Referring to Table 1, the electricity tariff model is specified in Table 3 for net consumption and maximum demand calculation according to electricity tariff categories on commercial and industrial sectors.

Table 3. Tariff rates under Malaysian utility billing scheme.

Tariff	Unit	Category	Total Bill
Net consumption, P_{load_net}	MYR/kWh, U_{load_net}	C1 & E1	C_{net}
Maximum Demand, P_{MD}	MYR/kW, U_{MD}	C1, C2, E1 & E2	C_{MD}

The total electricity bill (C_{bill}) for commercial and industrial customers as calculated as follows [6]:

$$C_{MD_kW} = E_{MD_kW} * P_{MD} \quad (1)$$

$$C_{net_kWh} = E_{load_net} * P_{load_net} \quad (2)$$

$$C_{bill} = \int P_{load_net} * E_{load_net} + \int P_{MD} * E_{MD} \quad (3)$$

where the combination of maximum demand bill (C_{MD_kW}) in Equation (1) and net consumption bill (C_{net_kWh}) in Equation (2) will be added on a monthly basis. Equations (1)–(3) are formulated based on the Malaysian electricity tariff category for the commercial and industrial sector. Based on Table 4 and Figure 3, a Malaysian higher learning institution's load profile under C1 electricity tariff is chosen for the case study. Since the case studies is focusing on solar PV-battery sizing based on maximum demand (MD) reduction approach, the concept can be explained using one (1) type of load profile from any commercial or industrial sector. In this paper, C1 category load profile for four (4) consecutive months from January 2017 until April 2017 is used for validation studies. Based on energy data evaluation, highest load or maximum demand is recorded at 1300 kW during beginning of academic calendar for the higher learning institution. Therefore, four (4) months of load profile data is sufficient to cater for optimal sizing of solar PV and battery system based on the Malaysian electricity tariff.

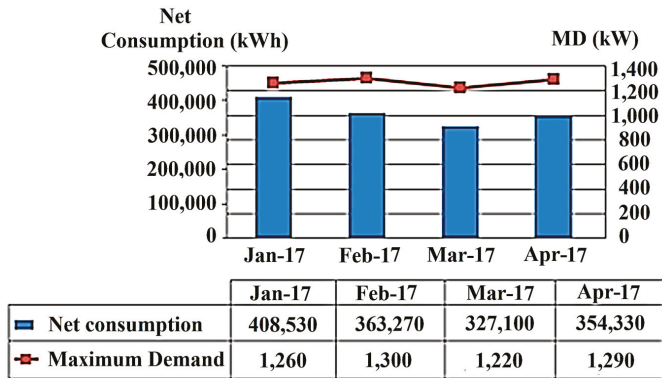


Figure 3. Energy consumption for C1 category commercial sector.

The MD is recorded between 1200 kW and 1300 kW during peak hours in between 8.30 a.m. and 10.30 a.m. Figure 3 shows the monthly net consumption and maximum demand recorded in electricity billing of the commercial building. Table 4 shows the maximum demand recorded throughout the months during peak hours only. It can be observed that the highest MD occurs in the month of February 2017 at 1300 kW. Besides that, the highest load has been consumed in between 8.30 a.m. and 10.00 a.m. for first four months in the year 2017. These data will be used in a MATLAB (2016a, The Mathworks, Natick, MA, USA) GA optimization algorithm for solar PV and battery sizing. The weather condition in Malaysia is suitable for solar PV generation. Based on Figure 4, the weather condition is almost predictable with intermittent sunlight from 8.30 a.m. until 5.30 p.m. The peak PV generation is normally achieved at 1000 W/m² and with solar PV module temperature and ambient temperature reaching 50 °C and 33 °C, respectively.

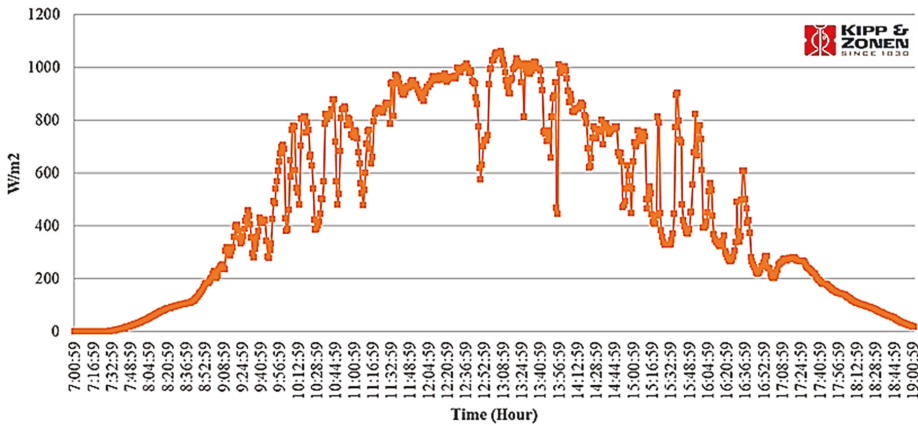


Figure 4. Actual solar irradiance measurement data at Nilai, Negeri Sembilan, Malaysia.

Table 4. Maximum demand captured during peak hours.

Month-Year	Time	Load (kW)	Total Cost (MYR)
Jan-17	9:30:00	1260	38,178.00
Feb-17	9:00:00	1300	39,390.00
Mar-17	10:00:00	1220	36,966.00
Apr-17	8:30:00	1290	39,087.00

3.1.2. Solar PV Model

The difficulty of calculating the energy generated by a solar PV has been extensively studied in the technical literature. The calculation of solar PV power of a grid-connected solar PV system is classified under two categories which is indirect method and direct method. As the operation and the performance of a PV focuses mainly on its maximum power, the indirect method describing the PV module's maximum power output behaviors are more theoretical for solar PV system valuation. Indirect method directly calculates the maximum power without calculating first the I-V curve of the solar PV array [25]. This simplified indirect method provides the modelled power to be used in MDRed modelling. Based on Rus-Casa et al., indirect method directly provides power from atmospheric parameters and information provided by the manufacturers in the datasheets. PV modelled power in per-unit conversion is based on PV module temperature and solar irradiance level at Standard Testing Condition (STC). The formula for PV modelled power in per-unit convention, P_{mod} is given as follows [25]:

$$P_{mod} = P_{PV_kwp} * (G/G_{STC}) [1 - \gamma * (T_C - T_{STC})] \quad (4)$$

where $G_s(t)$ is the measured solar irradiance (hourly) and P_{PV_kwp} is the rated PV power at Standard Testing Condition (STC). G_{STC} and T_{STC} is the solar irradiance (1000 W/m^2) and PV module temperature (25 degC) at Standard Testing Conditions (STC), respectively. Besides that, γ is the temperature correction based on measured polycrystalline silicon PV module temperatures with a power decrease in between $0.30\%/^{\circ}\text{C}$ and $0.5\%/^{\circ}\text{C}$.

The measured module temperature, T_C is set at $50 \text{ }^{\circ}\text{C}$ at solar irradiance of 3.5 up to 4 h per day averagely based on Malaysian climate. Solar irradiance measurement was taken at Nilai, Negeri Sembilan, Malaysia using a CMP3 pyranometer (KIPP & ZONEN, Delft, The Netherlands). Apart from the measured solar irradiance, the actual generated power will be obtained with respect to solar irradiance and PV module temperature. The cost of the solar PV system and batteries are the important parameters for optimal sizing of the solar PV-battery system. Table 5 shows the historical prices of the solar PV-inverter system from the year 2010–2016 in Peninsular Malaysia [26]. The P_{PV_rated} can be calculated as follows:

$$P_{PV_rated} = P_{PV_kwp} / \eta_{inv} \quad (5)$$

where P_{PV_rated} is the rated dc output power of the proposed PV array in kWp and η_{inv} is the conversion efficiency from dc to ac according to inverter efficiency. Nowadays, the PV inverters can operate at 90% of conversion efficiency.

Table 5. National trends in PV-inverter system prices.

Year	2010 ^a	2011 ^a	2012 ^a	2013 ^a	2014 ^a	2015 ^a	2016 ^a	2017
Price (MYR)/kWp	19,120	11,000	9000	7500	8500	7500	7300	-

^a Data is collected from [5].

3.1.3. Battery Energy Storage System (BESS) Model

The battery energy storage system (BESS) comprises batteries, control and power conditioning system (C-PCS). Typically, batteries will absorb power from the grid during the off-peak hours and discharge power during peak demand. Currently, significant research and development in battery technology are being carried out. Tesla (Arizona, AZ, USA) has designed and commercialized the Powerwall 2, the second iteration of its home battery system. Tesla Powerwall 2 costs MYR24,200 (USD5500) and delivers 14 kWh of capacity [27].

As the core battery technology matures and the unit pricing decays, bi-directional converters providing both battery charging (AC to DC) and battery inverting (DC to AC) will grow due to the new market for power converters. Various technologies for BESS are available, namely lead acid (LA), vanadium redox flow (VRB), zinc–bromine flow (ZnBr), polysulfide bromide battery (PSB),

nickel–cadmium battery (NiCd), sodium sulfur and lithium-ion (Li-ion) battery [28]. Four battery technologies are chosen for the investigation of BESS systems such as LA, VRB, ZnBr, and Li-ion. The key parameters for these batteries are tabulated in Table 6.

Table 6. Key parameters of batteries.

Technology	DOD ^a	Round Trip ^b	Cycle Life ^c		Cost of Energy ^b (RM/kWh)	
	(%)	Efficiency (%)	Low	High	Low	High
LA	50	85	500	2800	185	1147
VRB	100	85	12,000	13,342	648	3700
ZnBr	100	75	1500	2000	740	2220
Li-ion	85	90	1000	10,000	2220	9250

^a Data is collected from [29]; ^b Data is collected from [30]; ^c Data is collected from [31].

The batteries are rated in terms of their energy and power capacities. Some of the other essential features of a battery are its efficiency, life span, operating temperature, depth of discharge (DOD), self-discharge and energy density. In most cases, lithium-ion batteries and lead-acid batteries are the best choices for peak shaving techniques, although other battery types can be more affordable [32]. While lead-acid batteries have a relatively short lifespan and lower DOD than other battery types, they are also one of the least expensive options in the energy storage sector. Lithium-ion batteries are lighter and better than lead-acid batteries [33]. They also have higher DOD and longer lifespan when compared to lead-acid batteries. Since the battery is also operated on DC, an AC-to-DC converter is necessary for charging the battery and a DC-to-AC converter is necessary during discharging the battery. For simplicity, we assumed that both converters have the identical constant conversion efficiency satisfying:

$$P_{\text{conv}}(t) = \begin{cases} \eta_B P_B(t), & \text{if } P_B(t) < 0 \\ \frac{P_B(t)}{\eta_B} & \text{otherwise} \end{cases} \quad (6)$$

Note that, η_B is the round trip efficiency of the battery converters. In other words, P_{conv} is the power exchanged with the AC bus when the converters and the battery are treated as a single entity. Similarly, we can derive:

$$P(t) = \begin{cases} \frac{P_{\text{conv}}(t)}{\eta_B} & \text{if } P_{\text{conv}}(t) < 0 \\ \eta_B P_{\text{conv}}(t) & \text{otherwise} \end{cases} \quad (7)$$

Apart from that, the rated capacity of the battery, P_{Bat} is calculated by considering the optimal size of the battery, E_{bat} as follows:

$$P_{\text{bat}}(\text{kWh}) = E_{\text{bat}}(\text{kWh}) * \frac{\eta_{\text{bat}}}{\text{DOD}} \quad (8)$$

The battery Depth of Discharge (DOD) has a significant impact on a battery's life cycle. The battery life cycle is inversely proportional to the DOD. The DOD of a battery defines the fraction of the power that can be withdrawn from the battery. For instance, if a battery system is 100% fully charged, it means the DOD of this battery is 0% and vice versa. Generally, battery state of charge (SOC) provides the ratio of the amount of energy presently stored in the battery to the nominal rated capacity.

3.2. Economical Model

The cost of optimal PV array, $C_{\text{PV_inv}}$ can be calculated as follows:

$$C_{\text{PV_inv}} = U_{\text{PV}} * P_{\text{PV_rated}} \quad (9)$$

where $U_{\text{PV_kWp}}$ is the unit cost of PV array per kWp. Apart from that, reducing the cost of PV inverter system will lead to lower miscellaneous costs such as operation and maintenance costs and replacement

costs. The overall cost of the solar PV system is the combination of both costs of power conversion units and cost of inverter. In this paper, the overall solar PV system cost, $C_{total_PV_inv}$ is evaluated by referring to a specific planning period and is given by:

$$C_{total_PV_inv} (MYR) = C_{PV} + C_{O\&M_PV} + C_{RC_PV} \quad (10)$$

The cost of batteries, C_{Bat} is calculated as follows:

$$C_{bat} (MYR) = U_{bat} (MYR/kWh) * P_{bat} (kWh) \quad (11)$$

where U_{Bat} is the unit cost of the batteries in kWh, P_{Bat} is the rated capacity of the batteries. The cost of power conversion units, C_{conv} is as follows:

$$C_{conv} (MYR) = U_{conv} (MYR/kWh) \times P_{conv} (kW) \quad (12)$$

where U_{Conv} is the unit cost of the power conversion units in kWh and P_{conv} is the power rating of the converter. The overall cost of the BESS is the combination of both costs of power conversion units and cost of batteries. In this paper, the total overall BESS cost, C_{total_BESS} is evaluated by referring to a specific planning period and is given by:

$$C_{BESS} = C_{bat} + C_{conv} \quad (13)$$

$$C_{total_BESS} (MYR) = C_{BESS} + C_{o\&m_BESS} + C_{rep_BESS} + C_{disp_bat} + C_{LS_bat} \quad (14)$$

where C_{BESS} is the capital cost, $C_{o\&m_BESS}$ is the operation and maintenance cost, C_{rep_BESS} is the replacement cost, C_{disp_bat} is the disposal cost related to the potential cost achievable from recycling old batteries and lifespan cost (C_{LS_bat}) of all the main components including its system. However, this is not added in MDRed modeling since the cost of the BESS is very high and will lead to longer ROI. Cost of energy savings on net consumption and MD are according to Malaysian electricity tariff allocated for each category of commercial and industrial customers. For commercial consumers with tariff rates of C1 category, the annual savings, S_{yr_shave} can be calculated as follows:

$$P_{shave_MD} = [\max (\sum P_{load_net}) \quad (15)$$

$$S_{yr_shave} = (\sum P_{load_shave} * E_{load_net}) + (P_{shave_MD} * E_{MD}) + (\sum P_{PV_surplus} * E_{surplus}) * 12 \quad (16)$$

Under the NEM scheme, the rate of surplus generation, $E_{surplus}$ has been formulated at MYR 0.238 (USD 0.05)/kWh for medium voltage interconnection. Apart from that, overall loan payment is important to include all the incurred cost such as operation and maintenance cost ($C_{O\&M}$), replacement cost (C_{RC}) and lifespan cost (C_{LS}) of all the main components including its system. This is applied to PV-inverter and BESS components which includes the batteries and converter unit. Therefore, the overall cost of the system comprises of:

$$C_{full_loan} = (C_{total_PV} + C_{total_BESS}) * \text{interest rate (\%)} \quad (17)$$

The energy flow schedule of solar PV-battery system integration has been included to lower the daily operating cost mainly on the MD reduction at the specific limit. For GA optimization, 7% of interest rate for total load payment has been included.

4. Modeling of System Reliability

Several approaches have been used to achieve the optimal configuration of solar PV-battery systems from the technical and economical perspective. In this paper, the technical algorithm for the optimal sizing is developed according to the concept of MDRed model to evaluate the reliability

of solar PV-battery system. The GA model attains the optimal size in terms of various degrees of reliability. A binary coded GA was introduced to solve the optimal capacity of solar PV and battery. Input data includes hourly data per year, solar irradiation by indirect power calculation, load power consumption and timeframe of battery DOD and SOC with respect to peak hours and off-peak hour's tariff charges. The flowchart of the GA process applied to PV-battery sizing problem with respect to MDRed modelling is illustrated in Figure 5. One of the key parameters that represent the battery sizing is the capacity of battery charging, P_{bat_chg} and battery discharging, P_{bat_dischg} . Based on Figure 5 and Table 7, the amount of maximum demand reduction (MDRed) is based on battery discharging capacity (P_{bat_dischg}) to maintain the maximum demand limit (P_{MD_limit}), in the presence and/or absence of generated PV power (P_{PV}) during peak hours from 8.00 a.m. and 10.00 p.m. Battery charging capacity (P_{bat_chg}) will be in operation during off-peak hours in between 10.00 p.m. and 8.00 a.m. As per Figure 7, the battery energy management system works to monitor the net load continuously in the presence of solar PV and will immediately activate the battery operation to discharge if the new net load exceeds the MD limit. Besides that, the battery discharging will not take place if the new net load is below the MD limit. Besides that, as per Figure 7, the Battery Energy management system scenarios for MDRed modeling approach is based on any scenarios (efficient, intermittent or zero solar PV). Therefore, the proposed optimization method will deliver the optimal operation condition or optimal sizing of solar PV-battery in real time scenario.

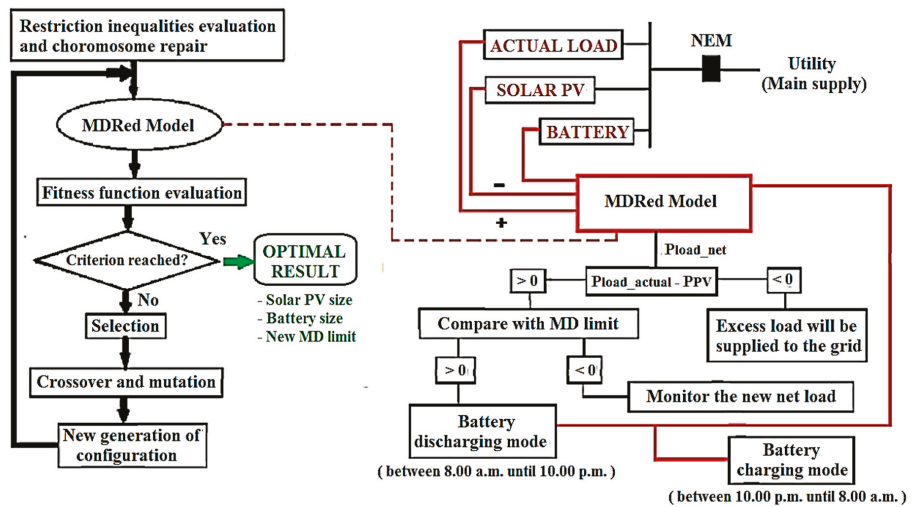






Figure 5. Flowchart of MDRed model for optimal sizing simulation using Genetic Algorithm.

Table 7. Battery Energy management system for MDRed modeling approach.

Scenario \ Concept	Control Algorithm	Peak Hours [8.00 a.m.–10.00 p.m.]	Off Peak Hours [10.00 p.m.–8.00 a.m.]
Actual load below the MD limit $P_{load_actual} < P_{MD_limit}$	Solar PV	Efficient	
	Battery	$PPV_surplus = P_{load_actual} - PPV$ when $PPV > P_{load_actual}$ [Battery will not operate]	[Battery will not change since 0% DOD]
	Fully charged	 DOD: 0%	
Actual load above the MD limit $P_{load_actual} > P_{MD_limit}$	Solar PV	Intermittent or Zero	
	Battery	$P_{load_net} = [P_{load_Actual} + P_{bat_chg}] - [PPV + P_{bat_discha}]$ [Battery will discharge]	[Battery will change to achieve 0% DOD]
	Fully charged	 DOD: >50%	

As per Equation (18), the generated PV power, P_{PV} will be supplied for self-consumption to reduce the actual load, P_{load_actual} . Therefore, new net load, P_{load_net} will be obtained. However, the battery will not discharge if the P_{load_net} is below P_{MD_limit} . Due to the intermittent solar irradiance during bad weather condition, the optimal battery sizing can be calculated using Equations (19) and (20) to cater for the MD limit. If the P_{load_net} is above P_{MD_limit} , the battery will discharge (P_{bat_dischg}) to maintain the required MD limit. During off-peak hours, the batteries will be charged (P_{bat_chg}) during off-peak hours until minimum DOD is reached. Therefore, new net load, P_{load_net} can be calculated as:

[Condition #1: $P_{MD_limit} < P_{load_net}$ with solar PV]:- Condition #1: $P_{MD_limit} < P_{load_net}$ with solar PV

$$\int P_{load_net} = \int P_{load_actual} - \int P_{PV} \tag{18}$$

[Condition #2: $P_{MD_limit} > P_{load_net}$ with solar PV]:-

$$P_{load_net} = [P_{load_actual} + P_{bat_chg}] - [P_{PV} + P_{bat_dischg}] \tag{19}$$

[Condition #3: $P_{MD_limit} > P_{load_net}$ without solar PV]:-

$$P_{load_net} = [P_{load_actual} + P_{bat_chg}] - [P_{bat_dischg}] \tag{20}$$

The total load net consumption reduction will be based on sum of the new net load mainly due to generated PV power. Therefore, total load shaving (P_{load_shave}) can be calculated as:

$$\sum P_{load_shave} = \sum P_{load_actual} - \sum P_{PV} \tag{21}$$

MD reduction shaving varies according to system performance which mainly relies on total generated PV power and battery capacity. The excess PV power, P_{PV_suplus} will be achieved when generated PV power is more than actual load and it can be calculated as: [Condition #4: $P_{PV} > P_{load_actual}$ with solar PV]:

$$P_{PV_suplus} = \sum [P_{PV} - P_{load_actual}] \tag{22}$$

The basic Return on Investment (ROI) is calculated based on payment of loan in regard to interest rate using total profit achieved using solar PV-battery system. The ROI can be calculated as:

$$ROI \text{ (in years)} = C_{load_payment} / S_{yr_shave} \tag{23}$$

5. System Optimization

As per Table 8, the system parameters used for GA optimization covers the technical and economical data of PV, inverter, converter and battery energy storage system. In this paper, the GA optimization gives an optimal sizing of solar PV and battery system without considering the lifespan cost of battery since replacement of battery will be neglected after completion of life span period.

Table 8. Detail of the components.

Component	Unit	PV-Inverter	Battery	Converter
Cost of the system	MYR (USD)/kWp	7000 (1600)		
	MYR (USD)/kWh		2200 (500)	
	MYR (USD)/kW			1100 (250)
Lifespan	Years	21	12	
Efficiency	%	90	95	90
DOD	%		85	
O&M cost		5% of C_{PV_INV}	10% of C_{BESS}	
RC cost		5% of C_{PV_INV}	10% of C_{BESS}	
Interest Rate	%	7	7	7

5.1. Problem Formulation

The aim of this study is to attain an optimal sizing of a solar PV-battery system, which should be properly designed in terms of technical, economic and reliability measures subject to physical and operational constraints/strategies. The objective function of the optimization is to achieve the optimal sizing with respect to highest energy savings on maximum demand and net consumption.

5.1.1. System Constraints

In this study, battery charging and discharging mechanism and the distribution lines are ideal. Besides that, the inverter efficiency, battery efficiency and manufacturers' round-trip efficiency is constant regardless of the operation period. Since the battery cost is very high, the life span cost or total cost of the new battery system will be set to zero after achieving the life span of the battery operation. For any period, t , the total power supply from the solar PV-battery system must supply the total demand with a certain reliability criterion. This relation can be represented by Equation (24) as follows:

$$P_{PV} + P_{Bat} \leq P_{load_actual} \quad (24)$$

This minimizes the excess power supply to the grid since the self-consumption of PV power or existing net consumption rate [MYR 0.365 (USD 0.08)/kWh] will be higher than net metering rate [MYR 0.238 (USD 0.05)/kWh].

5.1.2. Bounds of Design Variables

The proposed solar PV-battery system optimization parameters including the solar PV capacity, P_{PV_kWp} and maximum demand limit, P_{MD_limit} should be within a certain range:

$$\text{Load profile (Min)} < P_{PV_kWp} < \text{Load profile (Max)} \quad (25)$$

$$\text{Load profile (Ave)} < P_{MD_limit} < \text{Load profile (Max)} \quad (26)$$

The bounds of the design variable on PV and MD limit sizing is to maximize the self-consumption instead of surplus to the grid.

5.2. Validation of Numerical Results

Experimental data on PV model using indirect method is verified using a 50 kWp PV system. The experimental data and figure are shown in Figure 6 and Table 9 respectively. Based on the results, based on the indirect method of Equation (4), at 1000 W/m² of measured solar irradiance, a 50 kWp solar PV system only delivers up to 35 kW of actual PV power and 38 kW of PV modelled power.

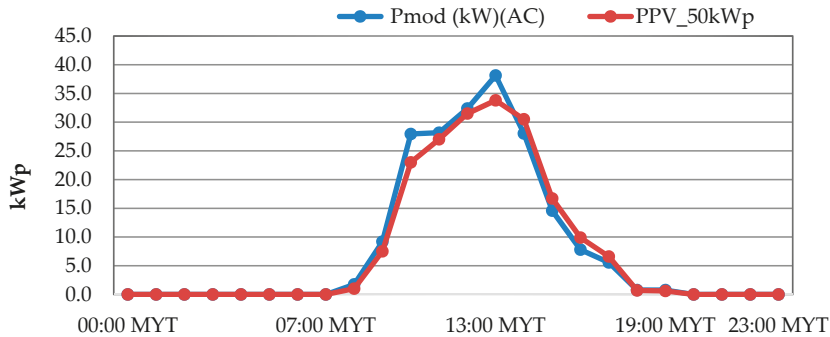


Figure 6. Modelled PV power (Indirect method).

Table 9. PV model validation data with 50 kWp PV system.

Time (Hr)	Pmod = PPV_Kwp* (Gs/GSTC) [1 - γ * (TC - TSTC)]							$\frac{P_{PV_rated}}{P_{PV_kwp}/\eta_{inv}}$	50 kWp PV System (Actual)
	Gs (W/m ²)	GSTC (W/m ²)	γ	Tc (DegC)	TSTC (DegC)	P _{mod} (In Per Unit)	P _{mod} (kW) (DC)	PV Modelled Power,	Actual PV Generated Power
								P _{mod} (KW)(DC)	P _{PV_Actual_AC}
00:00 MYT	0	1000	0.005	0.0	0.0	0.00	0.0	0.0	0.0
01:00 MYT	0	1000	0.005	0.0	0.0	0.00	0.0	0.0	0.0
02:00 MYT	0	1000	0.005	0.0	0.0	0.00	0.0	0.0	0.0
03:00 MYT	0	1000	0.005	0.0	0.0	0.00	0.0	0.0	0.0
04:00 MYT	0	1000	0.005	0.0	0.0	0.00	0.0	0.0	0.0
05:00 MYT	0	1000	0.005	0.0	0.0	0.00	0.0	0.0	0.0
06:00 MYT	0	1000	0.005	35.0	25.0	0.00	0.0	0.0	0.0
07:00 MYT	0	1000	0.005	38.0	25.0	0.00	0.00	0.0	0.0
08:00 MYT	42	1000	0.005	40.0	25.0	0.04	1.94	1.7	1.0
09:00 MYT	227	1000	0.005	45.0	25.0	0.20	10.22	9.2	7.5
10:00 MYT	690	1000	0.005	45.0	25.0	0.62	31.05	27.9	23.0
11:00 MYT	736	1000	0.005	55.0	25.0	0.63	31.28	28.2	27.0
12:00 MYT	872	1000	0.005	60.0	25.0	0.72	35.97	32.4	31.5
13:00 MYT	1027	1000	0.005	60.0	25.0	0.85	42.36	38.1	35.8
14:00 MYT	755	1000	0.005	60.0	25.0	0.62	31.14	28.0	30.5
15:00 MYT	393	1000	0.005	60.0	25.0	0.32	16.21	14.6	16.7
16:00 MYT	204	1000	0.005	55.0	25.0	0.17	8.67	7.8	9.9
17:00 MYT	141	1000	0.005	50.0	25.0	0.12	6.17	5.6	6.6
18:00 MYT	19	1000	0.005	45.0	25.0	0.02	0.86	0.8	0.7
19:00 MYT	18	1000	0.005	40.0	25.0	0.02	0.83	0.7	0.6
20:00 MYT	0	1000	0.005	0.0	0.0	0.00	0.0	0.0	0.0
21:00 MYT	0	1000	0.005	0.0	0.0	0.00	0.0	0.0	0.0
22:00 MYT	0	1000	0.005	0.0	0.0	0.00	0.0	0.0	0.0
23:00 MYT	0	1000	0.005	0.0	0.0	0.00	0.0	0.0	0.0

For this paper, load profile with actual MD load of 1050 kW has been used. Apart from that, two different phenomena of solar irradiance pattern with perfect data is used for solar PV-battery system integration to verify the MDRed scheme. For validation purposes, an MD limit of 750 kW and a PV-inverter rating of 1200 kWp are used to formulate the required battery capacity together with the financial data. Validation data is important to verify that the solar PV-battery system works according to MDRed scheme. In this paper, the MDRed control algorithm is based on a few conditions to achieve the new MD limit of 750 kW as shown in Table 10 and Figure 7.

Table 10. MDRed model validation data with solar PV-battery system.

Time (Hr)	$P_{MD_Limit} = 750\text{ kW}$		MDRed scheme During Perfect Weather Condition (Sunny Day)			
	Load Profile $P_{load_Actual},\text{ kW}$	PPV = 1200 kWp (Based on Equation (4))	Battery Capacity, $P_{bat_kWh} = 48\text{ kWh}$		New Net Load $P_{load_net}\text{ (kW)}$	Control Algorithm
			P_{bat_DOD}	P_{bat_SOC}		
00:00 MYT	390	0	0	-11	401	Condition #2
01:00 MYT	360	0	0	-11	371	
02:00 MYT	360	0	0	-11	371	
03:00 MYT	340	0	0	-11	351	
04:00 MYT	320	0	0	0	320	No operation
05:00 MYT	320	0	0	0	320	
06:00 MYT	310	0	0	0	310	
07:00 MYT	310	0	0	0	310	
08:00 MYT	520	46.6	0	0	473	Condition #1
09:00 MYT	1050	252.0	48	0	750	Condition #2
10:00 MYT	1020	724.5	0	0	296	Condition #1
11:00 MYT	990	772.8	0	0	217	
12:00 MYT	900	915.6	0	0	-16	Condition #4
13:00 MYT	940	1078.4	0	0	-138	
14:00 MYT	980	675.2	0	0	305	Condition #1
15:00 MYT	970	412.7	0	0	557	
16:00 MYT	970	214.2	6	0	750	Condition #2
17:00 MYT	880	148.1	0	0	732	Condition #1
18:00 MYT	630	20.0	0	0	610	
19:00 MYT	580	0	0	0	580	MD monitoring
20:00 MYT	620	0	0	0	620	
21:00 MYT	540	0	0	0	540	
22:00 MYT	510	0	0	0	510	
23:00 MYT	500	0	0	-11	511	Condition #2

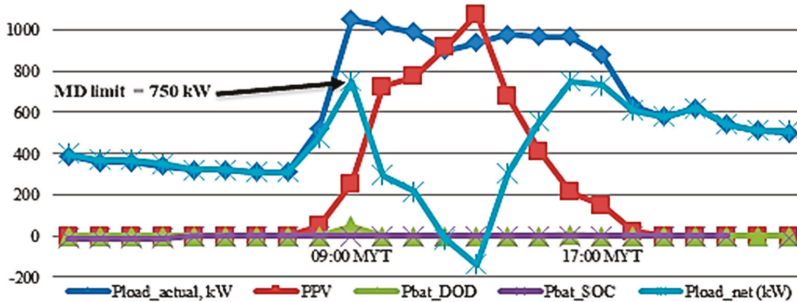


Figure 7. MDRed model validation graph (for Table 10 data.)

Apart from that, the MDRed model shows the control algorithm battery management system to cater for MD reduction with the support of solar PV power at preset MD limit. However, the rated sizing of solar PV-battery system is higher than the formulated optimal values since the calculation of rated values are based on Equations (5) and (8). The total savings is the combination of net consumption savings at rate of MYR 0.365/kWh, surplus power supplied to the grid at rate of MYR 0.238/kWh and maximum demand savings at rate of MYR 30.3/kW. Based on assumption, the annual total savings is calculated for 12 months period. Besides that, the cost of the solar PV-battery system will increase drastically due to additional cost of O&M and replacement apart from the interest rate of 7% incurred to the total cost of the system.

Control algorithm of MDRed modeling scheme falls under any of the conditions applied on Table 11 where battery management system works based on maximum demand to maintain the MD limit setting of 750 kW. However, battery discharging mode will take place in between 8.00 a.m. until 10.00 p.m. and battery charging mode in between 10.01 p.m. until 7.59 a.m. everyday with respect to the MD limit of different load profiles.

Table 11. Summary of validation data at 750 kW MD limit setting.

Control Algorithm	Status	PV Status	Numerical Formula
Condition #1	$P_{MD_limit} < P_{load_net}$	Yes	$\int P_{load_net} = \int P_{load_actual} - \int P_{PV}$ $P_{load_net} = [P_{load_actual} + P_{bat_chg}] - [P_{PV} + P_{bat_dischg}]$ $P_{load_net} = [P_{load_actual} + P_{bat_chg}] - [P_{bat_dischg}]$ $P_{PV_suplus} = P_{PV} - P_{load_actual}$
Condition #2	$P_{MD_limit} > P_{load_net}$	Yes	
Condition #3	$P_{MD_limit} > P_{load_net}$	No	
Condition #4	$P_{PV} > P_{load_actual}$	Yes	

6. Optimization Results

Based on Figure 8, on average 25% of total energy savings can be achieved on a monthly basis which can be used to calculate the Return on Investment (ROI). GA optimization results on MDRed modelling revealed that optimal sizing of solar PV-battery system contributed to energy bill savings up to 20% of net consumption via solar PV self-consumption, 3% of maximum demand (MD) via MD shaving and 2% of surplus power supplied to grid via net energy metering (NEM) in regards to Malaysian electricity tariff scheme and cost of overall system.

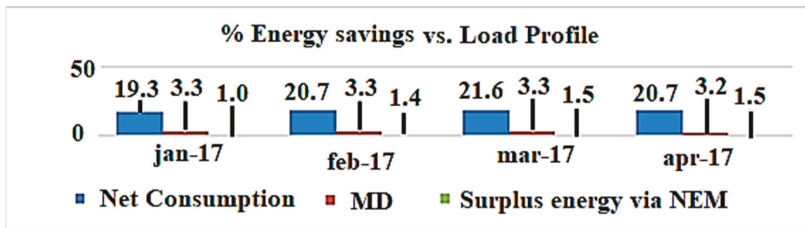


Figure 8. Percentage of energy savings based on load profile.

GA optimization results from 10 population sizes and via 300 iterations are shown in Figure 9. In this paper, GA optimization studies is based on 21-years of load pattern assumption to cater for optimal sizing of solar PV-battery system. Since all actual MDs are captured during peak hours between 8.30 a.m. and 10.00 a.m., it does not show huge differences in solar PV-battery optimal sizing. Therefore, the total energy savings achieved in the range of 23% to 26% with the use of solar PV-battery system. However, the differences in optimal sizing are influenced by the load margin in between maximum demand and average load consumed during peak hours throughout the month.

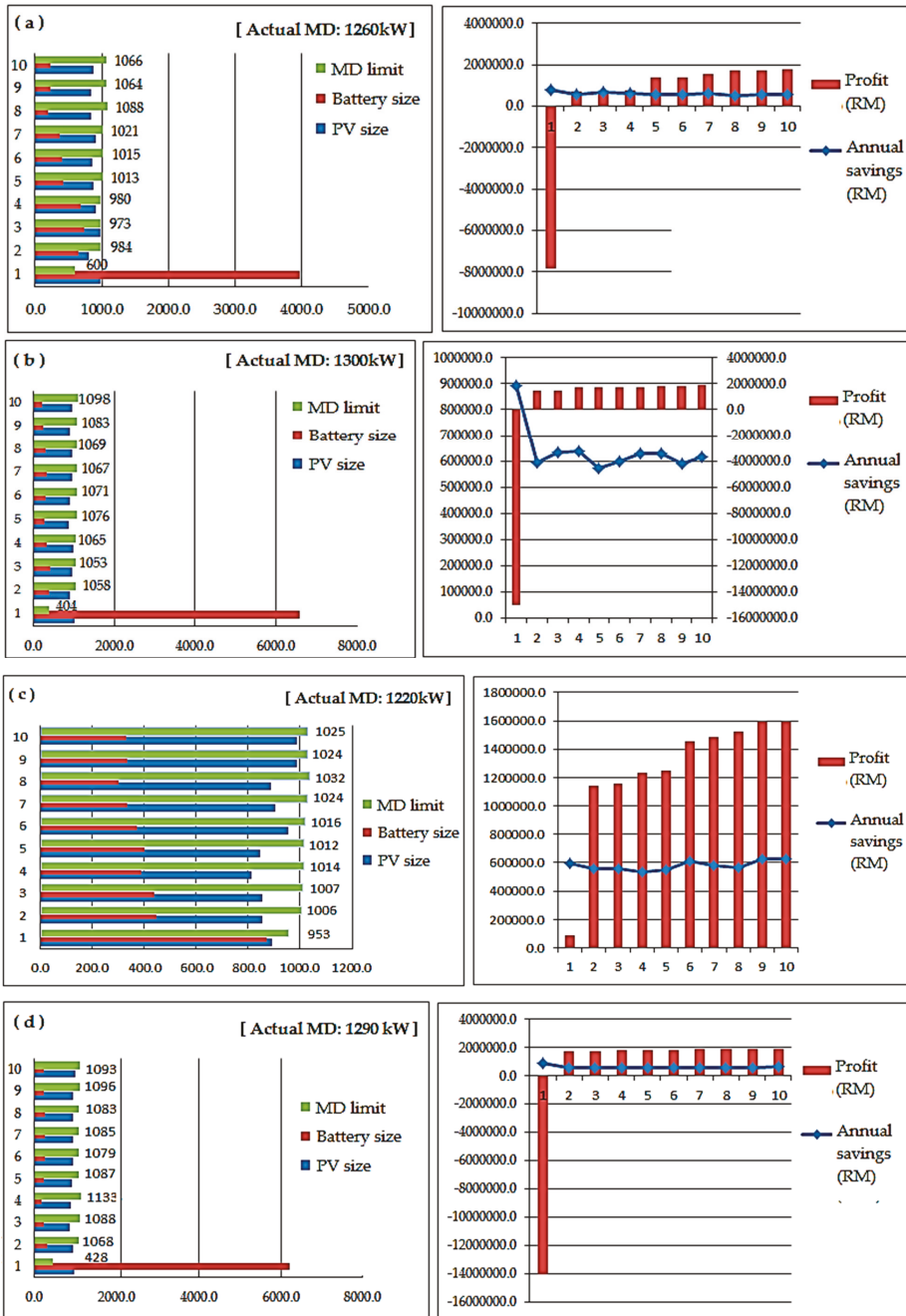


Figure 9. GA optimization results of difference load profiles: (a) Jan-17 [Actual MD: 1260 kW], (b) Feb-17 [Actual MD: 1300 kW], (c) Mar-17 [Actual MD: 1220 kW] and (d) Apr-17 [Actual MD: 1290 kW].

The surplus energy savings under Net Energy Metering (NEM) achieved at minimal level due to low NEM billing rate compared to net consumption rate. The commercial sector may experience

fluctuating load pattern with different ranges of maximum demand. Therefore, the optimal solar PV-battery sizing at various load pattern falls in between 870 kWp and 970 kWp of solar PV and 230 kWh up to 330 kWh of total battery capacity. In addition, the new MD limit has been achieved in the range 1025 kW and 1098 kW of MD reduction using solar PV-battery system.

Load profile of the system influence the MDRed modelling optimal sizing on the solar PV-battery system using a GA algorithm. The load profile of the system influences the MDRed modelling optimal sizing on the solar PV-battery system using the GA algorithm. Based on Table 12, the month of March 2017 is proven to give the best optimal sizing for solar PV-battery system with highest percentage of total energy savings. This is due to the load profile changes especially the load margin in between maximum and average loading for every month. Based on Figure 10, load margin and maximum demand of March 2017 is lowest compared to other months which gives the significant impact on MD shaving compared to net consumption savings. Therefore, the acceptable sizing of solar PV and battery capacity will be 986 kWp and 330 kWh respectively. This will be the best choice to allow the MDRed model to work efficiently at any load pattern to achieve high MD load reduction with yearly energy savings up to MYR 600,000.

Table 12. GA optimization results for different load profiles.

Load Profile	Energy Savings (MYR)	Percentage of Total Energy Savings (%)	Optimal Sizing		MD Limit (kW)
			PV (kWp)	Battery (kWh)	
(Actual MD)					
Jan-17 [1260 kW]	42,534.14	23.7	869	228	1062
Feb-17 [1300 kW]	46,661.90	25.4	970	225	1098
Mar-17 [1220 kW]	47,021.84	26.5	986	330	1025
Apr-17 [1290 kW]	46,850.45	25.4	980	232.3	1093

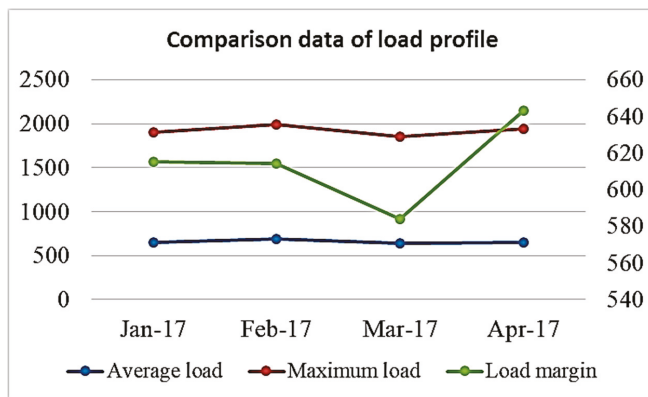


Figure 10. Comparison data analysis of load profile.

7. Conclusions

The proposed MDRed modeling scheme works as an optimization model which focuses on maximum demand (MD) shaving. This reduces the maximum demand and net consumption costs when using solar PV generation and battery systems. GA optimization results on MDRed modelling reveal that optimal sizing of the solar PV-battery system contributed to energy bill savings up to 20% of net consumption via solar PV self-consumption, 3% of maximum demand (MD) via MD shaving and 2% of surplus power supplied to grid via net energy metering (NEM) in regards to the Malaysian electricity tariff scheme and cost of the overall system. In addition, the optimal battery sizing will be

based on the amount of MD savings annually with respect to the cost of the battery system including the bi-directional converters. If the load demand is reduced as a result of effective energy management systems in place or low production in the factory or buildings, re-optimization may be useful to increase or maintain the current solar PV-battery size to maximize the net consumption and MD savings. In future, with higher demand for energy storage system and reduction in battery prices will lead to the realization of a higher rate of maximum demand shaving for commercial and industrial sector via MDRed modeling.

Author Contributions: Conceptualization, G.S. and P.S.; Methodology, V.K.R.; Validation, all co-authors; Formal Analysis, J.B.H.-N.; Investigation, P.S.; Writing-Original Draft Preparation, G.S., V.K.R. and P.S.; Writing-Review & Editing, P.S., P.K., and L.Z.; Supervision, P.S., L.Z. and P.K.; Funding Acquisition, L.Z. and P.K. All co-authors contributed substantially to the work.

Funding: This research received partial funding from EEEIC International, Poland.

Acknowledgments: The authors acknowledge the financial assistance from the Ministry of Higher Education (MOHE), Malaysia for the support to embark on renewable energy research.

Conflicts of Interest: The authors declare no conflict of interest.

Nomenclature

MDRed	Maximum demand reduction
PV	Photovoltaic
BESS	Battery energy storage system
DOD	Depth of Discharge (%)
SOC	State of Charge (%)
MD	Maximum demand
P_{load_net}	Net consumption (kW)
P_{MD}	Maximum demand (kW)
ROI	Return on Investment (%)
P_{conv}	Power rating of the converter (kW)
P_{Bat}	Rated capacity of the battery (kWh)
E_{bat}	Optimal size of the battery (kWh)
U_{PV}	Unit cost of PV array (MYR/kWp)
C_{total_PV}	Cumulative cost of PV system (MYR)
$C_{O\&M_PV}$	O&M cost of PV system (MYR)
C_{RC_PV}	Replacement cost of PV system (MYR)
C_{Bat}	Cumulative cost of batteries (MYR)
U_{Bat}	Unit cost of the batteries (MYR/kWh)
C_{LS_bat}	Cost of battery lifespan (MYR)
U_{Conv}	Unit cost of the converter (kW)
P_{shave_MD}	Maximum demand shaving load (kW)
S_{yr_shave}	Total energy savings annually (MYR)
P_{load_shave}	Total net consumption savings load (kWh)
P_{PV_STC}	Rated PV power at Standard Testing Condition (kWp)
C_{bill}	Cumulative amount of net consumption and MD (MYR)
C_{net_kWh}	Cumulative amount of net consumption (MYR)
C_{MD_kW}	Cumulative amount of Maximum demand (MYR)
C_{PV_inv}	Cumulative cost of optimal PV array (MYR)
C_{BESS}	Cumulative cost of BESS and converter MYR)
C_{full_loan}	Cumulative cost of overall PV-battery system (MYR)
U_{load_net}	Unit price of net consumption (RM/kWh)
U_{MD}	Unit price of maximum demand (RM/kW)
E_{load_net}	Total net consumption recorded (kWh)
E_{MD}	Total maximum demand recorded (kW)
P_{PV_rated}	Rated dc output power of PV array (kWp)

P_{PV_kWp}	DC output power of PV array (kWp)
η_{inv}	Conversion efficiency of inverter (%)
η_B	Round trip efficiency of the converter (%)
P_{MD_limit}	Maximum demand limit (kW)
P_{load_actual}	Actual consumed load (kWh)
P_{bat_chg}	Battery charging load (kWh)
P_{bat_dischg}	Battery discharging load (kWh)
P_{PV}	Solar PV generation load (kWh)
P_{mod}	Solar PV modelled power (per unit)
C_{total_BESS}	Capital cost of overall BESS (MYR)
$C_{o\&m_BESS}$	O&M cost of BESS (MYR)
C_{rep_BESS}	Replacement cost of BESS (MYR)
C_{disp_bat}	Disposal cost of BESS (MYR)
$P_{PV_surplus}$	Surplus PV power (kWh) (kWh)
$E_{surplus}$	Unit price of surplus PV (MYR/kWh)
$G_s(t)$	Measured solar irradiance (W/m^2)
γ	PV module temperature correction ($\%/^{\circ}C$)

References

- ExxonMobil Energy. *Outlook for Energy: A View to 2040*; ExxonMobil Energy: Irving, TX, USA, 2013.
- Wu, H.; Wang, S.; Zhao, B.; Zhu, C. Energy management and control strategy of a grid-connected PV/battery system. *Int. Trans. Electr. Energy Syst.* **2015**, *25*, 1590–1602. [[CrossRef](#)]
- Castillo, A.; Gayme, D.F. Grid-scale energy storage applications in renewable energy integration: A survey. *Energy Conversat. Manag.* **2014**, *87*, 885–894. [[CrossRef](#)]
- Coordinated Low Emissions Assistance Network. *Review of Networks and Platforms for Low Emission and Climate Compatible Development Planning*; Coordinated Low Emissions Assistance Network: Witzwort, Germany, 2011.
- The Sustainable Energy Development Authority of Malaysia. Available online: <http://www.seda.gov.my/> (accessed on 21 September 2014).
- TNB. *Electricity Tariff Schedule*; Tenaga Nasional Berhad: Kuala Lumpur, Malaysia, 2014.
- Braam, F.; Hollinger, R.; Engesser, L.M.; Müller, S.; Kohrs, R.; Wittwer, C. Peak shaving with photovoltaic-battery systems. In Proceedings of the Innovative Smart Grid Technologies Conference Europe, Istanbul, Turkey, 12–15 October 2014; pp. 1–5.
- Wang, B.; Zarghami, M.; Vaziri, M. Energy management and peak-shaving in grid-connected photovoltaic systems integrated with battery storage. In Proceedings of the North American Power Symposium, Denver, CO, USA, 18–20 September 2016; pp. 1–5.
- Pimm, J.A.; Cockerill, T.T.; Taylor, P.G. The potential for peak shaving on low voltage distribution networks using electricity storage. *J. Energy Storage* **2018**, *16*, 231–242. [[CrossRef](#)]
- Ru, Y.; Kleissl, J.; Martinez, S. Storage size determination for grid-connected photovoltaic systems. *IEEE Trans. Sustain. Energy* **2013**, *4*, 68–81. [[CrossRef](#)]
- Linssen, J.; Stenzel, P.; Fler, J. Techno-economic analysis of photovoltaic battery systems and the influence of different consumer load profiles. *Appl. Energy* **2017**, *185*, 2019–2025. [[CrossRef](#)]
- Hanna, R.; Kleissl, J.; Nottrott, A.; Ferry, M. Energy dispatch schedule optimization for demand charge reduction using a photovoltaic-battery storage system with solar forecasting. *Sol. Energy* **2014**, *103*, 269–287. [[CrossRef](#)]
- Moghimi, M.; Garmabdari, R.; Stegen, S.; Lu, J. Battery energy storage cost and capacity optimization for university research center. In Proceedings of the IEEE/IAS 54th Industrial and Commercial Power Systems Technical Conference (I&CPS), Niagara Falls, ON, Canada, 7–10 May 2018.
- Liu, X.; Gao, B.; Zhu, Z.; Tang, Y. Non-cooperative and cooperative optimisation of battery energy storage system for energy management in multi-microgrid. *IET Gener. Transm. Distrib.* **2018**, *12*, 2369–2377. [[CrossRef](#)]

15. Dongol, D.; Feldmann, T.; Schmidt, M.; Bollin, E. A model predictive control based peak shaving application of battery for a household with photovoltaic system in a rural distribution grid. *Sustain. Energy Grids Netw.* **2018**, *16*, 1–13. [[CrossRef](#)]
16. Subramani, G.; Ramachandaramurthy, V.K.; Padmanaban, S.; Mihet-Popa, L.; Blaabjerg, F.; Guerrero, J.M. Grid-Tied Photovoltaic and Battery Storage Systems with Malaysian Electricity Tariff—A Review on Maximum Demand Shaving. *Energies* **2017**, *10*, 1884. [[CrossRef](#)]
17. Chauhan, A.; Saini, R.P. A review of an integrated renewable energy system-based power generation for stand-alone applications: Configurations, storage options, sizing methodologies and control. *Renew. Sustain. Energy Rev.* **2014**, *38*, 99–120. [[CrossRef](#)]
18. Bilal, B.O.; Sambou, V.; Kebe, C.M.F.; Ndiaye, P.A.; Ndongo, M. Methodology to Size an Optimal Stand-Alone PV/wind/diesel/battery System Minimizing the Levelized Cost of Energy and the CO₂ Emissions. *Energy Procedia* **2012**, *14*, 1636–1647. [[CrossRef](#)]
19. Tudu, B.; Majumder, S.; Mandal, K.K.; Chakraborty, N. Optimal unit sizing of stand-alone renewable hybrid energy system using bees algorithm. In Proceedings of the Energy, Automation, and Signal (ICEAS), Bhubaneswar, India, 28–30 December 2011.
20. Maleki, A.; Askarzadeh, A. Optimal sizing of a PV/wind/diesel system with battery storage for electrification to an off-grid remote region: A case study of Rafsanjan, Iran. *Sustain. Energy Technol. Assess.* **2014**, *7*, 147–153. [[CrossRef](#)]
21. Maleki, A.; Ameri, M.; Keynia, F. Scrutiny of multifarious particle swarm optimization for finding the optimal size of a PV/wind/battery hybrid system. *Renew. Energy* **2015**, *80*, 552–563. [[CrossRef](#)]
22. Gupta, R.A.; Kumar, R.; Bansal, A.K. BBO-based small autonomous hybrid power system optimization incorporating wind speed and solar radiation forecasting. *Renew. Sustain. Energy Rev.* **2015**, *41*, 1366–1375. [[CrossRef](#)]
23. Alsayed, M.; Cacciato, M.; Scarcella, G.; Scelba, G. Design of hybrid power generation systems based on multi-criteria decision analysis. *Sol. Energy* **2014**, *105*, 548–560. [[CrossRef](#)]
24. Lara-Fanego, V.; Ruiz-Arias, J.A.; Pozo-Vazquez, D.; Santos-Alamillos, F.J.; Tovar-Pescador, J. Evaluation of the WRF model solar irradiance forecasts in Andalusia (southern Spain). *Sol. Energy* **2012**, *86*, 2200–2217. [[CrossRef](#)]
25. Rus-Casas, C.; Aguilar, J.D.; Rodrigo, P.; Almonacid, F.; Perez-Higueras, P.J. Classification of methods for annual energy harvesting calculations of photovoltaic generators. *Energy Convers. Manag.* **2014**, *78*, 527–536. [[CrossRef](#)]
26. Ghazali, A.; Salleh, E.; Haw, L.C.; Sohif, M.; Sopian, K.B. Feasibility of vertical photovoltaic system on a high-rise building in Malaysia: Performance evaluation. *Int. J. Low Carbon Technol.* **2017**, *12*, 1–9. [[CrossRef](#)]
27. Divya, K.C.; Østergaard, J. Battery energy storage technology for power systems—An overview. *Electr. Power Syst. Res.* **2009**, *79*, 511–520. [[CrossRef](#)]
28. Bulman, P. Tesla's Powerwall battery production requires 'super-charged' supply chain. *Renew. Energy Focus* **2015**, *16*, 126–127. [[CrossRef](#)]
29. Akhil, A.A.; Huff, G.; Currier, A.B.; Kaun, B.C.; Rastler, D.M.; Chen, S.B.; Cotter, A.L.; Bradshaw, D.T.; Gauntlett, W.D. *DOE/EPRI Electricity Storage Handbook in Collaboration with NRECA*; Sandia National Lab.: Albuquerque, NM, USA, 2015.
30. Poullikkas, A. A comparative overview of large-scale battery systems for electricity storage. *Renew. Sustain. Energy Rev.* **2013**, *27*, 778–788. [[CrossRef](#)]
31. Luo, X.; Wang, J.; Dooner, M.; Clarke, J. Overview of current development in electrical energy storage technologies and the application potential in power system operation. *Appl. Energy* **2015**, *137*, 511–536. [[CrossRef](#)]
32. Arul, P.G.; Ramachandaramurthy, V.K.; Rajkumar, R.K. Control strategies for a hybrid renewable energy system: A review. *Renew. Sustain. Energy Rev.* **2015**, *42*, 597–608. [[CrossRef](#)]
33. Aneke, M.; Wang, M. Energy storage technologies and real-life applications—A state of the art review. *Appl. Energy* **2016**, *179*, 350–377. [[CrossRef](#)]



Article

Location-Based Optimized Service Selection for Data Management with Cloud Computing in Smart Grids

Sivapragash C. ^{1,*}, Sanjeevikumar Padmanaban ^{2,*}, Hossain Eklas ³, Jens Bo Holm-Nielsen ² and R. Hemalatha ⁴

¹ Department of Electrical and Electronics Engineering, Swarnandhra College of Engineering and Technology, Narasapuram 534275, India

² Center for Bioenergy and Green Engineering, Department of Energy Technology, Aalborg University, 6700 Esbjerg, Denmark; jhn@et.aau.dk

³ Oregon Renewable Energy Center (OREC), Department of Electrical Engineering and Renewable Energy, Oregon Institute of Technology, Klamath Falls, OR 97601, USA; eklas.hossain@oit.edu

⁴ Department of Electrical and Electronics Engineering, Anna University, Chennai 600025, India; erhema@gmail.com

* Correspondence: sivadr2002@gmail.com (S.C.); san@et.aau.dk (S.P.); Tel.: +45-71-682-084 (S.P.)

Received: 21 September 2019; Accepted: 21 November 2019; Published: 27 November 2019

Abstract: To maximize the utilization, reliability and availability of power resources, some distribution strategy has to be implemented, which is possible nowadays with the support of modern information technologies (IT). To further develop power utilization, the customer should be aware of efficient power utilization, and the problem of customer management has to be resolved, where payment of electric bills could be through online solutions. A customer-aware power regulatory model is proposed that provides awareness to the consumer regarding the usage of electrical energy, in a secure and reliable solution that combines the features of electrical engineering with cloud computing to ensure better performance in notifying issues, which is done based on location and enhances the operation of smart grids. Instant electric meters are equipped with remote gadgets which communicate with a central cloud administration to produce electric bills for the client. The model provides mindfulness by showing history/notifications and suggestions for energy utilization through the smart meters. The user is provided with security keys to view the reading values and pay bills. To make the solution more accessible, the electronic data will be maintained on various servers at different locations of the cloud. Subsequently, there will be a service provider who manages service requests. A hardwired electric meter transmits the electric readings, which in turn access the particular service to make an entry for the particular connection on the cloud. The usage data will also be maintained at different locations in the cloud, which are accessible to different levels of users with appropriate security measures. The user accessibility is controlled by a Third Party Auditor (TPA) that computes the trustworthiness of users using a trust management scheme. This article also proposes a hash function, which computes and verifies the signature of the keys submitted by the users and also has a higher completeness ratio, which reaches 0.93, than typical methods. This is noteworthy, and the investigation results prove the system's proficiency in providing assured service.

Keywords: cloud services; trust management; secure computing; smart meter; LBSS; user-aware power regulatory model

1. Introduction

The Smart Grid (SG), is an enhancement of the 21st-century electrical grid, which is treated as a system that uses two-way communication. It includes information technologies (IT) and computational intelligence in an integrated way to address electricity generation, its transmission, and distribution to

achieve an electric system that is clean, secure, reliable, efficient, and sustainable. The evolution of SGs relies heavily on the utilization and integration of modern IT for the development of new applications and services that can leverage the technological upgrades that are enabled by the advanced information system. This allows electric grid systems to work in smarter ways. However, an overwhelming amount of heterogeneous information is generated in the SG, mainly due to widely deployed monitoring, metering, measurement and control devices. This calls for a dominant and cost-effective information management paradigm for data processing, analysis, and storage.

Our problem analysis is based on the situation in the regional state of Tamilnadu (India), where electric bills have to be produced for service payment, and the billing requires human intervention. In smart grids, the grid resource plays a significant role without the assistance of humans for such operations. The smart meters present in the SGs record the current energy utilization of users. Additionally, a remote gadget connected to the smart meter can send readings to a remote sink point at a specific time. The remote sink point is the cloud service, which gets the electronic reading from the gadget and creates a record in a database. Therefore, this paper suggests that the IT industry should be involved to assist in the information management of the SG. More specifically, the paper explores how cloud computing (CC), a next-generation computing paradigm, can serve the information management needs in the SG. The concept of CC is based on large data centers with massive computation and storage capacities operated by cloud providers, which deliver computing as a service. Shared resources, software, information, and storage are provided, with computers and other devices as a utility over a network. This SG information management paradigm, in which the management is (partially) accomplished via CC, is called Cloud Service (CS)-based SG Information Management [1].

Generally, the usage of electricity is measured by a human meter reader and later fed into the system manually. There can be errors during the reading process or when feeding the readings into the system, which makes the whole system error-prone. A cloud platform is one where there are multiple layers and services at different layers, which can be broken up into three primary services:

- (1) Software-as-a-Service (SaaS): A service provider delivers software and applications through the internet. Users subscribe to the software and access it via the web or vendor APIs.
- (2) Infrastructure-as-a-Service (IaaS): A vendor provides clients with pay-as-you-go access to storage, networking, servers and other computing resources in the cloud.
- (3) Platform-as-a-Service (PaaS): A service provider offers access to a cloud-based environment in which users can build and deliver applications. The provider supplies the underlying infrastructure.

These three services make up what Rackspace calls the Cloud Computing Stack, with SaaS on top, PaaS in the middle, and IaaS on the bottom. To access the service at different layers, various restrictions can be enforced by the service provider [1]. The cloud consists of service providers who provide services in different forms like infrastructure services, platform services, and software services. Each kind of service belongs to a layer of the cloud. This paper focuses on two different layers, namely software and databases. The cloud services are a set of software interfaces through which legitimate users can access the cloud resource. The cloud is a loosely coupled environment where the cloud system does not know anything about the user and cannot trust the user easily. On a cloud platform, the data can be stored in any of the cloud servers and can be accessed through a set of available services.

The users of the cloud have been allowed to access the service, according to their trust level. Only a registered user is permitted to access the services and data. The trust in different users is managed and verified using a Third Party Auditor (TPA) who maintains the details of users and their access permissions. Only if the TPA has verified the identity of a user successfully, he can access the service or data from the cloud [2]. The TPA, using various approaches, performs the authentication or verification of the users of the cloud. Each method has its demerits and deficiencies. Any security protocol faces different network threats. However, the authentication algorithm should be more rigid and less time-complex one. The popular key-based approaches have the problem of the higher

computational complexity of keys and their higher verification time. This encourages the invention of rigid verification algorithms.

In this paper, to ensure the regular provision of power, a user-aware power regulation method is proposed, which is updated regarding the usage of current meter readings via smart meters. The entire electrical data is updated to the cloud. Depending on the power usage of a user, the proposed power regulatory model provides directions to the user to cut/reduce their power consumption. However, no such service or idea is provided in the existing literature. Additionally, the authors use a location-based service selection scheme to reduce the time complexity. The main novelty of the proposed method involves finding the users who use auditing service and have been cleared by the auditing service and then the way performs service selection, which is explained in detail in Section 3.

2. Background Survey

There exist a variety of methods for the development of cloud services and smart meters; this paper discusses a few of them that apply to our problem statement. In [3], smart meter analytics were examined from a software performance perspective and a performance benchmark design inclusive of a typical smart meter analytics tasks. This system uses both an offline model for feature extraction and online anomaly detection. Due to privacy issues, an algorithm is presented to generate large realistic datasets from a small set of real data.

In [4], a thorough analysis of 100 anonymized 5-min commercial building meter data sets was used to explore time series of electricity consumption using a simple forecast model. This method improves energy management with the support of grid control and provides a model for detecting any anomalies.

In [5], a novel design of a smart metering system was developed as a graphical user interface (GUI)-based NTL detection platform. A 3-tier model of a detection algorithm is proposed to combine three mechanisms that complement each other for enhanced performance. The triangulation technique facilitates validation of detection results through cross verification of the three sources of measurement data. Furthermore, the system also supports better flexibility with built-in or externally developed AI methods and a user-friendly GUI-based platform to monitor and analyze the NTL status of the power grid in real-time for revenue recovery.

In [6], a smart metering technique with different technologies to capture the data from smart meters is presented. In [7] the user privacy is maintained using the tools from information theory and a hidden Markov model for the measurements. It further addresses the issues due to the trade-off between privacy and utility. In [8], open-source tools are used to measure the smart meter data and data storage, and an analytics ecosystem based on publicly available test data set is studied.

There exist a variety of methods for the development of cloud services and smart meters; the paper discusses a few of them here that relate to our problem statement. Reference [9], using a tabu search algorithm, presented an efficient search algorithm to identify the locations of data and software components in data clouds. The main goal of this approach is to minimize the cost incurred in operations and emissions, modelled using mixed-integer programming. The proposed model is solved with the search algorithm discussed earlier. Virtual data center embedding (VDCE) across distributed infrastructures (DI) was introduced to make the infrastructure user-friendly and increase the revenue of providers. Reference [10], performs an analysis of different VM-based cloud environments like Eucalyptus, Open Nebula, and Nimbus. All those platforms have been evaluated with High-Level Petri Nets (HLPN).

In [11], a formal analysis, modelling, and verification of three open-source state-of-the-art VM-based cloud platforms—Eucalyptus, Open Nebula, and Nimbus—is provided. HLPN are used to model, analyze the structural and behavioral properties of the systems. Moreover, to verify the models, they have used the Satisfiability Modulo Theories Library (SMTL) and Z3 Solver.

In this article, we modelled about 100 VM to verify the correctness and feasibility of proposed original models. The results reveal that the models function correctly. Moreover, the increase in the

number of VMs does not affect the working of the models, which indicates the practicability of the models in a highly scalable and flexible environment.

Reference [12] analyzes the robustness of advanced DCNs. First, the authors present multi-layered graph modelling of various DCNs, and they study the traditional robustness metrics considering different failure scenarios to perform a comparative analysis. Finally, they describe the inadequacy of the conventional network robustness metrics to appropriately evaluate the DCN robustness and propose new procedures to quantify DCN robustness. Currently, there is no detailed study available centering on DCN robustness.

Reference [13], designs a protocol to enable secure, robust, cheating-resistant, and efficient outsourcing of MIC to a malicious cloud in this paper. The main idea to protect the privacy is by employing some transformations on the original matrix to get an encrypted matrix, which is sent to the cloud; and then transforming the result returned from the cloud to get the correct inversion of the original matrix. Next, a randomized Monte Carlo verification algorithm with one-sided error is employed to successfully handle result verification. Further, in this paper, the superiority of this novel technique in designing inexpensive result verification algorithm for secure outsourcing and well demonstrated. They analytically show that the proposed protocol simultaneously fulfils the goals of correctness, security, robust cheating- resistance, and high-efficiency. Extensive theoretical analysis and experimental evaluations also show its high-efficiency and immediate practicability.

In [14] Cloud Capacity Manager (CCM), a prototype system and its methods for dynamically multiplexing the computing capacity of virtualized data centers at scales of thousands of machines, for diverse workloads with variable demands are presented. Extending prior studies primarily concerned with accurate capacity allocation and ensuring acceptable application performance. CCM also sheds light on the tradeoffs due to two unavoidable issues in large scale commodity data centers: (i) maintaining low operational overhead given the variable cost of performing management operations necessary to allocate resources, and (ii) coping with the increased incidences of these operations' failures.

Reference [15] adopts the intuitive idea of High-QoS First-Replication (HQFR) to perform data replication. However, this greedy algorithm cannot minimize the data replication cost and the number of QoS-violated data replicas. To achieve these two minimum objectives, the algorithm transforms the QADR problem into the well-known minimum-cost maximum-flow (MCMF) problem. By applying the existing MCMF algorithm to solve the QADR problem, the second algorithm can produce the optimal solution to the QADR problem in polynomial time. Still, it takes more computational time than the first algorithm.

Reference [16], utilizes Voronoi partitions to determine which data center requests should be routed based on the relative priorities of the cloud operator. In [17], the ability to forecast electricity demand, respond to peak load events, and improve sustainable use of energy by consumers, are made possible by energy informatics. Information and software system techniques for a smarter power grid include pattern mining and machine learning over complex events and integrated semantic information, distributed stream processing for low latency response, cloud platforms for scalable operations and privacy policies to mitigate information leakage in an information-rich environment. Reference [18], proposes a new prototype system, in which the cloud-computing system is combined with a so-called Trusted Platform Support Service (TSS) based on a Trusted Platform Module. In this design, better effects can be obtained in authentication, role-based access and data protection in a cloud computing environment.

Reference [19] presents a pruning algorithm in which a threshold parameter is used to control the tradeoff between computation time and solution accuracy qualitatively. The algorithm is iterative with decoupled state values in each iteration, and the paper parallelizes the state estimations to reduce the overall computation time. They illustrate the proposal with examples where the pruning algorithm reduces the computation time significantly without losing much precision in-game solutions, and that parallelization further reduces the computation time.

An interdisciplinary MIT study [20] focused on integrating and evaluating existing knowledge rather than performing original research and analysis. Besides, this study's predecessors focused on implications of national policies limiting carbon emissions, while do not make any assumptions regarding future carbon policy initiatives. Instead, they mainly consider the impact of a set of ongoing trends and existing policies. Reference [21] identifies and reviews several low-cost technology products that enable various load control functions and in an innovative prepaid power meter that will have the capacity to direct cash exchanges through remote intervention is built, keeping in mind the end goal is to empower the client to energize his record from home. The user interface comprises an LCD, which shows the power used and a measure of the bill to be paid, and will sound an alert when the balance goes beneath a specific sum utilizing GSM. Prepaid meters are now present in the market and used widely in a few African and European nations. Additionally, this will help service organizations in staying aware of power thievery.

The review concludes that interval metering is not necessary to carry out load control functions. Available technology can remotely switch loads without requiring a connection to a meter. While one-way communication is essential to carry out remote switching of loads, two-way communication is not necessary to carry out remote switching of loads. Metering, in some form, is required for the settlement of the financial transactions associated with load control programs.

Reference [22] examined uncertainty in demand response baseline models and variability in automated responses to dynamic pricing. It defined several demand response (DR) parameters, which characterize changes in electricity use on DR days, and then presented a method for computing the error associated with DR parameter estimates. In addition to analyzing the magnitude of DR parameter errors, in this article, the authors develop a metric to determine how much observed DR parameter variability is attributable to real event-to-event variability versus only baseline model error. Using data from 38 C&I facilities that participated in an automated DR program in California, it was found that DR parameter errors are significant. For most facilities, observed DR parameter variability is more likely explained by baseline model errors, not real DR parameter variability; however, and several facilities do exhibit real DR parameter variability.

Reference [23] proposes a mathematical model for the dynamic evolution where in particular supply, demand, and clearing prices under a class of real-time pricing mechanisms are characterized by passing on the real-time wholesale prices to the end consumers. The effects that such mechanisms could have on the stability and efficiency of the entire system are investigated, and several stability criteria are discussed. It is shown that relaying the real-time wholesale electricity prices to the end consumers creates a closed-loop feedback system, which could be unstable or lack robustness, leading to extreme price volatility. Finally, a result is presented, which characterizes the efficiency losses incurred when, to achieve stability, the wholesale prices are adjusted by a static pricing function before they are passed on to the retail consumers.

Fault current coefficient and time delay assignment for a microgrid protection system with a central protection unit was discussed in [24], which utilizes relays of type-distributed generators providing more protection between generators. This approach performs critical parameter assignments like fault current coefficient and relay hierarchy. This method overcomes the difficulty of the manual task of distributed generation (DG) and protection units.

Reference [25] proposed an approach for distributed network reinforcement using a time segmentation algorithm, which reduces the computation overhead. Discrete particle swarm optimization is used to overcome the problem of nonlinear and discrete optimization.

Reference [26] was focused on load models of appliances. The loads for different appliances are generated using the profiles maintained and validated with actual distribution circuits. Then on-demand sensitive load models are used to reduce the consumption of different consumer ports, introduced the improvement of such load models at the machine level, and incorporated traditional controllable burdens, i.e., space cooling/space warming, water heater, garment dryer and electric vehicles. Approval of the machine level load models' is done by contrasting the models' output and

the actual power utilization information for the related apparatus. The machine-level load models' are combined to create stack profiles for a dispersion circuit, which are approved against the load profiles of a real distribution circuit. The DR-touche load models are utilized to examine changes in power utilization at both the household and the distribution levels, given an arrangement of client practices and additional actions by a utility.

In [27], an approach for real-time voltage-stability margin control via reactive power reserve sensitivities is proposed. In detail, a man-in-loop control method is used to boost reactive power reserves (RPRs) while maintaining a minimum amount of voltage stability margin bus voltage limits. The objective is to determine the most effective control actions to reestablish critical RPRs across the system. Initially, the concept of reactive power reserve sensitivity concerning control actions is introduced. In the sequel, a control approach based on convex quadratic optimization is used to find the minimal amount of control necessary to increase RPRs above their pre-specified (offline) levels. Voltage stability margin constraints are incorporated using a linear approximation of critical RPRs.

Reference [28], discussed an evaluation method for renewable DG in distributed networks. This approach allocates DGs to maximize the usage of connections to the local distribution company and customers. Reference [29] presents the algorithms and associated analysis, but guidelines, rules, and implementation considerations are also discussed, especially for the more complicated situations where mathematical analysis is difficult. In general, it is challenging to codify and taxonomize the scheduling knowledge because there are many performance metrics, task characteristics, and system configurations. Also, adding to the complexity is the fact that a variety of algorithms are designed for different combinations of these considerations. In spite of the recent advances, there are still gaps in the solution space, and there is a need to integrate the available solutions.

Security-aware scheduling strategy for real-time applications on clusters (SAREC) [30], proposes a security-aware scheduling strategy, or which integrates security requirements into scheduling for real-time applications by employing our security overhead model.

Scheduling real-time data-intensive applications (SARDIG) is a security-attentive dynamic real-time scheduling algorithm architecture and a dynamic grid scheduling algorithm for providing security for real-time data-intensive applications [31]. It proposes a grid architecture, which describes the scheduling framework of real-time data-intensive applications. Also, the authors introduced a mathematical model for providing security of the real-time data-intensive applications and a security gain function to quantitatively measure the security enhancement for applications running in the grid sites. They have also proved that the SARDIG algorithm always provides optimum security for real-time data-intensive applications.

It could be concluded that the system has a problem of service selection in all the above approaches when there is the considerable number of customers from different locations, so a new location-based service and selection approaches are proposed in this paper. In the following Section 3, the proposed location-based service selection approach is discussed, while Section 4 discusses the results achieved by the proposed method.

3. User-Aware Power Regulatory System with a Location-Based Service Selection Scheme

The proposed user-aware power regulatory scheme gets updates about the power usage of users through smart meters. The smart meters update the power usage details to the cloud service. Based on the power usage details, the power regulatory model provides inputs to the users to control the power usage of the connection. The selection of a location-based service selection scheme to provide additional comprehensive and consistent services has to be done in a more tactical approach where the time complexity should be reduced. The method audits the identity of the user using the auditing service, and if the user has cleared the auditing service, then the way performs service selection. The entire process is split into several stages, namely Location-Based Service Selection, Hash Function for Key Generation, Signature Verification, Trust Management, and Profile-Based Access Restriction. In this section, we will explain each of the functional stages in detail. Figure 1 presents the architecture of

the proposed user aware power regulatory model with a location-based service selection framework, and it shows the various stages of the proposed model.

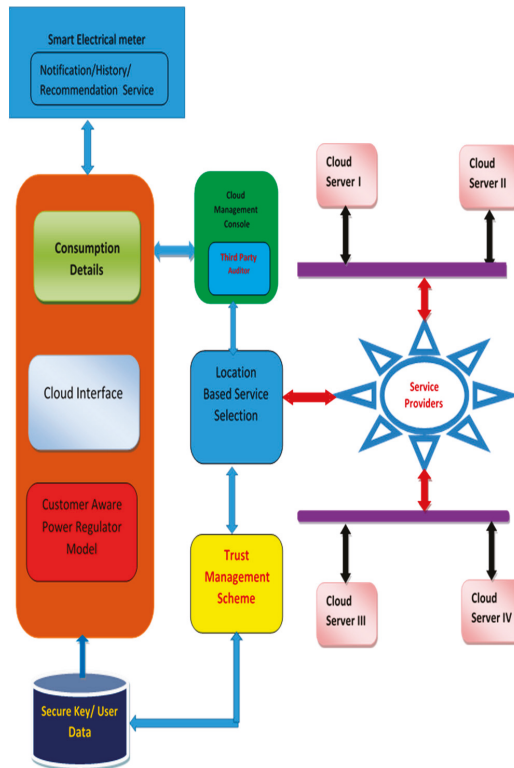


Figure 1. The architecture of the LBSS Model.

3.1. User-Aware Power Regulatory Model

The smart meter accesses the cloud service intermittently to send power use details, prior month use, cost, every month’s average units, number of units utilized at peak times, number of units used during off peak-times and their relative offered price. Additionally, the shutdown date and complaints registered, number of aggregate units, number of units utilized at peak time, number of units used during the off-peak times and their relative offered cost are included, and user notifications are shown on a smart meter display. The power regulatory model controls the flow of electric supply to the user connection. At intermittent periods, the model produces electric bills and regulates the power supply. At whatever point the instalment for the electrical supply not been paid, the substation sends a control message to the smart meter to detach the electric supply. When the user pays his bills again, then the substation sends the turn-on message to the meter, which provides the power back. The power regulatory model utilizes the ZigBee convention to the correspondence between the smart meter and substation.

Algorithm 1: User-Aware Power Regulatory System

Input: User Usage Details
Output: Power to be regulated.
Start
Initialize the value of time slot T_i .
 T_v = value of time slot T_i .
For each Time window T_i
Read Current usage units C_u .
Compute Number of units at peak time NPT_u .
Compute Number of units at Off-Peak Time $NOPT_u$.
Compute the cost of power usage CPU .
Compute Previous month usage Pmu .
Compute Previous month cost Pmc .
Compute Number of units on previous month Npm .
Compute No of units on peak time $Nupt$.
Compute No of units on off-peak time $Nuopt$.
Identify complaints registered $Compl$.
Compute shutdown date Sd .
Access Cloud Service Cs .
Cloud-Update-Service (C_u , NPT_u , $NOPT_u$, CPU ,
 PMU , Pmc , Npm , $Nupt$, $Nuopt$, $Compl$).
Display details to the smart meter.
End
If payment date Alive
Else
Access Payment-Detail Service.
If true then
Reset Payment date.
Else
Disconnect the power supply.
End
End
Stop.

Algorithm 1, above generates user awareness. It accesses the cloud service to update the cloud, so the smart meter can also show the recently registered estimations of energy utilization to the user. The model controls the power supply by checking the instalment status by accessing the cloud service. In light of the state of the instalment, the power status controls the electric supply through the smart meter.

3.2. Location-Based Service Selection

The user electronics readings are maintained at different locations of the county on different servers. Each geographic region reading is stored on separate servers located in different geographic regions. The user can view generated bills and make payment of bills through the cloud services. Upon creating a request, the cloud platform selects the respective service, according to the location of data or the server where the data is stored. To provide a more complete, and reliable service, the selection is made in a more strategic way where the time complexity should be minimized. The range of services is based on the location of the data, and then the user communicates with the selected service. The cloud management console makes the selection, and once the service is selected, then the user request is transferred to the service chosen (see Algorithm 2).

Algorithm 2: Location-Based Service Selection

LBSS(UserId Uid, UserLocation Uloc)

Output: Selected cloud service CS.

Step1: Read user-id Uid.

Step2: Read user location Uloc.

Step3: Read service details SD, service History Sh.

Step4: Select available services according to the location Uloc.

$$Ss = \int_{i=1}^N Mx(sh) \times (Sd(Uloc))$$

N = number of available services.

Mx = Minimum frequency of service

Sh = service history

Step5: Return SS.

3.3. Hash Function for Key Generation

The cloud user is assigned a secure key using which the user is identified and authenticated. The generation of the secret key is a dynamic process which is initiated for each reading, and the key is destroyed when the user completes the task. The key generation mechanism uses a hash function where the parameter of the hashing function also is changed when the existing or other users enter the system the next time. The selection of parameters and functions will also be adjusted according to the region of the user to provide more security and to avoid guessing attacks (see Algorithm 3).

Algorithm 3: Hashing Function for Key Generation

Intake: Locations loc, Schemes S.

Outcome: Secret key SecK.

Read location details LD from the database.

Compute NI = Number of locations from Ld.

NI = sizeof(LD).

Generate Random Number Rn.

$$Rn = f(x) = \int \emptyset(1, S).$$

Selected Scheme SeS = S(Rn).

If (SeS %2) = 0 then

Generate Secret Key SecK.

Initialize SecK = $\int_{i=1}^8 \text{SecK}(i) = 0$ // initialize the key to the size of 8 bit and set all bit to 0.

//Set the bit 1,2 = for region 1,2,3

//Set the bit 3,4 = for scheme 1-Feb no, 2-ams no, 3-Mona

//Set bit 5 and 6 = for the value -

//Set the bit 7,8 with meter no

User region ur = select the region of the user.

Select a random number for the addressing scheme RanS.

If(RanS = 1)

Ms = Select a Fibonacci number within ur.

$$Ms = f(x) = \int \textcircled{\otimes} \cap (\sum \text{Fibonacci} \in (1, UR))$$

Else if (RanS = 2)

Ms = select a amstrong number within ur.

$$Ms = f(x) = \int \textcircled{\otimes} \cap (\sum \text{Amstrong} \in (1, UR))$$

Else

Ms = select a manorama number within ur.

$$Ms = f(x) = \int \textcircled{\otimes} \cap (\sum \text{Manorama} \in (1, UR))$$

End

Construct sk = {Ur,RanS,NS,Mr}.

Else

Create a Secret Key SecK.

Initialize SecK = $\int_{i=1}^{16} \text{SecK}(i) = 0$ // initialize the key to the size of 16 bit and set all bit to 0.

//Set the bit 1 to,4 = for region 1,2,3

//Set the bit 5 to 8 = for scheme 1-Feb no, 2-ams no, 3-Mona

//Set bit 9 to12 = for the value -

//Set the bit 13 to 16 with meter no

User region ur = select the region of the user.

Select a random number for the addressing scheme RanS.

If(RanS = 1)

Ms = Select a Fibonacci number within ur.

$$Ms = f(x) = \int \textcircled{\otimes} \cap (\sum \text{Fibonacci} \in (1, UR))$$

Else if (RanS = 2)

Ms = select a amstrong number within ur.

$$Ms = f(x) = \int \textcircled{\otimes} \cap (\sum \text{Amstrong} \in (1, UR))$$

Else

Ms = select a manorama number within ur.

$$Ms = f(x) = \int \textcircled{\otimes} \cap (\sum \text{Manorama} \in (1, UR))$$

End

Construct SecK = {Ur,RanS,NS,Mr}.

End

Return SecK.

3.4. Signature Verification

In this stage, the user key has been verified. The verification process is performed by extracting the bit level information of the received key. If the key size is 16 bits, then a 16 bits keying mechanism is used; otherwise, an 8 bits keying mechanism is used (see Algorithm 4).

Algorithm 4: Signature Verification

Intake: SecK.
 Outcome: True/False
 Read Given Secret Key SecK.
 Read Key Set KeyS from Key Base Kb.
 Identify Key Size of SecK.
 $Ks = \sum \text{Bits} \in \text{SecK}$
 If $Ks = 8$ then
 Split SecK by the 2-bit key base.
 $Ur = \text{SecK}(1,2)$.
 Scheme $SN = \text{SecK}(3,4)$.
 Number $Mn = \text{SecK}(5,6)$.
 Meter No $Mr = \text{SecK}(7,8)$.
 Else
 Split SecK into 4 bit Key Base.
 $Ur = \text{SecK}(1,2,3,4)$.
 Scheme $ScN = \text{SecK}(5,6,7,8)$.
 Number $Mn = \text{SecK}(9,10,11,12)$.
 Meter No $Mr = \text{SecK}(13,14,15,16)$.
End
 If $(ScN = 1)$
 $Ms = \text{Select a Fibonacci number within ur.}$
 $Ms = \int_1^{Ur} \text{Feb}(1, Ur)$
 Else if $(ScN = 2)$
 $Ms = \text{select an amstrong number within ur.}$
 $Ms = \int_1^{Ur} \text{Ams}(1, Ur)$
 Else
 $Ms = \text{select a manorama number within ur.}$
 $Ms = \int_1^{Ur} \text{Man}(1, Ur)$
End
 If $Ms = Mn$ and $Mr \in Db$ then
 Return True.
 Else
 Return False.

End

3.5. Trust Management

Trust management is the critical process in service selection because the user is allowed to accessing the service only if he passes the trust evaluation. The trust management is categorized based on the type of users. By identifying the user type from the request, the identity of generic users is verified based on the crucial secret mechanism. For the internal registered users, the primary public/private critical method is used. Any user is allowed to access the service based on the trust verification result.

3.6. Profile-Based Access Restriction

The cloud platform is comprised of different users and has to be restricted to minimize access by different users. For example, the internal user needs to view the readings of various users and needs to

generate reports on them, and so on. The internal users must be able to access the data more frequently, whereas the external users do not. The external user needs one-time access or access for a short time to pay the bills so that the proposed work restricts the access based on the roles. It provides role-based access restriction to offer more security to the cloud platform and thus, outsiders cannot make flooding attacks on the proposed system.

4. Results and Discussion

The proposed SG is entirely simulated using the CloudSim platform, and the coding is written using 32 bit Java language for Windows 7 or 8. The processor used is a Core i5 with 8 GB RAM for higher computational operation. The application server used is Tomcat 5.0.6. The proposed user-aware Power Regulatory Model with Location-Based Service Selection approach, is implemented and evaluated for its efficiency. The technique has been assessed utilizing different setups with a vast number of service points and numbers of users. The strategy has been tried with varying situations of re-enactment for various periods. Table 1 lists the details of the simulation parameters utilized to assess the execution of the proposed technique. Figure 2 shows a preview of the smart meter intended for the proposed system. Figure 3 is a preview of the user interface utilized by the power station staff to refresh the unit costs for an assortment of associations. Table 2 shows the completeness ratio of three different algorithms, and it shows that the proposed method has a higher completeness measure value that indicates its efficiency in providing guaranteed service.

Table 1. Simulation Parameters.

Parameter	Value
Laxity Time	100–500 s
Network Bandwidth	10 Mbps
Number of Cloud Servers	32
Number of cloud services	2
Number of service providers	2
Number of Users	1 million
Number of Insiders	10,000

Details	Meter Display	Complaints	Logout
Energy used	Energy user per cost	Previous month unit	Previous month usage cost
520 Kwhr	Rs 2262	430 Kwhr	Rs 1120
Current	Voltage	Power	Frequency
9.5 A	228 V	1200 W	50 Hz
Number of units used at peak time	Peak time usage cost	No. of units used at OFF peak time	OFF peak time usage cost
300 Kwhr	Rs 1492	220 Kwhr	Rs 770
Previous month number of units used at peak time	Peak time usage cost	Previous month number of units used at OFF peak time	OFF peak time usage cost
250 Kwhr	Rs 850	180 Kwhr	Rs 270
Average unit per month	Average unit per month per cost	Power factor	Shut down date
8.67 Kwhr	Rs 37.7	0.96 PF	12/02/2015

Figure 2. Snapshot of the smart meter display.

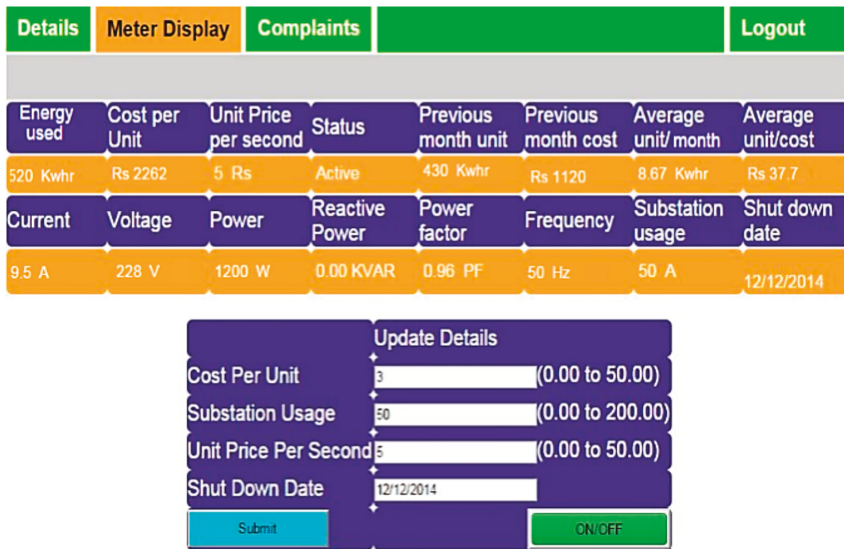


Figure 3. Snapshot of the power station interface.

Table 2. Comparative of completeness ratio results.

Laxyty (S)	Completeness Ratio			
	EDF	SAREG	SARDIG	Location-Based
100	0.79	0.82	0.83	0.89
200	0.80	0.81	0.85	0.90
300	0.83	0.85	0.87	0.91
400	0.84	0.86	0.89	0.92
500	0.85	0.87	0.91	0.93

The proposed solution has been implemented is Hadoop, which is a cloud computing platform integrated with the proposed solution to evaluate the proposed methodology. Three different clouds are created, with each one is running at various locations and on three service providers, which are running at N locations. The proposed solution is hardwired with the electric meter, and wireless communication is enabled to access the cloud service. Another web interface is specially designed for users to use and complete the payment procedures. To evaluate the performance of the proposed solution, Availability Ratio, Completeness Ratio, Security Value, Overall Performance Ratio, measures were the metrics examined. Availability is the ratio of total requests submitted and total requests handled. Completeness is the ratio between total submitted requests and the number of requests processed successfully. The security level is measured by total requests generated and completed. Overall performance is the ratio of the total number of requests submitted and the number of jobs completed in a particular time-frame.

The performance of the proposed method is compared with three well-known scheduling methods of the grid environment, namely Earlier Deadline First (EDF) [29] algorithms, Security-Aware scheduling strategy for Real-time applications on Clusters (SAREC) [30] and the Security of Real-Time Data-Intensive Applications on Grids (SARDIG) [31]. Table 2 shows the simulation results of the completeness ratio for the four algorithms. The completeness ratio is computed using different deadline bases or latency time (from 100 to 500 s). The proposed algorithm shows a better completeness ratio than the other algorithms as the deadline base or latency increases. Table 2 shows that the proposed

method has a higher ratio, which raised from 0.85 to 0.93, which demonstrates its efficiency in providing guaranteed service.

Table 3 shows the service availability ratio of four different algorithms, and it shows that the proposed method provides more service availability than other methods. Table 4 shows the simulation results of the security value for the four algorithms. The security value is computed using the total number of requests submitted and several requests fulfilled per number of users present in the network.

Table 3. Shows the comparison results of serviceability.

Availability Ratio %				
No. of Users	EDF	SAREG	SARDIG	Location-Based
1 million	72	82	89	98.7
2 million	69	79	85	97.6
3 million	67	75	81	96.6
5 million	63	72	77	95.8
10 million	59	69	72	95.1

Table 4. Shows the comparison results of the security level.

Security Level Value				
No. of Users	EDF	SAREG	SARDIG	Location-Based
1million	0.89	0.92	0.95	0.99
2 million	0.83	0.85	0.90	0.96
3 million	0.77	0.79	0.86	0.93
4 million	0.61	0.72	0.82	0.91
5 million	0.55	0.65	0.77	0.89

Figure 4 shows the time complexity of different methods to access the service where the service and data are available at various locations of the region. The time complexity is $\Phi(N \times M)$, where N—is the number of locations where the service is available, and M—is the number of service providers available. The overall time complexity is computed as follows:

$$\text{Time complexity } T_c = N \times \text{Log}(M)$$

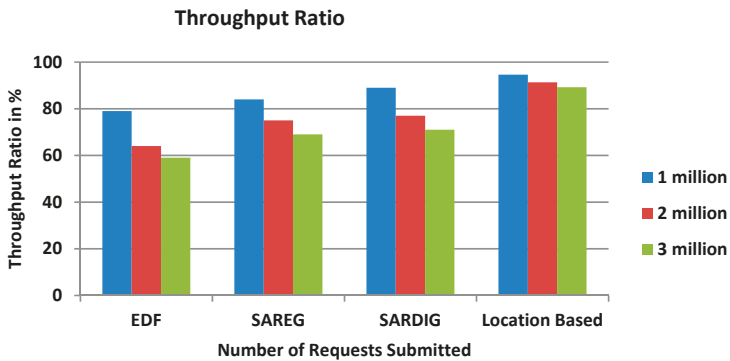


Figure 4. The time complexity of different approaches.

Figure 4 shows that the proposed method produces more efficient results compared to the other algorithms.

5. Conclusions

In this paper, we have proposed a user-aware power regulatory model with a location-based service selection approach for smart grids. The model provides functionality for smart meters to update the user details to the cloud as well be displayed on a smart meter display. Depending on the recommendations from the smart meter display, the users can change their usage patterns. As per the design, the proposed model manages the power supply to all its connecting units and a location-based service selection for secure and reliable access for the cloud services in a smart grid. It maintains a list of trustworthy users with different authentication mechanisms. For a registered internal user, it provides role-based access and user access restriction is provided based on their frequency of access. A malicious intruder or an unauthorized user is restricted from accessing the system through various hash-based signature verification mechanisms that ensure that the cloud is secure. Further, the access session duration is limited to prevent the system from being affected by flooding attacks. The experimental results show that the proposed model obtains higher performance in terms of high throughput and quality of assurance than other existing methods. The next step to introduce a secure and trusted solution is the requirement that needs to be focused on and to be addressed by the cloud-computing infrastructure.

Author Contributions: All authors have involved in this research activities for the final presentation of the work as a comprehensive research current article.

Funding: No source of funding for this research activities.

Conflicts of Interest: The authors declare no conflict of interest.

References

1. Sivapragash, C.; Thilaga, S.R.; Kumar, S.S. Advance Cloud Computing in Smart Power Grid. In Proceedings of the IET Chennai 3rd International on Sustainable Energy and Intelligent Systems (SEISCON 2012), Tiruchengode, India, 27–29 December 2012; pp. 356–361.
2. Rathi, A.; Parmar, N. Secure Cloud Data Computing with Third Party Auditor Control. In Proceedings of the 3rd International Conference on Frontiers of Intelligent Computing: Theory and Applications (FICTA), Bhubaneswar, Odisha, India, 14–15 November 2014; pp. 145–152.
3. Liu, X.; Golab, L.; Golab, W.; Ilyas, I.F.; Jin, S. Smart meter data analytics: Systems, algorithms, and benchmarking. *ACM Trans. Database Syst.* **2017**, *42*, 2. [[CrossRef](#)]
4. Mohammad, R. AMI Smart Meter Big Data Analytics for Time Series of Electricity Consumption. In Proceedings of the 2018 17th IEEE International Conference on Trust, Security and Privacy in Computing and Communications/12th IEEE International Conference on Big Data Science and Engineering (TrustCom/BigDataSE), New York, NY, USA, 1–3 August 2018; pp. 1771–1776.
5. Kee, K.K.; Shahab, S.M.F.; Loh, C.J. Design and development of an innovative smart metering system with GUI-based NTL detection platform. In Proceedings of the 4th IET International Conference on Clean Energy and Technology Conference, Kuala Lumpur, Malaysia, 14–15 November 2016.
6. Alahakoon, D.; Yu, X. Advanced analytics for harnessing the power of smart meter big data. In Proceedings of the 2013 IEEE International Workshop on Intelligent Energy Systems (IWIES), Vienna, Austria, 14 November 2013; pp. 40–45.
7. Sankar, L.; Rajagopalan, S.R.; Mohajer, S. Smart meter privacy: A theoretical framework. *IEEE Trans. Smart Grid* **2013**, *4*, 837–846. [[CrossRef](#)]
8. Prasad, S.; Avinash, S.B. Smart meter data analytics using OpenTSDB and Hadoop. In Proceedings of the 2013 IEEE on Innovative Smart Grid Technologies-Asia (ISGT Asia), Bangalore, India, 10–13 November 2013; pp. 1–6.
9. Larumbe, F.; Sanso, B. A Tabu Search Algorithm for the Location of Data Centers and Software Components in Green Cloud Computing Networks. *IEEE Trans. Cloud Comput.* **2013**, *1*, 22–35. [[CrossRef](#)]
10. Amokrane, A.; Zhani, M.F.; Langar, R.; Boutaba, R.; Pujolle, G. Greenhead: Virtual Data Center Embedding across Distributed Infrastructures. *IEEE Trans. Cloud Comput.* **2013**, *1*, 36–49. [[CrossRef](#)]

11. Malik, S.U.; Khan, S.U.; Srinivasan, S.K. Modeling and Analysis of State-of-the-art VM-based Cloud Management Platforms. *IEEE Trans. Cloud Comput.* **2013**, *1*, 1. [[CrossRef](#)]
12. Bilal, K.; Manzano, M.; Khan, S.U.; Calle, E.; Li, K.; Zomaya, A.Y. On the Characterization of the Structural Robustness of Data Center Networks. *IEEE Trans. Cloud Comput.* **2013**, *1*, 1. [[CrossRef](#)]
13. Lei, X.; Liao, X.; Huang, T.; Li, H.; Hu, C. Outsourcing Large Matrix Inversion Computation to A Public Cloud. *IEEE Trans. Cloud Comput.* **2013**, *1*, 1. [[CrossRef](#)]
14. Kesavan, M. Practical Compute Capacity Management for Virtualized Data Centers. *IEEE Trans. Cloud Comput.* **2013**, *1*, 1. [[CrossRef](#)]
15. Lin, J.W.; Chen, C.H.; Chang, J.M. QoS-Aware Data Replication for Data-Intensive Applications in Cloud Computing Systems. *IEEE Trans. Cloud Comput.* **2013**, *1*, 1. [[CrossRef](#)]
16. Doyle, J. Stratus: Load Balancing the Cloud for Carbon Emissions Control. *IEEE Trans. Cloud Comput.* **2013**, *1*, 1. [[CrossRef](#)]
17. Simmhan, Y.; Aman, S.; Cao, B.; Giakkoupis, M.; Kumbhare, A.; Zhou, Q.; Paul, D.; Fern, C.; Sharma, A.; Prasanna, V.K. *An Informatics Approach to Demand Response Optimization in Smart Grids*; Report; Computer Science Department, University of California: Los Angeles, CA, USA, 2013.
18. Zen, Z.D. Cloud computing based on trusted computing platform. In Proceedings of the International Conference on Intelligent Computation Technology and Automation, Changsha, China, 11–12 May 2010.
19. Ma, C.Y.T. Scalable Solutions of Markov Games for Smart-Grid Infrastructure Protection. *IEEE Trans. Smart Grid* **2013**, *4*, 47–55. [[CrossRef](#)]
20. Kassakian, J.G.; Schmalensee, R.; Desgroseilliers, G.; Heidel, T.D.; Afridi, K.; Farid, A.M.; Grochow, J.M.; Hogan, W.W.; Jacoby, H.D.; Kirtley, J.L.; et al. *The Future of the Electric Grid: An Interdisciplinary MIT Study*; Massachusetts Institute of Technology: Cambridge, MA, USA, 2011.
21. Crossley, D. *The Role of Advanced Metering and Load Control in Supporting Electricity Networks*; Tech. Rep. No 5 Task XV, International Energy Agency Demand Side Management Programme; Energy Futures Australia PTY LTD: Brisbane, Australia, 2008.
22. Mathieu, J.L.; Callaway, D.S.; Kiliccote, S. Examining uncertainty in demand response baseline models and variability in automated responses to dynamic pricing. In Proceedings of the 50th IEEE Conference on Decision and Control (CDC), Orlando, FL, USA, 12–15 December 2011; pp. 4332–4339.
23. Roozbehani, M.; Dahleh, M.; Mitter, S. On the stability of wholesale electricity markets under real-time pricing. In Proceedings of the 49th IEEE Conference on Decision and Control (CDC), Atlanta, GA, USA, 15–17 December 2010; pp. 1911–1918.
24. Ustun, T.S. Fault current coefficient and time delay assignment for micro grid protection system with central protection unit. *IEEE Trans. Power Syst.* **2013**, *28*, 598–606. [[CrossRef](#)]
25. Ziari, S. Optimal distribution network reinforcement considering load growth, line loss, and reliability. *IEEE Trans. Power Syst.* **2013**, *28*, 587–597. [[CrossRef](#)]
26. Shao, S.H. Development of physical-based demand response-enabled residential load models. *IEEE Trans. Power Syst.* **2013**, *28*, 607–614. [[CrossRef](#)]
27. Lianordi, B. An approach for real time voltage stability margin control via reactive power reserve sensitivities. *IEEE Trans. Power Syst.* **2013**, *28*, 615–625. [[CrossRef](#)]
28. Shaaban, M.F. DG allocation for benefit maximization in distribution networks. *IEEE Trans. Power Syst.* **2013**, *28*, 639–649. [[CrossRef](#)]
29. Stankovic, J.A.; Spuri, M.; Ramamritham, K.; Buttazzo, G.C. *Deadline Scheduling for Real-Time Systems: EDF and Related Algorithms*; Kluwer: Dordrecht, The Netherlands, 1998.
30. Xie, T.; Qin, X.; Sung, A. SAREC: A security-aware scheduling strategy for real-time applications on clusters. In Proceedings of the 34th International Conference on Parallel Processing, Oslo, Norway, 14–17 June 2005.
31. Islam, M.R.; Hasan, M.T.; Ashaduzzaman, G.M. An architecture and a dynamic scheduling algorithm of grid for providing security for real-time data-intensive applications. *Int. J. Netw. Manag.* **2011**, *21*, 402–413. [[CrossRef](#)]



Wavelet Packet Decomposition for IEC Compliant Assessment of Harmonics under Stationary and Fluctuating Conditions

Stefano Lodetti, Jorge Bruna, Julio J. Melero * and José F. Sanz

Instituto Universitario de Investigación CIRCE (Fundación CIRCE—Universidad de Zaragoza), C/Mariano Esquillor 15, 50018 Zaragoza, Spain; slodetti@fcirce.es (S.L.); jbruna@fcirce.es (J.B.); jfsanz@unizar.es (J.F.S.)

* Correspondence: melero@unizar.es; Tel.: +349-7676-2402

Received: 10 October 2019; Accepted: 15 November 2019; Published: 19 November 2019

Abstract: This paper presents the validation and characterization of a wavelet based decomposition method for the assessment of harmonic distortion in power systems, under stationary and non-stationary conditions. It uses Wavelet Packet Decomposition with Butterworth Infinite Impulse Response filters and a decomposition structure, which allows the measurement of both odd and even harmonics, up to the 63rd order, fully compliant with the requirements of the IEC 61000-4-7 standard. The method is shown to fulfil the IEC accuracy requirements for stationary harmonics, obtaining the same accuracy even under fluctuating conditions. Then, it is validated using simulated signals with real harmonic content. The proposed method is proven to be fully equivalent to Fourier analysis under stationary conditions, being often more accurate. Under non-stationary conditions, instead, it provides significantly higher accuracy, while the IEC strategy produces large errors. Lastly, the method is tested with real current and voltage signals, measured in conditions of high harmonic distortion. The proposed strategy provides a method with superior performance for fluctuating harmonics, but at the same time IEC compliant under stationary conditions.

Keywords: harmonic analysis; power quality; wavelet transform; wavelet packet; measurement techniques

1. Introduction

The fast evolution of electrical and electronic technologies is generating an exponential growth in the use of non-linear loads, such as switch-mode power supplies, electronic lighting ballasts [1], and other harmonic sources whose penetration can be expected to increase substantially in the future [2]. Harmonic distortions coming from new-generation sources and loads are generally larger and less regular than those due to traditional sources and loads, making power and energy more difficult to measure [3,4]. International standards have been developed to define acceptable limits and suitable measurements techniques for power systems' harmonics, e.g., [5,6]. Fourier spectral analysis is the most widely used approach for the evaluation of the harmonic content in power systems, due to its excellent accuracy under stationary conditions. This choice is reflected in the IEC 61000-4-7 [5] standard, which defines harmonics measurements and instrumentation requirements. This standard proposes the use of the Fast Fourier Transform (FFT), a fast and efficient algorithm for performing the Discrete Fourier Transform (DFT). Although the DFT is valid under general conditions, it is well known that limitations arise when it is applied to non-stationary signals, which is the normal situation in modern power systems. When fluctuating harmonics are analyzed with a DFT, the energy contained in the harmonics is distributed across the spectrum, affecting the accuracy [7]. For this reason, the IEC 61000-4-7 standard proposes a grouping strategy in order to improve the accuracy in

non-stationary conditions and, at the same time, explicitly mentions the possibility to employ more advanced processing tools. During the last few years, alternatives to DFT have been proposed in the literature. A common workaround is to use the Short Time Fourier Transform (STFT), which assumes the signal to be piecewise stationary, but other methods have been suggested as well [8]. Among them, there is Wavelet Transform (WT), typically in the form of Discrete Wavelet Transform (DWT). The main advantage of DWT is that, while DFT requires a stationary, perfectly periodic sinusoidal signal to work properly, this is not a requirement for DWT. This signal processing tool has a wide range of applications, including power systems, where it proved to be extremely useful in signal denoising, short time predictions, fault detection, and energy management [9–14], as well as for Power Quality [15–19]. From WT, Wavelet Packet Decomposition (WPD) was derived, generalizing the link between wavelets and Multiresolution Analysis (MRA). Thanks to the uniform frequency bands that can be obtained with WPD, its application in Power Quality has been proposed for power calculation [20,21] and harmonic measurements [22–24]. However, the WPD harmonic analyses proposed in the literature do not look complete from the point of view of compliance with international standards and capabilities under stationary conditions, as will be discussed in Section 2.

To complete the current scenario, this paper presents a WPD method for a full harmonic analysis, in contrast with the valuable, but partial work developed in recent years, e.g., [22–25]. The proposed method takes advantage of the superior performance of WPD with fluctuating harmonics with respect to Fourier analysis. On the other hand, it is for the first time compliant with the IEC 61000-4-7 standard. This result, never achieved before, is possible thanks to the accurate selection of the filtering implementation and to the uniform frequency bandwidth division of WPD, as studied by the authors in [26]. To assess the method's implementation and validate its superior performance within the IEC standard requirements, several voltage signals with known harmonic content, both in stationary and fluctuating conditions, were tested. The accurate assessment of individual harmonic values was the main focus of the proposed method, and therefore, they were the objective of the validation. Other indices, like for instance Total Harmonic Distortion (THD), were not considered since they are the result of a further processing stage that can be performed in the same way as for FFT, as explained in Section 2.2. In Section 4.4, a comparison of the computational effort is provided, and finally, in Section 5, the method is tested with real voltage and current signals measured in a high harmonic distortion environment.

2. The Proposed WPD Method

2.1. Wavelet Transforms in Power Systems

WT is a mathematical transform that provides a representation of a function by a series of orthonormal functions, generated by scaling and translating a wavelet. It is particularly powerful in the measurement of the time-frequency variations of spectral components, but not suitable for power harmonics analysis because of the non-uniform frequency bands obtained. WPD is an extension of WT where the frequency axis is divided into equally wide intervals, instead of the traditional division in dyadic intervals, whose sizes have an exponential growth [27]. The advantage is that, with an accurate selection of the sampling frequency and the decomposition structure, it can lead to uniform frequency bands of the desired size and can therefore be employed for harmonics analysis. Previous works on WPD based algorithms for harmonics analysis can be found in the literature, but up to this moment, no IEC compliant approach, with complete harmonic analysis, has been proposed. Hamid et al. presented in [21] a WPD method for Root Mean Squared (RMS) and power measurements, from which harmonic distortion can be obtained. However, with this approach, only odd harmonics can be evaluated, and the wide frequency bands that can be obtained are not compliant with IEC standards. Eren et al. proposed a decomposition scheme in [22], but again, only bands centered in odd harmonics were taken into account. Moreover, results were shown only up to the seventh order. A more refined strategy was proposed by Diego and Barros in [24], where the 50 Hz wide frequency bands were compatible with

IEC 61000-4-7 [5], but the decomposition was performed only up to the 15th order, far from compliance with the IEC standards.

Additionally, a major drawback of WPD based algorithms is their difficulty to compete with FFT in terms of computational speed. The FFT algorithm is the result of many years of developments and advances of Fourier analysis, while newly proposed methods (such as WPD) are not yet optimized for high performances. However, this gap is reducing, thanks to the constant increase in available computational power and the possibility of hardware implementation. In [23], it was shown that WPD can be efficiently implemented and be employed online for harmonics analysis. However, although the work showed the feasibility of online measurements, the same limitations on the results were found, i.e., the evaluation of only odd harmonics, limited total bandwidth (only up to 15th order), and too wide frequency bands (even harmonics contributions were included in the odd ones).

WPD algorithms continue to be interesting for power system researchers, as suggested by recent works [20,23], but in order to move forward and make WPD a feasible and better alternative to DFT, a complete algorithm for harmonic assessment must be designed. Modern power systems, with the increasing presence of non-linear loads, require a method compatible with the IEC standards, able to measure not only odd harmonics, but also even harmonics, and up to the highest possible order.

2.2. Characteristics of the Proposed Method

The past limitations of WPD arose from the difficulty of adjusting the algorithm to the constraints given in the IEC 61000-4-7 standard, which is not trivial. Among these constraints, there are: a fixed rectangular sampling window of 10 cycles of the fundamental (200 ms at 50 Hz), frequency bands of 50 Hz centered in integer multiples of the fundamental (both even and odd), a bandwidth up to the 50th harmonic order (2500 Hz), and mainly, the fulfillment of the accuracy requirements for the stationary case. Therefore, the implementation of an IEC compliant algorithm is not just an extension of previous studies, since it requires overcoming the previous limitations and keeping the accuracy within the prescribed limits.

In this paper, it is shown that this can be achieved by an accurate study of the WPD implementation. The novel algorithm hereafter presented is the continuation of the work performed by the authors in [26], where a detailed study was conducted to define a methodology for the selection of the most suitable filter and convolution technique for WPD applied to power systems' harmonics. The methodology proposed in [26] is here employed to develop and characterize a complete measurement method. In order to obtain the IEC frequency bands, up to at least the 50th order, a sampling rate of 6400 Hz is necessary, and seven levels of decomposition must be implemented. These necessary features set high requirements on the frequency selectivity of the decomposition filters. The work performed in [26] showed that a maximally-flat Butterworth Infinite Impulse Response (IIR) filter of order 29 was the most suitable choice, and for this reason, it was employed in this paper as the mother wavelet. Its superior behavior in frequency selectivity, number of coefficients, and spectral leakage under realistic conditions, compared with traditional mother wavelet functions (e.g., db20, db10, Vaidyanathan, etc.) provides the high level of accuracy required to comply with the IEC standards in both stationary and non-stationary conditions. It must be noted that, although IIR filters have a non-linear phase, it does not represent a problem because the purpose of the method is to extract the RMS content of each frequency band, and the convolution technique presented in [26] allows preserving this information even with non-linear phase filtering.

In the following, the filtering procedure at each node of the decomposition tree is explained: the input signal f is recursively convolved by a pair of Quadrature Mirror Filters (QMFs), high pass and low pass filters ($h(n)$ and $g(n)$, respectively), and then, the filtered signals are downsampled by a factor of two, taking into account that the employed filters are half band filters (see Equations (1) and (2)). Thus, the high pass and low pass QMFs used were obtained from the corresponding IIR Butterworth filter of order 29, as discussed before. This WPD scheme was designed and implemented using MATLAB, allowing the authors to speed up the validation and testing procedure under realistic

input conditions, i.e., with the evaluation of real voltage waveforms. The following equations describe the basic filtering stage of the WPD method, in which the wavelet coefficients at level l , node i , are obtained from the convolution of the input signal at the previous level with the filters' coefficients and subsequent downsampling.

$$D_1^{2i}(k) = \sum_n g(n) D_{1-1}^i(2k - n) \tag{1}$$

$$D_1^{2i+1}(k) = \sum_n h(n) D_{1-1}^i(2k - n) \tag{2}$$

where $i = 0, 1, \dots, 2(l - 1) - 1$, and $h(n)$ and $g(n)$ are the high pass and low pass filter coefficients, respectively. In this regard, Figure 1 shows the decomposition tree scheme employed.

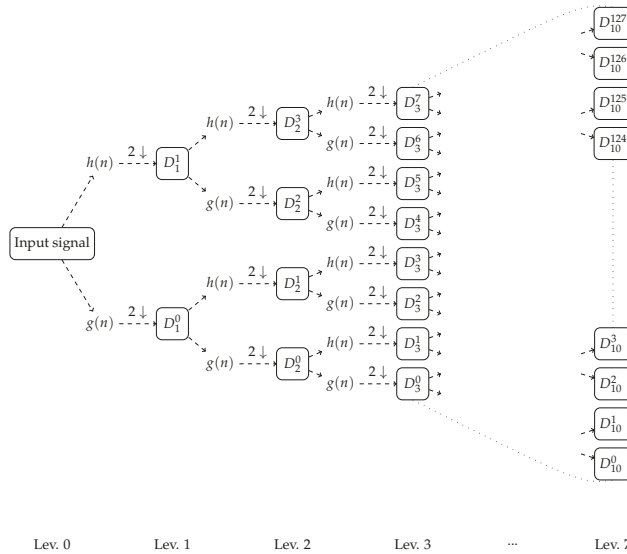


Figure 1. Wavelet Packet Decomposition (WPD) filtering and decimation scheme.

Table 1 summarizes the characteristics of the decomposition structure at each node, including information about the number of nodes per level, samples per node, effective time resolution, and bandwidth for every node at each level.

Table 1. Decomposition tree summary.

Level Number	Number of Nodes	Samples/Node	Δt (ms)	Bw /Node (Hz)
1	2	640	0.312	1600
2	4	320	0.625	800
3	8	160	1.250	400
4	16	80	2.500	200
5	32	40	5.000	100
6	64	20	10.000	50
7	128	10	20.000	25
7*	128/2 = 64	10 + 10 = 20	N/A	25 + 25 = 50

It is possible to observe that nodes at the seventh decomposition level have a bandwidth of 25 Hz. The required 50 Hz bands were obtained by a two-nodal-grouping (7*, last level in Table 1). Aggregated RMS harmonic values are derived from individual node content as follows [15]:

$$x_{rms}(j, p + q) = \sqrt{\frac{\sum_k (d_{j,k}^p)^2 + \sum_k (d_{j,k}^q)^2}{N}} \quad (3)$$

where p and q are the two grouped nodes, N the total number of data, k the index counter, and j the level at which the RMS calculation is performed. In order to obtain the correct IEC bands, the grouping must satisfy: $q = p + 1, p = 2, 4, 6, \dots$ (the first node is discarded).

Thanks to this two-nodal-grouping, each band corresponded exactly to an IEC harmonic group, and therefore, any further processing stage, e.g., THD calculation or time aggregation according to IEC 61000-4-30, is perfectly possible. The algorithm was indeed designed to represent an alternative to FFT for power quality analyzers, assuming sampled values as input and producing compliant individual harmonic values as output. As a result, the method did not have any additional requirements than those of FFT.

3. Compliance with IEC Accuracy Requirements

This section presents a test of accuracy, showing that the proposed method fulfills the IEC precision requirements for the stationary case and overperforms the IEC standard method for the non-stationary case.

IEC 61000-4-7 prescribes, for Class I accuracy, a maximum error of 5% in the evaluation of harmonic components, in case of single frequency and steady-state signals. In order to test the compliance of the proposed method, fifty steady-state signals $u_i(t)$, of single harmonic frequency ranging from harmonic order one to 50, were generated with a MATLAB script and subsequently analyzed using both the IEC method and the proposed WPD method. The input signals have the following expression:

$$u_i(t) = 100\sqrt{2} \sin(i 2\pi f_0 t) \quad (4)$$

where i is the i th test containing the i th pure tone, f_0 is the power frequency (50 Hz), and t is the time.

The top graph in Figure 2 shows the errors obtained with the proposed method for each i th harmonic order, with respect to the expected values, which in this case was always 100. It can be seen that the errors were well below the limit for Class I instruments for every harmonic order. The slightly higher errors for order 31st and 33rd were due to an intrinsic characteristic of WPD, which affected the central decomposition bands, as explained in [26]. This, however, did not compromise the accuracy, and compliance with IEC 61000-4-7 was proven.

The same test was repeated for non-stationary single frequency signals. To obtain non-stationary signals, the fluctuation pattern proposed in IEC 61000-4-7 Annex C.3 was employed, i.e., a reduction of the RMS of the signal from 100% to 20% at $t = 85$ ms in a 200 ms window. Since FFT is not suitable for measuring fluctuating harmonics, the standard proposes a grouping strategy, where the FFT bins are summed into harmonic groups to reduce the uncertainty. However, no accuracy limits are prescribed for this scenario. The bottom graph in Figure 2 shows the errors obtained in the case of fluctuating signals using the conventional FFT, the grouped IEC strategy, and the proposed WPD method. It can be seen that the conventional FFT produced errors of the order of 20%, while the IEC grouping strategy allowed a reduction of the error below the 5% limit. In this case, the proposed WPD method further reduced the error, for every order but 31 and 33, never exceeding the IEC stationary-state limits. The proposed method was therefore equally valid as the grouped FFT for single frequency signals, both stationary and fluctuating, and significantly superior to standard FFT, as expected.

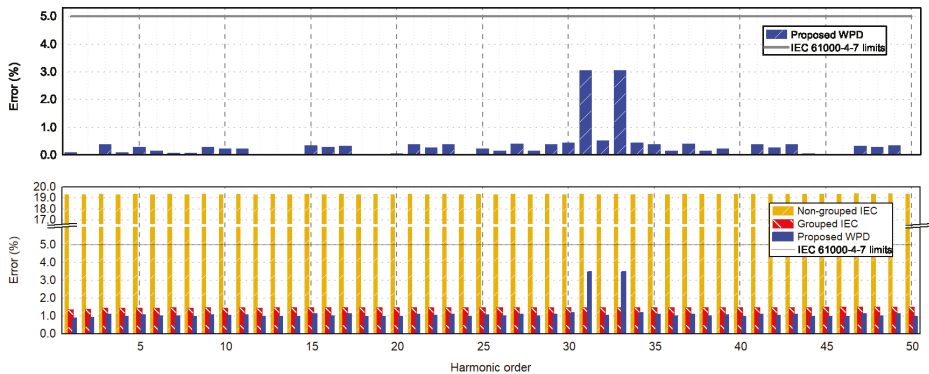


Figure 2. Top: errors of the proposed method with steady-state single frequency signals. Bottom: comparison of the error produced by the conventional FFT, the grouped IEC, and the WPD methods in case of single frequency signals, under fluctuating conditions (as explained in the text). The grey lines show the limits provided by IEC 61000-4-7 for stationary conditions.

4. Validation of the Method

The validation of the method required a more complex harmonic content than single frequency signals. Moreover, in order to be able to assess the accuracy of the method and compare it with the accuracy of Fourier analysis, the true harmonic content of the signals needed to be known a priori, i.e., synthetic signals must be employed. For this reason, realistic signals were generated, starting from the National Physics Laboratory (NPL) Power Quality Waveform Library [28], a public repository of waveforms with known harmonic content, representative of voltage signals found in the grid or used for calibration of equipment. This approach allowed obtaining waveforms whose true harmonic content was known and, at the same time, was realistic harmonic content.

4.1. Test Waveforms

The 13 employed waveforms are presented in Table 2. It was decided to employ all the waveforms of the NPL library coming from direct measurements in the grid (11), together with two synthetic waveforms, to further test the method. The synthetic waveforms were a square wave, allowing testing harmonic contents up to the 49th order, and a waveform whose harmonic content was created using IEC 61000-3-2:2000 limits for harmonic voltage emissions [28]. In each case, the power frequency was 50 Hz, so the duration of the test waveform was 200 ms, as prescribed in IEC 61000-4-7, while the RMS amplitude of the fundamental components was 230 V. Table 2 also shows the THD factors calculated from the nominal harmonic content values reported in [28]. For the study of the non-stationary case, the following modulation patterns were applied to the test waveforms:

- Constant modulation: instantaneous reduction of the amplitude from 100% to 20%, 85 ms after the beginning of the signal. This is the modulation proposed in IEC 61000-4-7.
- Linear modulation: amplitude linearly reduced from 100% to 75% in the last 115 ms of the signal. This modulation represents a motor start.
- Rectangular modulation: flicker-type modulation of 5% amplitude and 8.8 Hz modulation frequency.

The last two modulations were considered to provide a more reliable validation, since they could be realistically found in the grid, in the case of the connection of large loads or in the case of flicker [29]. More information about the modulation patterns is given in Section 4.3.

Table 2. Validation test waveforms, taken from [28], showing the total number of harmonic components included n , the most intense harmonic order H , and the calculated THD.

ID	Description	n	H	THD (%)
1	IEC 61000-3-2 voltage limits for the power amplifier	38	3	1.26
2	Voltage waveform for an accounting operation building	4	5	2.80
3	Voltage waveform for an apartment building	6	5	1.95
4	Voltage waveform for a commercial and residential load	3	5	2.44
5	Voltage waveform of fluorescent lights with electronic ballast	5	5	3.74
6	Voltage waveform of fluorescent lights with magnetic ballast	3	5	2.69
7	Voltage waveform for an industrial and residential load	3	5	3.00
8	Possible limits of voltage harmonics of a single phase feeder	49	3	6.72
9	Voltage waveform for a machining plant	4	5	2.00
10	Voltage waveform for a residential load	3	5	2.55
11	Square wave	24	3	47.30
12	Voltage waveform for a supermarket	4	5	2.42
13	Voltage waveform for a welded pipes plant	4	5	2.40

4.2. Validation for Stationary Conditions

In this section, an extensive analysis is presented for the case of Waveform 1, in steady state conditions. Figure 3 shows the obtained results for Waveform 1, along with the calculated errors.

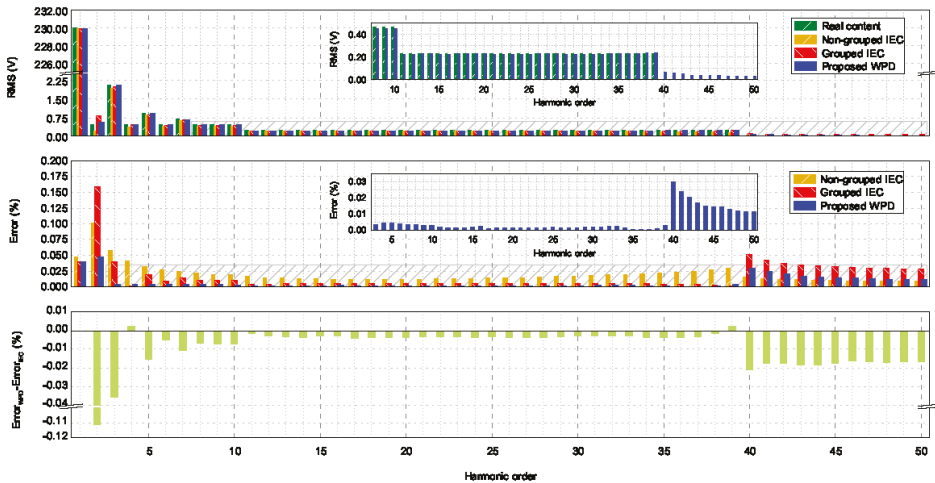


Figure 3. Analysis of the IEC 61000-3-2 limits waveform under stationary conditions. The comparison is made between the IEC, the grouped IEC, and the proposed WPD methods. The upper graph shows the spectrum of the RMS content of each IEC frequency band for the three methods, compared to the real content. The middle graph shows the errors for each frequency band. The difference between the errors is shown in the bottom graph.

The harmonic content was significantly more complex than single frequency signals, and it is possible to see that the results of the FFT slightly deviated from the expected values. The same happened with the grouped FFT and the proposed WPD method. In all of the cases, however, the errors were very low, always lower than 0.2%. Depending on the harmonic order and on the frequency content, the WPD errors were higher or lower than FFT. The bottom graph of Figure 3 shows a plot of the difference between the error of the WPD results and the error of the results of the grouped FFT (which resulted in being more accurate than standard FFT). This value indicated how worse WPD

was performing with respect to the grouped FFT. Negative values mean that WPD was performing better. It is possible to see from Figure 3 that the error of the proposed WPD method was always lower than the IEC method, except for the orders four and 39 where, however, the difference was negligible (less than 0.005%). In any case, all the errors presented were extremely low, and all the methods were perfectly suitable for stationary harmonics.

The other 12 waveforms were assayed with the same methodology, and a summary of the obtained results is presented. Figure 4 shows that, among all the assayed waveforms, the maximum difference between the errors of the two methods was less than 0.35%, which represented the worst case. This means that in the case of stationary signals, the presented method was almost never worse than the FFT or the grouped FFT, and when it was, the deviation was negligible.

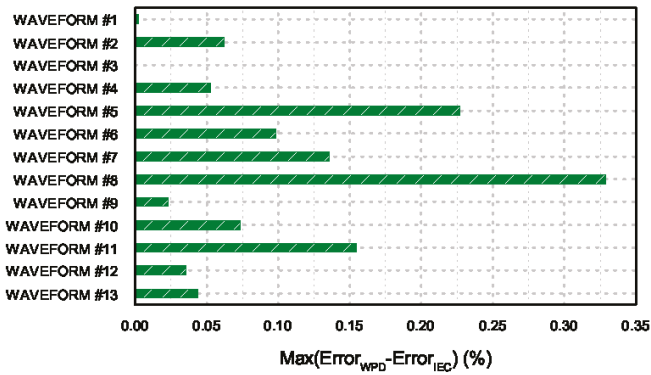


Figure 4. Maximum positive difference between the error of the WPD and grouped IEC methods.

4.3. Validation for Non-Stationary Conditions

In this section, the performance of the proposed method in the case of non-stationary realistic waveforms is assessed. The results were compared to the strategy proposed by IEC 61000-4-7, i.e., grouped FFT. Among the scenarios discussed so far, this was the most relevant one, since it was the closest to reality, where voltage and current waveforms are often, if not always, non-stationary. As stated in Section 4.1, three different fluctuation patterns were applied to the 13 waveforms previously identified. In this regard, Figure 5 illustrates the three types of modulations that were used.

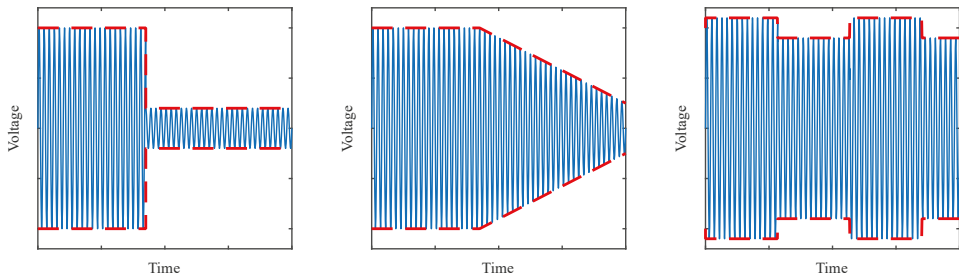


Figure 5. Schematic illustration of the employed modulation patterns. From left to right: constant modulation, linear modulation, and flicker-type modulation.

Figure 6 shows the results obtained for Waveform 1 with constant modulation. It can be easily seen how the proposed WPD method was significantly more accurate than the grouped FFT, which produced large errors. When the measured RMS content was less than 1%, the percentage of error was

calculated with respect to the nominal voltage, according to the IEC 61000-4-7 standard [5]. The results of the conventional FFT produced even larger errors and, for the sake of clarity, are not presented. Depending on the harmonic order, the deviation of the proposed WPD method from the real content of the signal could vary, but it was always more accurate than the grouped IEC method. This is confirmed by the bottom graph of Figure 6, which shows the difference between the errors made by the two methods. As can be seen, all the values were negative, meaning that WPD always gave more accurate results than grouped FFT, and in some cases with a large difference. It can also be seen that, in both methods, the largest errors were usually produced when no harmonic content was expected. In this case, the appearance of non-zero values was due to the so-called energy leakage, i.e., part of the harmonic content of nearby bands leaked to a band where no content should be present. This affected both methods, but it was evident that WPD was significantly superior in dealing with this issue, providing a far better overall accuracy.

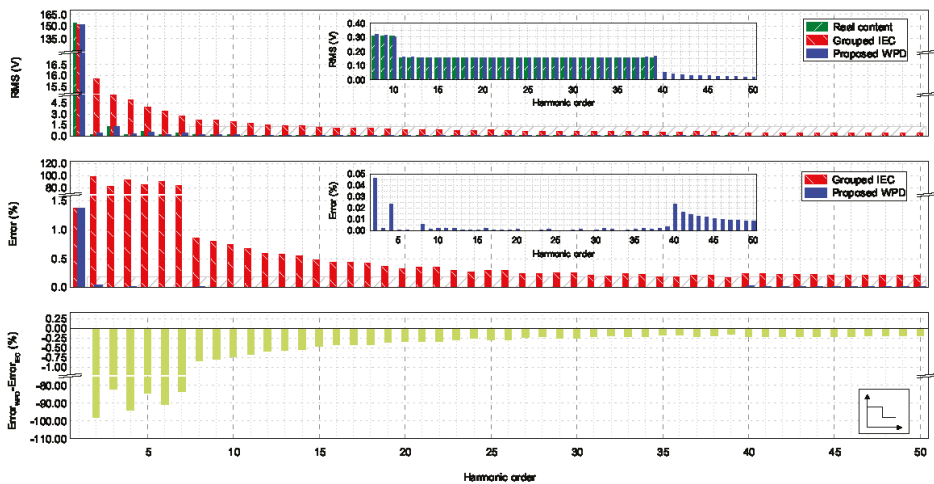


Figure 6. Analysis of the IEC 61000-3-2 limits waveform under non-stationary conditions (constant modulation). The upper graph shows the spectrum of the RMS content of each IEC frequency band for the three methods, compared to the real content. The middle graph shows the errors for each frequency band. The difference between the errors is shown in the bottom graph.

The other 12 waveforms were assayed with the same methodology, and a summary of the obtained results is presented. In this case, to quantify and compare the overall accuracy of the two methods, the Root Mean Squared Error (RMSE) can be employed:

$$RMSE = \sqrt{\frac{\sum_{h=1}^N \epsilon_h^2}{N}} \tag{5}$$

where ϵ_h is the error produced for order h , and N is the total number of bands, 50 in this case. This quantity is typically used in statistics to measure how well a distribution fits experimental data. However, in this case, it was used to aggregate the errors of each tested method over all harmonic orders into a single measure and have an estimation of the overall accuracy. The higher the RMSE, the lower the overall accuracy. Figure 7 shows the RMSE obtained with both methods, for all the considered waveforms (see Table 2). The constant modulation was employed (the same proposed by IEC 61000-4-7 for fluctuating harmonics). In order to better appreciate the large differences, results are plotted in logarithmic scale. The significantly lower RMSE for the proposed WPD method means a

higher overall accuracy of the proposed method. Figures 8 and 9 present the same analysis, but using the linear modulation and the flicker-type modulation, respectively.

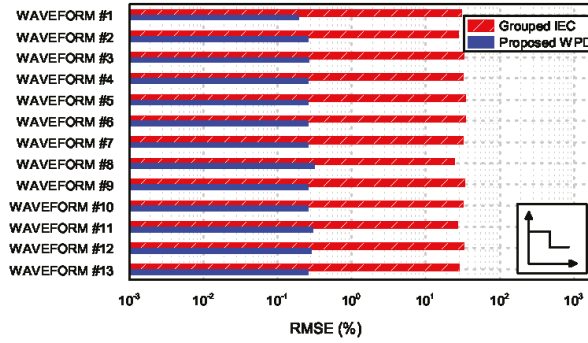


Figure 7. RMSE for each assessed waveform under fluctuating conditions, for grouped IEC and WPD, in the case of constant modulation.

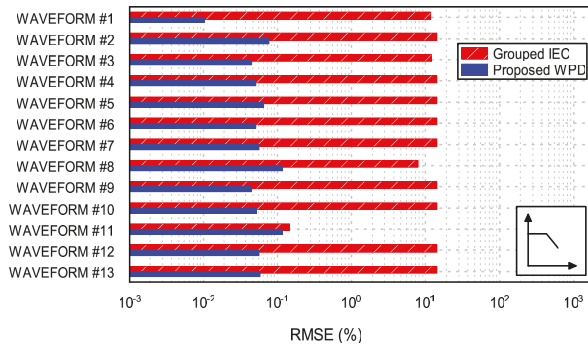


Figure 8. RMSE for each assessed waveform under fluctuating conditions, for grouped IEC and WPD, in the case of linear modulation (motor-start type).

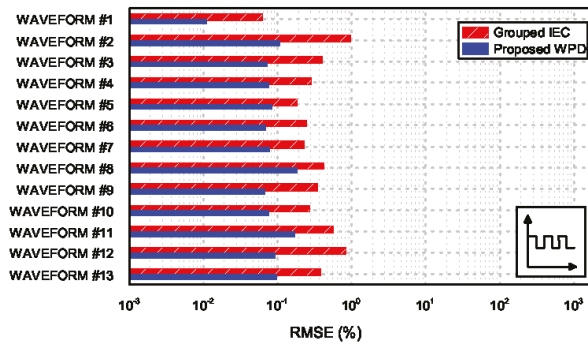


Figure 9. RMSE for each assessed waveform under fluctuating conditions, for grouped IEC and WPD, in the case of flicker-type rectangular modulation.

It can be seen that the overall accuracy of the WPD method was always significantly superior to the grouped FFT, for all the tested waveforms and types of modulations. The only case where the overall accuracy of WPD was comparable with the grouped FFT was the case of Waveform 11 (square wave) with the linear modulation. However, even in this extremely non-realistic case, WPD showed a better performance. Table A1, reported in Appendix A, provides a summary of the maximum errors obtained in the calculation of individual harmonic components, for all the assayed waveforms, in the four validation scenarios (stationary and fluctuating). It can be seen that the maximum error never exceeded 1%, with the maximum obtained error being 0.678%. Although this was far from being a mathematical formulation of the error, it could be considered as an indication of the accuracy of the proposed method.

4.4. Computational Effort

A drawback of the proposed WPD method could be the high number of operations that must be performed. At each level of decomposition, the number of filtering operation increased exponentially, although the decimation allowed reducing the number of samples that were convolved with the filter coefficients. In order to characterize the computational effort required, a comparison was performed by analyzing the same waveform, under the same conditions, with both methods. Although it did not represent an exhaustive study of the computational complexity, a comparison of the time required by the two methods on the same computer, for the same signal, and under the same operating conditions can be considered as an indication of the relationship between the computational effort of the two methods. The same analysis was repeated 1000 times for each of the 13 waveforms described in Section 4.1, and later, the 13,000 results were averaged. The results, obtained on a 3.00 GHz Intel Core i5-7400 CPU with 16 MB RAM computer, are reported in Table 3.

Table 3. Comparison of the average computational time for both methods on the same computer.

Computational Time (FFT) (s)	Computational Time (WPD) (s)	Ratio WPD/FFT
3.6×10^{-4}	5.2×10^{-2}	148

As can be seen, the time required by the proposed WPD algorithm resulted in being, on average, 148-times higher than FFT. However, it can be seen that, at least on the testing machine, the method had the capability of being performed online, since the time required for the calculation was less than the duration of the analyzed signal, i.e., 10 cycles of the power frequency (approximately 200 ms). A possible strategy to reduce the computation time is to implement the proposed method on an Field Programmable Gate Array (FPGA) since the structure, based on the iterative application of the same filter, is particularly suitable for hardware implementation and the time reduction could be significant, as demonstrated by recent works [23,30].

5. Analysis of Real Signals

The newly proposed method, after being validated, was employed to analyze real waveforms. In order to obtain real waveforms, measurements were taken at the point of connection of an Active Front End (AFD) device. It as a three leg 50 kW converter, with a 20 kHz switching frequency. Current and voltage waveforms were acquired using a NI PXIe-6124 module (installed on an NI PXIe-1071 chassis), equipped with a Pico TA044 70 MHz 7000 V differential voltage probe and a Tektronix TCP2020 50 MHz 20 A AC/DC current probe. The assayed AFD was designed to obtain low power losses, high efficiency (>96%), and most importantly, to produce low harmonic distortion. At nominal power, the THD was less than 0.6%. Therefore, in order to obtain signals with higher harmonic content, the harmonic distortion was enhanced by operating the device at 5% of its nominal power. In this way, the fundamental current was greatly reduced, while the harmonic components were only slightly reduced, increasing the current THD up to 50%.

The top graphs of Figure 10a,b show the acquired voltage and current waveforms, respectively, with a total duration of 10 cycles of the fundamental (approximately 0.2s), according to the IEC 61000-4-7 standard. It must be noted that in these cases, the error could not be calculated since the real energy content of each harmonic group was not known a priori. For this reason, the bottom plots of Figure 10a,b show the absolute difference between the RMS values obtained with the two methods, for each harmonic group, and not the error. Hence, it is not possible to know which method performed better, but only how different the results could be from each other. The voltage waveform in Figure 10a offers the possibility to analyze a mostly stationary signal. It can be observed that, in this case, the results obtained with the proposed WPD method were very similar to those obtained with the IEC method, and the differences between RMS values were close to zero for all harmonic orders. On the other hand, the current waveform in Figure 10b has a visible fluctuating character, offering the possibility to test the proposed WPD method with a real non-stationary signal. In this case, the differences between the two methods were higher, up to almost 1%. These results confirmed the conclusions of Section 4, i.e., that the WPD method was equally valid as the IEC Fourier strategy for analyzing stationary signals, but that differences arise under fluctuating conditions, where FFT is known to be inaccurate.

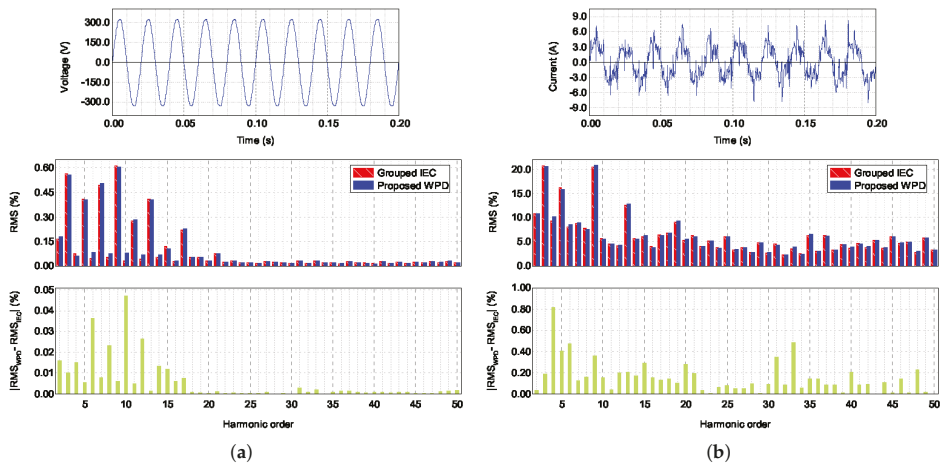


Figure 10. Analysis of real waveforms with a stationary (a) and non-stationary (b) character. The top graphs show the waveforms in the time domain, the middle graphs the harmonic content, and the bottom graphs the absolute difference between the proposed method and the IEC strategy.

6. Conclusions

This paper presented the validation and characterization of a wavelet based method for the accurate assessment of harmonic content in power systems under stationary and non-stationary conditions, using a WPD algorithm. Although other methods have been proposed in the last few years, some of them even using wavelets, Fourier analysis is still the preferred choice for power quality analyzers and the recommended approach according to IEC standards. It is however evident that Fourier analysis is inadequate for assessing harmonic content under non-stationary conditions, which is the most common situation in power systems. Even IEC 61000-4-7 recognizes this limitation, proposing a grouping strategy for adapting FFT to fluctuating harmonics. The IEC grouping strategy, however, can produce large errors in the case of fluctuating signals, as shown in this paper. The proposed method was therefore compared not only to standard FFT, but also to the IEC grouped FFT method, showing its superior performance with respect to both. After verifying compliance with the IEC precision requirements and validating the method using simulated waveforms with real harmonic

content, the method was employed to measure real voltage and current signals. This produced results similar to those obtained in the validation. The reliability of the method was clearly proven, and its performance was superior under fluctuating conditions. On the one hand, researchers are more and more transitioning to more reliable tools, while on the other hand, no methods have been shown to be able to comply with IEC standards and at the same time be precise enough to measure fluctuating harmonics. This paper intended to fill the gap between the research community and the application in the field, illustrating and validating a method whose performance was largely superior to the grouped FFT in assessing fluctuating harmonics. Moreover, the proposed method was shown to perform better than grouped FFT even under stationary conditions, and in the few cases when it did not perform better, the error was always within the IEC accuracy limits for steady-state signals. Lastly, the proposed frequency bands, time window, and bandwidth were, for the first time, compliant with the IEC 61000-4-7 and IEC 61000-4-30 requirements. This was achieved by an accurate selection of the decomposition tree and filter characteristics. The features of the proposed method made it suitable for implementation in Class I Power Quality analyzers, allowing a highly accurate estimation of harmonic content in power systems, both in stationary and non-stationary conditions.

Author Contributions: Conceptualization, J.J.M. and J.B.; methodology, J.B. and S.L.; validation, J.B., S.L., and J.J.M.; formal analysis, S.L.; investigation, J.B. and S.L.; data curation, J.B. and S.L.; writing, original draft preparation, J.B. and S.L.; writing, review and editing, J.J.M. and J.F.S.; supervision, J.J.M. and J.F.S.

Funding: This paper has received funding from the European Union's Horizon 2020 research and innovation program under Marie Skłodowska-Curie Grant Agreement No. 676042.

Conflicts of Interest: The authors declare no conflict of interest.

Appendix A

Table A1 shows the maximum error ϵ_{\max} obtained with the proposed WPD method in each of the 13 tests described in Sections 4.2 and 4.3, reporting the harmonic order that registered the maximum error. For each test type (modulation), the maximum error obtained among all waveforms is identified in bold. The maximum error overall is marked with a star (*).

Table A1. Maximum errors obtained for each validation assay.

ID	Stationary		Constant		Linear		Rectangular	
	ϵ_{\max} (%)	Order	ϵ_{\max} (%)	Order	ϵ_{\max} (%)	Order	ϵ_{\max} (%)	Order
1	0.048	2	0.079	1	0.041	2	0.048	2
2	0.416	5	0.504	5	0.281	3	0.486	5
3	0.416	5	0.514	5	0.271	5	0.479	5
4	0.374	5	0.458	5	0.232	5	0.428	5
5	0.322	4	0.372	5	0.285	4	0.327	4
6	0.319	5	0.390	5	0.184	4	0.341	5
7	0.348	5	0.428	5	0.213	4	0.394	5
8	0.589	7	0.625	7	0.446	7	0.678 *	5
9	0.363	5	0.443	5	0.221	5	0.406	5
10	0.366	5	0.449	5	0.225	5	0.418	5
11	0.566	7	0.667	5	0.437	2	0.671	5
12	0.401	5	0.488	5	0.258	5	0.462	5
13	0.397	5	0.484	5	0.254	5	0.476	5

References

1. Kalair, A.; Abas, N.; Kalair, A.R.; Saleem, Z.; Khan, N. Review of harmonic analysis, modeling and mitigation techniques. *Renew. Sustain. Energy Rev.* **2017**, *78*, 1152–1187. [[CrossRef](#)]
2. Sharma, H.; Rylander, M.; Dorr, D. Grid impacts due to increased penetration of newer harmonic sources. *IEEE Trans. Ind. Appl.* **2016**, *52*, 99–104. [[CrossRef](#)]
3. Liang, X. Emerging Power Quality Challenges Due to Integration of Renewable Energy Sources. *IEEE Trans. Ind. Appl.* **2017**, *53*, 855–866. [[CrossRef](#)]
4. Moeed Amjad, A.; Salam, Z. A review of soft computing methods for harmonics elimination PWM for inverters in renewable energy conversion systems. *Renew. Sustain. Energy Rev.* **2014**, *33*, 141–153. [[CrossRef](#)]
5. Electromagnetic Compatibility (EMC)—Part 4-7: Testing and Measurement Techniques—General Guide on Harmonics and Interharmonics Measurements and Instrumentation, for Power Supply Systems and Equipment Connected Thereto. IEC 61000-4-7:2002+AMD1:2008.
6. IEEE Recommended Practices and Requirements for Harmonic Control in Electrical Power Systems. In IEEE Std. 519-2014; IEEE, 2014.
7. Clarkson, P.; Wright, P.S. A wavelet based method of measuring fluctuating harmonics for determining the filter time constant of IEC standard harmonic analyzers. *IEEE Trans. Instrum. Meas.* **2005**, *54*, 488–491. [[CrossRef](#)]
8. Jain, S.K.; Singh, S.N. Harmonics estimation in emerging power system: Key issues and challenges. *Electr. Power Syst. Res.* **2011**, *81*, 1754–1766. [[CrossRef](#)]
9. Mostarac, P.; Malarić, R.; Mostarac, K.; Jurčević, M. Noise reduction of power quality measurements with time-frequency depth analysis. *Energies* **2019**, *12*, 1052. [[CrossRef](#)]
10. Wang, C.; Yang, R.; Yu, Q. Wavelet transform based energy management strategies for plug-in hybrid electric vehicles considering temperature uncertainty. *Appl. Energy* **2019**, *256*, 113928. [[CrossRef](#)]
11. Telesca, L.; Guignard, F.; Helbig, N.; Kanevski, M. Wavelet Scale Variance Analysis of Wind Extremes in Mountainous Terrains. *Energies* **2019**, *12*, 3048. [[CrossRef](#)]
12. Zhu, H.; Li, X.; Sun, Q.; Nie, L.; Yao, J.; Zhao, G. A power prediction method for photovoltaic power plant based on wavelet decomposition and artificial neural networks. *Energies* **2016**, *9*, 11. [[CrossRef](#)]
13. Avdakovic, S.; Lukac, A.; Nuhanovic, A.; Music, M. Wind speed data analysis using wavelet transform. *World Acad. Sci. Eng. Technol.* **2011**, *51*, 829–833.
14. Karmacharya, I.M.; Gokaraju, R. Fault Location in Ungrounded Photovoltaic System Using Wavelets and ANN. *IEEE Trans. Power Deliv.* **2018**, *33*, 549–559. [[CrossRef](#)]
15. Yoon, W.K.; Devaney, M.J. Reactive power measurement using the wavelet transform. *IEEE Trans. Instrum. Meas.* **2000**, *49*, 246–252. [[CrossRef](#)]
16. Morsi, W.G.; El-Hawary, M.E. On the application of wavelet transform for symmetrical components computations in the presence of stationary and non-stationary power quality disturbances. *Electr. Power Syst. Res.* **2011**, *81*, 1373–1380. [[CrossRef](#)]
17. Deokar, S.A.; Waghmare, L.M. Integrated DWT-FFT approach for detection and classification of power quality disturbances. *Int. J. Electr. Power Energy Syst.* **2014**, *61*, 594–605. [[CrossRef](#)]
18. De Apráiz, M.; Barros, J.; Diego, R.I. A real-time method for time-frequency detection of transient disturbances in voltage supply systems. *Electr. Power Syst. Res.* **2014**, *108*, 103–112. [[CrossRef](#)]
19. Latran, M.B.; Teke, A. A novel wavelet transform based voltage sag/swell detection algorithm. *Int. J. Electr. Power Energy Syst.* **2015**, *71*, 131–139. [[CrossRef](#)]
20. Alves, D.K.; Costa, F.B.; de Araujo Ribeiro, R.L.; de Sousa Neto, C.M.; de Oliveira, T. Power Measurement Using the Maximal Overlap Discrete Wavelet Transform. *IEEE Trans. Ind. Electron.* **2017**, *64*, 3177–3187. [[CrossRef](#)]
21. Hamid, E.Y.; Yokoyama, N.; Kawasaki, Z.I. Rms and Power Measurements: A Wavelet Packet Transform Approach. *IEEE Trans. Power Energy* **2002**, *122*, 599–606. [[CrossRef](#)]
22. Eren, L.; Unal, M.; Devaney, M.J. Harmonic Analysis Via Wavelet Packet Decomposition Using Special Elliptic Half-Band Filters. *IEEE Trans. Instrum. Meas.* **2007**, *56*, 2289–2293. [[CrossRef](#)]
23. Tiwari, V.K.; Umarikar, A.C.; Jain, T. Fast Amplitude Estimation of Harmonics Using Undecimated Wavelet Packet Transform and Its Hardware Implementation. *IEEE Trans. Instrum. Meas.* **2017**, *1*–13. [[CrossRef](#)]

24. Diego, R.I.; Barros, J. Global Method for Time-Frequency Analysis of Harmonic Distortion in Power Systems Using the Wavelet Packet Transform. *Electr. Power Syst. Res.* **2009**, *79*, 1226–1239. [[CrossRef](#)]
25. Barros, J.; Diego, R.I. Analysis of Harmonics in Power Systems Using the Wavelet Packet Transform. *IEEE Trans. Instrum. Meas.* **2008**, *57*, 63–69. [[CrossRef](#)]
26. Bruna, J.; Melero, J.J. Selection of the Most Suitable Decomposition Filter for the Measurement of Fluctuating Harmonics. *IEEE Trans. Instrum. Meas.* **2016**, *65*, 2587–2594. [[CrossRef](#)]
27. Mallat, S.G. *A Wavelet Tour of Signal Processing*, 2nd ed.; Academic Press: Cambridge, MA, USA, 1999.
28. NPL. Power Quality Waveform Library. Available online: <http://resource.npl.co.uk/waveform/> (accessed on 30 October 2019).
29. Brekke, K.; Seljeseth, H.; Mogstad, O. Rapid Voltage Changes—Definition and Minimum Requirements. In Proceedings of the 20th International Conference on Electricity Distribution (CIRED), Prague, Czech Republic, 8–11 June 2009. [[CrossRef](#)]
30. Tiwari, V.K.; Jain, S.K. Hardware Implementation of Polyphase-Decomposition-Based Wavelet Filters for Power System Harmonics Estimation. *IEEE Trans. Instrum. Meas.* **2016**, *65*, 1585–1595. [[CrossRef](#)]



© 2019 by the authors. Licensee MDPI, Basel, Switzerland. This article is an open access article distributed under the terms and conditions of the Creative Commons Attribution (CC BY) license (<http://creativecommons.org/licenses/by/4.0/>).

Article

Small Signal Stability with the Householder Method in Power Systems

Asghar Sabati ^{1,*}, Ramazan Bayindir ², Sanjeevikumar Padmanaban ^{3,*}, Eklas Hossain ⁴ and Mehmet Rida Tur ⁵

¹ Energy R&D Center, EUROPOWER, PC 06980 Ankara, Turkey

² Department of Electrical & Electronics Engineering, Gazi University, PC 06500 Ankara, Turkey

³ Department of Energy Technology, Aalborg University, 6700 Esbjerg, Denmark

⁴ Oregon Renewable Energy Center (OREC), Department of Electrical Engineering and Renewable Energy, Oregon Tech, Klamath Falls, OR 97601, USA

⁵ Department of Electrical & Energy Engineering, Batman University, PC 72500 TBMYO, Batman, Turkey

* Correspondence: asker.sabati@europowerenerji.com.tr (A.S.); san@et.aau.dk (S.P.)

Received: 1 August 2019; Accepted: 30 August 2019; Published: 4 September 2019

Abstract: Voltage collapse in power systems is still considered the greatest threat, especially for the transmission system. This is directly related to the quality of the power, which is characterized by the loss of a stable operating point and the deterioration of voltage levels in the electrical center of the region exposed to voltage collapse. Numerous solution methods have been investigated for this undesirable degradation. This paper focuses on the steady state/dynamic stability subcategory and techniques that can be used to analyze and control the dynamic stability of a power system, especially following a minor disturbance. In particular, the failure of one generator among the network with a large number of synchronous generators will affect other synchronous generators. This will become a major problem and it will be difficult to find or resolve the fault in the network due to there being too many variables, consequently affecting the stability of the entire system. Since the solution of large matrices can be completed more easily in this complex system using the Householder method, which is a small signal stability analysis method that is suggested in the thesis, the detection of error and troubleshooting can be performed in a shorter period of time. In this paper, examples of different rotor angle deviations of synchronous generators were made by simulating rotor angle stability deviations up to five degrees, allowing the system to operate stably, and concluding that the system remains constant.

Keywords: rotor angle; small signal stability; householder algorithm; power systems

1. Introduction

Developing technology, ever-growing urbanization and environmental conditions have forced energy systems to work close to the stability limit. This has increased the importance given to the subject of voltage stability and it has become much more important. The stability of a power system is the ability to keep the amplitudes of continuous or transient load bus bars within certain limits. In addition, voltage stability is the ability of these power systems to return to their former stable state when confronted with a disturbing effect and to retain the voltage in all bus bars within a certain level. One of the criteria for qualifying a system as a stable system is if the power given to a bus bar increases numerically, the amplitude of the voltage in that bus bar increases and this process proceeds similarly for all other bus bars in the system. If the reactive power given to that bus bar is increased in any of the bus bars in the system, and the voltage amplitude does not increase, it can then be said that there is voltage instability in this system [1]. Also, if the V-Q sensitivity for each bus bar is directly proportional or positive, the system is stable in terms of voltage. Thus, if the V-Q sensitivity is negative

for at least one bus bar, the system voltage is unstable. Failure of power systems to reach a voltage stability state is referred to as a “voltage failure”, which occurs in the event of overload, failure, or insufficient reactive power. In recent years, the voltage stability problem called voltage collapse has been experienced quite a lot. This has led to an increase in voltage stability studies [2,3]. In some studies, solutions are made by providing a methodology aimed at maintaining frequency stability by taking into account the latency associated with the frequency measurement process, while acquiring virtually equal inertia limitations from virtual operational generators [4]. Voltage stability and voltage instability are described depending on the size of static faults that may occur [5]. The oscillations in power systems raise voltage-related problems along with a small signal stability problem, which is one of the most important factors that limit power transmission capacity and jeopardize safe operation [6,7]. Analytical solutions and mathematical models were used to analyze the effect of stochastic continuous disturbances on the power system small signal stability [8,9].

This study aims to estimate the modal characteristics of the system including modal frequency, damping and shape. Most of the signal processing algorithms described in this section are the basis of developing several software tools. The majority of these tools are used to perform an engineering analysis on the grid in an offline or post-degradation environment [10]. Online real-time software tools and applications have recently been developed [11] and will continue to be the focus of research for the power system community. Voltage stability is sometimes referred to as load balancing [12]. The terms voltage instability and voltage collapse are often used interchangeably. Voltage instability is a dynamic process involving voltage dynamics, as opposed to rotor angle (synchronous) stability. Voltage collapse is defined as a process in which voltage instability in a significant portion of the system leads to a very low voltage profile. The voltage instability limit is not directly connected to the maximum power transmission limit of the grid [5,11,12]. Generally, local modes are in the range of 1–2 Hz, while in-field modes can range from 0.2 to 1.0 Hz [13]. Typically, in-field modes cause a little more trouble. Consistent with the dynamic system of a power system, it can be linearized at an operating point of the power system [10,11]. The proposed method offers an advantage for the difficulty of stability analysis of nonlinear systems. In addition, it is impossible to practically analyze very large powerful complex systems. The systems examined in this article are not actually of a linear nature. Since the deviations occurring at the equilibrium are small (small signal), they can be approximated to the linear system. Therefore, instead of analyzing the nonlinear system, we can analyze the system approximated to being linear, which is easier.

Stability in a power system means that the system normally has the desired parameters. In other words, it can be defined as the ability of the system to return to its nominal state in a short period in case of a failure. In some studies, a small signal and a large signal stability analysis were performed using the Lyapunov linearization method. A combined stability criterion was then proposed to predict small and large signal stability problems [14–16]. In a power system, when the system is in a stable state, there is equilibrium between the incoming mechanical momentum and the outgoing electrical momentum. This equilibrium causes the velocity to remain constant. When short-circuit faults are also included, the equilibrium may be explained in terms of static stability. If an error occurs between power systems, the balance between the incoming mechanical momentum and the outgoing electrical momentum is relatively eliminated. According to the law of motion of rotating objects, the synchronous machine rotor will have a positive or negative speed, so it will rotate at high or low speed compared to other generators. This uncoordinated rotation will alter the stability of the system by changing the rotor angle. Furthermore, this problem is solved by using an approach based on the largest Lyapunov base for online transient rotor angle stability assessment using data from large area measurement systems only [17,18].

Thanks to the studies conducted on maintaining small signal stability, a few advantages in large power systems will be addressed. One of the benefits of small signal stability is that each synchronous generator present in the system can be linearized around the operating point. However, differential equations need to be solved systematically in transient stability, where the differential equations that

dominate the pre-fault system, the during-fault power system, and the equations that dominate the post-fault system must be solved. Furthermore, if the protection relays do not work in the system during this time, the system will lose its synchronized state. It is not possible to find differential equations, even when solved in a systematic manner, that determine the cleaning time and security index in the relays after the fault. In order to find the critical time, the system needs to be simulated several times in all error-occurring situations, which will result in a great loss of time, and the fact that the system inspects its behavior for errors will reduce the time to intervene and cause even more time loss. However, the time spent in inspection of small signal stability is between 10 and 20 s. In the case of small signal stability, the stability of the system can be determined very easily through the master data, and only the positive or negative data will be sufficient to examine the stability of the system, without the need to inspect the data even after the calculations.

This article provides an overview of the challenges applied to the prediction of time-synchronized data of more successful analysis techniques of electromechanical mode. The theoretical basis, applications and performance characteristics of these methods are explained. When inter-zone modes are studied in a power system, several generators fluctuate in the opposite direction compared to other generators due to other failures. This is caused by a connection of two groups of generators over a weak line. The frequency of these fluctuations is between 0.2 and 1 Hz. Regional and comprehensive modes are today's most modern modes and are studied in stability studies of power systems. As modern power systems are directly connected to each other, the connection lines are often outdated and due to their high costs, the renewal of the lines is avoided. Despite the construction of new power plants, inter-regional fluctuations often occur because these power plants are connected to power systems through weak lines. Many PSS studies today are focused on power systems. The PSS system should not use local signals. However, it can use signals from other regions as input signals. In this case, too, a delay may occur when the signal is sent from other regions, which may impair the small signal stability. When there are multiple synchronous machines, the variable parameters will increase, and the mathematical analysis of the system will become more difficult. It is very difficult to find the determinant of a large matrix. Therefore, the straightforward method can only be discussed theoretically, but it does not have much use in practice. In the determination of the main quantities by means of numerical methods such as the square method, inverse square method and the Arnold method, the largest main amount is obtained in terms of absolute magnitude. Consequently, different measures should be taken to find other main quantities. For this reason, the method of similar transformations is one of the practical methods. In the Gionesis Rotation method, which is based on orthogonal similarities, only one element in the given matrix is reset at each stage after transformation. Because of repeated transformations, the given matrix is orthogonally homologized to an upper triangle or Hasenberg Matrix. Thus, the given matrix can be decomposed as QR (Q, an orthogonal matrix; R, an upper triangular matrix). The main advantage of the Householder method presented in this article is that each column of the given matrix is transformed into the column of an upper-triangular matrix at each transformation stage. This method is important when compared particularly to the Gionesis method because, in the Gionesis method, for the transformation of an $(n \times n)$ matrix to an upper-triangular matrix, a conversion (matrix multiplication) operation must be performed $n(n - 1/2)$ times. However, the conversion operation must be performed, at most, n times in the Householder method. In numerical terms of the data, the number of computational operations is important, because rounded errors can accumulate due to the large number of operations and ultimately have an impact on the result. In particular, when the actual specific quantities are close to zero, these rounded errors may not be able to determine the sign of that main quantity. Therefore, the method presented is of great importance—both in terms of the number of computational operations and in terms of obtaining all the main quantities—and has undeniable superiority over similar methods.

2. Materials and Methods

2.1. Mathematical Model of Small Signal Problems

Synchronizing and Damping Momentums: When a short circuit occurs, the momentum of a synchronous machine is divided into two components. In order for a power system to exist, both components must be present. The lack of synchronizing momentums in a power system leads to instability that is dependent on the rotor angle and is not of the fluctuation type. The lack of damping momentums causes fluctuation instability. If one generator runs temporarily faster than the other does, the angular position of the rotor will increase in connection to that of the slow machine. The resulting angular difference transfers a portion of the load from the slow machine to the fast machine based on the theoretically known power angle relationship. This tends to reduce the speed difference and therefore the angular aperture. Further angular aperture may lead to a decrease in power transfer, leading to greater instability [19].

$$\Delta T_e = T_s \Delta \delta + TD \Delta \omega \tag{1}$$

$T_s \Delta \delta$: Synchronous momentum;

T_s : Coefficient of synchronous momentum;

$TD \Delta \omega$: Damping momentum (has the same phase as $\Delta \omega$);

TD : Coefficient of damping momentum.

This involves the protection of predetermined bus voltages by a power system to reach a stable state after a fault or short circuit occurs [20]. Therefore, the main reason for the instability in voltage is that the power system fails to provide reactive power. In other words, because the reactive power is directly proportional to the voltage, the electric power system has not been able to provide the reactive power required in its network well [1,21]. If for some reason (such as the input or output of a large production unit) the voltage drops in a part of the network and other generators or systems that compensate for the reaction power return to the current system, the voltage returns to its normal state [22]. Otherwise, the voltage drop will reach an unacceptable value and cause a power failure in another part of the power system network, which is called a voltage collapse [3,23,24].

2.2. Definition of the Single Machine Infinite Bus (SMIB)

The infinite bus is a source of voltage with constant voltage and frequency. Due to the infinite bus, the generator dynamics will not change EB voltage and frequency. In terms of small signal stability, both space- and block-type display methods are used to represent the small signal. In topics related to stability, the classical model is used to model the generator [25]. In this model shown as Figure 1, the generator is modeled as a voltage source connected to the reactance; however, all resistances in the generator or synchronous machine are ignored.

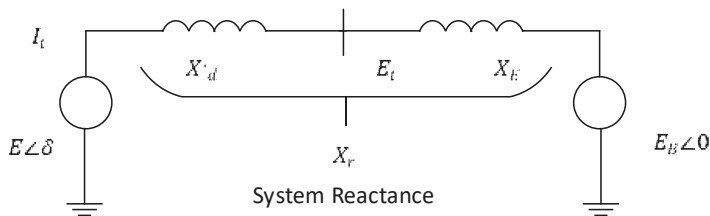


Figure 1. Classic model diagram in a Single Machine Infinite Bus (SMIB) system.

Calculation of complex and active forces in the network using flow equations:

$$X_T = X'_d + X_E \tag{2}$$

$$\tilde{I}_t = \frac{E'_{\angle 0} - E_{B\angle -\delta}}{jX_T} = \frac{E' - E_B(\overbrace{\cos\delta - j\sin\delta}^{\delta})}{jX_T} \tag{3}$$

'p' is the power of air distance. p does not indicate the voltage of the terminal generator. However, since the stator resistance is ignored while the generator model is conventionally shown, P is also shown as the power of the terminal generator so that other analyzes can be performed.

$$S = P + jQ = \tilde{E} \tilde{I}_t \tag{4}$$

$$S = \frac{E'E_B}{X_T} \sin\delta + j \frac{E'(E' - E_B \cos\delta)}{X_T} \tag{5}$$

Another important point is that the air distance momentum is equal to the air distance power. The air distance momentum is as in Equation (6).

$$T_e = P = \frac{E'E_B}{X_T} \sin\delta \tag{6}$$

One of the most important equations related to rotor angle stability is the air distance momentum equation, and the other is the fluctuation equation (motion equation) [26].

2.2.1. Linearization Model of Equations in Small Signal Stability (Sinδ, Cosδ)

In order to achieve small signal stability, the air distance momentum must be converted to a linear equation around the working point δ = δ0. To achieve this goal, first the sine in the air distance equation is linearized, so that the entire air distance equation can then be linearized [27]. Sinδ, Cosδ linearization around δ = δ0 equilibrium: a small deviation indicated by Δδ can be linearized as in the following equations:

$$\Delta\delta = \delta - \delta_{0} \Rightarrow \delta = \Delta\delta + \delta_{0} \tag{7}$$

δ0 = rotor angle at equilibrium

Based on Sinδ, Cosδ equations and trigonometric relations:

$$\cos\delta = \cos(\delta_0 + \Delta\delta) = \cos\delta_0 \cdot \cos\Delta\delta - \sin\delta_0 \cdot \sin\Delta\delta \tag{8}$$

$$\sin\delta = \sin(\delta_0 + \Delta\delta) = \sin\delta_0 \cdot \cos\Delta\delta + \cos\delta_0 \cdot \sin\Delta\delta \tag{9}$$

The most important result obtained from the above equations is Δδ = 1.

$$\begin{cases} \cos(\delta_0 + \Delta\delta) = \cos\delta_0 + \Delta\delta \cdot \sin\delta_0 \\ \cos(\delta_0 + \Delta\delta) - \cos\delta_0 = \Delta\delta \cdot \sin\delta_0 \\ \sin(\delta_0 + \Delta\delta) - \sin\delta_0 = \Delta\delta \cdot \cos\delta_0 \end{cases} \tag{10}$$

Considering the above equations, when Te becomes linear at the working point δ = δ0, it becomes as follows in Equation (11).

$$T_e = \frac{\partial T_e}{\partial \delta} \Delta\delta = \frac{EE'_B}{X_T} \cos\delta_0 (\Delta\delta) \tag{11}$$

$$\begin{cases} \frac{d\Delta\omega_r}{dt} = \frac{1}{2H} (T_m - T_e - K_D \Delta\omega_r) \\ \frac{d\delta}{dt} = \omega_0 \Delta\omega_r \end{cases} \tag{12}$$

$$\Rightarrow \begin{cases} \frac{d\Delta\omega_r}{dt} = \frac{1}{2H} (T_m - K_s \Delta\delta - K_D \Delta\omega_r) \\ \frac{d\delta}{dt} = \omega_0 \Delta\omega_r \end{cases} \tag{13}$$

Tm: Mechanical momentum;

Ks: Synchronous momentum coefficient.

$$K_s = \left[\frac{E'E_B}{X_T} \right] \text{Cos}\delta_0 T_e = P = \frac{E'E_B}{X_T} \text{Sin}\delta \tag{14}$$

Small signal stability can be analyzed by obtaining the master data. The representation of the linearized equation in the space matrix is as in Equation (15).

Ks: Synchronous momentum coefficient;
 KD = Stabilizer momentum coefficient (stabilizer);

$$\begin{aligned} \dot{X} &= AX + BU \\ \begin{bmatrix} \Delta\dot{\omega}_r \\ \dot{\Delta\delta} \end{bmatrix} &= \underbrace{\begin{bmatrix} -\frac{KD}{2H} & -\frac{K_s}{2H} \\ \omega_0 & 0 \end{bmatrix}}_A \begin{bmatrix} \Delta\omega_r \\ \Delta\delta \end{bmatrix} + \underbrace{\begin{bmatrix} \frac{1}{2H} \\ 0 \end{bmatrix}}_B \Delta T_m \end{aligned} \tag{15}$$

H = Coefficient of inertia.

Equations belonging to the system are determined by considering the input and output of the system; then the system’s main data is found using these equations and the system’s small signal stability can be examined [28].

$$\Delta\delta = \frac{\omega_0}{S} \left[\frac{1}{2HS} (-K_s\Delta\delta - K_D\Delta\omega_r + \Delta T_m) \right] \tag{16}$$

$$\Delta\delta = \frac{\omega_0}{S^2} \left[\frac{1}{2HS} (-K_s\Delta\delta - K_D S \frac{\Delta\delta}{\omega_0} + \Delta T_m) \right] \tag{17}$$

$$S^2(\Delta\delta) + \frac{kD}{2H} S(\Delta\delta) + \frac{ks}{2H} \omega_0(\Delta\delta) = \frac{\omega_0}{2H} \Delta T_m \tag{18}$$

$$\frac{\Delta\delta}{\Delta T_m} = \frac{\frac{\omega_0}{2H}}{S^2 + \frac{kD}{2H}S + \frac{ks \cdot \omega_0}{2H}} \tag{19}$$

At this stage, in order to find the main data, the Equation (20) must be equal to zero [29].

$$S^2 + \frac{kD}{2H}S + \frac{ks \cdot \omega_0}{2H} = 0 \tag{20}$$

The general representation of second-order equations will be as in Equation (21): ζ = Stability ratio

$$S^2 + 2\xi\omega_n S + \omega_n^2 = 0 \tag{21}$$

The equations belonging to ω_n ve ζ can also be found using the equations in Equations (20) and (21):

$$\omega_n = \sqrt{k_s \frac{\omega_0}{2H} \left(\frac{\text{rad}}{\text{s}} \right)} \tag{22}$$

$$\xi = \frac{1}{2} \frac{kD}{2H\omega_n} = \frac{1}{2} \frac{kD}{\sqrt{k_s 2H\omega_0}} \tag{23}$$

- a. As Ks increases; the natural frequency increases, the stability rate decreases.
- b. The stability ratio increases as kD increases.
- c. As H increases, both the ω_n rate and the stability rate ζ decrease [30].

2.2.2. Control of Dynamic Systems

In a dynamic system, xi variables of the system affect each other. Each variable of the system is a function in terms of time. The aim of the analysis of dynamic systems is to examine the future

behavior of the system. These behaviors include the determination of critical points and limit circles, examination of system stability, chelation, and chaos control.

If there is no change in rotor angle and speed, i.e., $\Delta\omega(0) = \Delta\delta(0) = 0$, and no change in mechanical momentum, the system will remain stable as per $\Delta T_m(t) = 0$. For example, $\Delta T_m t = 0$, $\Delta\omega_0 = 0$, $\Delta\delta_0 = 50 \approx 0.0875$ Rad; in this case, $KD = 10$, $KS = 0.757$, $H = 3.5$, $\omega_0 = 377.0\delta$

$$\begin{bmatrix} \Delta\dot{\omega} \\ \Delta\dot{\delta} \end{bmatrix} = \begin{bmatrix} \frac{-10}{7} & \frac{-0.757}{7} \\ 377.0 & 0 \end{bmatrix} \begin{bmatrix} \Delta\omega \\ \Delta\delta \end{bmatrix} + \begin{bmatrix} \frac{1}{7} \\ 0 \end{bmatrix} 0$$

$$= \begin{bmatrix} \frac{-10}{7} & \frac{-0.757}{7} \\ 377.0 & 0 \end{bmatrix} \begin{bmatrix} \Delta\omega \\ \Delta\delta \end{bmatrix}$$

$$\det\left(\begin{bmatrix} \frac{-10}{7} - \lambda & \frac{-0.757}{7} \\ 377.0 & 0 - \lambda \end{bmatrix}\right) = 0$$

$$\begin{cases} \lambda_1 = -0.7143 + 6.3450i; \\ \lambda_2 = -0.7143 - 6.3450i; \end{cases}$$

The real portions of both quantities are negative, so the system is stable shown as Figure 2.

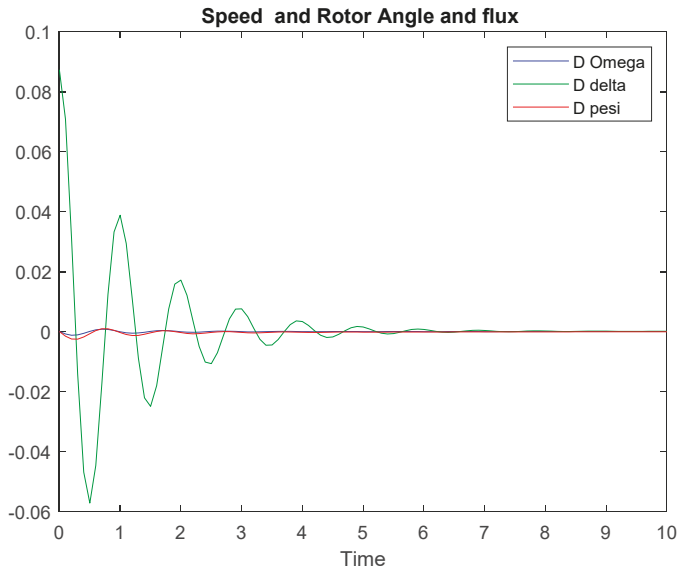


Figure 2. Diagram of the simulation of the rotor angle and speed changes up to 10 s.

If the damper coefficient becomes 0 ($KD = 0$) in the above example, the response and master data of the system will be as follows in Figure 3.

$$\begin{cases} \lambda_1 = -0.7143 + 6.3450i; \\ \lambda_2 = -0.7143 - 6.3450i; \end{cases}$$

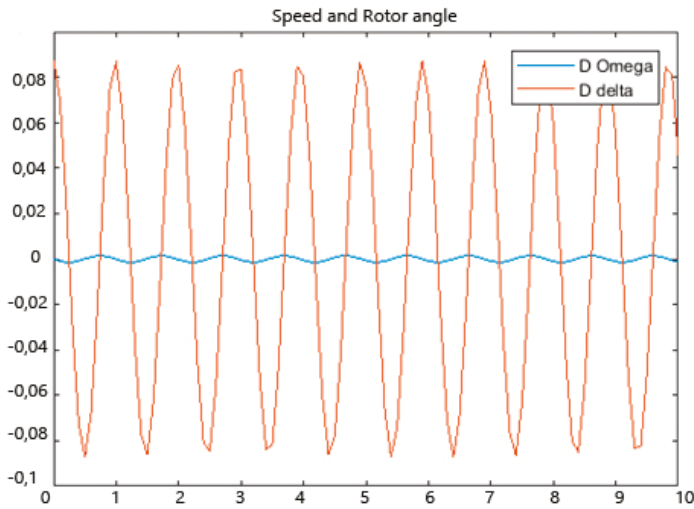


Figure 3. Response diagram of the system fluctuating between stability and instability.

The real part of both master data is equal to zero. Therefore, the system does not go towards zero (stability) or infinity (instability). Instead, it continues its own fluctuation state. In another case shown as Figure 4, if the damping coefficient always changes as $KD = -10$, the master data and the response diagram of the system change as follows:

$$\lambda_1 = 0.7143 + 6.3450i$$

$$\lambda_2 = 0.7143 - 6.3450i$$

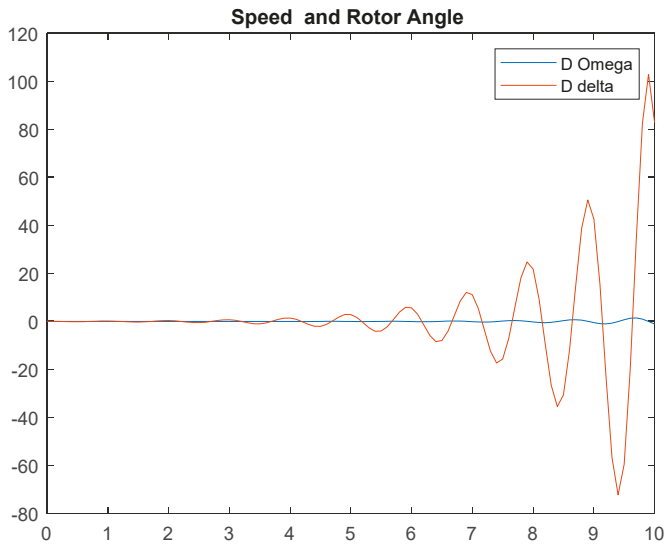


Figure 4. The system response in which there is a linear relationship between instability and time.

The response of the system, as can be seen, is positive for both quantities. Therefore, the system is unstable, as the diagram shows, and the fluctuation ranges of the system increase as time goes on. When the excitation system is taken into account, the matrix of the system is per Equation (24).

$$\begin{bmatrix} \Delta\dot{\omega} \\ \Delta\dot{\delta} \\ \Delta\dot{\psi}_{fd} \\ \Delta\dot{v}_1 \end{bmatrix} = \begin{bmatrix} a_{11} & a_{12} & a_{13} & 0 \\ a_{21} & 0 & 0 & 0 \\ 0 & a_{32} & a_{33} & a_{34} \\ 0 & a_{42} & a_{43} & a_{44} \end{bmatrix} \begin{bmatrix} \Delta\omega \\ \Delta\delta \\ \Delta\psi_{fd} \\ \Delta v_1 \end{bmatrix} + \begin{bmatrix} b_1 \\ 0 \\ 0 \\ 0 \end{bmatrix} \Delta T_m \quad (24)$$

The dynamics of a synchronous generator with PSS will be as in Equation (25) below.

$$\begin{bmatrix} \Delta\dot{\omega} \\ \Delta\dot{\delta} \\ \Delta\dot{\psi}_{fd} \\ \Delta\dot{v}_1 \\ \Delta\dot{v}_2 \\ \Delta\dot{v}_s \end{bmatrix} = \begin{bmatrix} a_{11} & a_{12} & a_{13} & 0 & 0 & 0 \\ a_{21} & 0 & 0 & 0 & 0 & 0 \\ 0 & a_{32} & a_{33} & a_{34} & 0 & 0 \\ 0 & a_{42} & a_{43} & a_{44} & 0 & 0 \\ a_{51} & a_{52} & a_{53} & 0 & a_{55} & 0 \\ a_{61} & a_{62} & a_{63} & 0 & a_{65} & a_{66} \end{bmatrix} \begin{bmatrix} \Delta\omega \\ \Delta\delta \\ \Delta\psi_{fd} \\ \Delta v_1 \\ \Delta v_2 \\ \Delta v_s \end{bmatrix} \quad (25)$$

2.2.3. Multi-Machine Synchronous Systems

As mentioned in the previous sections, the master data of the mode matrix plays an important role in system stability. The real parts of these quantities show exponential changes and the space matrix parts show fluctuation changes in sine. If the real part is negative, the exponential part of the response will tend towards zero. As a result, the fluctuating part will also be influenced by this and tend towards zero [31].

$$e^{a+ib} = e^a e^{ib} = e^a (\cos(b) + i\sin(b)) \quad (26)$$

However, if some of the master data contains non-negative real parts, the responses will not tend to zero over time. However, it either will tend towards infinity with growing fluctuations (if the master data is positive) or will continue with the previous fluctuation (if the master data is negative). Thus, even a small amount of chaos will be enough to disrupt the balance of the system. As it can be understood from these explanations, it is sufficient to know the position of the master data on the complex surface in the analysis of linear systems, but it is also sufficient to know the sign in the real part of the master data. In the following sections, methods of finding master data in large systems will be examined. If the dynamic system of each machine is as shown in Equation (27) below [32].

$$\dot{x} = Ax \quad (27)$$

$$A = \begin{bmatrix} a_{11} & a_{12} & a_{13} & 0 & 0 & 0 \\ a_{21} & 0 & 0 & 0 & 0 & 0 \\ 0 & a_{32} & a_{33} & a_{34} & 0 & 0 \\ 0 & a_{42} & a_{43} & a_{44} & 0 & 0 \\ a_{51} & a_{52} & a_{53} & 0 & a_{55} & 0 \\ a_{61} & a_{62} & a_{63} & 0 & a_{65} & a_{66} \end{bmatrix}, x = \begin{bmatrix} \Delta\omega \\ \Delta\delta \\ \Delta\psi_{fd} \\ \Delta v_1 \\ \Delta v_2 \\ \Delta v_s \end{bmatrix} \quad (28)$$

$$\Delta\dot{x} = \{A_D + B_D(Y + Y_N)^{-1}C_D\} \Delta x \quad (29)$$

$$A = \{A_D + B_D(Y + Y_N)^{-1}C_D\} \quad (30)$$

$$\begin{pmatrix} (\Delta\dot{\omega})_1 \\ (\Delta\delta)_1 \\ (\Delta\Psi_{fd})_1 \\ (\Delta\dot{v}_1)_1 \\ (\Delta\dot{v}_2)_1 \\ (\Delta\dot{v}_s)_1 \\ (\Delta\dot{\omega})_2 \\ (\Delta\delta)_2 \\ (\Delta\Psi_{fd})_2 \\ (\Delta\dot{v}_1)_2 \\ (\Delta\dot{v}_2)_2 \\ (\Delta\dot{v}_s)_2 \end{pmatrix} = \begin{pmatrix} (a_{11})_1 & (a_{12})_1 & (a_{13})_1 & 0 & 0 & 0 & 0 & 0 & 0 & 0 & 0 & 0 & 0 \\ (a_{21})_1 & 0 & 0 & 0 & 0 & 0 & 0 & 0 & 0 & 0 & 0 & 0 & 0 \\ 0 & (a_{32})_1 & (a_{33})_1 & (a_{34})_1 & 0 & 0 & 0 & 0 & 0 & 0 & 0 & 0 & 0 \\ 0 & (a_{42})_1 & (a_{43})_1 & (a_{44})_1 & 0 & 0 & 0 & 0 & 0 & 0 & 0 & 0 & 0 \\ (a_{51})_1 & (a_{52})_1 & (a_{53})_1 & 0 & (a_{55})_1 & 0 & 0 & 0 & 0 & 0 & 0 & 0 & 0 \\ (a_{61})_1 & (a_{62})_1 & (a_{63})_1 & 0 & (a_{65})_1 & (a_{66})_1 & 0 & 0 & 0 & 0 & 0 & 0 & 0 \\ 0 & 0 & 0 & 0 & 0 & 0 & (a_{11})_2 & (a_{12})_2 & (a_{13})_2 & 0 & 0 & 0 & 0 \\ 0 & 0 & 0 & 0 & 0 & 0 & (a_{21})_2 & 0 & 0 & 0 & 0 & 0 & 0 \\ 0 & 0 & 0 & 0 & 0 & 0 & 0 & (a_{32})_2 & (a_{33})_2 & (a_{34})_2 & 0 & 0 & 0 \\ 0 & 0 & 0 & 0 & 0 & 0 & 0 & (a_{42})_2 & (a_{43})_2 & (a_{44})_2 & 0 & 0 & 0 \\ 0 & 0 & 0 & 0 & 0 & 0 & (a_{51})_2 & (a_{52})_2 & (a_{53})_2 & 0 & (a_{55})_2 & 0 & 0 \\ 0 & 0 & 0 & 0 & 0 & 0 & (a_{61})_2 & (a_{62})_2 & (a_{63})_2 & 0 & (a_{65})_2 & (a_{66})_2 & 0 \end{pmatrix} \begin{pmatrix} (\Delta\omega)_1 \\ (\Delta\delta)_1 \\ (\Delta\Psi_{fd})_1 \\ (\Delta v_1)_1 \\ (\Delta v_2)_1 \\ (\Delta v_s)_1 \\ (\Delta\omega)_2 \\ (\Delta\delta)_2 \\ (\Delta\Psi_{fd})_2 \\ (\Delta v_1)_2 \\ (\Delta v_2)_2 \\ (\Delta v_s)_2 \end{pmatrix}$$

$$A = \{A_D + B_D(Y_N + Y_D)^{-1}C_D\} \tag{31}$$

Thus, the master data of the matrix of the above situation will determine the state of the system. In general, this matrix is a large sparse matrix and it is difficult to find its main data [33].

2.2.4. Householder Method Small Signal Stability

Many methods are based on orthogonal similarity. If two matrices are homologous, then the QR matrices present in the Homologous Transformations and a QR Algorithm will be as in Equation (32), since they have the same principal amounts as well as the same polynomials. For the separation of orthogonal and an upper triangular matrix, the transposed ‘p’ is obtained by multiplying the air distance by the force. The main advantage is obtained by transforming the resulting matrix.

$$A = P^{-1}BP \rightarrow A \sim B \tag{32}$$

$$A = Q^TBQ \rightarrow A \sim B, Q^{-1} = Q^T \tag{33}$$

$$A_0 = A \tag{34}$$

$$A_k = Q_k R_k \Rightarrow A_{k+1} = R_k Q_k \Rightarrow A_k = Q_k^T (R_k Q_k) Q_k = R_k Q_k = A_{k+1} \quad A_k \sim A_{k+1} \tag{34}$$

$$A_{k+1} = Q_k Q_{k-1} \dots Q_0 R_k Q_0^T Q_1^T \dots Q_k^T \rightarrow V \Lambda V^{-1} \tag{35}$$

If U is a unit vector, the Householder Matrix Hu is defined as follows per Equation (37):

$$H_u = I - 2uu^T, u^T u = 1 \tag{36}$$

$$\begin{aligned} H_u^T &= (I - 2uu^T)^T \\ &= (I - 2uu^T) \\ &= H_u \end{aligned} \tag{37}$$

$$\begin{aligned} H_u^2 &= (I - 2uu^T)(I - 2uu^T) \\ &= I - 2uu^T - 2uu^T + 4u(u^T u)u^T \\ &= I \end{aligned} \tag{38}$$

If A, n × n is a matrix, then B, the transformation of A through the Householder transformation, will be as in Equation (39).

$$A_n \times n AB = H_u A H_u \tag{39}$$

If the generated Hu matrix is indicated by H_{uj}: H_{uj} A H_{uj}

$$R = H_{u_n} (H_{u_{n-1}} \dots (H_{u_1} A)) = QA \Rightarrow A = QR \tag{40}$$

$$Q = H_{u_n} H_{u_{n-1}} \dots H_{u_1} \tag{41}$$

Thus, the matrix A is decomposed into QR. If the expression 2η(|a_{ij}| - η) is zero, U will not be able to be defined. Therefore, the matrix A cannot be homologous to an upper-triangular matrix

orthogonally by the QR algorithm. In this case, the matrix in discussion can be orthogonally made homologous to the previous Hessenberg Matrix. As a result, instead of the master data of matrix A, the master data of the Hessenberg Matrix is found. There are two famous assumptions on this topic.

3. Results

Considering a 20 bus bar grid model where current is injected by four generators, the Ad matrix having the damping coefficient difference will be a 24×24 cross-block matrix, as shown in Figure 5.

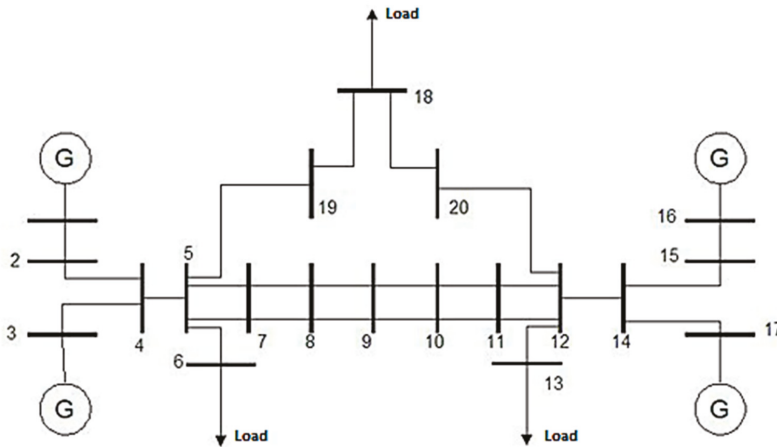


Figure 5. 20-bus bar power system.

It is possible to find the master data of the system matrix via the following program. In addition, the system's response to any change in parameters can be plotted and the output current of all generators can be monitored after each failure. In addition, the range of change of parameters can be determined upon system stability and the most appropriate mode can be selected shown as Table 1. The objective is to estimate $(\Delta\delta)_1 = 5^\circ$, $(\Delta\delta)_3 = 3^\circ$, $(\Delta\delta)_2 = (\Delta\delta)_4 = 0$ and 5° , 3° deviations in the first and third synchronous generators, respectively. The location of the 24th master data on a complex surface is shown in Figure 6.

The real part of the master data is completely negative, so the system is stable, and each minor fault returns to a stable state after a short time. The following Figure 7 shows how the condition variables of each generator, variation diagrams and other variables are changed by the deviation of the rotor angle by 5 degrees in the first generator and by 3 degrees in the third generator.

In general, the total active electrical power supplied by the generators should always be equal to the active power consumed by the loads, which also includes the losses in the system. A failure in the system can disrupt this balance, causing the rotors of the generators to accelerate or decelerate. If one generator temporarily runs faster than the other does, the angular position of the rotor will increase in connection to that of the slower machine shown as Figure 8. $\Delta\omega$ Variation diagram of four generators when $(\Delta\delta)_1 = 5^\circ$, $(\Delta\delta)_3 = 3^\circ$, $(\Delta\delta)_2 = (\Delta\delta)_4 = 0$.

Table 1. The data of special matrix values.

No.	Real Part	Imaginary Part
Landa1	-39.0967416	+0.000000000000000i
Landa2	-1.00550148	+6.607284341444071i
Landa3	-1.00550148	-6.607284341444071i
Landa4	-0.738513482	+0.000000000000000i
Landa5	-19.79697098	+12.822376834424755i
Landa6	-19.79697098	-12.822376834424755i
Landa7	-39.0967416	+0.000000000000000i
Landa8	-1.00550148	+6.607284341444071i
Landa9	-1.00550148	-6.607284341444071i
Landa10	-0.738513482	+0.000000000000000i
Landa11	-19.79697098	+12.822376834424755i
Landa12	-19.79697098	-12.822376834424755i
Landa13	-39.0967416	+0.000000000000000i
Landa14	-1.00550148	+6.607284341444071i
Landa15	-1.00550148	-6.607284341444071i
Landa16	-0.738513482	+0.000000000000000i
Landa17	-19.79697098	+12.822376834424755i
Landa18	-19.79697098	-12.822376834424755i
Landa19	-39.0967416	+0.000000000000000i
Landa20	-1.00550148	+6.607284341444071i
Landa21	-1.00550148	-6.607284341444071i
Landa22	-0.738513482	+0.000000000000000i
Landa23	-19.79697098	+12.822376834424755i
Landa24	-19.79697098	-12.822376834424755i

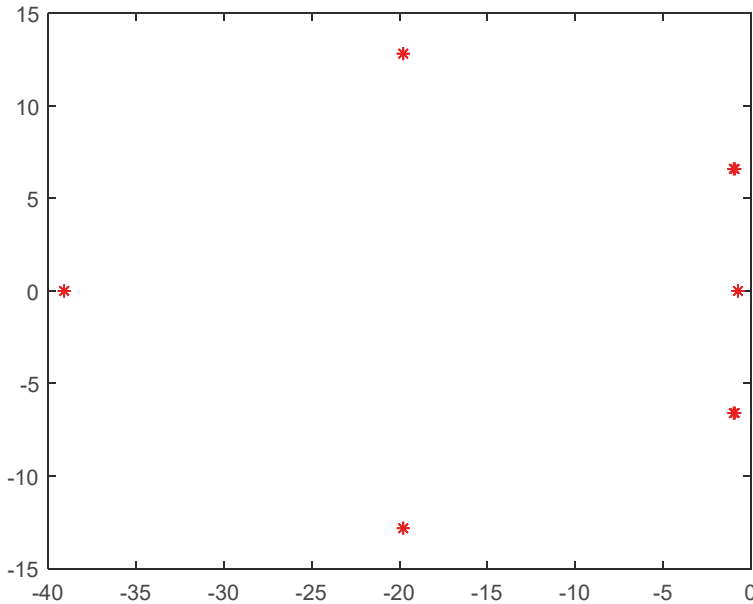


Figure 6. Location of the 24th master data on a complex surface.

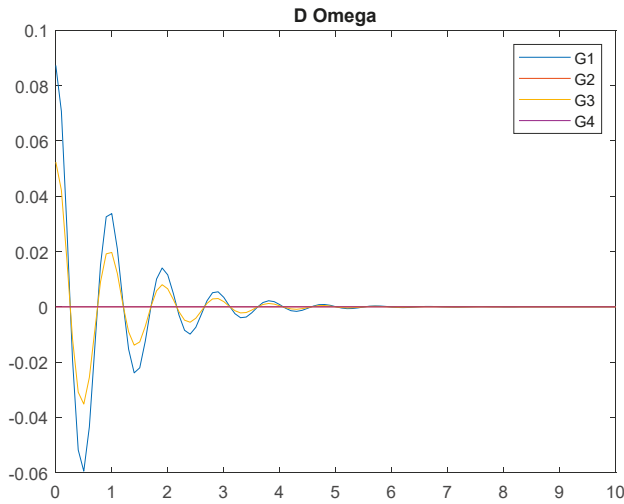


Figure 7. Shows the damping momentum $\Delta\omega$ stability diagram of the generators in the power system.

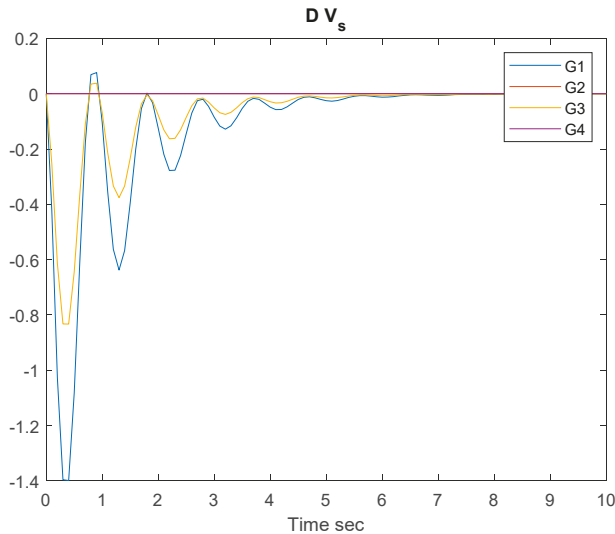


Figure 8. Δv_s Variations diagram of generators in a power system.

As can be seen in Δv_s variation diagram of four generators when $(\Delta\omega)_1=5^\circ, (\Delta\omega)_3=3^\circ, (\Delta\omega)_2 = (\Delta\omega)_4=0$, the system has remained stable as the real part of the master data is negative. The minimum changes of rotor angle $\Delta\delta$ and speed of some generators $\Delta\omega$ did not affect the stability of the system and the system regained its stability after these minimum failures.

Evaluation of the Proposed Solution Method

The analysis of linear systems is much simpler than that of nonlinear systems. As can be seen in this article, the position of the matrix state on the complex surface for the main quantities was found because of the analysis of linear systems. Furthermore, the sign of the real portions of the matrix state of the main quantities (positive or negative) showed the stability of the system. If these real parts

are negative, the system is stable and small deviations will not disrupt this stability, but after a short time, the system will regain its equilibrium. Any changes in the parameters of the generator and network will affect the elements of the matrix state; therefore, the location of the main quantities on the complex surface will vary, because of which the stability of the system will be affected. In this thesis, we attempted to examine how changes in the damping coefficient affect the main quantities of the state matrix, and the diagrams of the changes in the real parts of each main quantity were drawn against the changes in the $[-200,200]$ range of the damping coefficient (KD). The system is unstable in KDs where the real part of at least one main quantity is negative. Therefore, the above diagrams show the effect of the damping coefficient on system stability. In addition, these diagrams can be drawn based on changes of other parameters and system stability can be examined. As a result, the stability of large systems in the small signal depends only on finding the main quantities of a very large matrix. In fact, finding the main quantities is possible by finding the roots of a polynomial equation derived from the determinant, $\det(A-\lambda I)$. In other words, only $n-1$ steps are necessary for the conversion of the given matrix to an upper-triangular matrix. In the first stage, the elements below the element (1,1) are reset; in the second stage, the ones under element (2, 2) are reset; and in the final stage, only the ones under element $(n, n - 1)$ are reset.

4. Conclusions

This article demonstrates the formation of voltage stability in a system using conventional and small signal stability methods used to differentiate voltage stability. According to the literature, the non-linear system of the Household Method has been found to provide a linearization around the working point provided that the signal that changes the working point is small. Thus, it has been proved that easier linear systems can be analyzed instead of analysis of demanding nonlinear systems. However, it is not easy to obtain the Lyapunov Function to study the stability of a fixed point. This is because there is no general method for finding this function. The complex ambiance will be compared to non-linear functions with thousands of variables by using the concepts of coordinate functions. It has been shown that it is almost impossible to examine ultra-large systems with hundreds and thousands of variables without linearizing them. The only practical way of examining large systems is small signal analysis, since it can be linearized. The stability analysis of these systems is related to finding the master data of the mode matrix. Whether the real parts of these values are negative or positive determines whether the system is stable. Although it is highly challenging to find the master data of such a large matrix, it can be facilitated by making it linear so that the application capability of computer simulation can be improved.

The methods of finding the master data of large matrices are generally designed on homologous transformations (especially Householder transformations), because the successive transformations of the householder will result in many zeros in the columns of the matrix. The QR decomposition is made with the matrix obtained through the multiplication of the orthogonal matrix by the upper triangular matrix. The matrix obtained using the QR algorithm is then multiplied by the upper-triangular matrix (if this matrix does not exist, by the upper Hessenberg Matrix) and made homologous. Homologous transformations and degrees of the master data are retained so that, since the master data of the triangular matrix, the elements on the diagonal, the master data of the resulting matrix emerges from the triangular matrix. The QR algorithm can also generate the master data matrix (Modal Matrix). It is also designed to find the zero of functions in some other algorithms. These methods consider a particular polynomial as a function and try to find the zeros of the function by methods such as the Newton–Raphson Method. Other methods that are better suited than the Newton–Raphson Method are also used in finding the zero of different functions. Another method to find the master data is to use random algorithms. To achieve this goal, finding zeros is considered as minimizing, and then using complementary algorithms, such as genetic algorithms, solutions are provided for these issues. As a result, the most efficient method of finding main data in order to perform small signal stability analysis in large power systems is the Householder Method.

Author Contributions: Conceptualization, A.S. and M.R.T.; Methodology, A.S.; Software, E.H.; Validation, R.B., S.P. and A.S.; Formal Analysis, M.R.T.; Investigation, A.S.; Resources, A.S.; Data Curation, M.R.T. and E.H.; Writing-Original Draft Preparation, M.R.T.; Writing-Review & Editing, M.R.T.; Visualization, R.B.; Supervision, R.B. and S.P.

Funding: This research received no external funding.

Conflicts of Interest: The authors declare no conflict of interest

References

1. Pierre, D.A.; Trudnowski, D.J.; Hauer, J.F. Identifying reduced-order models for large nonlinear systems with arbitrary initial conditions and multiple outputs using Prony signal analysis. In Proceedings of the 1990 American Control Conference, San Diego, CA, USA, 23–25 May 1990; Volume 1, pp. 149–154.
2. Thompson, S.C.; Ahmed, A.U.; Proakis, J.G.; Zeidler, J.R.; Geile, M.J. Constant Envelope OFDM Abbrev. *IEEE MILCOM. Military Commun. Conf.* **2008**, *56*, 1300–1312.
3. Lindell, G.; Sundberg, C.E.W. An Upper Bound under bit error probability of combine convolution coding and continuous phase modulation. *IEEE Trans. Inform. Theory* **1988**, *1*, 1263–1269. [[CrossRef](#)]
4. Khan, S.; Bletterie, B.; Anta, A.; Gawlik, W. On Small Signal Frequency Stability under Virtual Inertia and the Role of PLLs. *Energies* **2018**, *11*, 2372. [[CrossRef](#)]
5. Taylor, C.W. *Power Systems Voltage Stability*; Electric Power Research Institute, McGraw Hill: New York, NY, USA, 1994.
6. Rajaraman, R.; Dobson, I.; Sarlashkar, J.V. Analytical modeling of thyristor-controlled series capacitors for SSR studies. *IEEE Trans. Power Syst.* **1996**, *11*, 15–32.
7. Martins, N. Retuning Stabilizers for the North-South Brazilian Interconnection. In Proceedings of the 1999 IEEE Power Engineering Society Summer Meeting, Edmonton, AB, Canada, 18–22 July 1999; Volume 1, pp. 58–67.
8. Lui, W. Research on a Small Signal Stability Region Boundary Model of the Interconnected Power System with Large-Scale Wind Power. *Energies* **2015**, *8*, 2312–2336. [[CrossRef](#)]
9. Xu, Y. Stochastic Small Signal Stability of a Power System with Uncertainties. *Energies* **2018**, *11*, 2980. [[CrossRef](#)]
10. Parashar, M.; Mo, J. Real Time Dynamics Monitoring System (RTDMSTM): Phasor applications for the control room. In Proceedings of the 42nd Annual Hawaii International Conference on System Sciences (HICSS-42), Big Island, HI, USA, 5–8 January 2009; Volume 1, pp. 5–8.
11. Abe, S.; Isono, A. Determination of power system voltage stability. *Electr. Enginland Jpn.* **1983**, *103*, 3–13.
12. Hauer, J.F. Application of Prony analysis to the determination of modal content and equivalent models for measured power system response. *IEEE Trans. Power Syst.* **1991**, *6*, 1062–1068. [[CrossRef](#)]
13. Bourgin, F.; Testud, G.; Heilbronn, B.; Verselle, J. Present Practices and Trends on the French Power System to Prevent Voltage Collapse. *IEEE Trans* **1993**, *8*, 3–13.
14. Willems, J.L. *Stability Theory of Dynamical Systems*; Wiley Interscience Division: London/Nelson, UK, 1970.
15. Chi-Tsong, T.C. *Linear Systems Theory and Design*; Academic Press: New York, NY, USA; London, UK, 1984.
16. Che, Y.; Xu, J.; Shi, K.; Liu, H.; Chen, W.; Yu, D. Stability Analysis of Aircraft Power Systems Based on a Unified Large Signal Model. *Energies* **2017**, *10*, 1739. [[CrossRef](#)]
17. Dher, D.K.; Doolla, S.; Bandyopadhyay, S. Electrical Power and Energy Systems Effect of placement of droop based generators in distribution network on small signal stability margin and network loss. *Int. J. Electr. Power Energy Syst.* **2017**, *88*, 108–118. [[CrossRef](#)]
18. Huang, D.; Chen, Q.; Ma, S.; Zhang, Y.; Chen, S. Wide-Area Measurement—Based Model-Free Approach for Online Power System Transient Stability Assessment. *Energies* **2018**, *11*, 958. [[CrossRef](#)]
19. Berrou, C.; Glavieux, A.; Thitimajshima, P. Near Shannon-Limit error correcting coding and decoding: Turbo codes. *Proc. ICC93* **1993**, *3*, 1064–1070.
20. Bezerra, H.L.; Martins, N. Eigenvalue methods for calculating dominant poles of a transfer function and their applications in small-signal stability. *Appl. Math. Comput.* **2019**, *347*, 113–121. [[CrossRef](#)]
21. Anderson, J.B.; Aulin, T. *Digital Phase Modulation*; Electronics & Electrical Engineering, Applications of Communications Theory; Springer Science & Business Media: New York, NY, USA, 1986.

22. Khodadad, A.; Divshali, P.H.; Nazari, M.H.; Hosseinian, S.H. Small-signal stability improvement of an islanded micro grid with electronically-interfaced distributed energy resources in the presence of parametric uncertainties. *Electr. Power Syst. Res.* **2018**, *160*, 151–162. [[CrossRef](#)]
23. Bourgin, F.; Testud, G.; Heilbronn, B.; Verseille, J. Present practices and trends on the French power system to prevent voltage collapse. *IEEE Trans. PWRS* **1993**, *8*, 3–13. [[CrossRef](#)]
24. Hill, D.J. Nonlinear dynamic load models with recovery for voltage studies. *IEEE Trans. PWRS* **1993**, *8*, 1. [[CrossRef](#)]
25. IEEE Special Stability Control Working Group. Static VAR Compensator Models for Power Flow and Dynamic Performance Simulation. *IEEE Trans. PWRS* **1994**, *9*, 1.
26. Robak, S.; Gryspanowicz, K. Rotor angle small signal stability assessment in transmission network expansion planning. *Electr. Power Syst. Res.* **2015**, *128*, 144–150. [[CrossRef](#)]
27. IEEE Task Force. Proposed Terms and Defin. for Power System Stability. *IEEE Trans.* **1982**, *7*, 1894–1898.
28. Lu, X.; Xiang, W.; Lin, W.; Wen, J. Small-signal modeling of MMC based DC grid and analysis of the impact of DC reactors on the small-signal stability. *Electr. Power Energy Syst.* **2018**, *101*, 25–37. [[CrossRef](#)]
29. Xie, R.; Kamwa, D.; Rimorov, D.; Moeini, A. Fundamental study of common mode small-signal frequency oscillations in power systems. *Electr. Power Energy Syst.* **2019**, *106*, 201–209. [[CrossRef](#)]
30. Weiyu, W. Virtual Synchronous Generator Strategy for VSC-MTDC and the Probabilistic Small Signal Analysis. *IFAC-Pap. Line* **2017**, *50*, 5424–5429. [[CrossRef](#)]
31. Sadhana, G.S. Small Signal Stability Analysis of Grid Connected Renewable Energy Resources with the Effect of Uncertain Wind Power Penetration. *Energy Procedia* **2017**, *117*, 769–776. [[CrossRef](#)]
32. Guo, C.; Zheng, A.; Yin, Z.; Zhao, C. Small-signal stability of hybrid multi-terminal HVDC system. *Electr. Power Energy Syst.* **2019**, *109*, 434–443. [[CrossRef](#)]
33. Yang, W.; Norrlund, P.; Chung, C.Y.; Yang, J.; Ludin, U. Eigen-analysis of hydraulic-mechanical-electrical coupling mechanism for small signal stability of hydropower plant. *Renew. Energy* **2018**, *115*, 1014–1025. [[CrossRef](#)]



© 2019 by the authors. Licensee MDPI, Basel, Switzerland. This article is an open access article distributed under the terms and conditions of the Creative Commons Attribution (CC BY) license (<http://creativecommons.org/licenses/by/4.0/>).

Article

Investigations on EMI Mitigation Techniques: Intent to Reduce Grid-Tied PV Inverter Common Mode Current and Voltage

Umashankar Subramaniam ^{1,*}, Sagar Mahajan Bhaskar ¹, Dhafer J. Almkhles ¹, Sanjeevikumar Padmanaban ² and Zbigniew Leonowicz ³

¹ Renewable Energy Lab, Department of Communications and Networks, College of Engineering, Prince Sultan University (PSU), Riyadh 66833, Saudi Arabia

² Department of Energy Technology, Aalborg University, 6700 Esbjerg, Denmark

³ Faculty of Electrical Engineering, Wrocław University of Science and Technology, Wyb. Wyspińskiego 27, 50370 Wrocław, Poland

* Correspondence: shankarums@gmail.com or san@et.aau.dk; Tel.: +966-11-494-8059

Received: 1 August 2019; Accepted: 29 August 2019; Published: 3 September 2019

Abstract: Power inverters produce common mode voltage (CMV) and common mode current (CMC) which cause high-frequency electromagnetic interference (EMI) noise, leakage currents in electrical drives application and grid-connected systems, which consequently drops the efficiency of the system considerably. This CMV can be mitigated by designing suitable EMI filters and/or investigating the effects of different modulation strategies. In this paper, the effect of various modulation techniques over CMV and CMC are investigated for two-level and three-level inverters. It is observed that the modified third harmonic injection method reduced the CMV and CMC in the system by 60%. This modified pulse width modulation (PWM) technique is employed along with EMI chokes which results in reduced distortion of the system.

Keywords: common mode current; common mode voltage; modulation techniques; electromagnetic interference; mitigation; grid connected inverters

1. Introduction

The PV-grid connected power inverter is a necessary part of the PV to electrical energy conversion system [1]. The quality of the voltage depends upon three phenomenons of voltage harmonics, voltage dips or swells and flicker [2]. In the present day, the intense use of electrical loads driven by power electronics (e.g., personal computers) has led to a severe increase of current harmonics drawn from the distribution system. These current harmonics, due to the impedance of the network, induce voltage harmonics into the utility. Voltage dips originate from fault currents in the electrical system or inrush currents of electrical motors and transformers [3]. The common mode circuit is formed in between Photo Voltaics (PVs) and the grid, as well as ground due to parasitic capacitance and deficiencies in galvanic isolation between the grid and PVs [1,4]. Electromagnetic interference (EMI) is the main source of unexpected transition at the output port of variable frequency drive (VFD). The fall time and rise time of semiconductor devices (employed in the converter section of VFD) are used to determine voltage transition times. These voltage transition times are around 100ns which is very fast. As a result, high dv/dt occurs. In the stray line to ground cables and capacitor, the magnitude of common mode noise current is higher if dv/dt is higher [4]. These noise currents affect the control signals and are the main source of EMI.

The instability and disturbances occur at the supply side due to the utilization of a higher number of power devices and components for energy conversion [5]. Mainly, non-linear devices are

responsible for this instability and disturbances. Due to this, harmonics are introduced in the power system. These harmonics causes EMI-related problems, overheating in the equipment, and damage the devices, etc. Inverter common mode voltage (CMV) and its leakage current are the primary concerns of radiated EMI. Noise with high-frequency components is emitted in the form of electromagnetic energy and may interfere with other components and equipment at the common coupling point [6]. To minimize common currents, commonly used methods are [1] improved power inverter structures with common mode current (CMC) suppression capabilities and advanced pulse width modulation (PWM) schemes [7], and (2) the addition of EMI filters [8] and bridge inverter topology based on DC and AC bypass [9]. It is also notable that the circuitry with fast switching semiconductors produces a very high amount di/dt and dv/dt and which is one of the reasons for the cause of EMI [10]. Decoupling effect-based configurations with constant CMV [11] and transformerless power converter configurations [12] are proposed to suppress CMC. The CM loop impedance can be increased in order to suppress current in CM loop effectively. In [13], the mid-point of DC and AC side voltage nodes are connected to the proposed new CM internal loop scheme in order to suppress CMC. In [14], a novel modulation scheme is presented to control inverter power switches in order to reduce CMC. In [15], a CM internal loop is formed by employing the RC branch in between the negative bus of DC and output terminals. However, detailed analysis of the CMC and its effect on CMC high-frequency components are not presented. In [16], a new scheme based on a dual CM internal loop for a PV grid-connected transformer-less system is proposed to suppress CMC high-frequency components. In [17] characteristics and analysis of the CMV based on the simplified modelling of a cascaded H-bridge power transformer and PWM strategy are presented under the fault grid condition and balanced condition. In [18], in order to reduce CM leakage current, a new hybrid modulation strategy is suggested. The suggested method is efficient and has reactive power provision with low distortion in the current. Filters at the input/output terminal are employed to suppress this unwanted emission or electromagnetic interference (EMI) [19,20]. Generally, filters are employed at the connector of power supply in order to restrict disturbance signals [21,22]. Generally, classical filters are designed by utilizing passive components, i.e., inductor and capacitor values to attenuate high-frequency voltage and current components [23,24]. However, the performance of the filter is dependent on the value of L and C and has limited achievable insertion loss that should be improved to meet the necessary condition. Moreover, passive filters are bulky, costly, and their volume mainly depends on the inductor size which is approximately directly proportional to the required attenuation. Moreover, there is always uncertainty in parasitic components. In order to reduce CMV and current effect, active [25] and passive filters [26] are suggested. However, these filters increase the size, cost of the system, and control of the equipment. As a result, it is good to advance control strategies in order to reduce the CMV's effect. In order to eliminate or reduce CMV, numerous control schemes are proposed based on the modulation strategy, such as the Sine PWM for three-level neutral point clamped (NPC) inverter [27], PWM based on non-nearest vectors, Space Vector PWM for high-level inverters [28,29], etc. In [30], a detailed comparison of SPWM and SVPWM techniques are presented for the three-phase inverter. Nevertheless, similar PWM schemes presented in [31,32] are restricted to 3–5 levels inverters. Synchronous reference frame and feedforward reference frame-based dynamic voltage restorer comparative study are presented in [33]. In [34], a new SVPWM scheme is presented with advanced features, such as the proposed scheme, which is suitable for inverters with any number of levels, zero CMVs can be achieved at any modulation index, the simple realization of CMV vectors, fast control scheme, etc. In [35], a new methodology called the spread spectrum (SS) technique is presented in order to reduce EMI of power converters over a wide range of frequency. However, this SS technique is competent to reduce EMI levels around 5–10 dB [36]. Based on the output voltage waveform and its alignment, another technique is suggested in [37,38]. However, this methodology has a specific application. In [39], a new technique based on software is presented to reduce EMI. The methodology is suitable for single- and three-phase power inverters. In [40], analysis on the CM EMI and methodology to mitigate EMI in power inverters is discussed by using a delay compensation

technique. In order to mitigate EMI, numerous passive filter methods are proposed based on the phases of the noise signal. In [41], a common mode-coupled inductor is designed in order to mitigate common mode noise. Nevertheless, differential mode noise is not able to be reduced by using this technique. Hence, later, a new method based on an integrated choke is presented in order to reduce differential, as well as common mode, noise at the same time [42].

In [43], a new method based on the parasitic component's determination is presented in order to predict EMI noise. In [44,45], computer-based three-dimensional modelling is presented for the noise current prediction by determining the value of parasitic components. A novel EMI filter is discussed with sufficient attenuation with a limited LC value in order to CM EMI [46]. Nevertheless, filters are additional components and increase the volume and cost of the system. Moreover, the implementation of the effective filter is important and the effort for the mitigation of EMI without knowing the system may degrade the performance and require additional cost. To reduce CM voltage, a new impedance balancing method is presented instead of impedance mismatching [47]. The three-phase phase-lock-loop for a distorted utility is discussed in [48]. In [49], controllable devices are used and active filters are presented to suppress CMC generated by the CMV method, called the active noise cancellation scheme, in order to mitigate the noise signal [50]. In [51], a new wavelet transform-based technique to mitigate EMI noise in power converter is presented with a frequency band of 3–30 MHz.

In this paper, EMI mitigation techniques are investigated with the aim to reduce CMV and CMC in a PV-grid tied power inverter. The effect of modulation techniques over CMV and CMC are investigated for two-level and three-level inverters to observe the mitigation of EMI. The modified third harmonic injection method reduced the CMV and CMC by 60% in the system. In order to reduce distortion and to improve the overall efficiency of the system, the modified PWM technique is employed along with EMI chokes.

The article is organized in the seven sections, discussing explicitly the important aspects for investigations and design of EMI filters for the mitigation of CMC and CMV in grid-tied inverter system. In Section 2, the modulation techniques for high power two-level and three-level inverters, are discussed in brief. Section 3 explains the concept of CMV of the inverters and design of filters or EMI chokes. Section 3 also deals with the comparative study of space vector-based and sine-based pulse width modulation (SVPWM and SPWM) techniques. A modified PWM strategy is discussed in Section 4. The results obtained through simulation and experimental works are presented in Section 5. Finally, the conclusion is given in Section 6.

2. Modulation Techniques for High-Power Inverters

Space vector-based and sine wave-based PWM techniques are the common techniques used to generate pulses for the switches of the inverter [29,30]. In the SPWM technique, high-frequency triangular carrier waves (typically several kHz) are compared with the modulating signal (50 Hz or 60 Hz) to generate pulses for a three-phase inverter. In the SVPWM technique, instead of modulating signals, a rotating vector reference is used to generate pulses of the inverter [29,30]. The prime objective of this control and pulse generation scheme is to generate a sinusoidal AC output whose magnitude is limited. The PWM switching scheme not only helps to achieve reduced Total Harmonic Distortion (THD), better harmonic spectrum, and maximum utilization of DC bus but also provides a solution to reduce EMI, switching loss. Figure 1 depicts the power circuitry of three-phase two-level inverter and neutral point clamped (NPC) three-level inverters [21] and its PWM strategies shown in Figures 2–5.

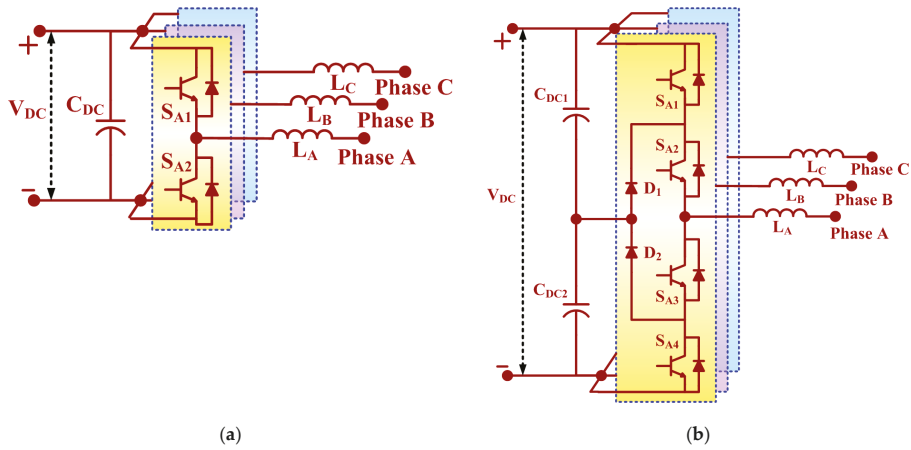
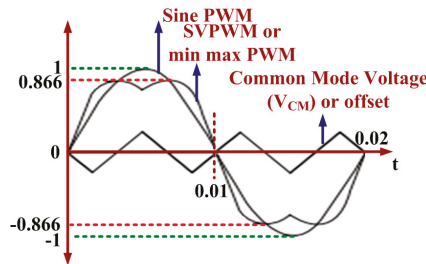
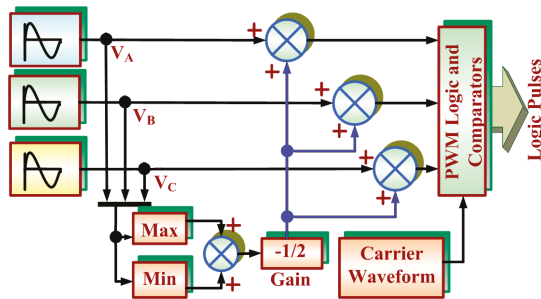


Figure 1. Power circuitries of (a) three-phase two-level inverter, and (b) neutral point clamped (NPC) three-level inverter.



(a)



(b)

Figure 2. Reference generation through Min–Max modulation strategy (a) associate waveform, and (b) mathematical model.

The Min–Max modulation strategy is supposed to be equivalent to the space vector modulation strategy. Thus, using this approach, the modulation index can be extended up to 1.15. Figure 2a,b explains the associated waveforms and mathematical model of the reference waveform generation technique through Min–Max modulation strategy, respectively [48]:

$$offset\ in\ (V) = -\left[\frac{\max(V_A, V_B, V_C) + \min(V_A, V_B, V_C)}{2}\right] \quad (1)$$

where:

$$\begin{cases} V_A = V_m \cos(\omega t) \\ V_B = V_m \cos(\omega t - \frac{2\pi}{3}) \\ V_C = V_m \cos(\omega t + \frac{2\pi}{3}) \end{cases} \quad (2)$$

$$V_{ref} = V_A + V_B + V_C + offset \quad (3)$$

The reference modulating signals are mathematically defined as follows:

$$\begin{cases} V_{Am} = V_m \cos(\omega t) + offset \\ V_{Bm} = V_m \cos(\omega t - \frac{2\pi}{3}) + offset \\ V_{Cm} = V_m \cos(\omega t + \frac{2\pi}{3}) + offset \end{cases} \quad (4)$$

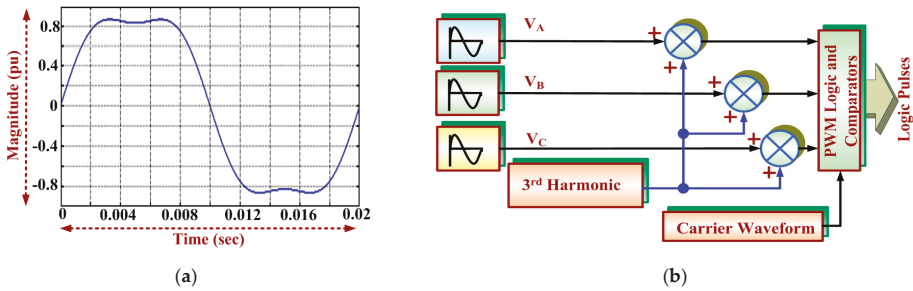


Figure 3. Modulating signal of third harmonic injection control technique (a) modulating signal, and (b) mathematical model.

In the third harmonic injection method [52,53], the third harmonic is injected in a modulation scheme to improve the gain of the pulse width modulator in the inverter. Figure 3a,b shows the third harmonic injection modulating signal control reference waveform and mathematical model, respectively.

The reference modulating signals are mathematically defined as follows:

$$\begin{cases} V_{Am} = V_m \cos(\omega t) + V_{m3} \cos(3\omega t) \\ V_{Bm} = V_m \cos(\omega t - \frac{2\pi}{3}) + V_{m3} \cos(3\omega t) \\ V_{Cm} = V_m \cos(\omega t + \frac{2\pi}{3}) + V_{m3} \cos(3\omega t) \end{cases} \quad (5)$$

In this technique, approximately 17% of third harmonics components are added in the reference waveform of classical SPWM [29,30,34]. The reference waveform of the method third harmonics injection can be also expressed as follows:

$$f(\omega t) = (1.15M_a \times \sin(\omega t) + 0.19M_a \times \sin(3\omega t)), 0 \leq \omega t \leq 2\pi \quad (6)$$

where M_a is the modulation index ratio.

3. Common Mode Voltage

The inverter common mode voltage is calculated by averaging the output voltage (V_A , V_B , and V_C) of each leg as follows [38]:

$$V_{CM} = \frac{V_A + V_B + V_C}{3} \quad (7)$$

For the three-phase two-level inverter, the achievable phase output voltage levels could be $-V_{DC}/2$ or $+V_{DC}/2$ where V_{DC} is input voltage. If the voltage at the DC link is zero then only the common mode voltage is zero. For the three-level inverter, the achievable phase output voltage levels could be

positive, negative, and neutral point voltage. Tables 1 and 2 tabulated the output vectors and possible common mode voltages for two-level and three-level inverters, respectively.

Table 1. Output vectors and common-mode voltages for two-level inverter.

Output Vector (V_A, V_B, V_C)	CMV (V_{CM})
(+ + +)	$(1/2) \times V_{DC}$
(+ + -), (+ - +), (- + +)	$(1/6) \times V_{DC}$
(+ - -), (- + -), (- - +)	$-(1/6) \times V_{DC}$
(- - -)	$-(1/2) \times V_{DC}$
(+ + +)	$(1/2) \times V_{DC}$
(+ + -), (+ - +), (- + +)	$(1/6) \times V_{DC}$

Table 2. Output vectors and common-mode voltages for three-level NPC inverter.

Output Vector (V_A, V_B, V_C)	CMV (V_{CM})
(+ + +)	$(1/2) \times V_{DC}$
(+ + 0), (+ 0 +), (0 + +)	$(1/3) \times V_{DC}$
(+ + -), (+ - +), (- + +), (+ 0 0), (0 + 0), (0 0 +)	$(1/6) \times V_{DC}$
(+ - 0), (+ 0 -), (- + 0), (0 + -), (- + 0), (0 - +), (0 0 0)	0
(+ - -), (- + -), (- - +), (- 0 0), (0 - 0), (0 0 -)	$-(1/6) \times V_{DC}$
(- - 0), (0 - -), (0 - -)	$-(1/3) \times V_{DC}$
(- - -)	$-(1/2) \times V_{DC}$

3.1. Filtering of Common Mode Voltage

The appropriate designed filter circuitry is needed to reduce the common mode voltage. The complete three-phase to grid (AC–DC–AC) system with the connection of a passive filter is shown in Figure 4. The DC link with voltage V_D is created between the AC–DC and DC–AC converter and passive filters are added at the input and output side. The filter consists of damping resistance, Y-connected capacitor and common mode chokes. In the given system, a damping resistor R_{CM2} is connected between grid and neutral point capacitor. Additionally, two chokes, L_{CM1} and L_{CM2} , and three Y-connected capacitors, C_{CM2} , are connected for filter purposes [12–14]. R_{CM1} and C_{CM1} are connected between the grid and negative terminal of the DC link. The range of the resonant frequency for the common mode circuitry is about 1.5 kHz [7] and is calculated as follows:

$$f_0 = 1 / (2\pi \sqrt{L_{CM} \times C_{CM}}) \tag{8}$$

where L_{CM} and C_{CM} are the equivalent inductance and capacitance values. The practical limitation of the real-time application needs to be considered while designing the capacitors. The capacitor size should be small for the designed frequency in order to reduce the bulkiness of the hardware unit.

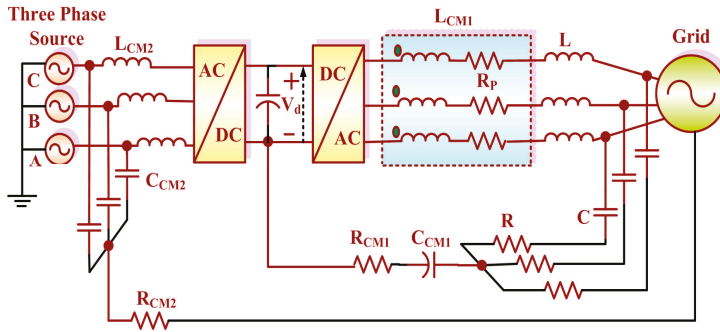


Figure 4. Complete three-phase to grid (AC–DC–AC) system with the connection of a passive filter.

3.2. Comparison of SPWM and Space Vector PWM Techniques for a Two-Level Inverter at a Higher Switching Frequency

The simple open-loop analysis is carried out for a two-level inverter for current and voltage distortions both with and without a filter. For the analysis, the modulation index is maintained at 0.8 and taken over a range of frequencies between 1 kHz and 150 kHz and the obtained results are tabulated in Table 3. After comparing SPWM and SVPWM results, it is known that SVPWM provides superior results for two-level inverter system. For reduction in CMV, the SVPWM technique provides the best results; however, due to tedious calculations, the requirement of high-end processors and complex hardware implementation, space vector modulation can be replaced with the carrier-based modulation strategy which will give the same results as that of the space vector modulation technique. If the reduction in the CMC can be achieved by using such a modulation strategy, the size of the common mode choke can be reduced.

Table 3. THD comparison of SPWM and SVPWM techniques.

Switching Technique	Switching Frequency	Without Filter (THD%)		With Filter (THD%)	
		Line Current (A)	Line Voltage (V)	Line Current (A)	Line Voltage (V)
SPWM	1 kHz	64.81	138.2	2.53	6.88
	10 kHz	24.9	88.46	1.04	4.16
	50 kHz	24.27	67.92	1.03	4.12
	100 kHz	24.27	67.92	1.03	4.12
	120 kHz	31.39	106.82	3.86	5.63
	150 kHz	43.95	301.92	7.42	7.89
SVPWM	1 kHz	4.82	52.84	0.14	0.66
	10 kHz	3.15	43.89	0.11	0.42
	50 kHz	3.15	43.89	0.11	0.43
	100 kHz	8.74	31.84	0.36	1.47
	150 kHz	5.75	56.33	0.45	1.03

4. Modified PWM Schemes

Among discussed PWM schemes, SVPWM provides quality results [30]. Nevertheless, due to some inherent disadvantages, the space vector modulation strategy is ruled out from the agenda. Thus, the next challenge was to obtain similar results, which were given by the space vector modulation, in carrier-based modulation as well. The modified carrier phase shift scheme is developed based on the concept of phase disposition PWM scheme. It is given that the input voltage is balanced and the possible two conditions are:

- One input phase voltage is negative and two input phase voltage is positive.
- One input phase voltage is positive and two input phase voltage is positive.

$$V_A + V_B + V_C = 1 \tag{9}$$

It is considered that $0 < V_A$, $0 > V_B$, and $0 > V_C$ and CMV are caused with the peak value to reach a higher voltage level than $1/6 \times V_{DC}$. The carrier signals and output voltage reference relation for the switching 0–1–1 is as follows:

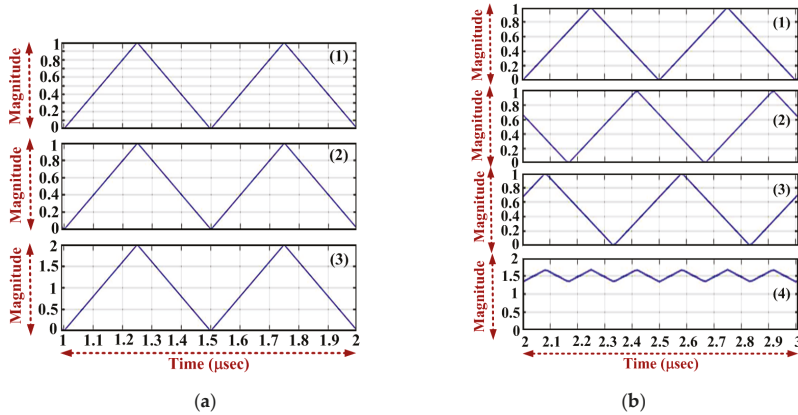


Figure 5. Waveform associated with PWM strategies (a) PDPWM method, max amplitude of the addition of the carrier waves is 2, (b) modified PWM method, max. amplitude of the addition of the carrier waves is around 1.5.

As phase disposition PWM (PDPWM) is used, at any point of time:

$$\text{for the state '0-1-1'} \begin{cases} V_{CarrierA} - V_{CarrierB} = 1 \\ 3 \times V_{CarrierA} - 2 > 0 \end{cases} \tag{10}$$

Hence, to avoid this state, $3 \times V_{CarrierA} - 2 < 0$, this condition is to be satisfied. This is done by using three carrier waves, which are 120° apart from each other. Figure 5 shows the waveform associated with PWM strategies. Figure 5a depicts the associated waveform of the PDPWM method where the max amplitude of the addition of the carrier waves is 2 (see amplitude in (3) in Figure 5a). Figure 5b depicts the associated waveform of the modified PWM method where the max amplitude of the addition of the carrier waves is around 1.5 (see amplitude in (4) in Figure 5b).

5. Simulation and Experimental Results

The simulation results are presented for the complete AC–DC–AC system. The circuit-level model was developed using the Simulink platform. The closed-loop analysis of both two-level and three-level inverters is carried out. The specifications of the system parameters are given in Appendix A.

5.1. Closed-Loop Analysis of the Two-Level Inverter

The model of the system is done in various stages. Figure 6 shows the complete closed-loop AC–DC–AC system Simulink model with the two-level inverter. The first section includes the diode rectifier model to obtain a constant DC voltage. Then the DC link capacitor was designed so as to provide a constant DC input voltage to the three-phase two-level inverter circuit which is modelled using Insulated Gate Bipolar Transistor (IGBTs) and SVPWM techniques were implemented for firing the inverter circuit.

The analysis of CMV and CMC for the given system is done without filter implementation and the achieved results are depicted in Figure 7a–d. The Fast Fourier Transform(FFT) analysis of the CMV and CMC waveform (150 kHz component) are done without filter, and it is observed that THD of the CMV

and CMC is 38.01% and 3152.31%, respectively. The analysis of the common mode voltage and current for the given system are done with a filter implementation and the achieved results are depicted in Figure 7e–h. The FFT analysis of the CMV and CMC waveform (150 kHz component) are done with a filter and it is observed that the THD of the CMV and CMC is 73.39% and 2213.58%, respectively.

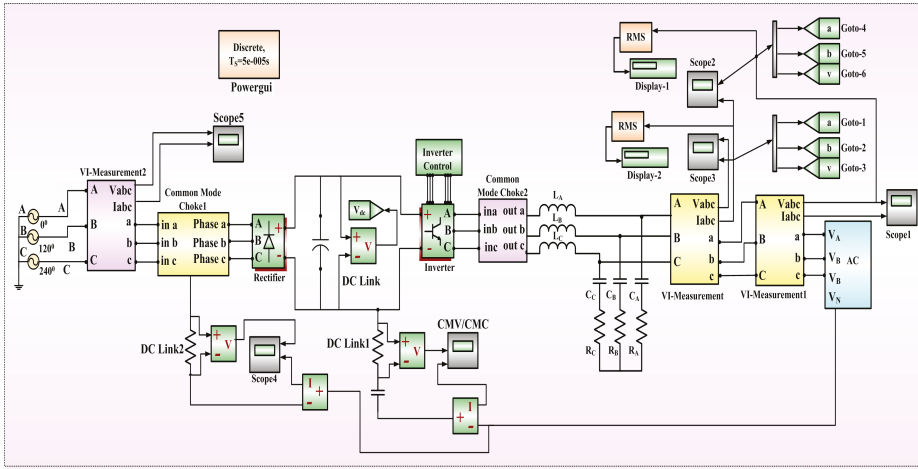


Figure 6. Complete closed-loop AC–DC–AC system Simulink model with the two-level inverter.

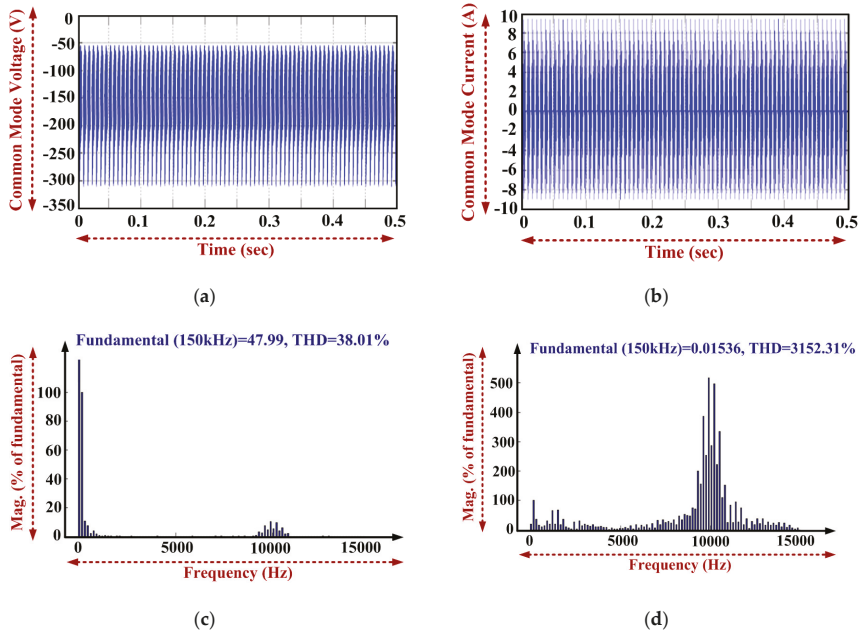


Figure 7. Cont.

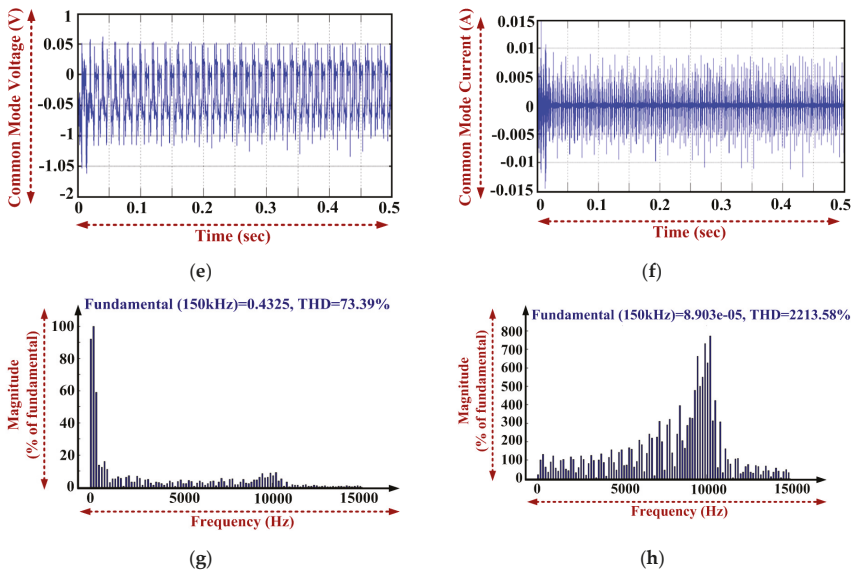


Figure 7. Simulation results: (a) CMV without filter; (b) CMC without filter; (c) without filter, common mode voltage FFT analysis; (d) without filter, common mode current FFT analysis; (e) CMV with filter; (f) CMC with filter; (g) with filter, common mode voltage FFT analysis; (h) with filter, common mode current FFT analysis.

From the investigation, the objective of reducing the CMC and CMV of the two-level inverter is achieved. From the analysis made, it can be concluded that when the two-level inverter is operating at a frequency above 10 kHz, the EMI increases drastically. Additionally, the CMV and CMC of the system cannot be reduced effectively by changing the reference, instead the size of the EMI filters have to be larger. Therefore, we need to consider the three-level inverter analysis.

5.2. Closed-Loop Analysis of the Three-Level Inverter

Based on the earlier explanation, the Simulink model of the three-level NPC system is designed in MATLAB. Figure 8 shows the Simulink model of the designed three-level NPC system.

5.2.1. Existing PWM Method

Using Min–Max and the third harmonic injection method, the common mode current and voltage are investigated for the three-level NPC inverter. Figure 9a–d depicts the waveforms of CMC using existing Min–Max method, CMV using existing Min–Max method, CMC using the existing third harmonic injection methods, and CMV using the existing third harmonic injection method, respectively.

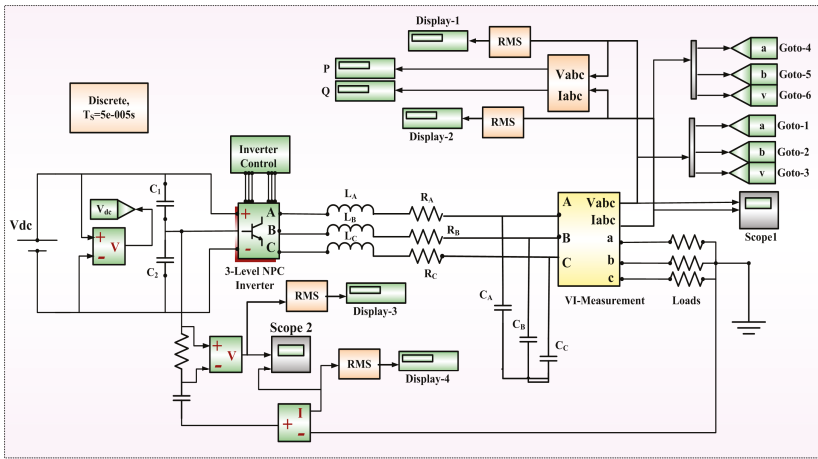


Figure 8. Matlab/Simulation model of the three-phase three-level NPC inverter.

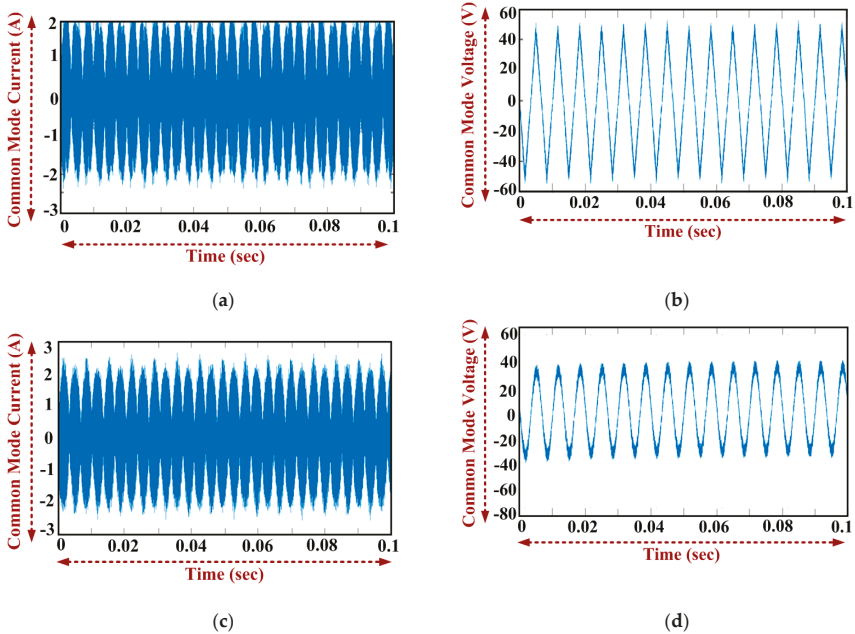


Figure 9. Simulation results: (a) CMC using existing Min–Max method; (b) CMV using existing Min–Max method; (c) CMC using the existing third-harmonic injection method; (d) CMV using the existing third-harmonic injection method.

The fast Fourier transform (FFT) is conducted for Min–Max and third harmonic injection PWM techniques and it is observed that common mode voltage THD is 14.74% for Min–Max strategy and 11.60% for the third harmonic injection method. In the existing PWM method, the magnitude of the common mode current (rms value) is 1.191 A using the Min–Max and 1.199 A in the case of the third harmonic injection method. This can be reduced further by using Modified PWM Technique.

5.2.2. Modified PWM Method

The simulation results for the modified Min–Max method and third harmonic injection methods as applied in the three-level NPC inverter. Figure 10a–d obtained waveform of CMC using modified Min–Max method, waveform CMV using modified Min–Max method, waveform of CMC using modified third harmonic injection methods, and waveform of CMV using modified third harmonic injection methods, respectively. Figure 10e,f show the FFT analysis of CMV and CMC with filter, respectively. It is observed that the THD of the CMV and CMC are 12.95% and 5.91%, respectively. Before modifying the PWM scheme, the common mode voltage and current of the inverter are experimentally investigated and shown in Figure 11a. Without modification, the RMS values of the common mode current and common mode voltage are 1.95 A and 4.73 V, respectively.

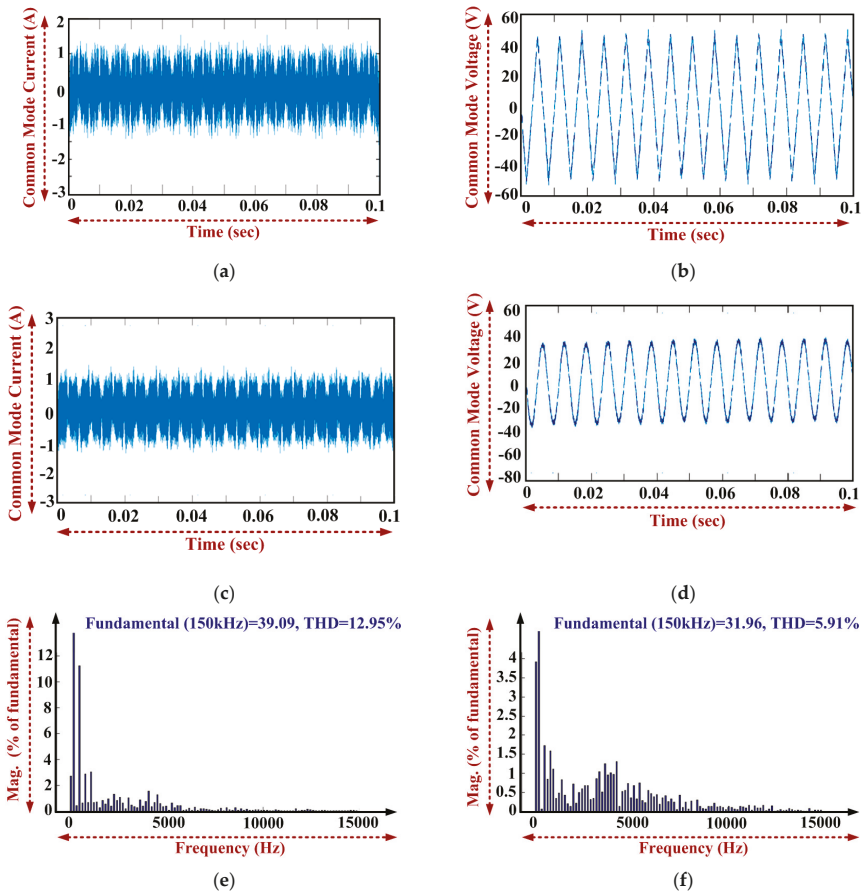
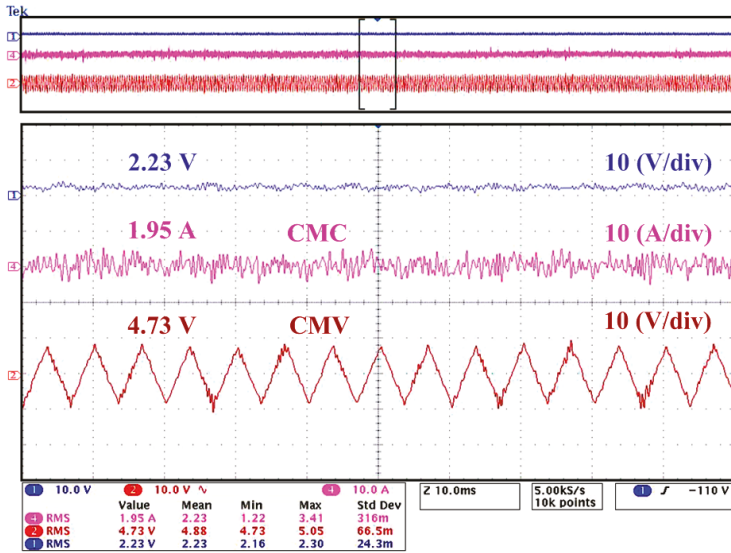
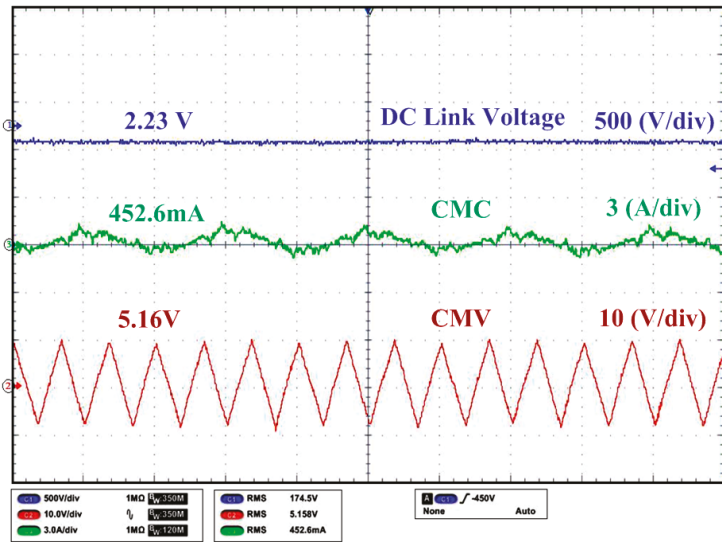


Figure 10. Simulation results: (a) CMC using the modified Min–Max method; (b) CMV using the modified Min–Max method; (c) CMC using the modified third-harmonic injection method; (d) CMV using the modified third-harmonic injection method; (e) with filter, common mode voltage FFT analysis; (f) with filter, common mode current FFT analysis.



(a)



(b)

Figure 11. Experimental results: common mode current and common mode voltage, (a) before modifying the PWM strategy, and (b) after modifying the PWM strategy.

After modifying the PWM scheme, the common mode voltage and current of the inverter are experimentally investigated and shown in Figure 11b. After modification, the RMS values of the common mode current and common mode voltage are 452.6 mA and 5.16 V, respectively. In Table 4, the observed results are tabulated and it is clear that, after modifying the PWM method, the common mode current is reduced significantly with a small increment in the common mode voltage.

Table 4. Experimental results.

Experimental Test	CMV (V)	CMC (A)
Before applying modified PWM	4.73 V	1.95 A
After applying Modified PWM	5.16 V	452.6 mA

In Table 5, a comparison of PWM strategies for reduction in CMC, CMV, and voltage THD of the three-level inverter is tabulated based on the obtained results. The simulated results show that when the modified PWM method is implemented there is a considerable reduction in CMC. The voltage THD of the system is also observed to be reduced considerably. This satisfies the objective of optimizing the PWM technique to reduce the CMV and current in grid-tied inverters. From the above comparison, it is clear that the modified third harmonic injection approach shows a significant amount of reduction in the CMV and CMC. EMI mitigation techniques are investigated with the aim to reduce the CM voltage and current in PV grid-tied power inverters. The common mode undesirable effects for grid-tied inverter systems has been discussed and compared for different PWM schemes. Two small passive filters are connected between the rectifier input and grid neutral point, and in between the grid and output port of the inverter and tested for a three-phase two-level inverter using a passive cancellation method.

Table 5. Comparison of PWM strategies for reduction in the CMC, CMV, and voltage THD of the three-level inverter.

Modulation Technique	CMV (V)	CMC (A)	Voltage THD (%)
Existing PWM Strategy			
Min–Max	34.7	1.863	14.27
Third Harmonic Injection	34.7	1.863	11.5
Modified PWM Strategy			
Modified Min–Max	43.31	0.74	12.95
Modified Third Harmonic Injection	34.84	0.74	5.77

6. Conclusions

In order to reduce distortion in the system, the modified PWM technique is employed along with EMI chokes. Various PWM strategies are analyzed to reduce the CMV and CMC, and a modified PWM approach is presented for a three-phase three-level inverter. The modified third harmonic injection method reduced the CMC by 60% in the system with a tradeoff to CMV. Simulation and experimental results are provided which show good agreement with each other and validate that the control strategies with different PWM techniques are valuable, optimize the output parameters, and are effective in preventing common mode undesirable effects along with and without filters. Hence, it is economic to use modified techniques so that the filter size can be reduced and the final product will be lightweight with a reduced cost compared with conventional strategies and existing PWM techniques.

Author Contributions: All authors were involved in developing the concept to make the article an error-free technical outcome for the set investigation work

Funding: This research received no external funding.

Acknowledgments: The authors would like to express their sincere gratitude to the Renewable Energy Lab, College of Engineering, Prince Sultan University, Riyadh, Saudi Arabia for giving the opportunity to execute the project in this area.

Conflicts of Interest: The authors declare no conflict of interest.

Nomenclature

CM	Common mode
CMC	Common mode current
CMV	Common mode voltage
DC	Direct current
AC	Alternating current
EMI	Electromagnetic interference
PWM	Pulse width modulation
PV	Photovoltaic
VFD	Variable frequency drive
dv/dt	Change in voltage
di/dt	Change in current
LC	Product of inductance and capacitance
SPWM	Sinewave pulse width modulation
NPC	Neutral point clamped
SVPWM	Space vector pulse width modulation
PDPWM	Phase disposition PWM
SS	Spread spectrum
V_A, V_B, V_C	AC voltage of each leg
V_{Ref}	Voltage of reference modulating signal
V_{Am}, V_{Bm}, V_{Cm}	Voltage of reference modulating signal for each leg
V_m	Peak value of output voltage
V_{m3}	Peak value of third harmonic of output voltage
$f(wt)$	Function of reference waveform of the method third harmonics injection
V_{dc}	DC input voltage
R_{CM1}, R_{CM2}	Damping resistor
L_{CM1}, L_{CM2}	Chokes
C_{CM1}, C_{CM2}	Capacitor
L_{CM}, C_{CM}	Common mode equivalent inductance and capacitor
f_o	Common mode resonant frequency

Appendix A

Table A1. Specifications of the system parameters.

Name of the Component	Rating
DC link voltage	560 V
DC link capacitor	2200 μ F
Filter inductance	450 mH
Filter capacitance	11.6 μ F
Rated phase voltage	230 V
Frequency	50 Hz
Grid Parameters	
Grid voltage and frequency	230 V, 50 Hz
Carrier frequency	20 kHz

References

1. Kerekes, T.; Teodorescu, R.; Liserre, M. Common mode voltage in case of transformerless PV inverters connected to the grid. In Proceedings of the IEEE International Symposium on Industrial Electronics, Cambridge, UK, 30 June–2 July 2008; pp. 2390–2395.
2. Esmaeli, A.; Tavassoli, F. A novel passive filter to reduce PWM inverters adverse effects in electrical machine system. *World App. Sci. J.* **2011**, *13*, 2536–2544.

3. Elnady, A.; Salama, M.M.A. Unified approach for mitigating voltage sag and voltage flicker using the DSTATCOM. In Proceedings of the IEEE Power Engineering, Society General Meeting, Denver, CO, USA, 6–10 June 2004; p. 645.
4. Yao, Z.; Xiao, L. Control of single-phase grid-connected inverters with nonlinear loads. *IEEE Trans. Ind. Electron.* **2011**, *60*, 1384–1389. [[CrossRef](#)]
5. Prasad, K.N.V.; Kumar, G.R.; Kumar, Y.S.A.; Narayana, G.S. In Proceedings of the IEEE International Conference on Computer Communication and Informatics, Coimbatore, India, 4–6 January 2013; pp. 1–6.
6. Khan, S.A.; Guo, Y.; Zhu, J. A high efficiency transformerless PV grid-connected inverter with leakage current suppression. In Proceedings of the 9th International Conference on Electrical and Computer Engineering, Dhaka, Bangladesh, 20–22 December 2016; pp. 190–193.
7. Grishanov, E.V.; Brovanov, S.V. Aspects of common-mode leakage current suppression in single-phase PV-generation systems. In Proceedings of the 18th International Conference of Young Specialists on Micro/Nanotechnologies and Electron Devices, Erlagol, Russia, 29 June–3 July 2017; pp. 541–546.
8. Zhu, H.; Liu, D.; Chen, H.; Chen, G. An improved foster model of common-mode inductor and its application in EMI filter design. In Proceedings of the IEEE International Symposium on Electromagnetic Compatibility and Asia-Pacific Symposium on Electromagnetic Compatibility, Singapore, 14–18 May 2018; 461–465.
9. Zhang, L.; Sun, K.; Xing, Y.; Xing, M. H6 transformerless full-bridge PV grid-tied inverters. *IEEE Trans. Power Electron.* **2013**, *29*, 1229–1238. [[CrossRef](#)]
10. Aggeler, D.; Canales, F.; Biela, J.; Kolar, J.W. Dv/Dt-control methods for the SiC JFET/Si MOSFET cascode. *IEEE Trans. Power Electron.* **2013**, *28*, 4074–4082. [[CrossRef](#)]
11. Kakosimos, P.; Sarigiannidis, A.; Beniakar, M.; Kladas, A. Investigation of transformerless topologies for renewable energy applications eliminating leakage currents. In Proceedings of the MedPower 2014, Athens, Greece, 2–5 November 2014; pp. 1–5.
12. Araujo, S.V.; Zacharias, P.; Mallwitz, R. Highly efficient single-phase transformerless inverters for grid-connected photovoltaic systems. *IEEE Trans. Ind. Electron.* **2010**, *57*, 3118–3128. [[CrossRef](#)]
13. Figueredo, R.S.; Carvalho, K.C.M.; Ama, N.R.N.; Matakas, L. Leakage current minimization techniques for single-phase transformerless grid-connected PV inverters—An overview. In Proceedings of the Brazilian Power Electronics Conference, Gramado, Brazil, 27–31 October 2013; pp. 517–524.
14. Zografos, D.; Koutroulis, E.; Yang, Y.; Blaabjerg, F. Minimization of leakage ground current in transformerless single-phase full-bridge photovoltaic inverters. In Proceedings of the 17th European Conference on Power Electronics and Applications, Geneva, Switzerland, 8–10 September 2015; pp. 1–10.
15. Yang, B.; Li, W.; Gu, Y.; Cui, W.; He, X. Improved transformerless inverter with common-mode leakage current elimination for a photovoltaic grid-connected power system. *IEEE Trans. Power Electron.* **2012**, *27*, 752–762. [[CrossRef](#)]
16. Liu, D.; Zhu, H.; Zhao, R. Novel common-mode current suppression method in transformerless PV grid-connected system. *Appl. Sci.* **2018**, *8*, 2072. [[CrossRef](#)]
17. Yang, Y.; Mao, C.; Wang, D.; Tian, J.; Yang, M. Modeling and analysis of the common mode voltage in a cascaded H-bridge electronic power transformer. *Energies* **2017**, *10*, 1357. [[CrossRef](#)]
18. Yang, T.; Hao, X.; He, R.; Wei, Z.; Huang, T.; Zhang, Y. Hybrid modulation strategy to eliminate current distortion for PV GRID-tied H6 inverter. *Appl. Sci.* **2018**, *8*, 2578. [[CrossRef](#)]
19. Swain, S.D.; Ray, P.K.; Mohanty, K.B. Improvement of power quality using a robust hybrid series active power filter. *IEEE Trans. Power Electron.* **2017**, *32*, 3490–3498. [[CrossRef](#)]
20. Hashempour, M.M.; Savaghebi, M.; Vasquez, J.C.; Guerrero, J.M. A control architecture to coordinate distributed generators and active power filters coexisting in a microgrid. *IEEE Trans. Smart Grid* **2016**, *7*, 2325–2336. [[CrossRef](#)]
21. Singh, B.; Jain, C.; Goel, S.; Gogia, R.; Subramaniam, U. A sustainable solar photovoltaic energy system interfaced with grid-tied voltage source converter for power quality improvement. *Electr. Power Compon. Syst.* **2016**, *45*, 171–183. [[CrossRef](#)]
22. Wong, M.C.; Dai, N.Y.; Lam, C.S. *Parallel Power Electronics Filters in Three-Phase Four-Wire Systems: Principle, Control and Design*; Springer: Berlin, Germany, 2016; pp. 59–165.
23. Sarajian, S. Design and control of grid interfaced voltage source inverter with output LCL Filter. *Int. J. Electron. Commun. Electr. Eng.* **2014**, *4*, 26–40.

24. Nazeri, A.A. Comparison of different filter types for grid connected inverter. In Proceedings of the 29th PIERS Proceedings, Marrakesh, Morocco, 20–23 March 2011.
25. Boonpirom, N. The EMI improvement on active filter using common-mode noise circuits balanced method. In Proceedings of the 18th International Conference on Electrical Machines and Systems, Pattaya, Thailand, 25–28 October 2015; pp. 1325–1328.
26. Chen, X.; Xu, D.; Liu, F.; Zhang, J. A novel inverter-output passive filter for reducing both differential- and common-mode dv/dt at the motor terminals in PWM drive systems. *IEEE Trans. Ind. Electron.* **2007**, *54*, 419–426. [[CrossRef](#)]
27. Kim, H.; Lee, H.; Sul, S. A new PWM strategy for common-mode voltage reduction in neutral point clamped inverter-fed AC motor drives. *IEEE Trans. Ind. Appl.* **2001**, *37*, 1840–1845.
28. Gupta, A.K.; Khambadkone, A.M. A space vector modulation scheme to reduce common mode voltage for cascaded multilevel inverters. *IEEE Trans. Power Electron.* **2007**, *22*, 1672–1681. [[CrossRef](#)]
29. Babu, B.C. Control of Voltage Source Inverters Using PWM/SVPWM for Adjustable Speed Drive Applications. Ph.D. Thesis, Department of Electrical Engineering, National Institute of Technology Rourkela, Rourkela, India, May 2009.
30. Kumar, K.V.; Michael, P.A.; John, J.P.; Kumar, D.S.S. Simulation and comparison of SPWM and SVPWM control for three phase inverter. *ARPN J. Eng. Appl. Sci.* **2010**, *5*, 61–74.
31. Mehra, M.; Pouresmaeil, E.; Zabihi, S.; Trujillo Caballero, J.C.; Catalão, J.P.S. A novel modulation function-based control of modular multilevel converters for high voltage direct current transmission systems. *Energies* **2016**, *9*, 867. [[CrossRef](#)]
32. Moranchel, M.; Huerta, F.; Sanz, I.; Bueno, E.; Rodríguez, F.J. A comparison of modulation techniques for modular multilevel converters. *Energies* **2016**, *9*, 1091. [[CrossRef](#)]
33. Jerin, A.R.A.; Palanisamy, K.; Umashankar, S.; Sanjeevikumar, P. Comparative analysis of feed-forward and synchronous reference frame control-based dynamic voltage restorer. *Adv. Power Syst. Energy Manag.* **2018**, 411–420. [[CrossRef](#)]
34. Tang, X.; Lai, C.; Liu, Z.; Zhang, M. A SVPWM to eliminate common-mode voltage for multilevel inverters. *Energies* **2017**, *10*, 715. [[CrossRef](#)]
35. Pareschi, F.; Rovatti, R.; Setti, G. EMI reduction via spread spectrum in DC/DC converters: State of the art, optimization, and tradeoffs. *IEEE Access* **2015**, *3*, 2857–2874. [[CrossRef](#)]
36. Park, H.; Kim, M.; Jung, J. Spread spectrum technique to reduce EMI emission for an LLC resonant converter using a hybrid modulation method. *IEEE Trans. Power Electron.* **2018**, *33*, 3717–3721. [[CrossRef](#)]
37. Kato, T.; Inoue, K.; Akimasa, K. EMI reduction method for a Single-Phase PWM inverter by suppressing common-mode currents with complementary switching. In Proceedings of the IEEE 5th International Power Electron and Motion Control Conference, Shanghai, China, 14–16 August 2006; pp. 1–5.
38. Morris, C.T.; Han, D.; Sarlioglu, B. Reduction of common mode voltage and conducted EMI through three-phase inverter topology. *IEEE Trans. Power Electron.* **2017**, *32*, 1720–1724. [[CrossRef](#)]
39. Perotti, M.; Fiori, F. Software based control of the EMI generated in BLDC motor drives. In Proceedings of the International Symposium on Electromagnetic Compatibility-EMC EUROPE, Wroclaw, Poland, 5–9 September 2016; pp. 417–421.
40. Perotti, M.; Fiori, F. Investigating the EMI mitigation in power inverters using delay compensation. *IEEE Trans. Power Electron.* **2019**, *34*, 4270–4278. [[CrossRef](#)]
41. Hedayati, M.H.; Acharya, A.B.; John, V. Common-mode filter design for PWM Rectifier-based motor drives. *IEEE Trans. Power Electron.* **2013**, *28*, 5364–5371. [[CrossRef](#)]
42. Ali, M.; Labouré, E.; Costa, F.; Revol, B. Design of a hybrid integrated EMC Filter for a DC–DC power converter. *IEEE Trans. Power Electron.* **2012**, *27*, 4380–4390. [[CrossRef](#)]
43. Yücel, A.C.; Bağcı, H.; Michielssen, E. An adaptive multi-element probabilistic collocation method for statistical EMC/EMI characterization. *IEEE Trans. Electromagn. Comp.* **2013**, *55*, 1154–1168. [[CrossRef](#)]
44. Yazdani, M.R.; Farzanehfard, H. Conducted electromagnetic interference analysis and mitigation using zero-current transition soft switching and spread spectrum techniques. *IET Power Electron.* **2012**, *5*, 1034–1041. [[CrossRef](#)]
45. Kovačević, I.F.; Friedli, T.; Muesing, A.M.; Kolar, J.W. 3-D electromagnetic modeling of EMI input filters. *IEEE Trans. Ind. Electron.* **2014**, *61*, 231–242. [[CrossRef](#)]

46. Son, Y.C.; Sul, S. A new active common-mode EMI filter for PWM inverter. *IEEE Trans. Power Electron.* **2003**, *18*, 1309–1314. [[CrossRef](#)]
47. Xing, L.; Sun, J. Conducted common-mode EMI reduction by impedance balancing. *IEEE Trans. Power Electron.* **2012**, *27*, 1084–1089. [[CrossRef](#)]
48. Salamah, A.M.; Finney, S.J.; Williams, B.W. Three-phase phase-lock loop for distorted utilities. *IET Electric Power Appl.* **2007**, *1*, 937–945. [[CrossRef](#)]
49. Morris, C.T.; Han, D.; Sarlioglu, B. Comparison and evaluation of common mode EMI filter topologies for GaN-based motor drive systems. In Proceedings of the IEEE Applied Power Electronics Conference and Exposition, Long Beach, CA, USA, 20–24 March 2016; pp. 2950–2956.
50. Ogasawara, S.; Ayano, H.; Akagi, H. An active circuit for cancellation of common-mode voltage generated by a PWM inverter. *IEEE Trans. Power Electron.* **1998**, *13*, 835–841. [[CrossRef](#)]
51. Alam, A.; Mukul, M.K.; Thakura, P. Wavelet transform-based EMI noise mitigation in power converter topologies. *IEEE Trans. Electromagn. Compat.* **2016**, *58*, 1662–1673. [[CrossRef](#)]
52. Tamasas, M.E.; Saleh, M.; Shaker, M.; Hammada, A. Comparison of different third harmonic injected PWM strategies for 5-level diode clamped inverter. In Proceedings of the IEEE Power and Energy Conference at Illinois, Champaign, IL, USA, 23–24 February 2017; pp. 1–6.
53. Colak, I.; Bayindir, R.; Kabalci, E. A modified harmonic mitigation analysis using Third Harmonic Injection PWM in a multilevel inverter control. In Proceedings of the 14th International Power Electronics and Motion Control Conference, Ohrid, Macedonia, 6–8 September 2010; pp. 215–220.



© 2019 by the authors. Licensee MDPI, Basel, Switzerland. This article is an open access article distributed under the terms and conditions of the Creative Commons Attribution (CC BY) license (<http://creativecommons.org/licenses/by/4.0/>).

Article

Economic Analysis of HRES Systems with Energy Storage During Grid Interruptions and Curtailment in Tamil Nadu, India: A Hybrid RBFNOEHO Technique

Karunakaran Venkatesan ^{1,*}, Uma Govindarajan ¹, Padmanathan Kasinathan ²,
Sanjeevikumar Padmanaban ^{3,*}, Jens Bo Holm-Nielsen ³ and Zbigniew Leonowicz ⁴

¹ Department of Electrical and Electronics Engineering, College of Engineering, Anna University, Chennai 600025, Tamil Nadu, India

² Department of Electrical and Electronics Engineering, Agni College of Technology, Thalambur, Chennai, Tamil Nadu 600130, India

³ Center for Bioenergy and Green Engineering, Department of Energy Technology, Aalborg University, 6700 Esbjerg, Denmark

⁴ Faculty of Electrical Engineering, Wroclaw University of Science and Technology, Wyb. Wyspianskiego 27, 50370 Wroclaw, Poland

* Correspondence: kanchikaruna8860@gmail.com (K.V.); san@et.aau.dk (S.P.)

Received: 30 June 2019; Accepted: 2 August 2019; Published: 7 August 2019

Abstract: This work presents an economic analysis of a hybrid renewable energy source (HRES) integrated with an energy storage system (ESS) using batteries with a new proposed strategy. Here, the HRES system comprises wind turbines (WT) and a photovoltaic (PV) system. The hybrid WT, PV and energy storage system with battery offer several benefits, in particular, high wind generation utilization rate, and optimal generation for meeting supply-demand gaps. The real recorded data of various parameters of a 22 KV hybrid ‘Regen’ feeder of 110/22 KV Vagarai Substation of TANTRANSOCO in Palani of Tamilnadu in India was gathered, studied for the entire year of 2018, and utilized in this paper. The proposed strategy is the hybridization of two algorithms called Radial Basis Function Neural Network (RBFNN) and Oppositional Elephant Herding Optimization (OEHO) named the RBFNOEHO technique. With the help of RBFNN, the continuous load demand required for the HRES and be tracked. OEHO is used to optimize a perfect combination of HRES with the predicted load demand. The aim of the proposed hybrid RBFNOEHO is to study the cost comparison of the HRES system with the existing conventional base method, energy storage method (ESS) with batteries and with HOMER. The proposed Hybrid RBFNOEHO technique is evaluated by comparing it with the other techniques; it is found that the proposed method yields a more optimal solution than the other techniques.

Keywords: energy storage system (ESS); hybrid renewable energy sources (HRES); grid; demand; load; RBFNOEHO technique

1. Introduction

In the present scenario, the energy demand is managed with both renewable and non-renewable sources in most of the countries around the world. More quantum generation of green energy than fossil fuels is the need of the hour due to both the cost factor as well as the mitigation of global warming. At the same time, the optimum production of green energy even during interruptions is a challenging task. Hence, a study of the economic analysis on this subject is more important. The Sun is the prime source of all energies and power. Heat and light, being the primary forms of solar energy are transformed and absorbed by the environment in various ways for sustainability; this has been reviewed in [1–4]. A review on the relationships between energy transformation from

renewable energy sources such as wind and solar with climate change mitigation has been presented in [5]. This, in turn, helps to mitigate greenhouse gas emissions and reduce global warming as has been explained in [6], along with the anticipated patterns of future energy use. A review on the scope of CO₂ mitigation through various renewable energy gadgets has been presented [7]. In general, wind energy is caused by airflow and solar energy is caused by irradiation. Hence, the amount of harvestable renewable energy predicted for a particular time span might not be accurate. In addition, renewable energy sources are intermittent, fluctuating and non-continuous. Many unsatisfactory issues due to implementation of renewable electricity systems alone have been addressed in detail [8]. Voltage, frequency, and waveform are the three important affecting factors of the ‘power quality’ of the distribution network, due to the synchronization of the generation from renewable energy sources into the power grid [9]. It has been reported that this could also affect the scheduling scheme, in turn, hence further affecting the normal operation of the distribution network. The grid synchronization of the power is discussed in detail by [10,11]. Energy storage technologies using batteries in hybrid wind power operations is analyzed in [12,13]. The characteristics and a comparison of energy storage systems have been reviewed in [14]. The need for energy storage in active distribution networks in spite of the uncertainty of wind power distributed generation is discussed in [15].

In this context, the study of the integration of hybrid renewable energy systems with the power grid is essential. The main essence of the energy storage is nothing but the properties of its ‘space transfer energy’ for stable operation of the power grid and thereby to improve the power quality. In [16], an OPF control of HRES with energy storage was discussed, and the achievement of a better dynamic response due to energy storage has been proved.

In recent years, a number of nature-inspired metaheuristic evolutionary algorithms have been studied in depth and are being applied to solve different types of optimization problems. Examples of such algorithms are the Genetic Algorithm (GA) [17–19], Biogeography-based Optimization (BBO) [20], Particle Swarm Optimization (PSO) [21,22], Artificial Bee Colony (ABC) [23], Different Evolution (DE) [24], Bacterial Foraging Optimization (BFO) [25], Ant Colony Optimization (ACO) [26], Cuckoo Search (CS) [27], Honey Bee Mating Optimization (HBMO) [28], BAT Algorithm [29], etc. These different types of algorithms are often being used to solve the various engineering problems that arise in different fields. Numerous research works are available in the literature for optimum power flow management using solar energy and wind energy transformation applying different techniques in different parts of the world. The steps taken by the Korea Electric Power Corporation (KEPCO) to develop a Renewable Energy Map (REM) in South Korea have been reviewed in [30]. In addition, they have explained the steps taken for optimal location identification for a renewable complex without violating any reliability standards.

An effective assessment approach to non-renewable energy sources has been developed in Taiwan; the country is dependent on the importation of energy, with more than 99% coming from foreign countries, as discussed in [31]. In [32], the many problems and challenges faced by China’s wind power industry are reviewed in detail. A comprehensive assessment was presented to discuss China’s wind power industry, power demand, cost and distribution of wind power. In [33] it was reported that the wind power access to power grids could have a great influence on the power stability and power quality of the distribution network of Henan Province in China.

In [34], the availability of the abundant solar radiation and the challenges for utilizing it for solar irrigation in Bangladesh has been reviewed. In [35] the availability of RES and the present technologies practiced in Bangladesh have been briefed with conclusions for the implementation of systematic changes from conventional to the non-conventional (renewable) methods to obtain benefits for the whole nation.

This work focuses on an economic analysis to integrate an energy storage system (ESS) using batteries along with different hybrid renewable energy source (HRES) devices using the proposed strategy. Here, the HRES system comprises wind turbines (WT) and a photovoltaic (PV) system. The proposed strategy is the hybridization of two algorithms called Radial Basis Function Neural

network (RBFNN) explained by [36] and Oppositional Elephant Herding Optimization (OEHO) described by [37], together named the RBFNOEHO technique.

Reference [38] has proposed an optimal energy management for a grid-connected PV-WT, MT and ESS hybrid energy system utilizing the ANFMDS approach and Homer. The technique has analyzed various load demands of the microgrid.

In the proposed study, a detailed analysis based on real data is discussed to insist on the need for an energy storage system to avoid the wastage of the production and utilization of green energy. Beneficially and economically; in particular, generation during various types of 'grid interruption' and utilization during the 'peak' hours and 'maintenance periods' of the solar and wind electric generators are studied. The research work is a comparative economic analysis of HRES without using energy storage and battery storage during grid interruption and curtailment. Curtailment has been a major concern for RES. Curtailment can be defined as a reduction in the output of a generator from what it could otherwise produce given the available resources (e.g., wind or sunlight), typically on an involuntary basis. Curtailment occurs when a transmission system operator issues an instruction to limit the energy output of a specific or a group of RES generators. There is lot of evidence for the incidence of curtailment across many states in India. Curtailment is heavily influenced by local factors, such as the status of the grid infrastructure near an RE generation site and resource variability at those sites. There is considerable variation in the quantum of curtailment across months, states, and even districts in a state, so there is a need to solve the issue during grid interruptions and curtailment using HRES combined with the optimal storage system.

In this paper, an existing Hybrid Renewable Energy Source (HRES) comprising a wind power generation and solar power generation system in a single 22 KV feeder at Vagarai located in the Palani Division in the Dindigul Circle of TANGEDCO in Tamil Nadu, India has been chosen for study. This dissertation focuses on an economic analysis to integrate the hybrid renewable energy sources (HRES) with an energy storage system (ESS) using batteries in the proposed strategy. Here, the HRES system comprises wind turbines (WT) and a photovoltaic (PV) system. The proposed strategy is the hybridization of two algorithms called Radial Basis Function Neural Network (RBFNN) and Oppositional Elephant Herding Optimization (OEHO) named the RBFNOEHO technique. The rest of the paper is organized as follows: Section 2 describes the topography of Tamil Nadu state. Section 3 contains a description of the chosen area. Section 4 describes the objective function formulation. Section 5 portrays the system configuration of HRES system. Section 6 postulates the economic analysis of battery storage system for HRES system using the proposed hybrid strategy. Section 7 defines the real data and simulation results and a discussion. Section 8 concludes the manuscript.

2. Topography of the State of Tamil Nadu

In general, in India, the Sun is visible on sunny days at 6.00 a.m. in the morning and disappears at 6.00 p.m. The solar insolation varies with seasons. However, in general, the peak of the irradiation during sunny days occurs between 7.30 a.m. and 4.00 p.m. The energy demand can be fulfilled by solar energy only during daytime hours. On the other hand, wind energy is available in the southwest monsoon months of May through September in the peninsula and Tamil Nadu. The rest of the months there will be poor generation from wind due to lull periods or shorter generation periods. The energy balance for the entire day and night and throughout the year by the hybrid system alone is very difficult and it is not at all possible. The coordinates of the location of Thoppampatti village and Vagarai village in Palani, India are 10.5844° N, 77.5727° E. The average and maximum wind speed and wind gust over the years in Palani, India as described in [39] are shown in Figure 1.

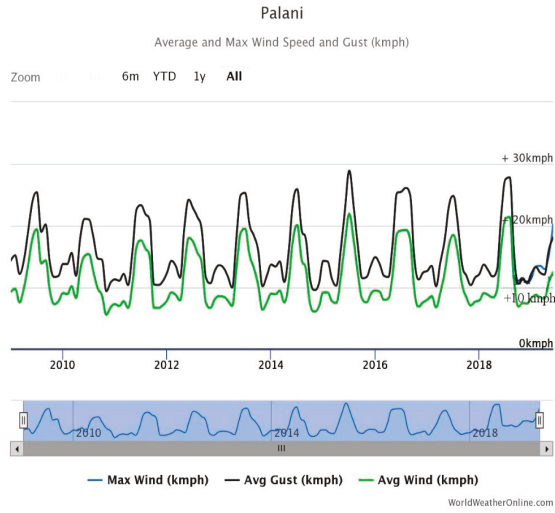


Figure 1. The average and maximum wind speed and wind gust over the years in Palani, India.

The average sun hours and sun days over the years in Palani, India is shown in Figure 2, as described in [39].

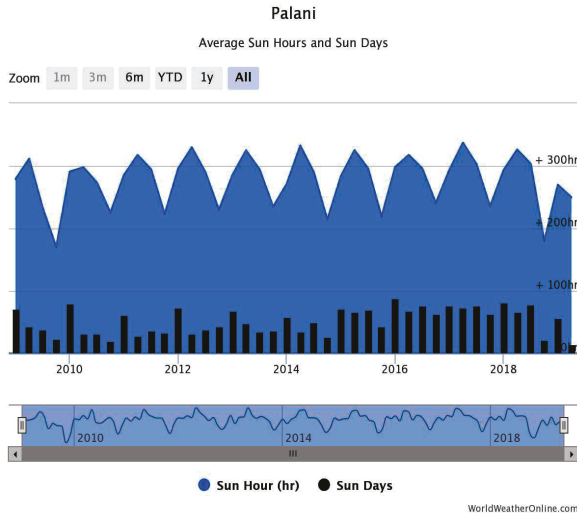


Figure 2. The average sun hours and sun days over the years in Palani, India.

3. Description of the Chosen Area

An existing hybrid system with both solar and wind generation combined and formed as 22 KV feeders and fed into 110/22 KV Vagarai Substation, in the Palani Division in the Dindigul Circle of TANGEDCO in the State of Tamil Nadu of India has been chosen for our study purposes. The presentation of the real data and analysis in this section will give the real picture of the present scenario and the need for energy storage for economical and beneficial usage of the green energy to meet the entire “Demand” requirement with the limited utilization of conventional energy. The switchyard arrangement of the 22 KV hybrid feeders in the 110/22 KV Vagarai SS is shown in Figure 3.

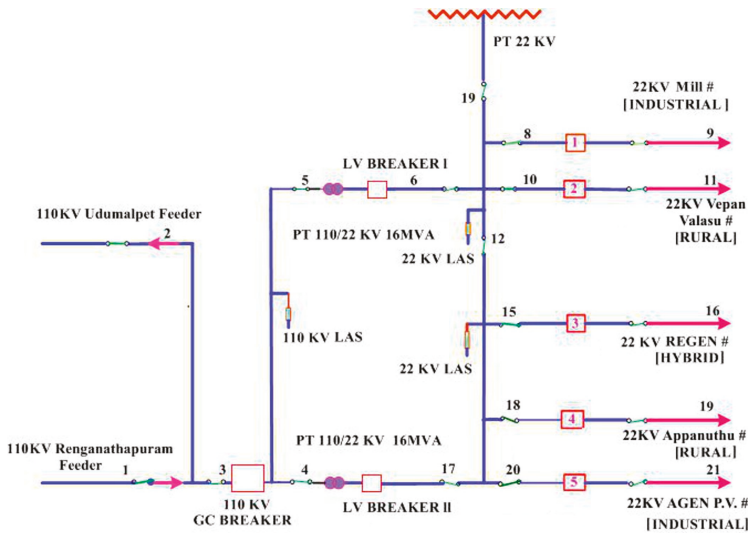


Figure 3. Switchyard arrangement of the 22 KV hybrid feeder in the 110/22 KV Vagarai SS.

4. Objective Function Formulation

The existing 22 KV Vagarai feeder consists of one standalone 1.5 MW wind turbine (W_1), and one 1.5 MW wind turbine (W_{2-PV}) combined in a hybrid configuration with a 0.300 MW solar PV system and one standalone 2.8 MW wind turbine (W_3). The cost of the entire system and the initial erection and commission cost is fixed. The objective function, which has to be minimized, can be expressed as follows:

$$Min(AC) = N_{PV}C_{PV} + N_{WT}C_{WT} + P_{ESS}C_{ESS} - C_{gs} + C_{gp} \tag{1}$$

where, AC is the annualized cost of the system. The annualized total costs of PV , WT and ESS are represented as C_{PV} , C_{WT} and C_{ESS} . The total price (\$/year) of electricity purchased from the grid annually is denoted as C_{gp} and the total price of electricity sold to the grid (\$/year) annually is C_{gs} . The annualized cost of each component comprises several parts, that is, annualized capital cost, and annualized operational and annualized replacement cost.

The entire hybrid system comprises several components and the cost of the replacement of components during normal wear and tear and major breakdown is the running cost for operations and maintenance. The salary of the operational crew and miscellaneous costs like taxes on land and maintenance of the control room building is also included in the running cost. It also includes the cost of purchasing power for the operation of the wind turbines, when synchronized with the grid. The system with the lowest cost would be classified as possessing the optimal strategy; it should overcome the constraints and one should measure the ‘per unit’ cost by dividing the total cost and the generation units in KWHr. In the proposed study, the production of power is the total supply of power to the grid at the instance of generation and the stored energy fed back, generated during predictable interruption periods. Hence when measuring per unit cost by dividing the total cost and the generation units in KWHr, it will be less when compared to the cost of the system without energy storage:

$$Max(Gen) = E_{W1} + E_{W2-PV} + E_{W3} - E_{Import-W1} - E_{Import-W2-PV} - E_{Import-W3} \tag{2}$$

$$Min(Cost) = C_{W1} + C_{W2-PV} + C_{W3} - C_{Import-W1} - C_{Import-W2-PV} - C_{Import-W3} \tag{3}$$

Here, the export of energy from the wind turbine (W_1) is denoted as E_{W1} , the export of energy from wind turbine (W_2) plus solar Photo Voltaic (PV) is denoted as (E_{W2-PV}) and the export of energy

from the wind turbine (W_3) is denoted as E_{W_3} . C_{W_1} is the cost of the sale of power to grid due to the standalone 1.5 MW wind turbine. C_{W_2PV} is the cost of the sale of power to the grid due to the hybrid 1.5 MW wind turbine combined with the 0.300 MW solar PV systems and C_{W_3} is the cost of the sale of power to the grid due to the standalone 2.8 MW wind turbine.

By substituting the real data of the energy supplied to the grid through the 22 KV hybrid feeder of the 110 KV Vagarai SS, into the expressions of (2) and (3), will become:

$$Max(Gen) = 3016380 + 3362200 + 6570120 - 10800 - 12420 - 11960 = 12913520 \text{ KWHr} \quad (4)$$

$$Min(Cost) = 144786.24 + 161385.60 + 354786.48 - 518.40 - 596.16 - 645.84 = 659198 \$ \quad (5)$$

In the existing grid-connected hybrid system, without any energy storage, the cost per unit sold without any storage for the year 2018 in the 22 KV hybrid feeder, considering all interruption periods is:

$$C_{actual} = Min(Cost) / Max(Gen) \quad (6)$$

By substituting the real data of the net energy sold and the net cost towards supply of energy in (6), one gets the following expression:

$$C_{actual} = 659198 / 12913520 = 0.05104 = 0.051 \$ \quad (7)$$

Hence, the annual average net cost of the energy sold to grid during the year 2018 without any storage system during the interruptions is worked out to be \$0.051.

In the first operational segment, the entire load of the 110 KV Vagarai SS is fully served by the connected hybrid feeder, which consists of three WTz and a 0.300 KW solarPV unit:

$$P_{W_1}(t) + P_{W_2-PV}(t) + P_{W_3}(t) = P_{Load} \quad (8)$$

In the second operational segment, the entire load is fully served by the connected hybrid feeder, which consists of three WTsz and the 0.300 KW solar PV system, when they are equal and higher than the load demand:

$$P_{W_1}(t) + P_{W_2-PV}(t) + P_{W_3}(t) > P_{Load} \text{ or } P_{W_1}(t) + P_{W_2-PV}(t) + P_{W_3}(t) \geq P_{Load} \quad (9)$$

The remaining power would be sent to the grid.

In the third operational segment, the load can be partly served by the connected hybrid feeder, which consists of three WTs and a 0.300 KW solar PV system, is less than the load demand:

$$P_{W_1}(t) + P_{W_2-PV}(t) + P_{W_3}(t) < P_{Load} \quad (10)$$

5. System Configuration of the HRES System

In this section, the system configuration of the HRES system is explained. The PV panel is connected with a rectifier to deliver alternating current. The proposed combination of the WT-PV system will act as a power injection system to the power grid and does not have the features needed to apply any sort of power quality control on the generated power. The output power of the WT is directly delivered by means of the AC grid to the distribution side. The output power produced by the solar panels is fed into the grid through the DC-AC converter. A bidirectional charge controller carries out the functions of charging and discharging the battery and thus performing both the AC-DC conversion and voltage boosting. The non-continuous availability of the renewable sources would hinder a system not equipped for gathering the power dispatch standards of the load dispatch centers. Likewise, during periods of high wind, the wind turbines are forced to shut down to safeguard the equipment. Coordinating the battery with the renewable energy source devices will enable to store the excess energy and it could be used beneficially during peak power demand periods, thus improving

the system reliability. It additionally enables the storage of energy during periods when low demand exists, so that it can be better utilized during the peak load periods. The system configuration of the HRES system in the proposed strategy is shown in Figure 4.

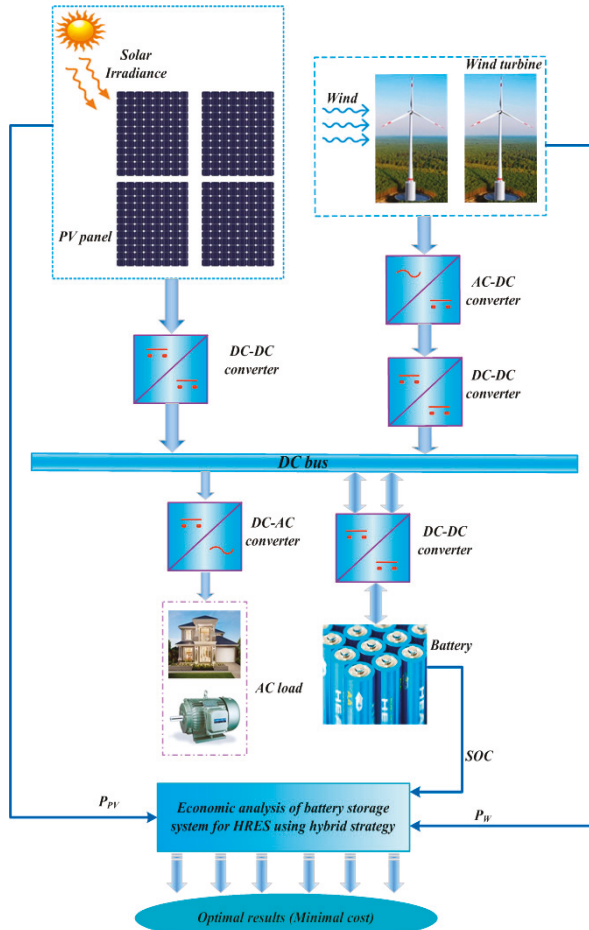


Figure 4. System configuration of the HRES system.

Photovoltaic systems and wind turbines are non-dispatchable resources. The battery system is an energy storage device. In the proposed approach, in the light of the annualized capital and replacement cost the objective functions are resolved. Along these lines, the optimal operation is accomplished when the objective of maximized revenues and minimized usage of HRES is fulfilled.

6. Economic Analysis of Battery Storage System for HRES System Using Hybrid Strategy

In this section, the proposed strategy for the economic analysis of battery storage system for the HRES system is described. The proposed strategy is the incorporation of Radial Basis Function Neural Network (RBFNN) and Oppositional Elephant Herding Optimization (OEHO) named RBFNNOEHO. RBFNN can be regarded as a feed-forward network composed with three layers of neurons [36]. The EHO algorithm is developed from the natural behavior of elephant herding [37]. Figure 5 portrays the procedure of economic analysis of the proposed system.

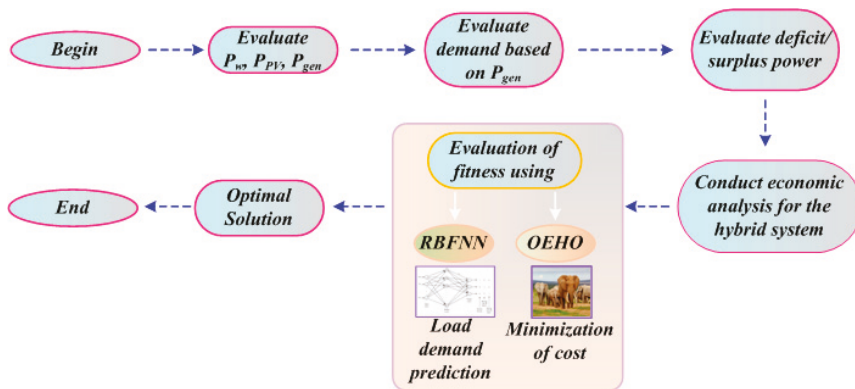


Figure 5. Process of economic analysis of the proposed system.

In order to accelerate the convergence rate and performance, the EHO is enhanced with the concept of oppositional-based learning (OBL). With the help of RBFNN, the required load demand for the HRES system is continuously tracked. With the consideration of the predicted load demand, OEHO is optimized for the HRES perfect combination. The involvement of the annualized capital cost and replacement cost of the HRES system is the main objective of the proposed methodology. The constraint is the renewable energy sources accessibility, power demand and storage elements state of charge. The systematic process of RBFNN and OEHO are discussed in the following section.

6.1. Prediction of Load Demand Using RBFNN

RBFNN is an artificial neural network. In the field of mathematical modelling, the proposed artificial neural network uses radial basis functions as activation functions. The first layer is called the input layer. It consists of the source nodes for the input data. The second layer is the single hidden layer in the network. It is made up of the radial basis functions. The nonlinear transformation is applied by these functions from the input layer into the hidden layer. The third layer is called the output layer. The output layer of the network is a linear combination of radial basis functions of the inputs and neuron parameters.

Here, the RBFNN is trained by the target power demand with the appropriate input time intervals of the day. To establish the proposed approach, the selection of the input variables to each node in the first layer and the output is computed using the Gaussian membership function.

Based on these corresponding inputs and the output values the RBFNN is trained. The structure and the training process of the ANFIS are described as follows:

Step 1: The Input Vector. In the input layer of the network, the input vector a is applied. In the proposed approach, the time interval T is the input of the network, load demand are the output of the network. Then the equation for the input vector is given by:

$$a = [a_1 \ a_2 \ \dots \ a_p]^T \tag{11}$$

Here, a represents the input vector of the RBFNN.

Step 2: The RBF Neurons. From the training set, each RBF neuron stores a ‘prototype’ vector, which is one of the vectors. Each RBF neuron compares the input vector to its prototype, and outputs a value between 0 and 1 which is a measure of similarity. Output of the RBF neuron will be 1 if the input is equal to the prototype. The value of the neuron’s response is called its ‘activation’ value. The prototype vector is called neuron’s ‘centre’.

Step 3: The Output Nodes. The output of the network consists of set of nodes; each output node computes a score sort for the associated category. Typically, by assigning the input to the category with the highest score a classification decision is made. From every RBF neuron, a score is computed by taking a weighted sum of the activation values. With each of the RBF neurons, an output node associates a weight value by weighted sum and before adding it to the total response, it multiplies the neuron's activation by this weight. Every output node has its own set of weights for a different category because each output node is computing the score. Output node give positive weight to the RBF neurons and negative weight is shared to the others.

Step 4: RBF Neuron Activation Function. In between the input and its prototype vector, each RBF neuron computes a measure of the similarity. Input vectors are similar to the prototype, which returns a result closer to 1. There are different possible choices of similarity functions based on Gaussian. The equation for the Gaussian with a one-dimensional input is postulated as follows:

$$f(a) = \frac{1}{\alpha \sqrt{2\pi}} e^{-\frac{(a-\beta)^2}{2\alpha^2}} \quad (12)$$

Here, input can be represented as a , mean as β , standard deviation can be represented as α . The RBF neuron activation function is slightly different, and is typically written as:

$$\psi(a) = e^{-\eta \|a-\beta\|^2} \quad (13)$$

Here, β is the mean of the distribution in the Gaussian distribution. After completing the algorithm, the RBFNN generates the load demand. Then the predicted values are used as the input of OEHO to get the optimal energy management outputs for the HRES system.

6.2. Minimization of Total Cost Using OEHO

An efficient OEHO approach is presented for the optimal energy management in the connected HRES system. EHO algorithm is developed from the natural behavior of elephant herding. An elephant group is composed of a number of clans headed by a matriarch. A clan consists of females and their calves. It is seen that the preference of the females is to always live with family members; whereas, the preference of males is to live a nomadic and solitary life. The improved version of the elephant herding optimization to solve the optimal energy management in the HRES system is achieved by introducing oppositional-based learning (OBL). In general, the initial population for all the evolutionary algorithms is generated randomly and gradually until they reached the destination of the 'optimal solution' in the subsequent iterations and stopped at the pre-defined condition. The convergence times of the algorithms are linked to the distances of these initial guesses from the optimal solution. The speed of the convergence and the time taken depend upon the selection of the initial solution. If it is, closer to the optimal solution, then it converges as quickly as possible; otherwise, its speed would be comparatively less and it takes a longer time to converge. The Oppositional-based Learning (OBL) is considered as one of the most efficient concepts. It can be used to improve the initial solution by evaluating both the current candidate solution and its opposite solution simultaneously; and by choosing the more fitted one as the initial solution. OEHO is used to establish the exact schedule of the HRES combinations as per the power variations in both source and load side of the grid. Two definitions are used in the OBL-based proposed system, opposite number and opposite point. The two stages utilized here are Opposition-based Population Initialization (OBPI) and Opposition-based Generation Jumping (OBGJ). The terms are described as follows:

Definition 1. *Opposite number:* Let the real number be S . The opposite number of $s(s^*)$ is described as follows:

$$s^* = a + b - s \quad (14)$$

Likewise, in Definition 2 this definition can be extended to higher dimensions, which are stated as follows.

Definition 2. *Opposite point:* In d -dimensional search space the equation is equated to be $S = s_1, s_2, s_3, \dots, s_D$, where $s_1, s_2, s_3, \dots, s_D \in \text{Real}$, real number is represented as Real, $s_i \in [a_i, b_i] \forall i \in \{1, 2, \dots, d\}$. The opposite point $OS = (s_1^*, s_2^*, s_3^*, \dots, s_D^*)$ is completely defined by its components:

$$OS = a_i + b_i - s_i \tag{15}$$

In the accompanying section, the steps of the OEHO algorithm are explained as follows:

Step 1: Opposition Based Initial Population. Opposition based initialize the population of the HRES sources such as WT, PV are taken as the input.

Step 2: Random Generation. The elephant herd population is randomly generated by using the load demand matrix d :

$$d = \begin{bmatrix} r_{11} & r_{12} & \dots & r_{1n} \\ r_{21} & r_{22} & \dots & r_{2n} \\ \vdots & \vdots & \vdots & \vdots \\ r_{n1} & r_{n2} & \dots & r_{nm} \end{bmatrix} \tag{16}$$

Here, load demand can be specified as d , random solutions can be expressed as r .

Step 3: Fitness Evaluation. The fitness function is evaluated by minimizing the error value and the equation is expressed in the following equation,

$$obj = \text{Min} (\text{Cost}) \tag{17}$$

After the fitness function, the clan updating operator and separating operator is evaluated and the equations are explained in the Step 4 and Step 5.

Step 4: Clan Updating Operator. Being the leaders of the elephant group, the matriarchs are influenced by all the members of a particular clan in each generation; the next position of the member's j -th elephant of the clan is calculated as follows:

$$f_{new,c_i,j} = f_{c_i,j} + \varphi \times (f_{best,c_i} - f_{c_i,j}) \times r \tag{18}$$

Here, the clan is represented as c_i , the fittest elephant of the clan as f_{best,c_i} and the new updated position of the j -th elephant in the clan can be expressed as $f_{new,c_i,j}$. The next updated position of the fittest elephant is expressed as:

$$f_{new,c_i,j} = \gamma \times f_{center,c_i} \tag{19}$$

$$f_{center,c_i} = \frac{1}{m_{c_i}} \times \sum_{m_{c_i}}^{j=1} f_{c_i} d \tag{20}$$

Here, the number of elephants of each clan can be represented as m_{c_i} , $1 \leq d \leq D$ is the d -th dimension and D is specified as a total dimension.

Step 5: Separating Operator. The worst elephant of each clan updates its position in each generation and the equation can be expressed as follows:

$$f_{worst,c_i} = f_{min} + (f_{max} - f_{min}) \times \text{random} \tag{21}$$

Here, the worst elephant of the clan of elephant group can be indicated as f_{worst,c_i} , maximum and minimum value of the search space can be represented as f_{max} and f_{min} , $\text{random} \in [0, 1]$ follows the uniform distribution.

Step 6: Opposition Based Generation Jumping. To hop to another candidate solution the completely evolutionary process can be constrained in the event that we apply a comparable approach to the

current population, which is more reasonable than the current one. The new population is created and opposite population is determined in the wake of following the EHO operator, dependent on a jumping rate and it is a random number from (0, 1). The fittest NF individuals are chosen from this correlation. To compute the opposite points search space is diminished in every generation:

$$OS_{i,j} = \min_j^{gen} + \max_j^{gen} - S_{i,j} \tag{22}$$

Here, $i = 1, 2, \dots, N_F; j = 1, 2, \dots, n, [\min_j^{gen} + \max_j^{gen}]$ is the current interval in the population which is becoming increasingly smaller than the corresponding initial range p_j, q_j, J_R as the jumping rate. The process of position updating is continued, until the stop condition is met.

The flowchart of the proposed technique is depicted in Figure 6.

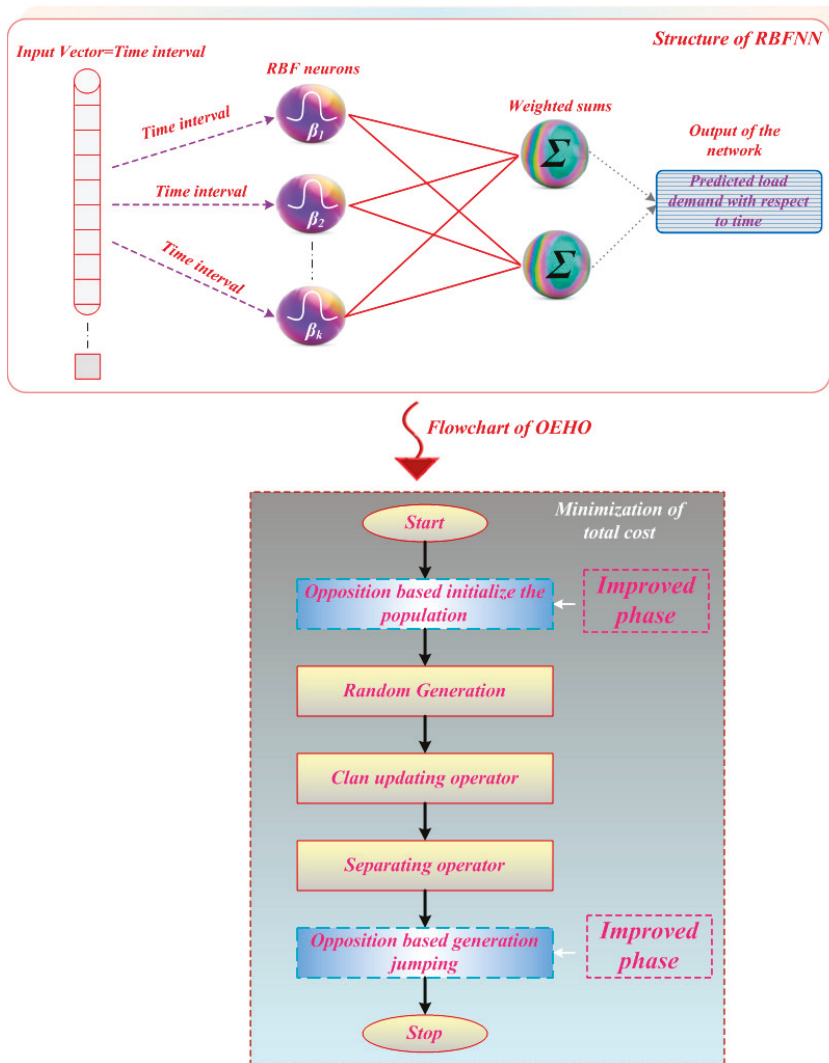


Figure 6. Flowchart of the proposed technique.

7. Results and Discussion

In this section, the economic analysis of the HRES system without and with energy storage is considered. The proposed technique is implemented in the MATLAB/Simulink platform. In order to meet the load demand of the system, PV, WT and battery have been utilized. HOMER is a free software application developed by the National Renewable Energy Laboratory in the United States. This software application is used to design and evaluate technically and financially the options for the off-grid and on-grid power systems for remote, stand-alone and distributed generation applications. It allows considering a large number of technological options to account for energy resource availability and other variables.

Here, two case studies are considered and discussed as follows:

Case Study A: Cost worked out for the interruption period without using energy storage.

Case Study B: Cost worked out using proposed technique for the interruption period with energy storage.

7.1. Case Study A

The existing 22 kV Vagarai feeder consists of one standalone 1.5 MW wind turbine (W_1), one 1.5 MW wind turbine (W_{2-PV}) combined in a hybrid system with a 0.300 MW solar PV system and one standalone 2.8 MW wind turbine (W_3). In this case, study A, the cost analysis for the interruption period without using energy storage has been analyzed. Here, there is no generation during load curtailment and interruption periods of the system due to non-availability of battery storage. The results of case study A mainly show the impacts of higher load curtailment i.e., fault trip, main supply failure, shutdowns, etc. Table 1 lists the amount of energy really sold to the TANTRANSCO grid in KWHr and the actual cost of the electricity (\$/month).

Table 1. Quantum of energy really sold to the TANTRANSCO grid in KWHr during the year 2018 and the realization of actual cost of electricity (\$/month).

Month	E_{W1}	$\$-C_{W1}$	E_{W2-PV}	$\$-C_{W2-PV}$	E_{W3}	$\$-C_{W3}$	Export in KWHr	Total Cost (\$)
January 2018	30,740	1476	152,380	7314	103,680	4977	286,800	13,766
February 2018	129,800	6230	154,180	7401	282,280	13,549	566,260	27,180
March 2018	26,400	1267	28,780	1381	50,480	2423	105,660	5072
April 2018	102,040	4898	113,080	5428	205,920	9884	421,040	20,210
May 2018	243,300	11,678	278,160	13,352	512,240	24,588	1,033,700	49,618
June 2018	605,760	29,076	592,980	28,463	1,490,320	71,535	2,689,060	129,075
July 2018	768,120	36,870	867,960	41,662	1,734,640	83,263	3,370,720	161,795
August 2018	676,560	32,475	686,100	32,933	1,341,680	64,401	2,704,340	129,808
September 2018	185,460	8902	188,400	9043	359,920	17,276	733,780	35,221
October 2018	53,240	2556	64,820	3111	100,240	4812	218,300	10,478
November 2018	77,260	3708	92,480	4439	151,800	7286	321,540	15,434
December 2018	117,700	5650	142,880	6858	236,920	11,372	497,500	23,880

The quantum of the energy really purchased from the TANTRANSCO grid in KWHr and the actual cost paid for the electricity (\$/month) is derived in Table 2. The MATLAB/Simulation proves the generation cost is optimum after considering the sale of excess stored power. The total price (\$/month) of electricity sold to grid monthly is denoted as $I_{Import-month}$.

The export of energy from the wind turbine (W_1) is denoted as E_{W1} , the export of energy from wind turbine (W_2) plus solar Photo Voltaic (PV) is denoted as (E_{W2-PV}) and the export of energy from the wind turbine (W_3) is denoted as E_{W3} (per unit of power purchased from TANTRANSCO in INR is 3.30 [\$ 0.48] for the W_1 and W_2 plus PV solar hybrid system and INR 3.70 for W_3 [1 INR = \$0.015]). C_{W1} is the cost of the sale of power to grid due to the standalone 1.5 MW wind turbine. C_{W2} is the cost of the sale of power to the grid due to the hybrid 1.5 MW wind turbine combined with the 0.300 MW solar PV systems and C_{W3} is the cost of the sale of power to the grid due to the standalone 2.8 MW wind turbine. The import of energy from the wind turbine (W_1) is denoted as I_{W1} . The export of

energy from the wind turbine (W_2) plus solar PV systems denoted as $I_{W_2 PV}$ and the export of energy from the wind turbine (W_3) is denoted as I_{W_3} and per unit of power purchased from TANTRANSCO in INR is 3.30 [\$0.48] for W_1 and W_2 plus solar PV hybrid system; and INR 3.70 is for W_3 [1 INR = \$0.015]. Similarly, the import of energy for the wind turbine (W_1) is denoted as I_{W_1} , the import of energy for the wind turbine (W_2) plus solar PV systems denoted as $I_{W_2 PV}$ and the import of energy for the wind turbine (W_3) is denoted as I_{W_3} . Here, the export of energy from wind turbine (W_1) is denoted as E_{W_1} in column (2); export of energy from wind turbine (W_2) plus solar PV is denoted as $E_{W_2 PV}$ in column (3); and export of energy from wind turbine (W_3) is denoted as E_{W_3} . The amount of energy really purchased by the grid through 22 kV feeders in the 110/22 kV Vagarai SS is tabulated in Table 2.

Table 2. Quantum of energy really purchased by the TANTRANSCO grid in KWHr and actual cost paid towards the electricity (\$/month).

Month	I_{W_1}	$\$-C_{W_1}$	$I_{W_2 PV}$	$\$-C_{W_2 PV}$	I_{W_3}	$\$-C_{W_3}$	Import (KWHr)	Total Cost (\$)
January 2018	780	25.16	1040	49.92	720	38.88	2540	126.24
February 2018	640	22.86	860	41.28	960	51.84	2460	123.84
March 2018	460	14.84	540	25.92	560	30.24	1560	78.24
April 2018	1540	51.33	1560	74.88	1760	95.04	4860	243.84
May 2018	1540	49.68	920	44.16	1240	66.96	3700	185.04
June 2018	480	16.00	180	8.64	200	10.80	860	42.48
July 2018	580	18.71	300	14.40	280	15.12	1160	57.36
August 2018	120	3.87	40	1.92	80	4.32	240	12.00
September 2018	860	28.67	1560	74.88	1400	75.60	3820	191.76
October 2018	1240	40.00	2120	101.76	1920	103.68	5280	264.96
November 2018	1140	38.00	1780	85.44	1400	75.60	4320	215.76
December 2018	1420	45.81	1520	72.96	1440	77.76	4380	218.88

The actual current flow at 01.00 hon 19 July 2018 in all segments like 22 kV side, LV 1, LV2, Bus 1 and Bus 2; 110 kV side, GC and 110 kV Udumalpet/Renganathapuram in the switch yard is shown in Figure 7.

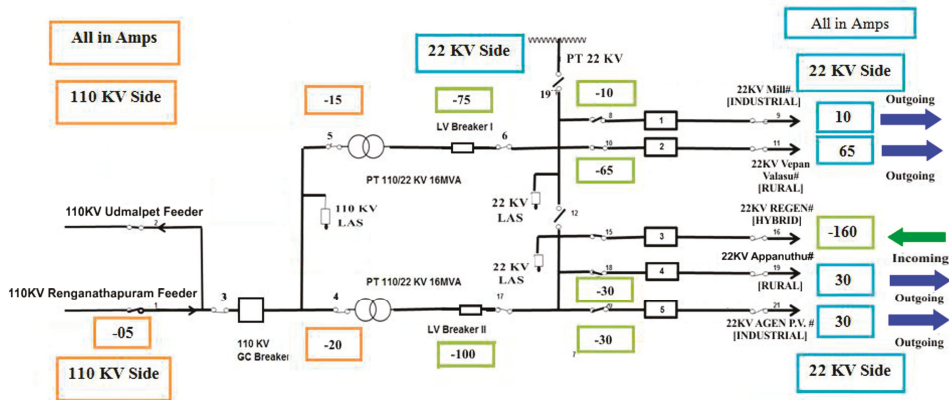


Figure 7. Actual flowchart of both the 110 kV and 22 kV sides @ 01.00 hour on 19 July 2018 in the 110 kV SS.

The hourly readings of the five 22 kV feeders in the 110/22 kV Vagarai substation and the L.V 1 and L.V 2 of the power transformers1 and 2 on 19 July 2018 are tabulated in Tables 3 and 4.

The 22 kV Bus 2 is connected with three 22 kV feeders, namely (1) Hybrid Generation Regen feeder, (2) Agen Vijay feeder and (3) Appanathu feeder; whereas the 22 kV Bus 1 is connected with two 22 kV feeders, namely (4) VepanValasu feeder and (5) Mill feeder in the 110/22 kV Vagarai substation.

Table 3. Readings of all the 22 kV feeders including the hybrid generation regen feeder in the 110/22 kV Vagarai SS on 19 July 2018.

Date	Hybrid		22 Industrial		Rural		Rural		Industrial	
19 July 2018	Regen Feeder		Agen Vijay		Appanuthu		VepanValasu		Mill	
Time	Current (A)	MW	A	MW	A	MW	A	MW	A	MW
1.00 a.m.	-160	-5.5	30	1.0	30	1.0	65	2.2	10	0.3
2.00 a.m.	-155	-5.3	30	1.0	30	1.0	65	2.2	10	0.3
3.00 a.m.	-160	-5.5	30	1.0	25	0.9	70	2.4	10	0.3
4.00 a.m.	-160	-5.5	25	0.9	25	0.9	70	2.4	10	0.3
5.00 a.m.	-160	-5.5	30	1.0	30	1.0	70	2.4	10	0.3
6.00 a.m.	-160	-5.5	30	1.0	35	1.2	80	2.7	10	0.3
7.00 a.m.	-150	-5.1	30	1.0	35	1.2	100	3.4	50	1.7
8.00 a.m.	-160	-5.5	30	1.0	40	1.4	110	3.8	55	1.9
9.00 a.m.	-150	-5.1	25	0.9	35	1.2	100	3.4	65	2.2
10.00 a.m.	-165	-5.7	25	0.9	30	1.0	95	3.3	65	2.2
11.00 a.m.	-140	-4.8	25	0.9	25	0.9	85	2.9	65	2.2
12.00 Noon	-135	-4.6	30	1.0	30	1.0	75	2.6	65	2.2
01.00 p.m.	-130	-4.5	30	1.0	25	0.9	80	2.7	60	2.1
02.00 p.m.	-130	-4.5	30	1.0	30	1.0	80	2.7	60	2.1
03.00 p.m.	-125	-4.3	30	1.0	30	1.0	80	2.7	55	1.9
04.00 p.m.	-125	-4.3	35	1.2	30	1.0	85	2.9	60	2.1
05.00 p.m.	-160	-5.5	30	1.0	30	1.0	85	2.9	60	2.1
06.00 p.m.	-170	-5.8	30	1.0	35	1.2	90	3.1	60	2.1
07.00 p.m.	-120	-4.1	30	1.0	35	1.2	75	2.6	60	2.1
08.00 p.m.	-165	-5.7	30	1.0	35	1.2	75	2.6	60	2.1
09.00 p.m.	-140	-4.8	30	1.0	30	1.0	80	2.7	55	1.9
10.00 p.m.	-130	-4.5	30	1.0	30	1.0	75	2.6	55	1.9
11.00 p.m.	-130	-4.5	30	1.0	30	1.0	75	2.6	55	1.9
12.00 Night	-150	-5.1	30	1.0	30	1.0	70	2.4	55	1.9

←-----22 kV Bus-2-----→ ←-----22 kV Bus-1-----→

Table 4. Readings of the 22 kV regen feeder, LV1 and LV2 of power transformers 1 and 2, respectively in the 110/22 kV Vagarai SS on 19 July 2018.

Date	Hybrid		Power Tr. 2		Power Tr. 1	
19 July 2018	Regen Feeder		L.V 2		L.V 1	
Time	Current (A)	MW	A	MW	A	MW
1.00 a.m.	-160	-5.5	-100	-3.42	75	2.57
2.00 a.m.	-155	-5.3	-95	-3.25	75	2.57
3.00 a.m.	-160	-5.5	-105	-3.60	80	2.74
4.00 a.m.	-160	-5.5	-110	-3.77	80	2.74
5.00 a.m.	-160	-5.5	-100	-3.42	80	2.74
6.00 a.m.	-160	-5.5	-95	-3.25	90	3.08
7.00 a.m.	-150	-5.1	-85	-2.91	150	5.14
8.00 a.m.	-160	-5.5	-90	-3.08	165	5.65
9.00 a.m.	-150	-5.1	-90	-3.08	165	5.65
10.00 a.m.	-165	-5.7	-110	-3.77	160	5.48
11.00 a.m.	-140	-4.8	-90	-3.08	150	5.14
12.00 Noon	-135	-4.6	-75	-2.57	140	4.79
01.00 p.m.	-130	-4.5	140	4.79	140	4.79
02.00 p.m.	-130	-4.5	140	4.79	140	4.79
03.00 p.m.	-125	-4.3	135	4.62	135	4.62
04.00 p.m.	-125	-4.3	145	4.97	145	4.97
05.00 p.m.	-160	-5.5	145	4.97	145	4.97
06.00 p.m.	-170	-5.8	150	5.14	150	5.14
07.00 p.m.	-120	-4.1	135	4.62	135	4.62
08.00 p.m.	-165	-5.7	100	3.42	135	4.62
09.00 p.m.	-140	-4.8	135	4.62	135	4.62
10.00 p.m.	-130	-4.5	130	4.45	130	4.62
11.00 p.m.	-130	-4.5	130	4.45	130	4.62
12.00 Night	-150	-5.1	135	4.62	135	4.62

←-----22 kV Bus-2-----→ ←-----22 kV Bus-1-----→

From Figure 7 and Table 3, it is seen that the required load was only 60 Amps (30 Amps each for the 22 kV Appanuthu and Agen Vijay feeders) on 22 kV Bus 2 and 75 Amps (10 Amps for 22 kV Mill feeder and 65 Amps for the 22 kV VepanValasu feeder). As the Bus coupler switch No. 12 was kept in an open condition, at 01.00 h on 19 July 2018, the power for an amount of 2.57 MW (75 Amps) out of 5.5 MW (160 Amps) from the hybrid feeder was stepped up to 110 kV by the power transformer (Pr. Tr)-2. And stepped down to 22 kV voltage level by power transformer (Pr. Tr)-1, (or, say from LV-2-Pr.Tr.2-Pr.Tr.1-LV-1) from the balance power of the 22 kV regen feeder, which is kept at 22 kV Bus-2.

An amount of current of 100 Amps at the 22 kV side got transformed through the power transformer, as 20 Amps at the 110 kV side; and only an amount of 15 Amps at 110 kV equivalent to 5 Amps for the 22 kV side required for Bus 1. The balance amount of 5 Amps would flow to the 110 kV GC and finally be exported through 110 kV Udumalpet/Ranganathapuram feeders. Or, one can say that the required load demand for the 22 kV Veppen Valasu and 22 kV turbine feeders was only 75 Amps @ 01.00 h, and the balance 25 Amps was fed into the power transformer 1 and stepped up to 110 kV.

The actual current flow on all the 22 kV feeders in the 22 kV side in both the 22 kV Bus 1 and Bus 2 are given in Table 4 and Figure 7. At 01.00 h, the demand of the 22 kV Agen Vijay and Appanuthu feeders was 30 Amps each, whereas the hybrid generation of the regen feeder was 160 Amps.

Similarly, during each hour of 19 July 2018, the actual incoming generation from the hybrid regen feeder and the load demand of the remaining four 22 kV feeders and power flow to/from the 110 kV GC are recorded and charted in Table 3.

The time vs. current (in Amps) graph is given in Figure 8. From the graph, it is understood that the wind generation alone on the 22 kV hybrid feeder balanced the entire load of four 22 kV feeders. The unutilized amount of energy had been exported through the 110 kV Udumalpet/Ranganathapuram feeders from 01.00 a.m. to 06.00 a.m. on 19 July 2018.

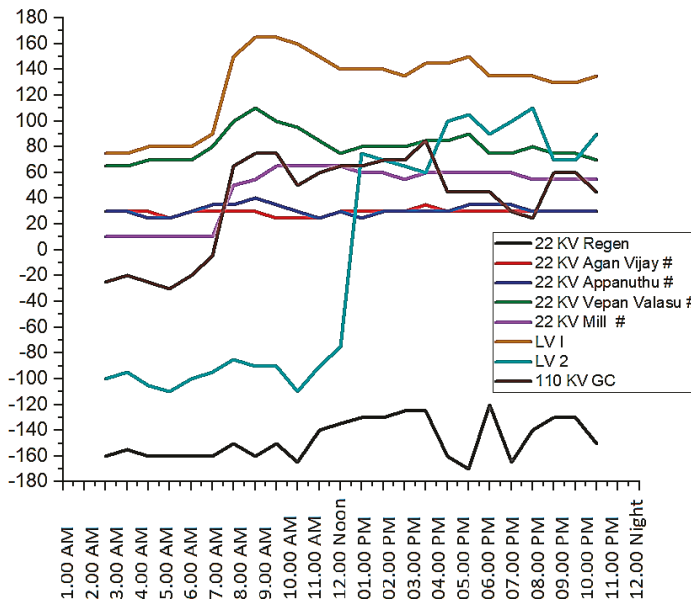


Figure 8. Time vs. current graph showing the actual current flowed with respect to hours of the day on each of the 22 kV feeders and LV1, LV2 and GC of the 110 Vagarai substation on 19 July 2018.

As the load increased during the day hours and as the hybrid generation could not cater to the load, 110 kV GC imported power through the 110 kV Udumalpet/Ranganathapuram feeders from 7.00 a.m. onwards. If the 22 kV regen feeder is kept connected only with the solar generation, then there

would not be any green energy from the wind and it would not fulfil the requirement at least up to some early hours of the day. In addition, if an energy storage system were implemented in the HRES, it would be more economical and beneficial and facilitate the generation of green energy even during predictable interruptions and curtailment periods also using the interconnectivity of the same grid.

The following Table 5 is a summary of various interruptions occurred in the 110 kV Vagarai SS during the year of 2018.

Table 5. Summary of all interruptions like fault trip, 110 kV main supply failure, load shedding, line clear, hand trip, break down and shut down in 110 kV Vagarai SS during the year of 2018.

Sl. No	Description	No. of Tripping	Duration of Interruptions
Group 1:			
a	Fault Trip	37	05 H 16 Min
b	Load Shedding	1	00 H 10 Min
c	Hand Trip	10	13 H 05 Min
d	Main 110 kV Supply failure	45	09 H 26 Min
Group 2:			
e	Total Shut down	9	65 H 35 Min
f	Line Clear	4	09 H 40 Min
g	Break Down of other feeders	11	109 H 15 Min
	Total	117	212 H 27 Min

From the table, it is understood that seven various types of generation interruption have occurred for a total of 212 hours and 27 min during the year 2018. The different types of interruptions are described as fault trip, (b) load shedding, (c) hand trip, (d) main 110 kV supply failure, (e) total shut down (f) line clear and (g) breakdown of other feeders and equipment. A summary of all month wise interruptions during the year of 2018 in the 110/22 kV Vagarai SS is presented in Table 6. All the interruptions can be grouped into two segments, some interruptions were predictable, and others were not predictable.

Table 6. Summary showing all interruptions month wise during the year of 2018.

Total Interruption					
Month	Hours	Min	Month	Hours	Min
January 2018	0	0.00	July 2018	14	11.00
February 2018	7	46.00	August 2018	81	9.00
March 2018	0	20.00	September 2018	55	17.00
April 2018	1	41.00	October 2018	10	40.00
May 2018	8	15.00	November 2018	14	46.00
June 2018	11	6.00	December 2018	7	16.00
Total	208 H plus 267 min = 208 + 4 H 27 Min, or say, 212 H 27 Min.				

7.1.1. Interruptions That Would Not Be Predictable and Can Occur Suddenly

Interruptions like (a) fault trip, (b) load shedding (c) hand trip and (d) main 110 kV supply failure are categorized in this group. These interruptions could not be predicted. However, if a proper energy storage system is available; the energy can be stored by diverting the output through the breaker to the energy storage system. The number of occurrences of said unpredictable interruptions was 93 in the year 2018 but the total duration of the interruptions is only 27 h and 57 min, as given in Table 7.

Table 7. Summary of unpredictable interruptions during the year 2018 in the 110 kV Vagarai SS.

Sl. No	Description	No. of Tripping	Duration of Interruptions
a	Fault Trip	37	05 h 16 min
b	Load Shedding	1	00 h 10 min
c	Hand Trip	10	13 h 05 min
d	Main 110 kV Supply failure	45	09 h 26 min
	Total	93	27 h 57 min

7.1.2. Interruptions That Are Predictable and Carried Out with Prior Intimation

Interruptions like (e) total shut down, (f) line clear and (g) proposed break down (BD) of other feeders and equipment are categorized in this group. The occurrence of the predictable interruptions during the year 2018, in the 110/22 kV Vagarai SS was 24 in number, but the duration was 184 h 30 min, as tabulated in Table 8.

Table 8. Summary of predictable interruptions during the year 2018 in the 110 kV Vagarai SS.

Sl. No	Description	No. of Tripping	Duration of Interruptions
e	Total Shutdown	9	65 h 35 min
f	Line Clear	4	09 h 40 min
g	Breakdown of other feeders	11	109 h 15 min
	Total	24	184 h 30 min

These interruptions are normally taken intentionally for maintenance of equipment in the yard of the substation, it can be predictable, and in fact, the details of the interruptions would be conveyed over phone before being carried out. The duration of the interruptions is very large and the green power from the renewable energy sources can be stored; if a proper energy system is incorporated. As there is an alternative supply available for running the wind turbines, it can be possible to harness the green energy and store it in the energy storage system to be sold to the grid in the future.

7.2. Case Study B

In the case study B, the cost analysis for the interruption period using the proposed technique with energy storage has been analyzed. Here, the loss of the production of the green energy during grid interruptions and wind curtailment of the system are minimized because of the presence of battery storage using the proposed technique. Consequently, the proposed system gives lower cost with an optimal solution. The power flow in the HRES system using battery storage is analyzed for one day and one year. The variation of load per day and for a year is depicted in Figure 9.

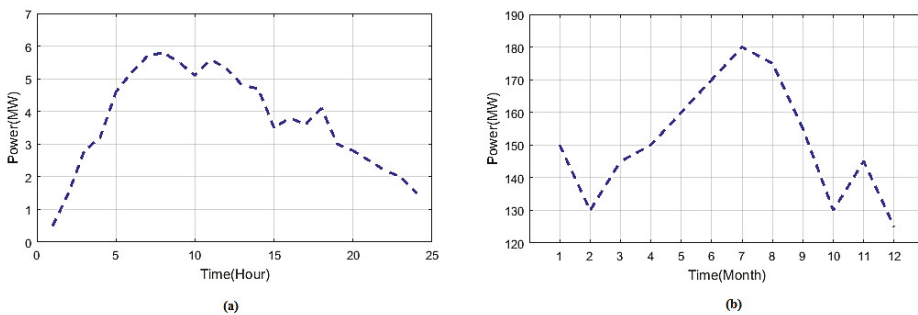


Figure 9. Demand versus time profile of the proposed technique for (a) one day (b) one year.

Figure 9a depicts how with the proposed technique the load demand is calculated during the time period of 24 h and Figure 9b illustrates the monthly load demand of the proposed technique. From Figure 9a, it is observed that the maximum hourly load demand of 5.9 MW is reached in the time intervals of 5 to 10 h. Likewise from Figure 9b, the maximum monthly load demand 1.39×10^4 KW is reached during the time period of 10 to 12 h.

The graphs of irradiance and wind speed for a 24 h. period are plotted in Figure 10. From Figure 10a, it is observed that the irradiance of the system is a maximum of 1000 W/m^2 during the time-period of 10 to 15 h. The maximum wind speed 12 m/s is predicted at the time moment of 5 to 15 h. in Figure 10b.

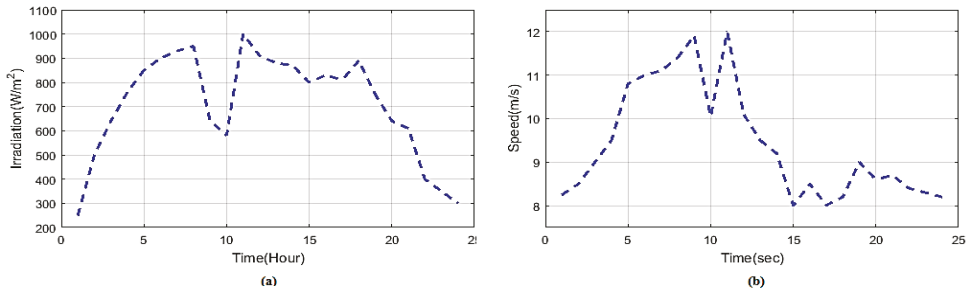


Figure 10. Analysis of (a) Irradiance (b) Wind Speed for one day.

Figure 11 shows the comparison analysis of power generated using energy storage, HOMER and the proposed technique for one day. Figure 11a depicts the graph of power versus time using the energy storage system. It is observed from Figure 11a, that by using the energy storage the maximum power 0.049 MW is generated in a period of 2 to 7 h. Figure 11b depicts the power generated using HOMER. By utilizing HOMER, the maximum power 0.047 MW is produced during the time interval of 20 to 25 h. Figure 11c shows the power generated using proposed technique. The maximum power generated using proposed technique is 0.05 MW at the time duration of 3 to 5 h.

Figure 12 shows the comparison analysis of power generated using energy storage, HOMER and proposed technique for one year. Figure 12a depicts a graph of power versus time using energy storage system. It is observed from the Figure 12a, which by using the energy storage the maximum power 1 MW is generated at the time period of 2 to 7 h. Figure 12b depicts the power generated using HOMER. By utilizing HOMER, the maximum power 1.3 MW is produced during the time interval of 2 to 4 h.

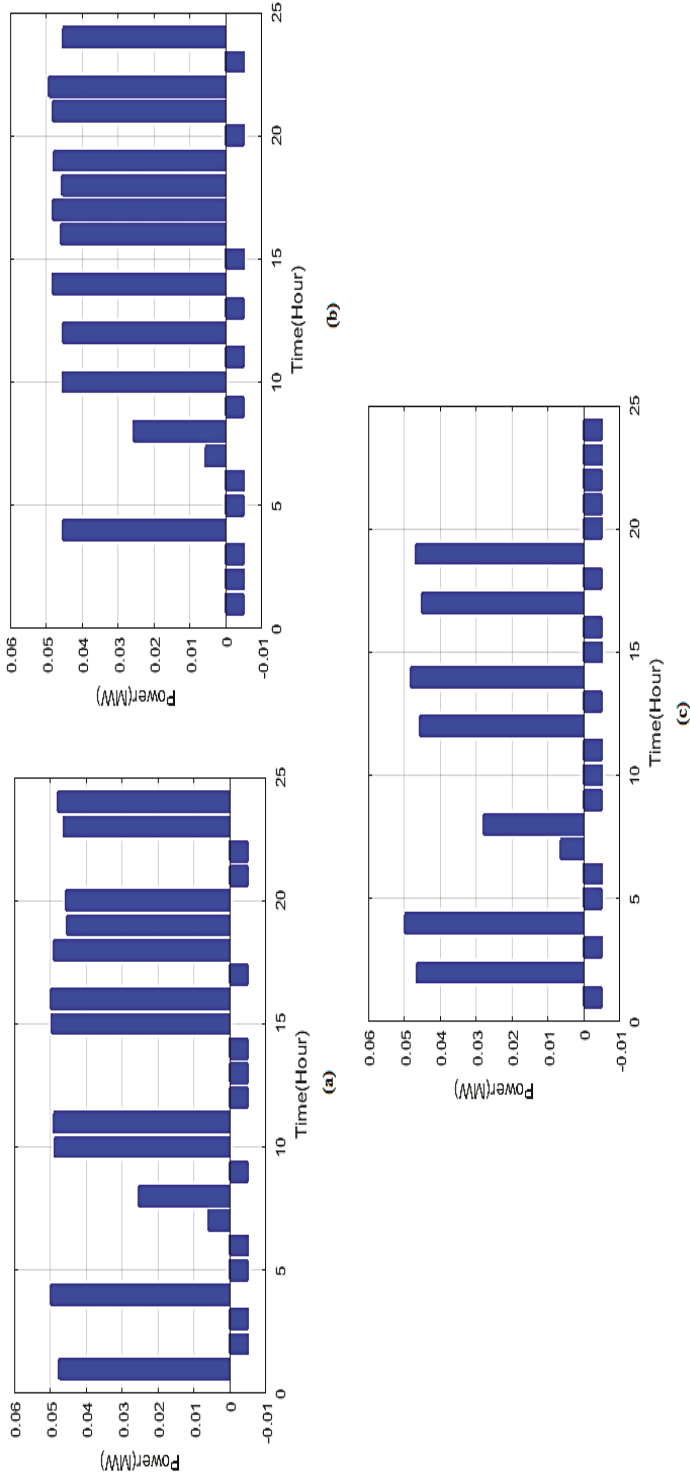


Figure 11. Comparison analysis of the power generated using (a) With ESS (b) HOMER (c) Proposed technique for one day.

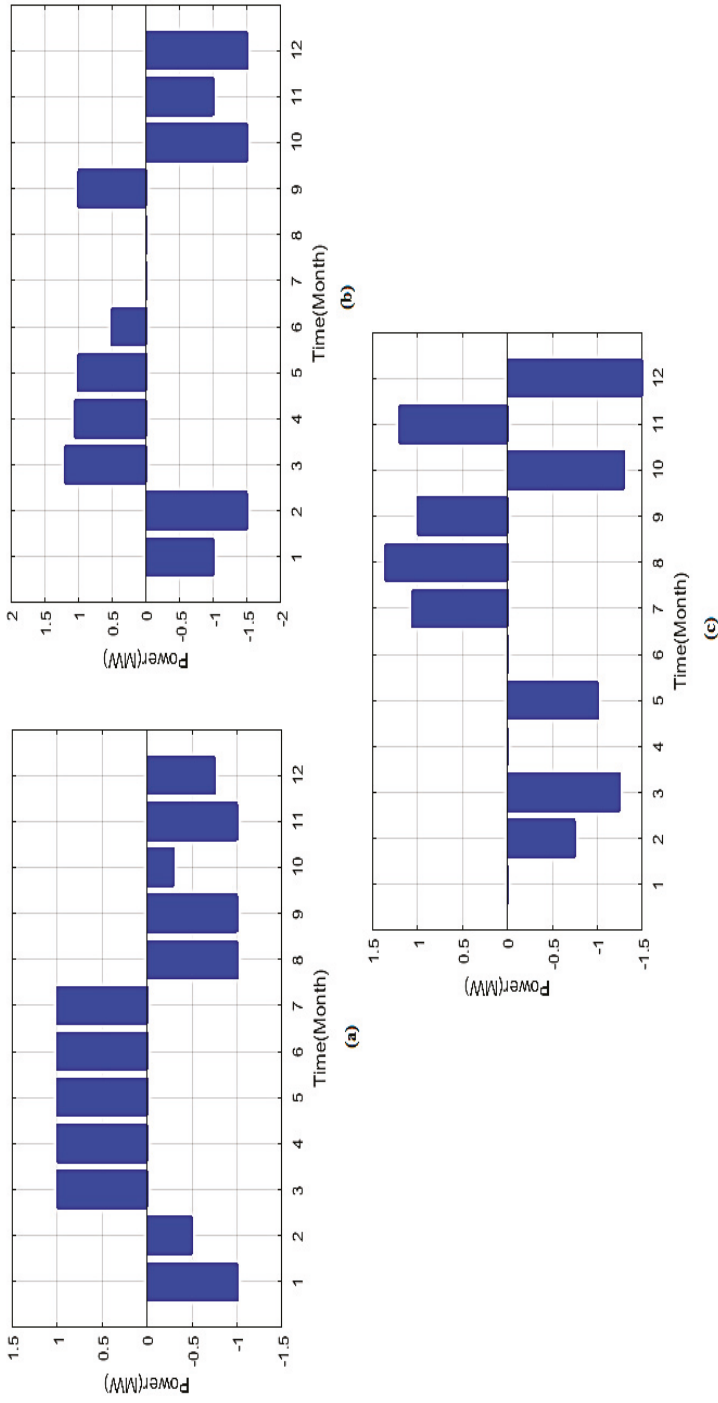


Figure 12. Comparison analysis of power generated using (a) With ESS (b) HOMER (c) Proposed technique for one year.

Figure 13 shows the individual generated power analysis using ESS, Without ESS, HOMER and Proposed for one day. Figure 13a shows the individual generated power using ESS. Figure 13a analyzes the PV, WT1, WT2 and WT3 generated power during the time period of 24 h. As seen from Figure 13a, the power generated by PV, WT1, WT2 and WT3 reaches the peak of 5.7 MW during the time instant of 5 to 10 h. Figure 13b shows the individual generated power without considering the ESS. From Figure 13b, it is observed that the power generated is in the maximum range of 5.75 MW at the time interval of 5 to 10 h. Figure 13c explains the individual generated power using HOMER. It is observed from the figure that the power generation is maximum 5.8 MW at the time duration of 5 to 10 h. Figure 13d delineates the individual generated power using the proposed technique. From Figure 13d, it is seen that the maximum power 5.9 MW is generated during the time interval of 5 to 10 h.

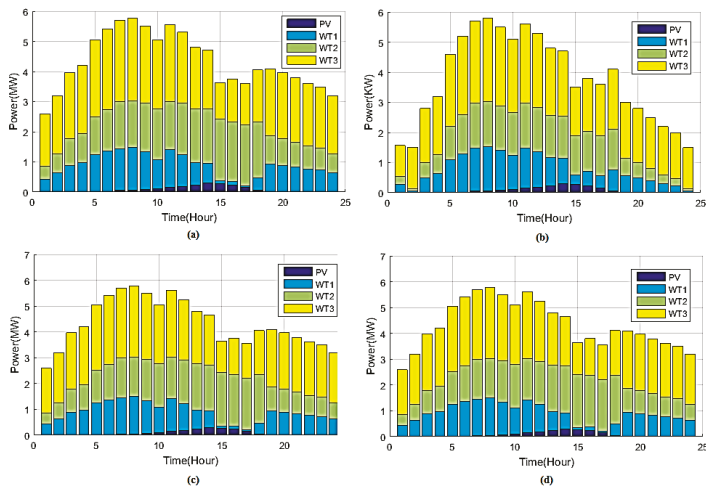


Figure 13. Individual Power analysis (a) With ESS (b) Without ESS (c) HOMER (d) Proposed technique for one day.

Figure 14 shows the individual generated power analysis using ESS, without ESS, HOMER and the proposed technique for one year. Figure 14a shows the individual generated power using ESS. Figure 14a analyzes the PV, WT1, WT2 and WT3 generated power during the time period of 24 h. As seen from Figure 14a, the power generated by PV, WT1, WT2 and WT3 reaches a peak of 160 MW during the time period of 6 to 8 h. Figure 14b shows the individual generated power without considering the BESS. From Figure 14b, it is observed that the power generated is in the maximum range of 155 MW during the time interval of 6 to 8 h. Figure 14c explains the individual generated power using HOMER. It is observed from the figure that the power generation is maximum 160 at the time period of 6 to 8 h. Figure 14d delineates the individual generated power using proposed technique. From the Figure 14d, the maximum power 170 MW is generated during the time interval from 6 to 8 h.

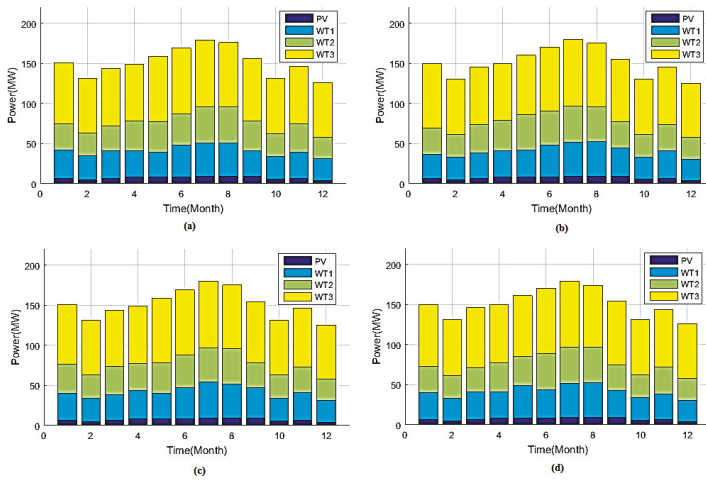


Figure 14. Individual power analysis: (a) With ESS (b) Without ESS (c) HOMER (d) Proposed technique for one year.

Figure 15 shows the investigation of fitness graph for one day. It depicts the fitness comparison for one day. As seen from the figure, the base method solution converges after an iteration count of 32. The HOMER fitness solution converges at the 38th iteration and the proposed technique gives the solution faster than the other techniques.

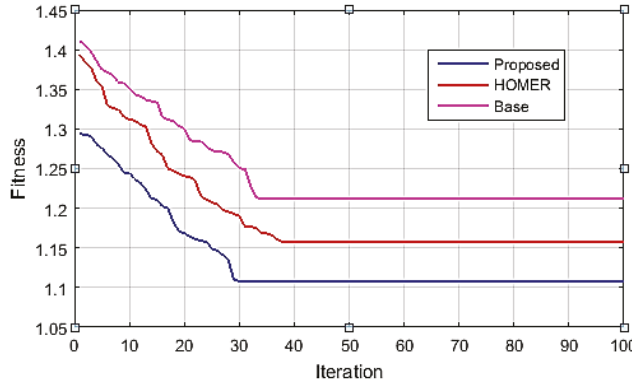


Figure 15. Investigation of Fitness comparison for one day.

Figure 16 shows the investigation of cost for one day and one year. Figure 16a depicts the graph of cost versus time. The cost of the proposed technique is more optimal for one day than the other techniques such as without ESS, Base and HOMER. Figure 16b depicts the graph of cost versus time. The cost of the proposed technique is more optimal for one year than the other techniques such as without ESS, Base and HOMER.

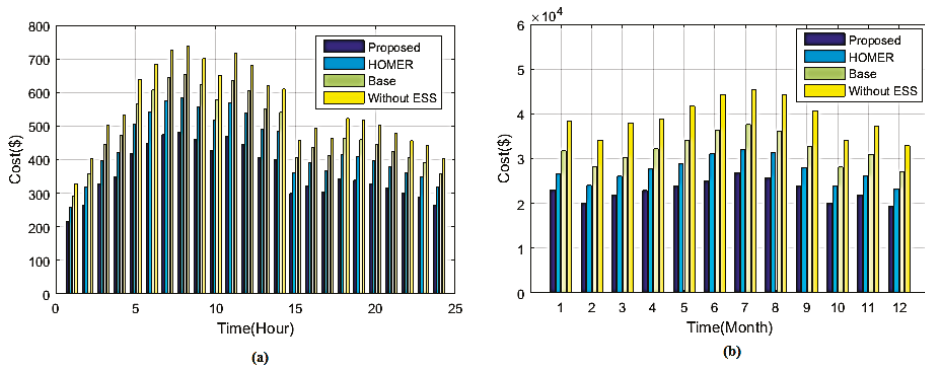


Figure 16. Investigation of cost for (a) One day (b) One year.

Figure 17 shows the investigation of fitness graph for one year.

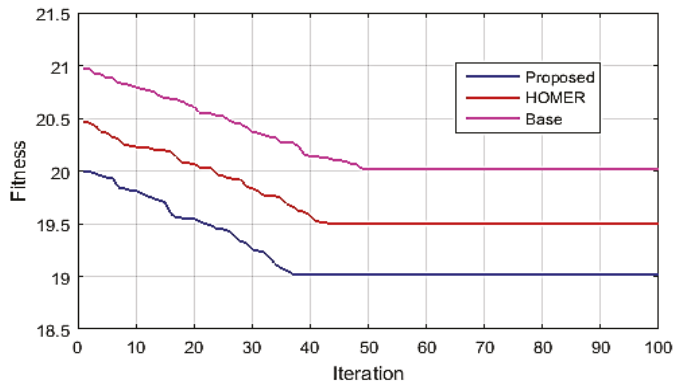


Figure 17. Investigation of Fitness comparison for one year.

As seen from the Figure 17, the base method solution converges after 49 iterations. The HOMER fitness solution converges at the 41st iteration and the proposed technique gives the solution faster than the other techniques.

8. Conclusions

The present study has been carried out for the optimization of hybrid renewable energy systems (HRES), where WT and PV function as generation systems and battery banks for storage as well as a backup system using the RBFNOEHO technique. Here, an existing hybrid system with both solar and wind generation combined and formed as 22 kV feeder and fed into the 110/22 kV Vagarai substation in the Palani Division in the Dindigul Circle of TANGEDCO in the State of Tamil Nadu of India has been chosen for study purposes. The economic analysis of battery storage for the HRES system using the proposed hybrid technique is discussed. By utilizing the proposed hybrid technique, the load demand is predicted and the total cost of the system is minimized. Here, two case studies are analyzed. First, the cost is worked out for interruption periods without using energy storage and in the second, the cost is worked out using the proposed technique for the interruption periods with energy storage. According to the results, it is concluded that the hybrid systems including WT and PV with battery backup are less costly compared to the other systems.

Author Contributions: All authors contributed equally to the research activity to present as full article.

Funding: This research was funded in part by EEEIC International, Poland.

Conflicts of Interest: The authors declare no conflict of interest.

Abbreviations

HRES	Hybrid Renewable Energy Sources.
RBFN	Radial Basis Function Neural Network
OEHO	Oppositional Elephant Herding Optimization
RBFNOEHO	Radial Basis Function Neural Network and Oppositional Elephant Herding Optimization
OBL	Oppositional based Learning
OBGJ	Oppositional based Generation Jumping
RBF Neuron	Radial Basis Function Neuron
WT	Wind Turbine
CT	Current transformer
SS	Sub Station
HOMER	Hybrid Optimization of Multiple Energy Resources
TANGEDCO	TamilNadu Generation and Distribution Corporation Ltd.
TANTRANSKO	TamilNadu Transmission Corporation Ltd.
TNEB Ltd.	Tamilnadu Electricity Board Ltd.
KEPCO	Korea Electric Power Corporation.
ESS	Energy Storage System
ANFIS	Adoptive Network based Fuzzy Inference system

References

1. Dincer, I. Renewable energy and sustainable development: A crucial review. *Renew. Sustain. Energy Rev.* **2000**, *4*, 157–175. [[CrossRef](#)]
2. Padmanathan, K.; Govindarajan, U.; Ramachandaramurthy, V.K.; Rajagopalan, A.; Pachaivannan, N.; Sowmmiya, U.; Padmanaban, S.; Holm-Nielsen, J.B.; Xavier, S.; Periasamy, S.K. A Sociocultural Study on Solar Photovoltaic Energy System in India: Stratification and Policy Implication. *J. Clean. Prod.* **2019**, *216*, 461–481. [[CrossRef](#)]
3. Padmanathan, K.; Govindarajan, U.; Ramachandaramurthy, V.K.; Sudar Oli Selvi, T. Multiple Criteria Decision Making (MCDM) Based Economic Analysis of Solar PV System with Respect to Performance Investigation for Indian Market. *Sustainability* **2017**, *9*, 820. [[CrossRef](#)]
4. Padmanathan, K.; Uma, G.; Ramachandaramurthy, V.K.; Sudar Oli Selvi, T.; Baskaran, J. Integrating solar photovoltaic energy conversion systems into industrial and commercial electrical energy utilization—A survey. *J. Ind. Inf. Integr.* **2018**, *10*, 39–54.
5. Owusu, P.; Asumadu-Sarkodie, S. A review of renewable energy sources, sustainability issues and climate change mitigation. *Cogent Eng.* **2016**, *3*, 1167990. [[CrossRef](#)]
6. Omer, A. Energy, environment and sustainable development. *Renew. Sustain. Energy Rev.* **2008**, *12*, 2265–2300. [[CrossRef](#)]
7. Panwar, N.; Kaushik, S.; Kothari, S. Role of renewable energy sources in environmental protection: A review. *Renew. Sustain. Energy Rev.* **2011**, *15*, 1513–1524. [[CrossRef](#)]
8. Heard, B.; Brook, B.; Wigley, T.; Bradshaw, C. Burden of proof: A comprehensive review of the feasibility of 100% renewable-electricity systems. *Renew. Sustain. Energy Rev.* **2017**, *76*, 1122–1133. [[CrossRef](#)]
9. Liang, X. Emerging Power Quality Challenges Due to Integration of Renewable Energy Sources. *IEEE Trans. Ind. Appl.* **2017**, *53*, 855–866. [[CrossRef](#)]
10. Blaabjerg, F.; Teodorescu, R.; Liserre, M.; Timbus, A. Overview of Control and Grid Synchronization for Distributed Power Generation Systems. *IEEE Trans. Ind. Electron.* **2006**, *53*, 1398–1409. [[CrossRef](#)]
11. Divya, K.; Ostergaard, J. Battery energy storage technology for power systems—An overview. *Electr. Power Syst. Res.* **2009**, *79*, 511–520. [[CrossRef](#)]
12. Zhao, H.; Wu, Q.; Hu, S.; Xu, H.; Rasmussen, C. Review of energy storage system for wind power integration support. *Appl. Energy* **2015**, *137*, 545–553. [[CrossRef](#)]

13. Choi, J.; Heo, S.; Kim, M. Hybrid operation strategy of wind energy storage system for power grid frequency regulation. *IET Gener. Transm. Distrib.* **2016**, *10*, 736–749. [[CrossRef](#)]
14. Ibrahim, H.; Ilinca, A.; Perron, J. Energy storage systems—Characteristics and comparisons. *Renew. Sustain. Energy Rev.* **2008**, *12*, 1221–1250. [[CrossRef](#)]
15. Sedghi, M.; Ahmadian, A.; Aliakbar-Golkar, M. Optimal Storage Planning in Active Distribution Network Considering Uncertainty of Wind Power Distributed Generation. *IEEE Trans. Power Syst.* **2016**, *31*, 304–316. [[CrossRef](#)]
16. Karunakaran, V.; Uma, G. Optimal Power Flow control of Hybrid renewable energy system with energy storage: A WOANN strategy. *J. Renew. Sustain. Energy* **2019**, *11*, 015501. [[CrossRef](#)]
17. Yin, P.Y. A fast scheme for multilevel thresholding using genetic algorithms. *Signal Process.* **1999**, *72*, 85–95. [[CrossRef](#)]
18. Hammouche, K.; Diaf, M.; Siarry, P. A multilevel automatic thresholding method based on a genetic algorithm for fast image segmentation. *Comput. Vis. Image Underst.* **2008**, *109*, 163–175. [[CrossRef](#)]
19. Zhang, J.; Li, H.; Tang, Z.; Lu, Q.; Zheng, X.; Zhou, J. An improved quantum inspired genetic algorithm for image multilevel thresholding segmentations. *Math. Probl. Eng.* **2014**, *112*, 1–12. [[CrossRef](#)]
20. Simon, D. Biogeography based optimization. *IEEE Trans. Evol. Comput.* **2008**, *12*, 702–713. [[CrossRef](#)]
21. Yin, P.Y. Multilevel minimum cross entropy threshold selection based on Particle swarm Optimization Algorithm. *Appl. Math. Comput.* **2007**, *184*, 503–513.
22. Kennady, J.; Eberhart, R.C. Particle swarm Optimization. In Proceedings of the IEEE International Conference of Neural Network, Perth, Australia, 27 November–1 December 1995; Volume 4, pp. 1942–1948.
23. Akay, B. A study on Particle swarm Optimization and artificial bee colony algorithms for multilevel thresholding. *Appl. Soft Comput.* **2013**, *13*, 3066–3091. [[CrossRef](#)]
24. Gandomi, A.H.; yang, X.S.; Talatahari, S.; Deb, S. Coupled eagle strategy and differential evaluation for unconstrained global optimization. *Comput. Math. Appl.* **2012**, *63*, 191–200. [[CrossRef](#)]
25. Sathya, P.D.; Kayalvizhi, R. Optimum multilevel image thresholding based on Tsallis entropy method with bacterial foraging algorithm. *Int. J. Comput. Sci.* **2010**, *7*, 336–343.
26. Tao, W.; Jin, H.; Liu, L. Object segmentation using ant colony optimization algorithm and fuzzy entropy. *Pattern Recognit. Lett.* **2007**, *28*, 788–796. [[CrossRef](#)]
27. Agarwal, S.; Panda, R.; Bhuyan, S.; Panigrahi, B.K. Tsallis entropy based optimal multilevel thresholding using Cuckoo Search algorithm. *Swarm Evol. Comput.* **2013**, *11*, 16–30. [[CrossRef](#)]
28. Horng, M.H. Multilevel minimum cross entropy threshold selection based on the honey bee mating optimization. *Expert Syst. Appl.* **2010**, *37*, 4580–4592. [[CrossRef](#)]
29. Yang, X.S. A new metaheuristic bat-inspired algorithm. In *Nature Inspired Cooperative Strategies for Optimization*; Springer: Berlin, Germany, 2010; Volume 284, pp. 65–74.
30. Kim, S.; Lee, H.; Kim, H.; Jang, D.H.; Kim, H.J.; Hur, J.; Cho, Y.S.; Hur, K. Improvement in policy and proactive interconnection procedure for renewable energy expansion in South Korea. *J. Renew. Sustain. Energy Rev.* **2018**, *98*, 150–162. [[CrossRef](#)]
31. Chen, F.; Lu, S.M.; Tseng, K.T.; Lee, S.C.; Wang, E. Assessment of renewable energy reserves in Taiwan. *Renew. Sustain. Energy Rev.* **2010**, *14*, 2511–2528. [[CrossRef](#)]
32. Dai, J.; Yang, X.; Wen, L. Development of wind power industry in China: A comprehensive assessment. *Renew. Sustain. Energy Rev.* **2018**, *97*, 156–164. [[CrossRef](#)]
33. Liu, Y.; Zhang, J. Research on the effects of wind power grid to the distribution network of Henan province. *AIP Conf. Proc.* **2018**, *1955*, 030005. [[CrossRef](#)]
34. Islam, M.R.; Sarker, P.C.; Ghosh, S.K. Prospect and advancement of solar irrigation in Bangladesh: A review. *Renew. Sustain. Energy Rev.* **2017**, *77*, 406–422. [[CrossRef](#)]
35. Islam, M.R.; Islam, M.R.; Beg, M.R. Renewable energy sources and technologies practice in Bangladesh. *Renew. Sustain. Energy Rev.* **2008**, *12*, 299–343. [[CrossRef](#)]
36. Pham, B.; Shirzadi, A.; Tien Bui, D.; Prakash, I.; Dholakia, M. A hybrid machine learning ensemble approach based on a Radial Basis Function neural network and Rotation Forest for landslide susceptibility modeling: A case study in the Himalayan area, India. *Int. J. Sediment Res.* **2018**, *33*, 157–170. [[CrossRef](#)]
37. Chakraborty, F.; Roy, P.; Nandi, D. Oppositional elephant herding optimization with dynamic Cauchy mutation for multilevel image thresholding. *Evol. Intell.* **2019**, 1–23. [[CrossRef](#)]

38. Murugaperumal, K.; Raj, P.A. Energy storage based MG connected system for optimal management of energy: An ANFMDA technique. *Int. J. Hydrog. Energy* **2019**, *44*, 7996–8010. [CrossRef]
39. World weather Home Page. Available online: <https://www.worldweatheronline.com/lang/en-in/palani-weather-averages/tamil-nadu/in.aspx> (accessed on 26 July 2019).



© 2019 by the authors. Licensee MDPI, Basel, Switzerland. This article is an open access article distributed under the terms and conditions of the Creative Commons Attribution (CC BY) license (<http://creativecommons.org/licenses/by/4.0/>).

Article

Rescheduling of Generators with Pumped Hydro Storage Units to Relieve Congestion Incorporating Flower Pollination Optimization

Padmini Sankaramurthy ¹, Bharatiraja Chokkalingam ^{1,2,*}, Sanjeevikumar Padmanaban ^{3,*}, Zbigniew Leonowicz ⁴ and Yusuff Adedayo ²

¹ Department of Electrical and Electronics Engineering, SRM Institute of Science and Technology, Chennai 603 203, India; padmini.s@ktr.srmuniv.ac.in

² Department of Electrical Engineering, University of South Africa, Florida Park, Roodepoort 1709, South Africa, yusufaa@unisa.ac.za

³ Department of Energy Technology, Aalborg University, 6700 Esbjerg, Denmark

⁴ Faculty of Electrical Engineering, Wrocław University of Science and Technology, Wyb. Wyspińskiego 27, 50370 Wrocław, Poland; zbigniew.leonowicz@pwr.edu.pl

* Correspondence: bharatiraja@gmail.com (B.C.); san@et.aau.dk (S.P.)

Received: 3 March 2019; Accepted: 4 April 2019; Published: 18 April 2019

Abstract: In this paper, a Flower Pollination Algorithm (FPA) has been proposed for relieving congestion in the deregulated power electricity industry. Congestion in the power market is one of the contemplative challenges to be overcome in the era of deregulation. The primary cause of congestion is due to the loss of the transmission line, an increase in load, or loss of generator(s). Hence, managing congestion is one of the issues which have to be tackled in the present scenario. There are several techniques to relieve congestion. It is quite well-known that the thermal limits of transmission lines in a power system are fixed. One of the methods to abate congestion is to reschedule the real power of the generators. The purpose of the present work is to benefit the Independent System Operator (ISO) in relieving congestion. (1) In order to meet this objective effectively, a FPA algorithm has been proposed for relieving congestion and is simulated on a modified IEEE 30-bus system initially. (2) Congestion cost, compared with and without the application of FPA, is computed. (3) To validate its effectiveness, the obtained results are compared with recent power system optimization algorithms present in the literature. (4) Further, the work has been extended with the incorporation of a Pumped Hydro Storage Unit (PHSU). Here an economic analysis of congestion cost reduction employing FPA before and after the incorporation of PHSU is investigated applying FPA. In comparison with other evolutionary algorithms, the uniqueness of generating a new population is attained in FPA by the levy flight procedure. It is one of the latest evolved algorithms and is suited for different power system problems due to fewer clear-cut tuning parameters in contrast with other algorithms. (5) Furthermore, the effects of other network parameters, including system losses and voltage, have been computed. The result obtained is tested in terms of congestion mitigation with and without the incorporation of PHSU, in terms of novel objective improvement, and with and without applying recently evolving FPA for the above application. Thus the objective-wise and algorithmic-wise innovative concept has been presented. This proves effectiveness of the algorithm in terms of minimized cost convergence and other parameters including system losses and voltage before and after the incorporation of PHSU as compared with other recent trendsetting reported optimization techniques.

Keywords: congestion management; power flow; generator rescheduling; Flower Pollination Algorithm (FPA); Pumped Hydro Storage Unit (PHSU)

1. Introduction

The integration of utilities being vertical, the task of separating the cost incurred in generation, transmission and distribution is quite difficult. Thus, the utilities put an average tariff on to their customer which relies on the aggregated fixed price for a specific period. Some of the external agencies fix the price which focuses more on consideration rather than economics. Occurrence of Congestion at a location in power transmission system will not be able to suit all the proposed bi/multilateral exchanges. It is due to the inability to incorporate the Existing Transmission Commitments (ETC), due to the infringement of operating constraints. A glimpse of a detailed survey related to managing the congestion issues occurring worldwide has been schemed in [1]. The authors have explained the techniques for consolidating deregulated market arrangements for the better utilizations of the power resources thereby providing solution to the issues [2]. A model with the inclusion of system stability criterion has been accounted for so as to relieve congestion [3]. A methodology for the embodiment of the reactive power services and real power loss while overseeing congestion has been considered [4]. The authors have examined the effects of FACTS arrangement for pacifying this problem [5]. The impact of congestion on the power system, and the financial signs of dispensing the associated cost venture have been discussed in [6]. The authors have proposed congestion management based zones/cluster; wherein the zones are being decided by the congestion distribution factors [7,8]. A combination of pool and bilateral trading has been considered for managing the congestion in a market based environment [9]. The author has assessed a detailed review on managing the congestion in different scenario of the market under privatization structure [10,11]. This paper ranks the management of congestion activities and its trappings on socio-economic impacts has been addressed in a divergent private mob. An analytical model based optimal technology comprising elements such as transformer taps and optimal switching has been incorporated for eliminating congestion [12]. A secure path of managing congestion with the due consideration of stability has been urged in [13,14]. Here the optimization problem has been effectively handled incorporated with penalty constraints [15,16].

Managing the congestion can be eased with different algorithm such as Simulated Annealing (SA), Random Search Method (RSM) and Particle Swarm Optimization (PSO) and tested on modified IEEE 30 bus system and IEEE 57 bus system. Further this issue has been dealt with the embodiment of nonconventional wind energy system [17]. This paper addresses the combined operation of energy utilization from hydro and wind is utilized for devising the mathematical model for bidding in a day-ahead energy market [18]. Adjusting the real power output of generators in order to meet the power demand is a real time challenge in the present scenario in the power grid. PHSU has commercially proven to meet the changes in power demand owing to its capability to start/stop quickly in accordance to change in load. The authors have presented the erection and devising of PHSU to serve peak demand. Further an insight analysis has been carried out on electricity pricing and its associated guidelines adopted [19]. This paper renders a wide vision into the recent development of PHSU in relation to its participation in deregulated energy market [20]. Further it addresses the flexibility of PHSU aiding in shift of generation thereby avoiding congestion and manages reliable supply of power in the grid. A formative structure has been incorporated with combined operation of hydro and PHSU for apprehending the volatility in pricing for in order to improvise the payoff from the generators [21]. Implementation of PSHU along with thermal plants enabled a steady decrease in emission [22,23]. This paper interprets the saving in cost yielded by optimal use of PHSU when operated during peak demand and thermal usage during off-peak demand [24]. The superiority of PHSU elevated the efficiency in energy transaction [25–27]. FPA and its variants have been developed in recent years which are found to yield better efficient outputs in applications for optimization designing due to its single probability switching parameter [28]. It associates the non-linearity Levy flight mechanism which proves to be effectively suited for multi-objective for enhancing the algorithmic performance of exploring the distant pollinator thereby globally exploring and locally exploiting by the consistency of flowers chosen [29,30]. FPA has been tested on IEEE 30 bus system with three different objective functions incorporating economic load dispatch and result obtained is compared with other

optimization techniques proving for its robustness over other existing algorithms [31]. Symbiotic Organisms Search algorithm [32], Ant lion algorithm [33], Gravitational Search Algorithm [34], Teaching Learning Based Optimization (TLBO) [35] are few of the latest algorithms have been found proposed for extenuating congestion. Switching the transmission lines in optimal sequence is one of the novel technologies to subdue congestion [36]. A novel distribution Algorithm has been proposed using nash equilibrium for effective cost reduction due to wheeling [37]. The technological advancements employing Power Electronic circuitry for Hydro Energy Electric Systems contributes widely in terms of economical payment and space reduction [38]. The reliability of the PHSU is effectively eased with the incorporation of Doubly-Fed Induction Motor [39]. The future prospects of adventing compressed air storage embedded with PHSU has been discussed. This could increase the performance utilization of energy. This proves to be a viable solution for the power industry in the future [40].

The major contributions of the paper are as follows. The main idea is to propose a methodology for managing the problem of congestion with cost reduction by rescheduling the generators active power. To achieve this task, FPA Algorithm is presented here. The stimulus of the present effort is to benefit the ISO in reliving the congestion. Here, modified IEEE 30 bus system is used as the test case. Initially an outage is created to cause the Congestion which results in power flow violation in certain transmission lines and the Congestion cost has been computed. Then the novel FPA is schemed as an efficient optimizing tool for rescheduling cost minimization as well as reduces the system losses. Further the rescheduling Congestion cost is compared with and without the application of FPA is computed. The effectiveness of the proposed Algorithm is proven in terms of minimized Congestion cost. To validate its effectiveness, the obtained results are compared with other optimization algorithms already reported in literature. Thereafter to replenish the varying load demand nature, a PHSU unit has been incorporated in it. The efficacy of FPA algorithm incorporating with PHSU is then investigated in terms of congestion cost minimization.

The paper is methodized as follows: Section 2 deals with the frame work criterion of managing congestion by rescheduling of generator's active power with the inclusion of PHSU in terms of congestion cost and loss minimization. Section 3 accomplishes FPA as an efficient optimizing tool for congestion cost minimization as well as reduces the system losses. Section 4 discusses the power flow violation due to congestion and the application of suitable methodology namely FPA. The efficacy of FPA in benefitting the Independent System Operator (ISO) in reliving the congestion is presented here. Here, modified IEEE 30 bus system is used as the test case. There after it is validated with other optimization techniques. Section 5 presents the significance of PHSU incorporated in the test system in aiding further reduction in congestion cost, losses and voltage profile improvement embodying BSF and GSF. Furthermore an economic analysis of congestion cost reduction using FPA before and after the incorporation of PHSU is investigated.

2. Problem Formulation

The main objective that is been focused is to reduce the congestion cost of the system taken into consideration.

$$\text{Minimize } \sum_{k=1}^{N_k} C_k^n (\Delta P_k^n) \Delta P_k^n \quad (1)$$

where,

C_k^n : Rescheduling cost of power by generators as per increase and decrease price bids at interval n .

ΔP_k^n : Incremental change in active power adjustment of the generator at interval n .

P_k^{min} & P_k^{max} : Minimum and maximum limits of generation.

Subject to constraints mentioned below.

$$P_{gj} - P_{dj} = \sum_{k=1}^n |V_j \|V_k \|Y_{jk}| \cos(\delta_i - \delta_k - \theta_{jk}) \tag{2}$$

$$Q_{gj} - Q_{dj} = \sum_{k=1}^n |V_j \|V_k \|Y_{jk}| \sin(\delta_j - \delta_k - \theta_{jk}) \quad j = 1, 2, \dots, n \tag{3}$$

$$P_{gk}^{min} \leq P_{gk} \leq P_{gk}^{max} \tag{4}$$

$$Q_{gk}^{min} \leq Q_{gk} \leq Q_{gk}^{max} \quad k = 1, 2, \dots, N_g \tag{5}$$

As the pumped storage units are connected on to the bus to reduce the congestion cost of the system, the additional constraints considered are as follows

$$e^n = e^{initial} \quad n = 0, \quad e^n = e^{final} \quad n = 24 \tag{6}$$

$$e^{n+1} = e^n + t \left(\eta_{Ps} P_{ps}^n - \frac{P_{Hs}^n}{\eta_{Hs}} \right) \tag{7}$$

$$P_{Ps}^{min} \leq P_{Ps}^n \leq P_{Ps}^{max} \tag{8}$$

$$P_{Hs}^{min} \leq P_{Hs}^n \leq P_{Hs}^{max} \tag{9}$$

$$e^l \leq e^n \leq e^u \tag{10}$$

2.1. Bus Sensitivity Factor

The bus sensitivity factor (BSF) is expressed as the ratio of incremental real power change flowing in bus ‘i’ connected between buses ‘j’ and ‘k’ to the incremental change in mth power of the bus as given below. BSF provides the optimal location for the placement of PHSU based on highest negative sensitive indexes.

$$BSF_m^i = \frac{\Delta P_{jk}}{\Delta P_m} \tag{11}$$

where, BSF_m^i indicates the quantum of real power change in real power flows in a transmission line in accordance to real power injection at bus m.

BSF can be derived from Equation (2) as illustrated below.

$$\Delta P_{jk} = \frac{\partial P_{jk}}{\partial \delta_j} \Delta \delta_j + \frac{\partial P_{jk}}{\partial \delta_k} \Delta \delta_k + \frac{\partial P_{jk}}{\partial V_j} \Delta V_j + \frac{\partial P_{jk}}{\partial V_k} \Delta V_k \tag{12}$$

$$\Delta P_{jk} = a_{jk} \Delta \delta_j + b_{jk} \Delta \delta_k + c_{jk} \Delta V_j + d_{jk} \Delta V_k \tag{13}$$

$$\Delta P_{jk} = a_{jk} \Delta \delta_j + b_{jk} \Delta \delta_k + c_{jk} \Delta V_j + d_{jk} \Delta V_k \tag{14}$$

where,

$$a_{jk} = V_j V_k Y_{jk} \sin(\theta_{jk} + \delta_k - \delta_j) \tag{15}$$

$$b_{jk} = -V_j V_k Y_{jk} \sin(\theta_{jk} + \delta_k - \delta_j) \tag{16}$$

$$c_{jk} = -V_k Y_{jk} \cos(\theta_{jk} + \delta_k - \delta_j) - 2V_k Y_{jk} \cos \theta_{jk} \tag{17}$$

$$d_{jk} = V_j Y_{jk} \cos(\theta_{jk} + \delta_k - \delta_j) \tag{18}$$

The Jacobian Matrix using Newton–Raphson (NR) method is given in Equation (19).

$$\begin{pmatrix} \Delta P \\ \Delta Q \end{pmatrix} = [J] \begin{pmatrix} \Delta \delta \\ \Delta V \end{pmatrix} = \begin{pmatrix} J_{11} & J_{12} \\ J_{21} & J_{22} \end{pmatrix} \begin{pmatrix} \Delta \delta \\ \Delta V \end{pmatrix} \tag{19}$$

where,

$$\Delta \delta = [J_{11}]^{-1} [\Delta P] = [M][\Delta P] \tag{20}$$

$$\Delta \delta_j = \sum_{l=1}^n m_{jl} \Delta P_l \quad j = 1, 2, \dots, n, \quad j \neq s \tag{21}$$

Thus

$$BSF_m^i = a_{jk} m_{jl} + b_{jk} m_{jl} \tag{22}$$

2.2. Generator Sensitivity Factor

The generator sensitivity factor (GSF) is expressed as the ratio of incremental change in real power flowing in bus ‘i’ connected between buses ‘j’ and ‘k’ to the incremental change in the active power supply of the generator as shown below. Generators are rescheduled based on highest negative indexes.

$$GSF_{gn} = \frac{\Delta P_{jk}}{\Delta P_{gn}} \tag{23}$$

Congestion management is formulated using the Newton–Raphson power flow method. Congestion results in the power flow violation in certain transmission lines and the congestion cost have been computed. Then the novel FPA is schemed as an efficient optimizing tool for rescheduling cost minimization as well as reducing the system losses. Further the rescheduling congestion cost is compared with and without the application of FPA is computed. The effectiveness of the proposed Algorithm is proven in terms of minimized congestion cost and its validation is presented in Figure 1. The efficacy of FPA algorithm incorporating with PHSU is then investigated in terms of congestion cost minimization, as shown in Figure 2. The impetus to carry out this work relies on a novel methodology for figuring out complexity that arises in managing the congestion. Despite the fact the problem of managing congestion has been endorsed in the literature for decades, at most gets committed on meta-heuristic and artificial intelligence approaches. Iteration number and population size are the typical monitoring criterion shared among these different methodologies. Distinct from these general monitoring criterions, some techniques incorporates algorithmic based specific tuning criterion like mutation rate and cross-over rate in the Genetic Algorithm (GA). Lack of proper tuning of algorithmic parameters can lead to local minima and increases time of computation for convergence. Particle Swarm Optimization (PSO) handles inertial weight adjustments. Although Simulated Annealing (SA) can solve optimization problems of complicated nature, the drawback is the inability to obtain the best solution without integrating another technique in it. Further, Harmony Search Algorithm (HSA) embodies the heed on memory rate and adjustments in pitch weight. Thus the fulfillment of the final solution is attained by the legitimate control of this algorithmic based specific tuning criterion. Commemorating these concepts, the proposed paper employs the implementation of FPA Algorithm. This relies on the mechanism of levy flight using a common probability switching parameter thus eliminating the need of algorithmic based specific tuning criterion and makes it effective for optimization problems.

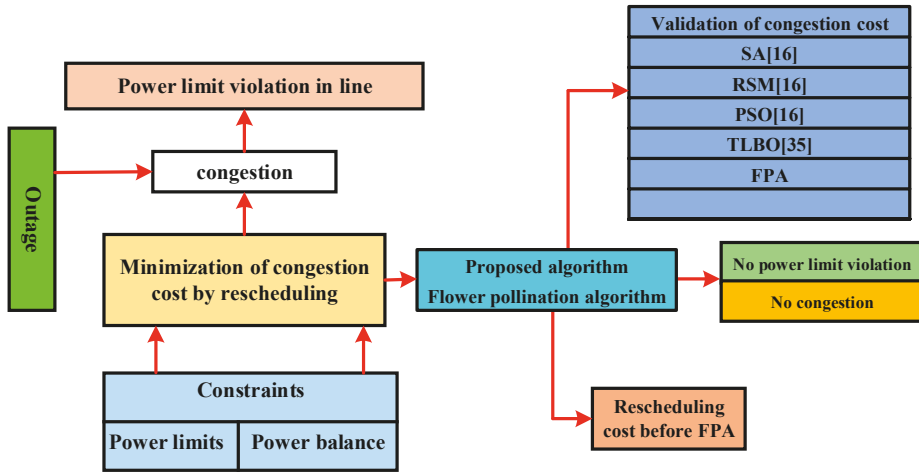


Figure 1. Congestion cost minimization using Flower Pollination Algorithm (FPA) and its validation with other optimization techniques (Part I).

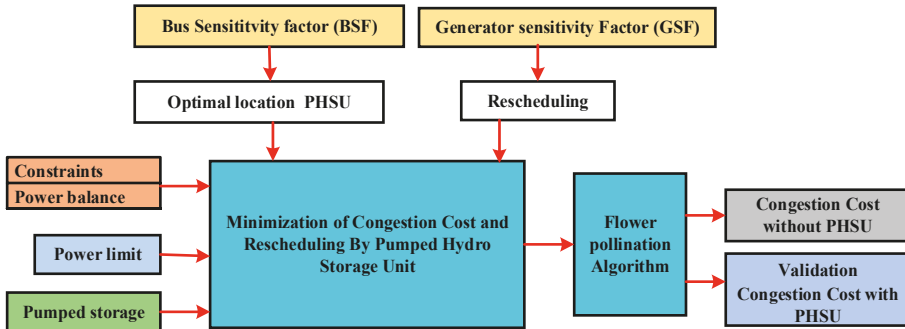


Figure 2. Congestion cost minimization using FPA incorporating Pumped Hydro Storage Unit (PHSU) and its validation (Part II).

3. Flower Pollination Technique

Flower pollination is a process adopted by flowers and plants to reproduce. It is classified into biotic and abiotic. Biotic pollination is done by living organisms whereas nonliving accounts for abiotic pollination. The other way of classifying pollination is self and cross. Self-pollination means fertilization of the same plant and cross-fertilization happens for different plants. The long distance process is called global pollination, and implantation, happening over short distance, is called local pollination. Flower constancy also provides an assurance of nectar for the pollinators with minimum effort of learning, exploration and exploitation. The global pollination is carried out by the equation

$$a_i^{m+1} = a_i^m + L(a_i^m - c_*) \tag{24}$$

where,

$$L \approx \lambda \Gamma(\lambda) \frac{\sin(\frac{\pi\lambda}{2})}{\pi} * \frac{1}{s^{1+\lambda}} \tag{25}$$

a_i^m — i th pollen at m th iteration

L —Levy weight-based size of each step ($s; s > 0$).

c_* —Best current solution at current iteration.

$\Gamma(\lambda)$ Gamma distribution function

The pollination occurring locally is carried out by the following equation

$$a_i^{m+1} = a_i^m + \epsilon (a_o^m - a_q^m) \tag{26}$$

a_i^m ith pollen at m th iterations

ϵ —takes a value of [0,1]

a_o^m and a_q^m —pollen from different flowers from same plant.

Biotic, also called cross-pollinators, follows movement of step flight, which aids in attaining. A set of N flower population is generated with random solutions. Global pollination follows the rule of biotic and cross-pollination; the reproduction probability depends on flower constancy.

The two indispensable concepts of FPA are local and global pollination steps. Pollinators carry the pollens of the flower to far reaching places due to its custom manner. This helps in the exploration of the larger search space. Here the general tuning parameter of levy flight mechanism, which essentially incorporates the various distant step sizes carried out by the pollinator. Usually the nearby flower is pollinated by the pollens of the local adjacent flowers rather than the far-off flowers. Thus, the general probability tuning parameter using levy fight mechanism switches effectively between global pollination and local pollination ensures the effective exploration and exploitation of the learning with minimum learning effect.

A simple numerical example is illustrated here for the implementation of FPA, as given below.

Consider a simple objective function $f(z) = z_1^2 + z_2^2$ subject to $z_{g,i} = (0.3,0.3)$. The fitness value obtained is $f(z_{g,i}) = 0.18$. Equation (26) is then applied and $z_{g+1,i} = (0.3,0.3)$ and then updated to $(0.1,1)$ for illustration. Then the newly updated. $z_{g+1,i} = (0.1,0.3)$. As a result, the new fitness value solution $f(z_{g+1,i}) = 0.04$. Here $f(z_{g+1,i}) < f(z_{g,i})$. This infers that the old fitness value solution can be replaced by the currently obtained fitness value. For example, if the newly updated. $z_{g+1,i} = (0.9,0.3)$, this results in the new fitness solution $f(z_{g+1,i}) = 0.9$. Here $f(z_{g+1,i}) > f(z_{g,i})$. This clearly indicates there is no progress to advance $z_{g,i}$. Thus, this value should be discarded and proceeded for the updating the next fitness value as indicated in pseudocode.

4. Algorithmic Steps in FPA

The sequential steps carried out in pseudocode of the flower pollination algorithm are presented as follows. The minimization objective function:

$$\min f(x), x = (x_1, x_2, \dots, x_n) \tag{27}$$

- Initially generate t population of flowers randomly
- Fitness solution c_* is then obtained from t population generated.
- While ($m < \maxgen$)
 - for $i = 1:t$
 - if r and $< p$,
 - A step vector has been drawn with levy’s distribution
 - And carry out Global population given by Equation (24)
- else
 - Uniform distribution in between the range 0 to 1 is then drawn for ϵ .
- Pollination is then carried out with local population with the random r and s variables by
- Equation (26).
- end if

- New solutions are then calculated
- If current solution obtained is better, replace the old solution by the current solution.
end for
- Best current solution c_* is then updated
- end while

Managing the congestion is coded using the Flower Pollination Algorithm. The process of carrying the pollens of the flower to far reaching places assures the fittest population for survival in the search space. The efficacy of FPA is implemented in terms of congestion cost minimization as shown in Figure 3. The parameters of FPA are λ , s , and size of population and iteration number. The criteria for optimal tuning obtained using FPA are $\lambda = 1.6$, $s = 1$, and size of population is 6 has been carried out for 25 iterations. Here the expedition between the global and local search using levy flight mechanism ensures the optimal output. Further FPA relieves congestion by suitable rescheduling of the real power of the generators. To validate its effectiveness, the obtained results are compared with other optimization algorithms already reported in literature.

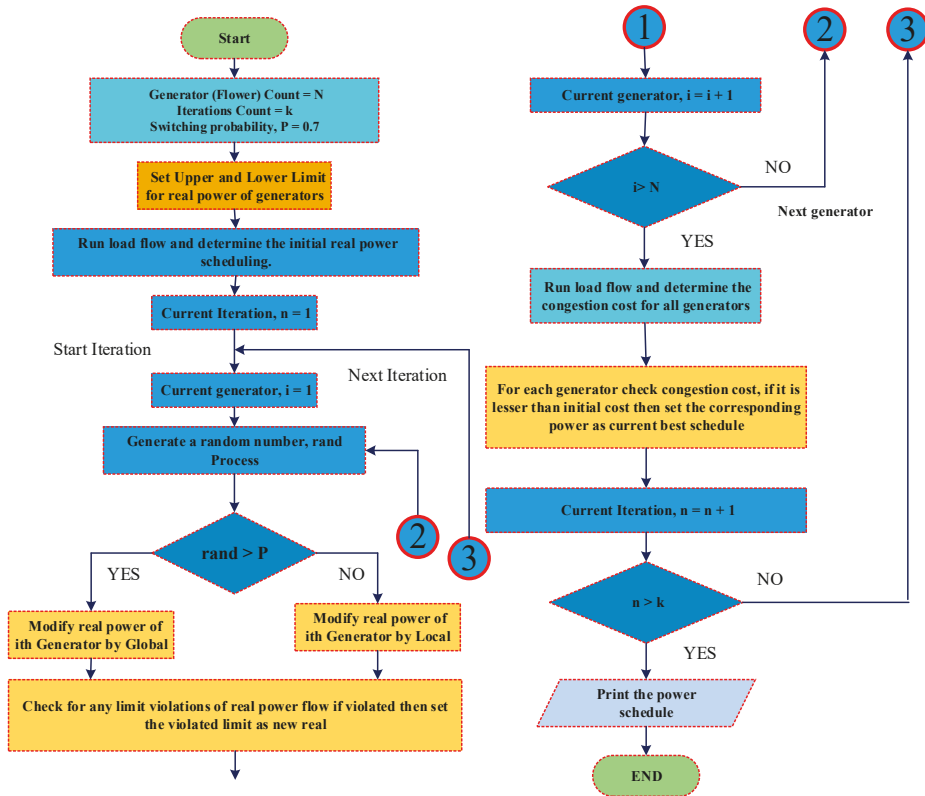


Figure 3. Implementation of FPA for congestion management.

5. Results and Discussions

The proposed method is schemed considering IEEE modified 30-bus system, which consists of six generator buses and 24 load buses. The slack node has been assigned as bus number 1. The numbering of buses has been done in a way that the generator buses are numbered first followed by load bus. Figure 4 depicts the single line diagram of the modified IEEE 30-bus system considered here.

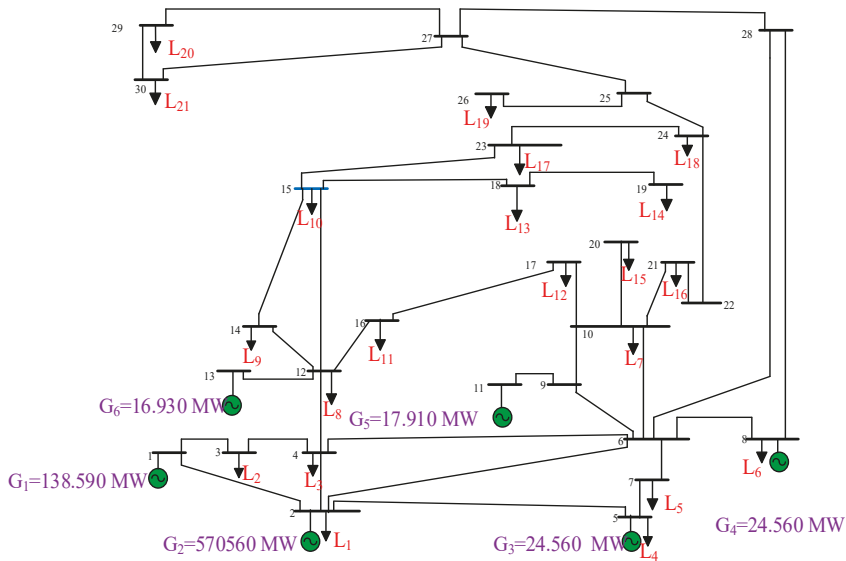


Figure 4. Single line diagram of modified IEEE 30-bus system.

Contingency analysis was conducted under the base load condition to identify the harmful contingencies. Here the outage of line 1–2 with normal loading is considered and has been illustrated out in Figure 5. It is ascertained from Figure 5. The actual power flow violation rises to 1.14%, 2.13%, and 1% in the lines connected between 1 and 3, 2 and 6, and 4 and 6, respectively. The system has been simulated with a line outage so as to create the contingency and results of line flow and its violations are reported in Table 1. Here, from Table 1 we can observe that there are three lines those are violating their limit that is line number 1, 5, and 6 which have 130 MW, 65 MW, and 90 MW of line flow limit, respectively. The power flows on the three violated lines are nearly 148 MW, 138 MW, and 90 MW. Even though the line 6 is violating by a small amount that is nearly equal to 0.59 MW, it has also been taken into consideration in the calculation. Congestion due to outage of line 1–2 and its effect on network framework parameters has been tabulated in Table 2. Here, due to congestion the percentage of overload on the congested line is reflected. The most overloaded line among the three lines that has to get congestion due to the line outage of lines 1–2 is the line connecting between buses 2 and 6.

The amount of power violated by each of the congested line is also shown in Figure 6. The line 2–6 has violated the limits the most that is nearly 73 MVA of power. The total amount of power violated due to the outage is 92.292 MVA. This power violation has to be now rescheduled through other lines so as to get rid of the congestion that has appeared. It is highlighted from Figure 7 the increase in overload amounts to 13.89%, 113.29%, and 0.65% in the lines connected between 1–3, 2–6, and 4–6, respectively. This violation is one of the issues critically faced by ISO. To achieve this task, the novel FPA is schemed as an efficient optimizing tool for congestion cost minimization as well as reduces the system losses. The stimulus of the present effort is to benefit the ISO in relieving the congestion. The rescheduling line flow is compared with and without the application of FPA is computed. The Flower Pollination Algorithm is used here as an optimization tool and it can be seen that the result obtained in Table 3 reflects its validity. The line which were violating the their line flow limits are now under the limits of their flow after the rescheduling of the generators is done by utilizing the FPA as shown in Figure 8.

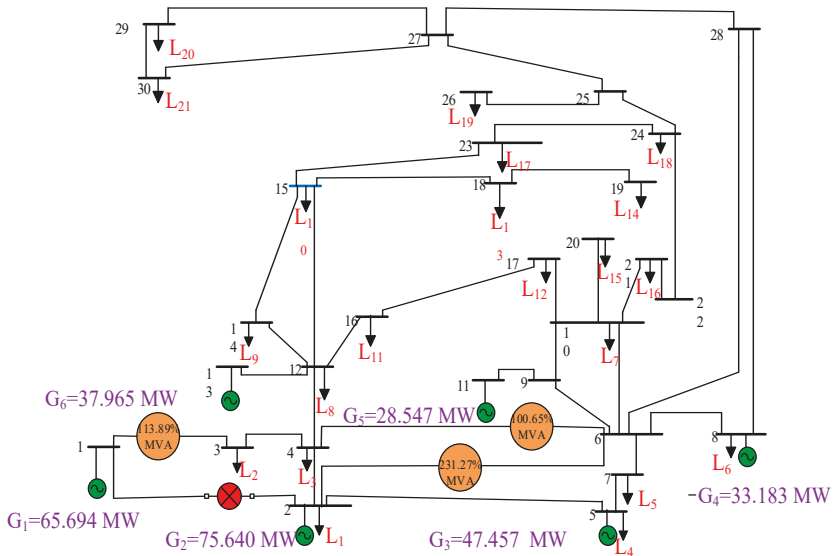


Figure 5. Effect of MVA violations due to an outage.

Table 1. Line flows in test case.

Line No.	MVA	Flow Rating (MVA)	Violation (MVA)	Line No.	MVA	Flow Rating (MVA)	Violation (MVA)
1	148	130	-18.0636	21	17.3	65	47.718
2	19	65	46.0397	22	8.34	16	7.66181
3	45.9	130	84.1025	23	19.9	32	12.0516
4	5.51	130	124.486	24	8.84	32	23.1584
5	139	65	-73.6385	25	1.85	32	30.1469
6	90.6	90	-0.590291	26	6.77	32	25.2275
7	37.7	70	32.2841	27	6.12	32	25.8765
8	34.1	130	95.9333	28	5.18	32	26.8177
9	51.3	65	13.7257	29	3.49	16	12.5059
10	24.5	65	40.5254	30	7.06	16	8.9363
11	13.8	65	51.1833	31	2.85	16	13.1489
12	12	65	53.0422	32	6.05	32	25.9523
13	16.5	65	48.482	33	2.86	16	13.1409
14	4.45	65	60.5462	34	1.35	16	14.6473
15	17.9	65	47.0647	35	4.27	65	60.7337
16	30.8	35	4.1557	36	5.26	16	10.7365
17	9.52	32	22.4836	37	6.42	16	9.58086
18	7.51	32	24.4883	38	7.29	16	8.70574
19	18.3	32	13.6829	39	19	32	28.2448
20	8.66	32	23.3388	40	3.76	32	12.9574

Table 2. Impact on network framework parameters due to outage of lines 1–2.

Type of Contingencies	Congested Lines	Line Limits MVA	Actual Power Flow (MVA)	Amount Power Violation (MVA)	Total Power Violation (MVA)	Overload %
Outage of line 1–2	1–3	130	148.06	18.06	92.29	13.89
	2–6	65	138.63	73.63		113.29
	4–6	90	90.590	0.59		0.65

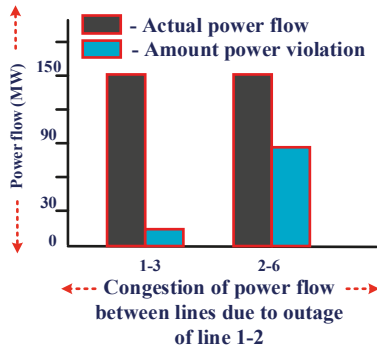


Figure 6. Power violation between lines due to line outage between lines 1–2.

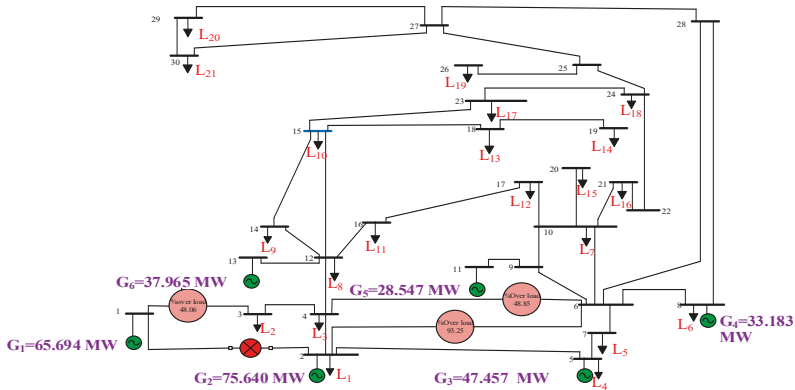


Figure 7. Effect of overload due to an outage.

Table 3. Comparison of congested line flow.

Congested Line	Limit (MVA)	Before Applying FPA (MVA)	After Applying FPA (MVA)
1–3	130	148.0636	63.5146
2–6	65	138.6385	60.6178
4–6	90	90.5903	43.2578

Table 4 indicates the economic cost analysis of cost before rescheduling is 941.208 \$/hr, while after rescheduling it reduces to 460.616 \$/hr. Here the expedition between the global and local search using levy flight mechanism ensures the optimal output. This validates the effectiveness of the algorithm. Further the changes in active power rescheduling have been graphically depicted in Figure 9.

Table 4. Rescheduling of generators in the modified IEEE 30-bus system.

Generator No.	Before Rescheduling (MW)	After Rescheduling (MW)	Increment in Generation (ΔP_{gi})
1	138.590	65.694	-72.896
2	57.560	75.640	18.080
3	24.560	47.457	22.897
4	35.000	33.183	-1.817
5	17.910	28.547	10.637
6	16.930	37.965	21.035
Total cost (\$/hr)	941.208	460.616	

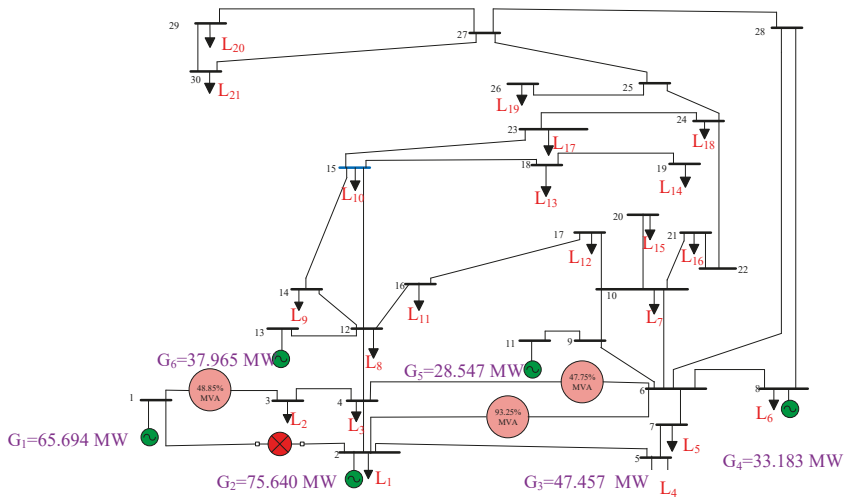


Figure 8. Mitigation of congestion employing Flower Pollination Algorithm.

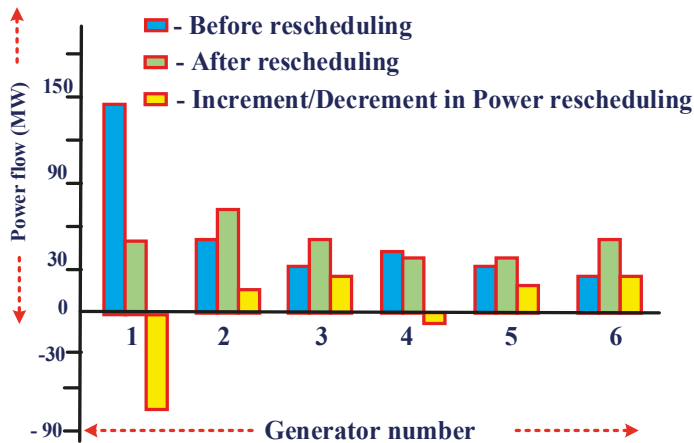


Figure 9. Comparison of power rescheduling in the modified IEEE 30-bus system employing FPA.

The results gained from the implementation of FPA for alleviation of congestion are tabulated in Table 5. With the results obtained in [16], the effectiveness of the proposed algorithm is illustrated with the reduction in congestion cost of 1.60%, 1.55%, 1.17%, and 1.07% as compared with other optimization algorithms like Simulated Annealing (SA), Random Search Method (RSM), Particle Swarm Optimization (PSO), and Teaching Learning-Based Optimization (TLBO). The best effective final solution is attained due to the legitimate control of the algorithmic based specific tuning criterion. Figure 10 infers that Flower Pollination Algorithm (FPA) yields the minimum congestion of 460.616 \$/hr as compared with the results obtained with other optimization techniques. Figure 11 validates the effectiveness of the algorithm in terms of its convergence in seven iterations as compared with 25 iterations in SA and RM, while 50 iterations are required in PSO to obtain solution consistency. Table 6 provides the parametric settings of the proposed FPA with other optimization techniques.

Table 5. Validation of proposed FPA with other optimization techniques.

Parameters	SA [16]	RSM [16]	PSO [16]	TLBO [26]	Proposed FPA
Total congestion cost (\$/hr)	719.86	716.25	538.95	494.66	460.62

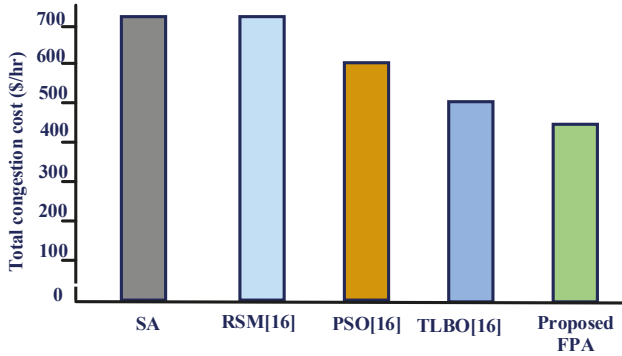


Figure 10. Effectiveness of proposed FPA with other optimization techniques.

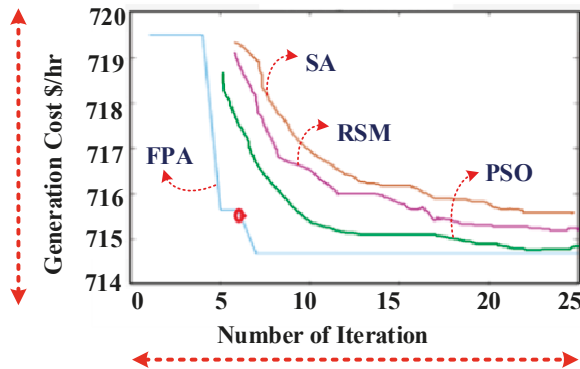


Figure 11. Convergence curve for managing congestion using FPA'.

Table 6. Parametric settings proposed FPA with other optimization techniques.

SA [16]	RSM [16]	PSO [16]	TLBO [26]	FPA
Start Set Temperature = 900 °C; End Set Temperature = 900 °C;		No. of swarms = 20	No. of learners = 6	No. of flowers = 6
No. of iter. = 1000	No. of iter. = 1000	No. of iter. = 300	No. of iter. = 30	No. of iter. = 25
		$C_1 = 2; C_2 = 2;$ $\omega_{min} = 0.4; \omega_{max} = 0.9$		$\Lambda = 1.6; \Upsilon = 0.12;$ $p = 0.80$

6. Congestion Management with PHSU

In this proposed work, to replenish the varying load demand nature, a PHSU unit has been incorporated with the test system. PHSU is operated in generator mode when there is power inadequacy while operated in pumping mode where there is power sufficiency. Thus PHSU helps in minimize the cost of congestion while maintaining the voltage figuration, The test case considering the modified IEEE 30 bus system has been simulated with a line outage 1–2 so as to create the contingency and results in violations of power flow between lines 1–3, 2–6, and 4–6, respectively. Considering this

outage, BSF are then computed for different load buses. The bus with the highest negative index is chosen to be the optimal location for PHSU placement. Here, it is evident from Table 7 that the ideal location for PHSU placement is obtained at bus 4. This is pictorially depicted in Figure 12 The feasible location of PSHU placement is attained assuming sufficient availability of water resource and reservoir area. GSF is then calculated for rescheduling active power of generators. Thus the placement of PHSU at bus 4 yields the minimized congestion cost of 361.450 \$/hr as compared to bus 16 with 756.03 \$/hr higher cost of congestion. This infers the efficiency of FPA in terms of congestion cost reduction. Active powers of the generators are then rescheduled through the computed GSF as inferred from Table 8. Generators with the highest negative sensitivities are opted for participation in rescheduling Table 9.

Table 7. Sensitivity factor without PHSU.

Load Bus No.	2	3	4	5	7	8	16	20	23
BSF	-0.0179	0.0315	-0.192	0.0107	0.0315	0.1532	0.0016	0.0804	0.0413

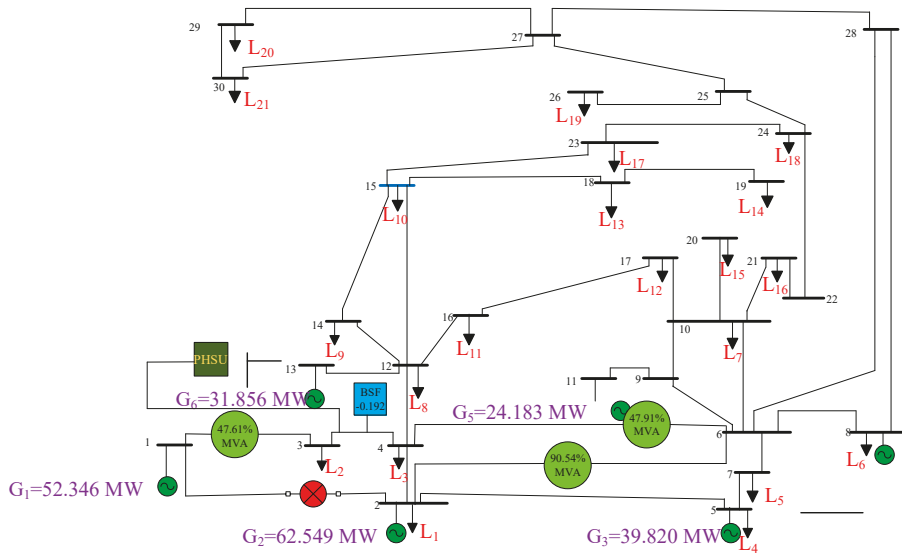


Figure 12. FPA-based suitable choice of PHSU for managing congestion.

Table 8. Sensitivity factor without PHSU.

Generators	G1	G2	G3	G4	G5	G6
GSF	-0.5563	-0.4217	-0.5326	-0.4862	-0.4326	-0.511

Table 9. Rescheduling with PHSU.

Generator No.	Before Rescheduling (MW)	After Rescheduling (MW)	Increment in Generation (ΔP_{gi})
1	138.590	52.346	-86.244
2	57.560	62.549	4.989
3	24.560	39.820	15.260
4	35.000	27.729	-7.271
5	17.910	24.183	6.273
6	16.930	31.856	14.926

Figure 12 interprets the incremental changes in value of rescheduling of real powers of the generators with the incorporation of PSHU. This facilitates meeting the objective of yielding minimum cost of congestion. The results gained from the implementation of FPA for alleviation of congestion influencing other network criterion is tabulated in Table 10. This investigates the effective minimization of power losses and security enhancement after employing EPA. The total loss in the system was 8.177 MW, which was also reduced to 5.217 MW after conducting congestion management, and further reduced to 4.208 MW after the incorporation of PSHU. Further the considerable improvement in voltage portrait is also tabulated.

Table 10. Influence of FPA on other network criterion in the test case.

Other Network Criteria	Rescheduling without Applying FPA	Rescheduling Applying FPA	Rescheduling Applying FPA Incorporating PSHU
Power loss (MW)	8.177	5.217	4.208
Voltage (p.u)	0.930	0.939	0.947

The PSHU is placed at load bus number 4 which is selected based on the most sensitive bus sensitivity factor. The PSHU is connected to the bus 16 and the results are tabulated. The generation cost is 736.426 \$/hr and the congestion cost incurred to the consumer is 361.450 \$/hr after the implementation of the pumped storage hydro unit at bus 4, as pictorially depicted in Figure 13. Table 11 infers the alleviation of congestion after the incorporation of PSHU employing FPA.

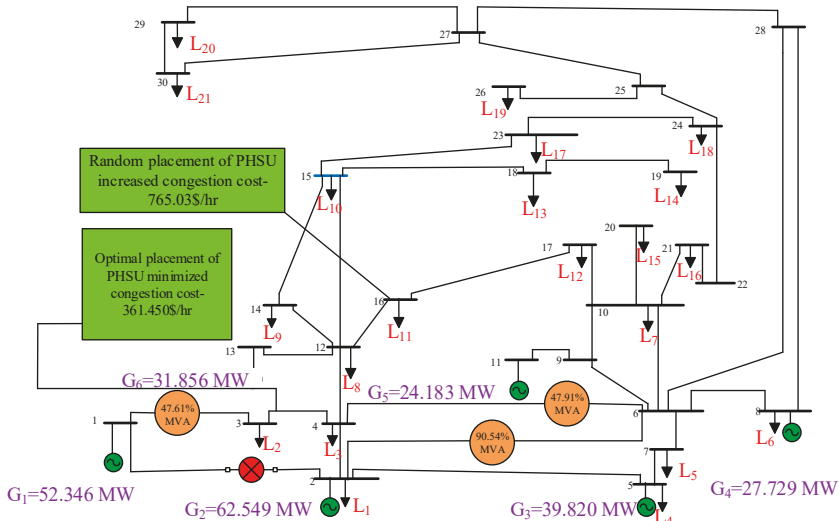


Figure 13. FPA-based cost comparison in placement of PSHU for managing congestion.

Table 11. FPA-based MVA line flow with and without PSHU.

Congested Line	Limit (MVA)	Before Applying FPA (MVA)	After Applying FPA (MVA)	After Applying FPA Incorporating PSHU (MVA)
1–3	130	148.0636	63.5146	61.9052
2–6	65	138.6385	60.6178	58.8522
4–6	90	90.5903	43.2578	43.1241

From Table 12, it is inferred that the rescheduling cost using FPA is considerably reduced by 1.27% with the PHSU placement. Furthermore, the superiority of the FPA is shown in terms of congestion cost reduction of 2.04% after the application of FPA algorithm employing PHSU placement as depicted pictorially in Figure 14. Thus the effectiveness of the FPA algorithm is proven in terms of minimized congestion cost and other parameters that influence the network framework criterion.

Table 12. Cost comparison with and without PHSU employing with and without FPA.

Parameter	Rescheduling Applying FPA without Incorporating PHSU	Rescheduling Applying FPA Incorporating PHSU
Congestion cost(\$/hr)	460.616	361.450

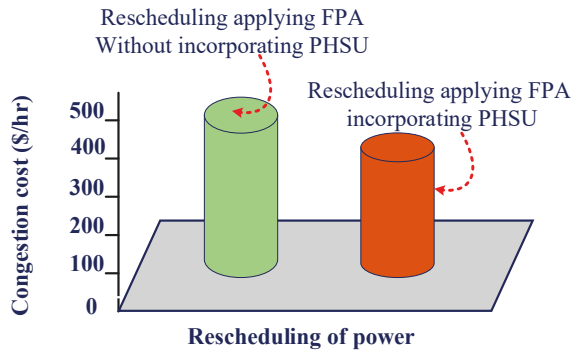


Figure 14. FPA-based cost comparison with and without placement of PHSU for managing congestion.

7. Conclusions

To relieve the congestion and recognize the congestion management’s importance in the power system, an attempt using FPA has been carried out in this paper. Generator rescheduling is used in this work for congestion management with that to reduce the transmission congestion cost. Here a study has been carried out to solve the congestion problem by generator rescheduling with the help of flower pollination algorithm aimed at reducing transmission congestion cost. Then the algorithm is compared with the other optimization techniques taking the same constraints and outage. The efficacy of FPA in benefitting the ISO in relieving the congestion in terms of minimized congestion cost. It is marked that there is a considerable amount of decrease in congestion cost by the incorporation of pumped storage unit and is validated effectively by Flower Pollination Optimization. Furthermore, the effects of other network parameters like system losses and voltage has been computed. The result obtained proves effectiveness of the algorithm in terms of minimized cost convergence as compared with other recent trendsetting reported optimization techniques.

Author Contributions: All authors were involved in developing the concept, simulation, and validation and making the article an error-free technical outcome for the set investigation work.

Acknowledgments: The would authors like to acknowledge the Department of Energy Technology, Aalborg University, Esbjerg, Denmark for supporting this research activity for the insight technical guidance and providing technical information for this project.

Conflicts of Interest: The authors declare no conflicts of interest.

List of Symbols and Abbreviations

e^n	Reservoir pumped storage energy level at interval n
e^{final}	Reservoir final limit
η_{Ps}	Pumping operation efficiency
η_{Hs}	Generation operation efficiency
P^n_{Ps}	Pumped storage power generation at interval n
P^n_{Hs}	Pumped storage power consumption at interval n
p^{min}_{Ps}	Minimum limit of power consumption
p^{max}_{Ps}	Maximum limit of power consumption
p^{min}_{Hs}	Minimum limit of power generation
p^{max}_{Hs}	Maximum limit of power generation
e^l	Reservoir lower limit
e^u	Reservoir upper limit
FPA	Flower Pollination Algorithm
GA	Genetic Algorithm
SA	Simulated Annealing
RSM	Random Search Method
HAS	Harmony Search Algorithm
PSO	Particle Swarm Optimization
TLBO	Teaching Learning-based Optimization
UC	Unit Commitment
EDRP	Emergency Demand Response Program

References

- Kumar, S.; Srivastava, C.; Singh, S.N. Congestion management in Competitive Power Market A Bibliographical Survey. *Electr. Power Syst. Res.* **2005**, *76*, 153–164. [[CrossRef](#)]
- Christie, R.D.; Wollenberg, B.; Wangensteen, I. Transmission management in the Deregulated Environment. *Proc. IEEE Trans. Power Syst.* **2000**, *88*, 170–195. [[CrossRef](#)]
- Ma, J.; Song, Y.H.; Lu, Q.; Mei, S. Market-Based Dynamic Congestion Management. *IEEE Power Eng. Rev.* **2002**, *22*, 54–56.
- Jian, F.; Lamont, J.W. A Combined Framework for Service Identification and Congestion Management. *IEEE Trans. Power Syst.* **2001**, *16*, 56–61. [[CrossRef](#)]
- Huang, G.M.; Yan, P. TCSC and SVC as Re-Dispatch Tools for Congestion Management and TTC Improvement. *Proc. IEEE Power Eng. Soc. Winter Meet.* **2002**, *1*, 660–665.
- Rau, N.S. Transmission Loss and Congestion Cost Allocation—An Approach Based on Responsibility. *IEEE Trans. Power Syst.* **2003**, *18*, 346–352. [[CrossRef](#)]
- Yu, N.; Ilic, M. Congestion clusters based markets for transmission management. In Proceedings of the IEEE Power Engineering Society, 1999 Winter Meeting, New York, NY, USA, 31 January–4 February 1999.
- Fang, R.S.; David, A.K. Transmission Congestion Management in an Electricity Market. *IEEE Trans. Power Syst.* **1999**, *14*, 877–883. [[CrossRef](#)]
- Doll, M.; Verstege, J.F. Congestion Management in a Deregulated Environment using Corrective Measures. *Proc. IEEE Power Eng. Soc. Winter Meet.* **2001**, *2*, 393–398.
- Masoud, E.; Ali, S.H.; Nima, A. Congestion management enhancing transient stability of power systems. *Int. J. Appl. Energy* **2010**, *87*, 971–981.
- Yesuratnam, G.; Thukaram, D. Congestion management in open access based on relative electrical distances using voltage stability criteria. *Electr. Power Syst. Res.* **2007**, *77*, 1608–1618. [[CrossRef](#)]
- Attaviriyunapap, P.; Kita, H.; Hasegawa, J. A hybrid LR-EP for solving new profit based UC problem under competitive environment. *IEEE Trans. Power Syst.* **2003**, *18*, 229–237. [[CrossRef](#)]
- Padmini, S.; Jegatheesan, R. A new model for Short-term Hydrothermal Scheduling of a GENCO in the competitive electricity market. *Indian J. Sci. Technol.* **2016**, *46*, 1–6. [[CrossRef](#)]

14. Padmini, S.; Srikanth, K. Optimal bidding strategy for Hydrothermal scheduling in a Deregulated Energy Markets. *Int. J. Control Theory Appl.* **2016**, *16*, 7783–7788.
15. Jacob Raglend, I.; Raghuvveer, C.; Rakesh Avinash, G.; Padhy, N.P.; Kothari, D.P. Solution to profit based unit commitment problem using Particle Swarm Optimization. *Appl. Soft Comput.* **2011**, *10*, 1247–1256. [[CrossRef](#)]
16. Balaraman, S.; Kamaraj, N. Transmission congestion management using particle swarm optimization. *J. Electr. Syst.* **2011**, *7*, 54–70.
17. Zeng, M.; Feng, J.; Xue, S.; Wang, Z.; Zhu, X.; Wang, Y. Development of China's pumped storage plant and related policy analysis. *Energy Policy* **2013**, *61*, 104–113.
18. Deb, R. Operating hydroelectric plants and pumped storage units in a competitive environment. *Electr. J.* **2000**, *13*, 24–32. [[CrossRef](#)]
19. Crampes, C.; Moreaux, M. Pumped Storage and Cost saving. *Energy Econ.* **2010**, *32*, 325–333. [[CrossRef](#)]
20. Yang, X.S. Flower pollination algorithm for global optimization: Unconventional Computation and Natural Computation. *Lect. Notes Comput. Sci.* **2013**, *7445*, 240–249.
21. Yang, X.S.; Karamanoglu, M.; He, X.S. Multi-objective flower algorithm for optimization. *Procedia Comput. Sci.* **2013**, *18*, 861–868. [[CrossRef](#)]
22. Yang, X.S.; Karamanoglu, X.S.; He, X.S. Flower Pollination algorithm—A Novel approach for Multiobjective Optimization. *Eng. Optim.* **2014**, *46*, 1222–1237. [[CrossRef](#)]
23. Verma, S.; Saha, S.; Mukherjee, V. A novel symbiotic organisms search algorithm for congestion management in deregulated environment. *J. Exp. Theor. Artif. Intell.* **2015**, *29*, 59–79. [[CrossRef](#)]
24. Verma, S.; Mukherjee, V. Optimal real power scheduling of generators for congestion management using a novel ant-lion algorithm. *IET Gener. Transm. Distrib.* **2016**, *10*, 2548–2561. [[CrossRef](#)]
25. Paul, K.; Kumar, N.; Agrawal, S. Optimal rescheduling of real power to mitigate congestion with incorporation of wind farm using gravitational search algorithm in deregulated environment. *Int. J. Renew. Energy Res.* **2017**, *7*, 1731–1740.
26. Verma, S.; Mukherjee, V. Optimal rescheduling of generators for congestion management using a novel teaching learning based optimization Algorithm. *J. Electr. Syst. Inf. Technol.* **2017**, 889–907. [[CrossRef](#)]
27. Salkuti, S.R. Congestion management using optimal transmission switching. *IEEE Syst. J.* **2018**, *12*, 3555–3564. [[CrossRef](#)]
28. Gao, B.; Ma, T.T.; Tang, Y. Power transmission scheduling for generators in a deregulated environment based on a game-theoretic approach. *Energies* **2015**, *8*, 13879–13893. [[CrossRef](#)]
29. Singh, R.R.; Chelliah, T.R.; Agarwal, P. Power Electronics in Hydro Electric Energy Systems—A Review. *Renew. Sustain. Energy Rev.* **2014**, *32*, 944–959. [[CrossRef](#)]
30. Joseph, A.; Chelliah, T.R.; Lee, S.S.; Lee, K.B. Reliability of Variable Speed Pumped Storage Plant. *Electronics* **2018**, *7*, 265. [[CrossRef](#)]
31. Andebili, M.R.; Shen, H. Energy management of end users modeling their reaction from a GENCO's point of view. In Proceedings of the International Conference on Computing, Networking and Communications, Santa Clara, CA, USA, 26–29 January 2017; pp. 571–581.
32. Zhao, Z.; Zu, L. Impacts of high penetration wind generation and demand response on LMP's in a day-ahead market. *IEEE Trans. Smart Grid* **2014**, *5*, 220–229. [[CrossRef](#)]
33. Albadi, M.H.; El-Saadany, E.F. Demand response in electricity markets: An overview. In Proceedings of the Power Engineering Society General Meeting, Tampa, FL, USA, 24–28 June 2007; pp. 1–5.
34. Strbac, G. Demand side management: Benefits and challenges. *Energy Policy* **2008**, *36*, 4419–4426. [[CrossRef](#)]
35. Yousefia, A.; Nguyen, T.T.; Zareipour, H.; Malikb, O.P. Congestion management using demand response and FACTS devices. *Int. J. Electr. Power Energy Syst.* **2012**, *37*, 78–85. [[CrossRef](#)]
36. Rahmani-Andebili, M.; Abdollahi, A.; Moghaddam, M.P. An investigation of implementing emergency demand response programs in unit commitment problem. In Proceedings of the IEEE PES'GM, San Diego, CA, USA, 24–29 July 2011.
37. Rahmani-Andebili, M. Investigating effects of responsive loads models on unit commitment collaborated with demand side resources. *IET Gener. Transm. Distrib.* **2013**, *7*, 420–430. [[CrossRef](#)]
38. Rahmani-andebili, M. Risk—Cost based generation scheduling smartly mixed with reliability driven and market driven demand response measures. *Int. Trans. Electr. Energy Syst.* **2015**, *25*, 994–1007. [[CrossRef](#)]

39. Rahmani-andebili, M. Nonlinear demand response programs for residential customers with non-linear behavioral models. *Energy Build.* **2016**, *119*, 352–362. [[CrossRef](#)]
40. Yao, E.; Wang, H.; Liu, L.; Xi, G.A. Novel Constant Pressure Pumped Hydro combined with Compressed Air Energy storage systems. *Energies* **2015**, *8*, 154–171. [[CrossRef](#)]



© 2019 by the authors. Licensee MDPI, Basel, Switzerland. This article is an open access article distributed under the terms and conditions of the Creative Commons Attribution (CC BY) license (<http://creativecommons.org/licenses/by/4.0/>).

Article

Software Architectures for Smart Grid System—A Bibliographical Survey

Ramesh Ananthavijayan ^{1,2}, Prabhakar Karthikeyan Shanmugam ^{2,*},
Sanjeevikumar Padmanaban ^{3,*}, Jens Bo Holm-Nielsen ³, Frede Blaabjerg ⁴ and Viliam Fedak ⁵

¹ Power Steering Systems, Robert BOSCH Engineering & Solutions, Coimbatore 641035, Tamilnadu, India; Ramesh.AV@in.bosch.com

² School of Electrical Engineering, VIT University, Vellore 632014, Tamilnadu, India

³ Center for Bioenergy and Green Engineering, Department of Energy Technology, Aalborg University, 6700 Esbjerg, Denmark; jhn@et.aau.dk

⁴ Center of Reliable Power Electronics (CORPE), Department of Energy Technology, Aalborg University, 9220 Aalborg, Denmark; fbl@et.aau.dk

⁵ Department of Electrical Engineering and Mechatronics, FEI TU of Košice, Letná 9, 04200 Košice, Slovakia; viliam.fedak@tuke.sk

* Correspondence: sprabhakarkarthikeya@vit.ac.in (P.K.S.); san@et.aau.dk (S.P.); Tel.: +45-716-820-84

Received: 3 January 2019; Accepted: 6 March 2019; Published: 26 March 2019

Abstract: Smart grid software interconnects multiple Engineering disciplines (power systems, communication, software and hardware technology, instrumentation, big data, etc.). The software architecture is an evolving concept in smart grid systems, in which system architecture development is a challenging process. The architecture has to realize the complex legacy power grid systems and cope with current Information and Communication Technologies (ICT). The distributed generation in a smart grid environment expects the software architecture to be distributed and to enable local control. Smart grid architecture should also be modular, flexible, and adaptable to technology upgrades. In this paper, the authors have made a comprehensive review of architectures for smart grids. An in depth analysis of layered and agent-based architectures based on the National Institute of Standards and Technology (NIST) conceptual model is presented. Also presented is a set of smart grid Reference Architectures dealing with cross domain technology.

Keywords: Advanced Metering Infrastructure (AMI); Distributed Energy Resources (DER); Distribution Management System (DMS); Graph Reduction in Parallel (GRIP); Intelligent Electronic Device (IED); Intelligent Platform Management Interface (IPMI); Service Oriented Architecture (SOA); Ultra Large-Scale System (ULSS)

1. Introduction

The Smart Grid combines electricity and IT infrastructure to integrate and interconnect all users (producers, operators, marketers, consumers, etc.) in order to efficiently balance demand and supply over an increasingly complex network. The smart grid software architecture is visualized as interconnecting sub-systems like Generation, Transmission, Distribution, and Utilization (GTDU). ISO/IEC/IEEE 42010 defines a software architecture as “a fundamental concept or properties of a system embodied in its elements, relationships, and in the principles of its design and evolution”. A software reference architecture is a generic architecture for a class of information systems that is used as a foundation for the design of concrete architectures from this class [1]. Smart grid is viewed as a software intensive system in which majority of devices and components contain electronics and software. Smart grid software architecture is characterized as a large scale, multi-disciplinary, highly interconnected, data driven system. Research in smart grids has seen a flurry of proposals

and experiments to explore software architecture techniques. Cloud interface with grid sub-systems is another important theme in smart grid research articles. The architectural standards (National Institute of Standards and Technology (NIST), International Electrotechnical Commission (IEC)) define the guiding principles to the evolving smart grid software structure. In this paper, we attempted to group and investigate the research articles based on structure of software architecture for smart grid applications.

Motivation

Application of software engineering methods in power grid domain is a multi-disciplinary, research-intensive topic. Design and development of software architecture for smart grids requires detailed research across multi domains. The software components are arranged in different layers to meet the intended objectives of smart grids. The literature survey on smart grid software architecture is aimed with the following objectives:

- ✓ Analysis of Standards
- ✓ Software layers definition and purpose
- ✓ Interface mechanisms amongst layers
- ✓ Data transmission mechanisms.

An electric grid is an interconnected grid of networks composed of several hardware and software components to distribute electricity from generation utilities to end-users [2]. The Software System runs on the embedded electronics in the power grid, residing at the various substations that are part of the smart grid. The ability of the electronics to communicate with each other and use feedback makes the power grid a smart grid. The communication channel between substations in its present form is wired, and the use of cloud interface and wireless enables smart grid.

The architecture of the electronics and the firmware configures, monitors, maintains, and controls energy equipment on the electric power grid. The core fundamentals of smart grid architecture pertain to reliability and definitive control (as per standards) over the power grid equipment, and focus on the security aspects as well. Smart grid architecture physically integrates the electronics and software systems of the grid together. A range of communication frameworks provide a wide flexibility for networking. The scenario is each sub-system operates with their own technique, and also agree upon a common data format for overall communication. Also, this architecture is to be capable of accommodating future communication techniques.

The rest of the paper is organized as follows. Smart grid software architecture concepts and requirements are addressed in Section 2. NIST and Joint Working Group's definition of architectural layers are briefly discussed in Section 2.1. Smart grid architectural view and requirements are addressed in Sections 2.2 and 2.3. Section 3 depicts the summary of the literature survey. A detailed report reference architecture is presented in Section 3.1. A detailed review of layered architecture is analyzed in Section 3.2, whereas Section 3.3 investigates agent-based architectural details with relevant research papers. Section 4 outlines the conclusions and the authors' ongoing research work in smart grid software.

2. Smart Grid Software Architecture

A distributed software system is defined as a set of processing elements running at different locations interconnected by a communication system. The processing elements are relatively independent software components that run on different hardware nodes and communicate to each other so that the design requirements are met. The grid architecture is significantly influenced by the physical location of power plants. Conventional power grids depend on larger, individual and remotely-located generating stations, whereas the modern smart grids depend on many Distributed Energy Resources (DER) with a relatively smaller generating capacity. Seamless integration of DERs and energy storage devices are necessary for their effective utilization and storage [3]. Producer and consumer active participation in buying and selling actions are to be integrated in the architecture.

Conventional systems are characterized by high voltage, and renewable energy sources are known for medium and low voltage generators. DERs should provide the flexibility and controllability required to support secure system operations. Each DER operates with its own local control units, and they must interface coherently to realize the smart grid architecture. This results in a paradigm shift of architectural design from traditional control philosophy of distributed control. DER components enable the fast realization of many functions for a stable grid operation [4].

The huge volume of data exchange in smart grids means the monitoring and control operations are more complex. This grid architecture is comparable with software architecture for automotive systems. The vehicle architecture has various sub components, such as engine management, chassis control, and steering. An integrated complete vehicle system is designed to meet the mobility requirement with focus from individual sub-systems. All the participating units shall adhere to the common architectural rules. This analogy is extended to smart grid systems.

2.1. Initiatives towards Standard Architecture

NIST [5] lays down standards for smart grid devices and protocol development. The NIST architectural framework is addressed below:

- Common understanding of smart grid elements and their relationships
- Traceability between the functions and the goals of the smart grid
- High-level and strategic views of the envisioned systems
- Integration of systems across domains, companies, and businesses
- Guide various architectures.

The report of the Joint Working Group (JWG) for standards for smart grids has outlined [6] the smart grid software architecture concepts, as defined in Table 1:

Table 1. Architecture layers as per Joint Working Group (JWG) standard.

Conceptual Architecture	High-Level Presentation of the Major Stakeholders and Their Interactions
Functional Architecture	Arrangement of functions and their sub-functions and interfaces and the conditions for control or data flow
Communication Architecture	Description of functional architecture focusing on connectivity
Information Security Architecture	Detailed description and guidelines of information security
Information Architecture	Representation of entities including their properties, relationships, and the operations that can be performed on them

The smart grid architecture has new challenges in not only balancing the volatile, largely distributed, small-volume energy production and consumption, but also in shifting of centralized overall control infrastructure to more localized and decentralized approaches [7]. The system representation captures central architectural concepts and their interaction. Smart grid architecture enables a unified and unambiguous representation of all connected sub system components [8]. Describing architecture with necessary flow diagrams and symbols is another challenging task. Many architectural documentations differ in their level of detail, completeness, and preciseness. The architectural documentation guidelines are well defined to balance with detailed descriptions and high-level explanations. [9]. The software architectural concepts can be adapted to the ULS smart grid systems [10,11].

Smart grid architecture bridges traditional power system automation (such as SCADA systems) with DERs and cloud systems. Standards like NIST and JWG-SG 2011 are laying down the architectural principles towards software layer arrangement and grid sub-system interfaces. These standards aim to catalyze innovations, to highlight best practices, and to open global markets for Smart Grid devices and systems [5,12]. However, these architectural view points and their level of granularity need to be carefully analyzed in power engineering with information technology.

2.2. Smart Grid Architecture—An Embedded Software View

Smart grid architecture is visualized with electronics and software elements, as represented in Figure 1. The smart grid features are realized by software algorithms that interface with grid sensors and actuators. The device drivers enabled with an operating system ensures the real time control and operation of the smart grid system. These components are placed in three prominent layers of distributed software architecture:

Physical (device) layer: This base layer consists of the modules with direct access to the microcontroller and peripherals. All device drivers and sensor interfaces are implemented in the base layer.

Communication (service) layer: Connects to various layers with an agreed information exchange protocol and realizes the functionality to abstract details from modules which are architecturally placed beneath them. The communication protocol interface, Operating systems (OS) interface, and device independent services are the key modules. In a smart grid environment, the energy suppliers and customers are located distributively, the communication network will assume a hybrid structure with core networks and many edge networks that connect all the suppliers and customers [13].

Application layer: Implements the actual software functionality that consists of sub-layers like component layer, service layer, etc. Smart grid specific features, such as load forecast and demand management, are realized in the application layer.

The abstraction components ensure the required separation of connected layers, while allowing the data communication. The RTE ensures communication between the individual software components, and with the help of the operating system, handles execution of the software components. In a typical scenario with huge wind flow availability the static loads (such as EVs Battery) are informed. All the relevant operations with relevant sub-systems are synchronized with RTE systems.

This architecture helps to perform the effective and intelligent distribution of energy to end users. It also helps to integrate renewable energy sources and their generation and distribution. Furthermore, it helps to have communication between the consumers and utility control center through the desired network. This will lead to electricity services becoming more reliable, efficient, cost-effective, self-repairing, self-optimizing, and environmentally conscious. There are two major objectives for having smart grid architecture: (i) to ensure reliability and availability of the grid, continuous and autonomous monitoring, measurement, and control of the grid; and (ii) management of energy utilization and distribution to ensure balanced demand and supply. To achieve this objective, a detailed analysis of smart grid requirements for optimized performance of networked sensors and software system is undertaken, which is discussed in the following section.

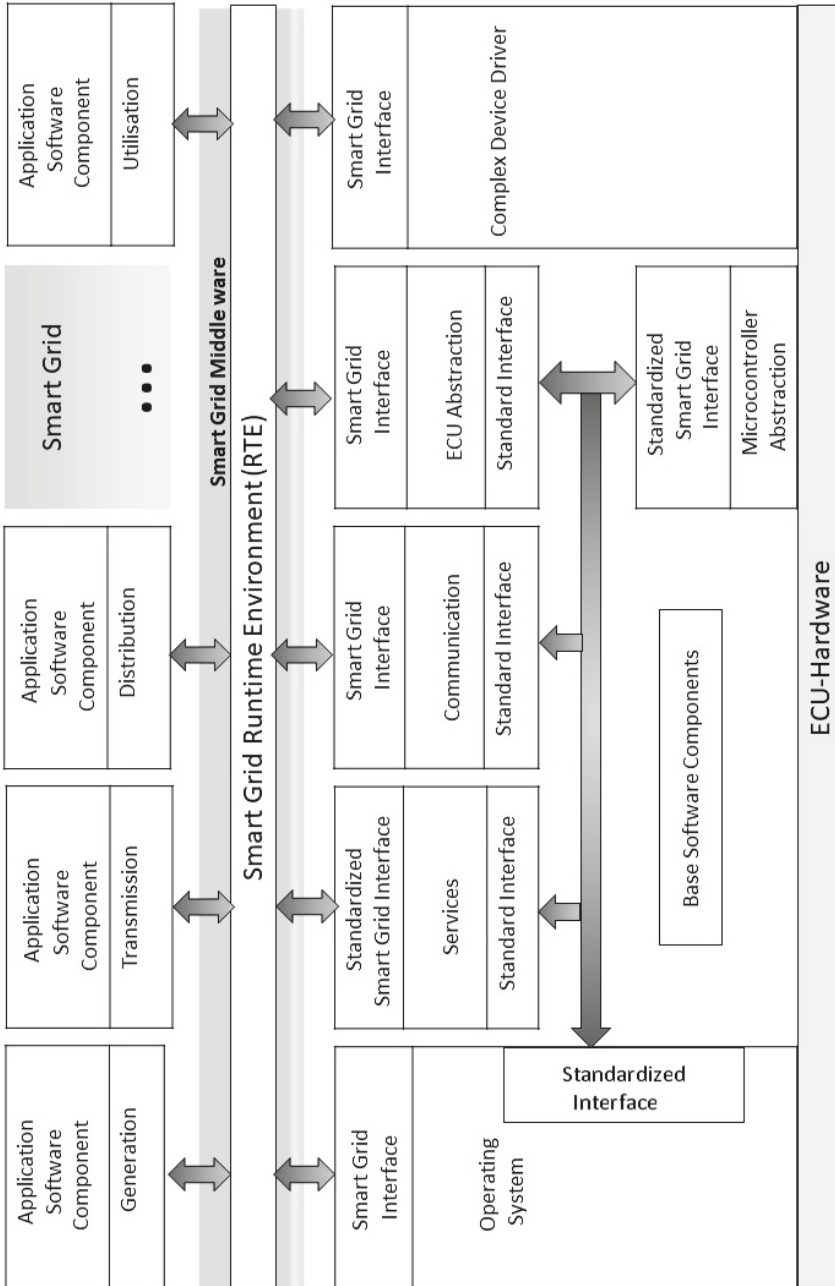


Figure 1. Smart grid. Architectural view.

2.3. Smart Grid Requirements

Smart grid software is characterized by highly interconnected, multi layered, enormous computations, and huge data traffic and security issues [14]. DERs in GTDU sub-systems and active stakeholder participation in grid operations enable intelligent features like load control, demand response, etc. The functional features are realized with the algorithms and interfaces, as defined in the requirements. Deriving smart grid requirements is the first step towards realizing its architecture [12,14–16]. Smart grid software architecture is designed to realize the requirements broadly listed in Table 2.

Table 2. Smart grid functional requirements.

Generation	Transmission	Distribution	Utilization	Operations	Cloud Interface
Load control and dispatch	Monitoring and control	Demand response	Enable active customer participation	Configuration management	Forecast (weather, generation, demand)
Load shaping	Maintaining Power quality	Peak clipping and load shaping	Variable pricing schemes	Device and asset management	Market services
Generation control and scheduling	Fault tolerant and Recovery mechanism	Fault handling and self-healing	Learning user profile	Enable new products and services	Geographic information system
Equipment maintenance	FACTS control	Outage management and power theft management	Consumer energy services	Firmware management, time Synchronization	Protection against cyber attack

3. Literature Survey

Smart grid architecture is an interdisciplinary system interface with a range of conventional technologies incorporating modern technological advancements. Smart grid architecture can be described based on factors such as representation, communication flow, and range of service. Based on the analysis of many research papers, the architecture is studied based on the below categories:

- ✓ Reference architectures—systematic experiments
- ✓ Layered architectures
- ✓ Agent-based architectures.

3.1. Reference Architecture

Smart grid software architecture is being explored by numerous researchers, service providers, and electricity producers. These works are aimed towards all stakeholders to accelerate smart grid component development and comply with uniform protocols. A reference model is a set of views and descriptions that provides the basis for discussing the characteristics, uses, behavior, interfaces, requirements, and standards of the smart grid [5]. Reference architecture provides a technology strategy that will holistically leverage standards-based solutions to realize these benefits consistently across multiple stakeholders [17–19]. Table 3 summarizes the various standard architectures found in the literature.

FREEDM architecture [24,25,28] facilitate seamless integration of distributed renewable power generation and storage resources and describes three states of operation, namely user level, solid state transformer level, and system level. FREEDM is an appropriate architecture if all of the hardware nodes and communication protocols are homogeneous, whereas CosGRID [18] architecture aims at smart grids based on different hardware platforms and protocols. CoSGRID architecture provides a generic platform suitable to develop improved electric power management services and applications for any environment and provide core smart grid control mechanisms. ScorePlus architecture [21] combines the merits from both hardware and software platforms to examine the performance of Smart Grid applications under realistic communication and computation constraints.

Table 3. Reference Architecture.

Reference Nr.	Name of Architecture	Salient Features	Demonstration
[5]	NIST framework	<ul style="list-style-type: none"> • Customer • Markets • Service provider • Operations • Bulk Generation 	NIST established a robust smart grid interoperability panel to develop additional standards
[11]	IEC 61499-based	<ul style="list-style-type: none"> • Load Balancing algorithm • Intelligent fault management algorithms 	Embedded controller (ARM based TS-7800 and verified using co-simulation approach
[18]	DIP (Duke Energy)	<ul style="list-style-type: none"> • Enhanced security • Near real-time resiliency 	Compatible with the OSI model and all 7 layers are mapped.
[20]	Controlling the Smart Grid (CoSGrid)	<ul style="list-style-type: none"> • Object-oriented • Distributed • Communication middleware 	Embedded Metering Device, Information Model, set of core services
[21]	ScorePlus	<ul style="list-style-type: none"> • Scalable • Flexible • Capable of remote access to configure physical devices 	Five solar generators, 5 storage devices, 15 demanders (Loads), 5 topology switches, and 1 interface device
[22]	BEMOSS platform	<ul style="list-style-type: none"> • Open source operating system • Improve sensing and control of equipment • Reduce energy consumption 	Enable developers with different skill sets to work on a different layer
[23]	GridOPTICS (Grid Operation and Planning Technology Integrated Capabilities Suite)	<ul style="list-style-type: none"> • Efficient solution for integrating the various projects • Event driven 	Demonstrate advanced smart grid operational capabilities like data management, operations and planning
[24–26]	FREEDM (Future Renewable Electric Energy Delivery and Management)	<ul style="list-style-type: none"> • Energy Internet • Enabling bidirectional flow of electricity 	Plug-and-play interface (e.g., RJ45 Ethernet interface) Open-standard operating system (e.g., TCP/IP and HTML).
[27]	NASPInet (North American Synchro-Phasor Initiative Network)	<ul style="list-style-type: none"> • Phasor Measurement Unit-centred • Reliability coordinators 	Impact analysis of the implementation of Quality of Service (QoS), cyber security, and network management service

GridOPTICS architecture [23] is layered architecture that addresses the data encapsulation and dependencies between layers. This promotes a clear separation of concerns and makes it possible to independently develop capabilities within each layer while ensuring data driven mechanisms. Smart grid architecture based on IEC 61499 and IEC 61850 has been experimented in previous studies [29,30]. IEC 61850 decomposes power substations, including functions for monitoring, control, protection and primary devices, down to objects, thus obtaining an object-oriented representation of the power system.

Duke Energy platform [18] implements an electric grid with “distributed intelligence” that significantly increases the operational efficiencies of the electric power system. It uses OSI model and Internet Protocol Suite as a reference to abstract and differentiate the connectivity and computing requirements. This architecture provides routing, bridging, and gateway capabilities to the IP based networks. NASPInet [27] architecture reflects the hierarchy among power grid operators, monitors, and regulators in order to provide a realistic deployment path.

Building Energy Management Open Source Software (BEMOSS) [22] is an open source operating system that is expected to improve sensing and control of equipment to reduce energy consumption.

This focusses on user management in addition to the operating system and connectivity [31]. BEMOSS is an open source architecture, which enables developers with different skillsets to work on different layers, thus enabling rapid deployment.

3.2. Layered Architecture in Smart Grid Software

The software architecture is a very high-level design of large software systems and the overall structure of a system with a set of defined rules. NIST recommended a conceptual model [5] for smart grid architecture, which is considered as reference architecture, including five domains pertaining to three areas: Smart Grid Service and Applications, Communication, and Physical Equipment.

1. Grid domain (generation, distribution, and transmission)
2. Smart metering (AMI)
3. Customer domain (smart appliances, electric vehicles, premises networks)
4. Communication network.

The NIST architecture model is represented in Figure 2, interconnecting the domains and service areas. NIST model enables the smart grid architecture to be flexible, uniform, and technology-neutral. This explains the simplified domain model in ICT perspective and the mapped domain model on the NIST smart grid interoperability framework. It is meant to foster understanding of smart grid operational intricacies and describes the data flow techniques amongst the participants.

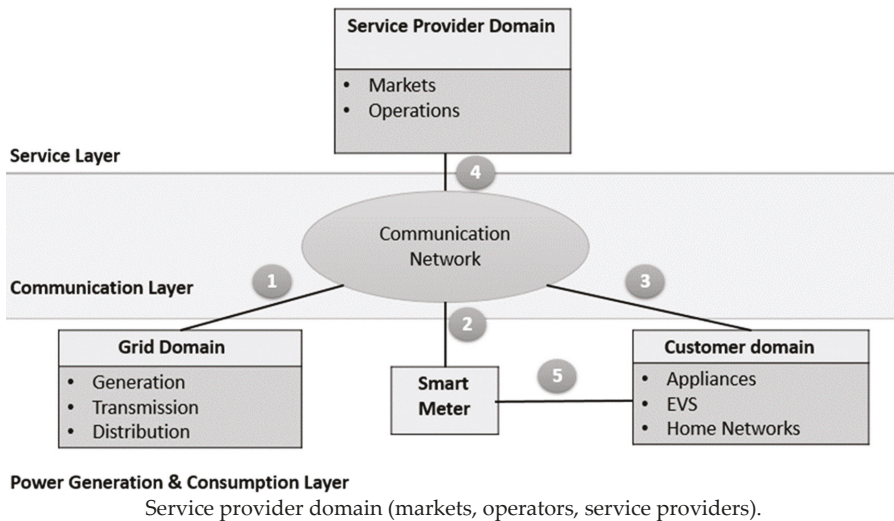


Figure 2. NIST reference model for smart grid architecture [32].

The NIST conceptual model revolves around the communication network and the information exchange within grid domains. The interoperability of the domain is represented with numbers (Port 1 to 5) in Figure 2. The insight of different architecture layers (in literature survey) is described under each communication port.

Communication Port 1: Describes information exchange between grid domain and communication network. This includes exchange of control signals between devices in grid domain and the service provider domain.

The data and control signal interactions are enabled with the physical layer [33], which consists of thousands of data points. IEDs have real-time capabilities for capturing and processing massive amounts of information of large-scale smart grids. This type of layer brings a component that translates

the different communication protocols and data models to the common communication technology and information model. The GTDU layer [3] implements key grid functionalities, such as distributed V-AR (Volt Ampere Reactive) compensation schemes, estimating generation schedules, and regulating power consumption.

In Gridstat architecture [34], data plane components [35] are designed to transmit the data from each source to many potential destinations, as directed by management-plane components. MultiFLEX architecture [36] implements the interoperability across heterogeneous devices using middleware technologies.

System Control Layer [36] represents the coordinated control required to meet the functional and performance-system-level objectives, such as coordinated volt-var regulation, loss minimization, economic and secure operation, system restoration, etc. The system control layer continuously monitors the system devices and keeps track of the system state by using applications such as state estimators. The sensor and actuator layer [37] ensure the local data processing amongst grid components.

Pérez et al. applied autonomic computing techniques towards a reference architecture for micro grids [14]. The autonomous behavior helps real time capabilities to acquire, distribute, process, analyze, connect, and disconnect distributed resources. This model implements the grid controller and the real time scenarios of all participating elements

Communication Port 2: Enables metering information exchange between the smart metering domain and communication network, which is a vital element in smart grid architecture. It also warrants the exchange of metering information and interactions through operators and service providers.

Smart meter communication is achieved by the storage layer [34] that collects the data from meters and devices in grid. The component layer [33] analyses data and behavior and provides intelligence to the power network. The data acquisition, processing, and analysis operations are performed on the information received from IED. The connectivity layer [22] takes care of the communication between the operating system and the framework layer and all physical hardware devices. This encompasses different communication technologies, data exchange protocols, and device functionalities.

The Meter Data Interface Layer [38] integrates smart meter architecture with Distribution Management Systems (DMS). A novel AMI communication architecture [39] is described with a Local Metering Concentrator layer. Such an architecture ensures command data processing and data acquisition. Meter Data Interface layers [38–40] perform: (i) pushing of AMI meter data to DMS; (ii) polling of DMS meter data from the AMI; and (iii) pushing of DMS control commands to AMI [41,42].

Communication Port 3: Enables the interactions between operators and service providers in the service provider domain and devices in the customer domain. The interface between the smart grid and the customer domain is of special importance as the most visible and user-focused interactive element. Electricity usage is measured, recorded, and communicated through this port.

The service layer [7] consists of those services that are provided to the stakeholders of each of the systems that constitute the large-scale smart grid. The customer services, such as stake on pricing and control of equipment, are implemented under customer-level control mechanisms [3]. The energy utilization is optimized by the information available, such as peak load, climate conditions, and power consumption. The local control layer [3] is used to implement the consumer level control functionalities and demand optimization.

The market layer [36] utilizes all the system control information and uses advanced economic and financial applications, such as reserve co-optimization, risk management, load and price forecasting, and architecture to reduce distribution losses [43] and is designed to coordinate between market dynamics and regional load despatch center.

Communication Port 4: Enables information exchange between the service provider domain and communication network domain. It enables communication between services and applications in the service provider domain to actors in other domains.

The service provider communication is enabled in M2M layer [44]. It increases the scalability because it removes the interdependencies between producer and consumer related to the information, allowing the development of services completely independent from the systems and deployed devices. Orchestration layer [33] represents those services that are implemented by the composition of simple services that are required by service providers.

The market (business) layer deals with the process of control decisions for the available resources, incorporating economic objectives [36,45]. This layer enables the service providers to participate in grid level transactions. The service provider domain operations, such as retail energy options, billing, etc., are described with utility provider and third-party provider services [46]. The protocol vulnerability risks for substation and transmission asset mitigation assessments are also addressed.

Communication Port 5: Enables the communication between smart metering and the customer domain. The coordination layer [3] defines the information exchanged between the GTDU layer and smart meter to control and optimize functionality implementation. The security layer [36,47] enables secure and trusted communication to control whether a device or service can be trusted or not. The mechanism triggers mutual authentication by providing the means to create a public key infrastructure.

In the MDI layer [38], translation means converting the AMI data to the DMS data when meter data from the AMI is delivered to the DMS, and vice versa. Service-oriented middleware [36] architecture is designed to support different kinds of smart meters and distributed power consumption information. Additionally, this architecture provides transparent interpretation of application and end users by controlling information exchange flow.

Comparative Study on Different Architectural Layers

Table 4 summarizes the comparison of layered architecture available in various literature. Analysis of various architectural features and key attributes are presented.

Table 4. Comparison of layered architectures.

Reference	Year	Layer Details	Salient Features
[3]	2013	<ul style="list-style-type: none"> • Local control layer • Utilization layer • Distribution layer • Transmission layer • Generation layer • Cooperation layer • Global optimizer layer • Coordination layer 	<ul style="list-style-type: none"> • It is an eight-layer architecture • Control and optimization functionality • Transform to smart grid in control perspective • Auto reconfiguration • Load balancing • Fault-detection approach
[14]	2014	<ul style="list-style-type: none"> • Resource layer • Autonomic Managers layer • Autonomic Orchestrating layer 	<ul style="list-style-type: none"> • Real time capabilities • Define a pattern of usage • Autonomous behaviour • Interoperability of the different devices • Self-balancing of demand/supply energy • Control the power flow of cells
[22]	2014	<ul style="list-style-type: none"> • User interface and data management • Operating system and framework • Connectivity 	<ul style="list-style-type: none"> • BEMOSS Architecture • Open Source protocol • Scalability, robustness • Plug and play, interoperability • Cost-effective • Local and remote monitoring • Advanced Control and monitoring • User interaction • Ease of deployment

Table 4. Cont.

Reference	Year	Layer Details	Salient Features
[33]	2015	<ul style="list-style-type: none"> Physical layer Communication layer Component layer Service layer Orchestration layer 	<ul style="list-style-type: none"> Suitable for Large-Scale Smart Grids Multi-tiered architecture based on the Event-Driven Oriented architecture Loosely coupled Flexibility in reconfiguration of architecture Tolerant to change and flexibility to expand
[36]	2011	<ul style="list-style-type: none"> Device layer Local control layer Device control layer Market layer 	<ul style="list-style-type: none"> Prosumer driven, service-oriented architecture Mechanism to realize the economic, reliability, and sustainability of the grid Interoperability and scalability Web services-based Service provider participation
[36]	2015	<ul style="list-style-type: none"> Integration M2M Storage Application Security 	<ul style="list-style-type: none"> Enable Secure communication Approach to integrate smart meters Improved Demand Response Energy optimization during ON peak duration Data accumulation on short term energy demand profile and the consumer behaviours
[38]	2010	<ul style="list-style-type: none"> Meter Data Interface layer 	<ul style="list-style-type: none"> Focus on AMI adaptation and Distributed Management Systems High performance data exchange Flexibility and scalability Loosely-coupled event infrastructure Extensibility
[43]	2009	<ul style="list-style-type: none"> Data Application and integration Communication Control and sensor layer 	<ul style="list-style-type: none"> Interfaces with WAMS Distribution automation Automation and reliability Interoperability, flexibility, scalability Decrease in transformer failure rates Cost reduction for energy utilization Revenue enhancement Identification of poor management of distribution networks
[48]	2013	<ul style="list-style-type: none"> User Port Control Port Transmission Port 	<ul style="list-style-type: none"> Service oriented architecture Access control and Power allocation Flexibility in scheduling Quality of service Dynamic information exchange infrastructure Security and consumer satisfaction
[49]	2015	<ul style="list-style-type: none"> Control level Supervisory level Area Level Operational management level Intra communication level 	<ul style="list-style-type: none"> Layered based on responsibilities Process control Process optimization Automation Global database management Reduced transmission delay (latency) Secure data transmission Interoperability
[50]	2016	<ul style="list-style-type: none"> Electric layer Cognitive layer Communication layer 	<ul style="list-style-type: none"> Standard framework based on IEEE-1516.2010 Reliable and robustness Proper bandwidth utilization

3.3. Agent Based Architecture for Smart Grids

Service Oriented Architecture (SOA) and Multi Agents (MAS) architecture are promising techniques for realizing smart grid systems. In both cases, smart grid components, such as Distributed Generators (DGs), intelligent switches, smart transformers, sensors, electric appliances, or electric vehicles, can be monitored and controlled by an autonomous software component, being either an agent in the MAS sense or a service in the SOA sense [51]. An intelligent agent processes several characteristics: reactivity (ability to learn the environment and act), proactiveness (self-initiative to meet expected goals), and social ability (negotiating and cooperating with other agents).

3.3.1. Description of Agents

Agents are autonomous systems which can operate in a fully-decentralized manner, i.e., it does not depend on a central (master) element. An agent can represent a group of appliances or bigger grid elements, such as a cluster of households. The utilities can retrieve data collected by the agents and use this information to control the power supply and decide which power sources to use. MAS-based software architecture for micro grids has been experimented in previous studies [35–49,51–53]. Agent-based software architectures are a potential technique in smart grids, hence plenty of research articles exist in this domain.

Existing distribution systems operate as a Master–Slave concept, responding to the central command with no possibility of dynamic reconfiguration. They do not support interoperability, and utilities often are locked into solutions from a single vendor. Multi agents' application in grid environments enables the local devices to be more self-operable and support decentralized monitoring and controlling operations. Data services, functional logic services, and business logic services are described in smart grid architectures. An intelligent agent consists of four components:

- ✓ Input interface
- ✓ Output interface
- ✓ Decision making system
- ✓ Communication system.

3.3.2. Agent Based Architecture in Literature

Multi Agent Systems are “autonomous decision makers that communicate their preferences, negotiate sub-goals, and coordinate their intentions in order to achieve the individual or system goals” [54,55]. They are suitable for smart grid architectures as they are intelligent and autonomous, exhibit distributed control, act flexibly to the changes in environment, and cooperate with each other towards a common goal.

Malik et al. analyzed various aspects of agent usage in a smart grid environment [3]. This paper evaluates the agent's application in smart grid functional areas, namely control, fault management, self-healing properties, energy balance management, and distribution side management. Zhabelova et al. investigated various aspects of distributed architectures for smart grid applications and unique contributions within this domain [29,54,56,57]. These works practically implement agent-based solutions for smart grids and facility migration of smart grid technology to the next level of research.

The limitations of current distribution systems are addressed with agent-based techniques [29]. The proposed integration of the two international standards IEC 61499 and IEC 61850 has enabled development of a prototype of the automation architecture, where the intelligence resides at the device level [56,58,59].

An agent-based architecture is proposed for fault location, isolation, and supply restoration (FLISR) applications [15,57]. A hybrid approach combining both the advantages of reactive and deliberative architecture approaches is implemented. This paper deals with two reactive behaviors, five plans, the intention stack, and the interpreter. The design process is methodological and agents are reproducible.

An actual fault condition in a substation environment is considered and the mechanism of agent reactions is tested.

The concept of a JIAC (Java Intelligent Agent Component) framework is integrated with a service-oriented paradigm [2]. The framework provides the agent-platform, comprising agent nodes, is physically distributed, and it enables runtime environments for JIAC agents. These are demonstrated in two projects: The Intelligente Lösungen zum Schutz vor Kaskadeneffekten in voneinander abhängigen kritischen Infrastrukturen (ILias) project, and Gesteuertes Laden V2.0.

Agent-based design in smart grid applications requires a modular software architecture [60]. This work attempts to implement different aspects of communication agents, namely communication perspective, access to services, and handling subscriptions. Agents can have the following attributes: name, parent, child, and unique ID. Protocol adapters are proposed to bridge between agents and appliances.

The Multi Agent Architecture for smart grids is explored in a previous study [61]. This paper defines different roles in the smart grid as producer, storage, consumer, prosumer, and distribution. It takes JADE as a base framework to implement the proposed architecture. The salient features of this research are time dependent monitoring and computation support for internal and external physical models, flexibility in computation, and it eases the integration of distributed control algorithms.

4. Future Work and Conclusions

4.1. Smart Grid Architecture Proposal Based on Data Exchange

Smart grid architecture is a complex, data intensive, and safety-critical system. The data collection and exchange among consumers, DERs, distribution, and cloud systems decides the basic structure of smart grid architecture. A typical smart grid system is similar to a datacenter system, in that the devices sit in a remote location and require a means for a supervisor or administrator to access the system remotely. Remote access is meant to happen over a secure connection and will also need reliable data transfer, a light, and fast protocol definition, which is one of the focus areas of this document. The bit-level protocol definition ensures fast, reliable, and secure communication in a smart grid environment [62]. Cloud integration techniques also enable leverage of many technologies (automotive, home automation) into the smart grid domain.

4.2. Conclusions

This review paper is a comprehensive analysis of various aspects of smart grid software architecture. It requires multi-disciplinary research, which involves power system, communication, and information technology. Even though various researchers follow a different naming convention for their layered architecture, a commonality exists in the functionality. A synergy in the functionality of the layers is also observed in many research papers. Agent technology directly enables all required features in a smart grid due to their autonomous nature. Self-centric (not Master-Slave) agents are directly suitable for the distributed smart grid software architecture. Most of the research work focuses on building a standard software architecture based on smart grid elements. The experimental methods and interfacing technologies are also analyzed with software architectures available in the literature. Some architectures, such as ScorePlus and GridOptics, are reconfigurable and implemented in hardware. BEMOSS is an open source software architecture for building energy management. FREEDM, known as Energy Internet, implements various smart grid elements and features. Basic research, architectural proposals, application of adjacent technologies, all demonstration with pilot projects shall all lead to smarter (i.e., intelligent, automated, decentralized, self-healing, adaptable, dynamic) intelligent power grids.

Author Contributions: All authors contributed equally to the final dissemination of the research investigation as a full article.

Funding: The authors would like to acknowledge the funds received from the VIT University, Vellore, India. The project VEGA 1/0187/18 for its support (VEGA is Slovak Research and Development Agency with the seat in Bratislava). The project title is Development of Optimal Electromechanical Systems with High Dynamics.

Acknowledgments: The authors would like to acknowledge the technical assistance received from the Center for Bioenergy and Green Engineering, Center for Reliable Power Electronics (CORPE), Department of Energy Technology, Aalborg University, Denmark for making this technical survey a full article.

Conflicts of Interest: The authors declare no conflict of interest.

Nomenclature

AMI	Advanced Metering Infrastructure
ARM	Advanced RISC Machine
BEMOSS	Building Energy Management Open Source Software
CoSGrid	Controlling the Smart Grid
DER	Distributed Energy Resources
DIP	Distributed Intelligence Platform
DMS	Distributed Management System
EV	Electrical Vehicle
FREEDM	Future Renewable Electric Energy Delivery and Management
FLISR	Fault, Location, Isolation and Supply Restoration
GridOPTICS	Grid Operation and Planning Technology Integrated Capabilities Suite
GTDU	Generation Transmission Distribution Utilization
GRIP	Graph Reduction In Parallel
HTML	Hyper Text Markup Language
IEC	International Electrotechnical Commission
IED	Intelligent Electronic Devices
IEEE	Institute of Electrical and Electronics Engineers
JADE	JAVA Agent DEvelopment Framework
NIST	National Institute of Standards and Technology
M2M	Machine to Machine
NASPinet	North American Synchro-Phasor Initiative Network
RTE	Real Time Environment
OSI	Open System Interconnection
RISC	Reduced Instruction Set Computer
SOA	Service Oriented Architecture
QoS	Quality of Service
TCP	Transmission Control Protocol
ULS	Ultra Large Scale
WAMS	Wide Area Management System

References

1. Angelov, S.; Grefen, P.; Greefhorst, D. A classification of software reference architectures: Analyzing their success and effectiveness. In Proceedings of the Joint Working IEEE/IFIP Conference on Software Architecture, Cambridge, UK, 14–17 September 2009; pp. 141–150.
2. Yilmaz, C.; Albayrak, S.; Lützenberger, M. Smart grid architectures and the multi-agent system paradigm. *Energy* **2014**, *90*, 90–95.
3. Srinivasan, S.; Kotta, U.; Ramaswamy, S. A layered architecture for control functionality implementation in smart grids. In Proceedings of the 2013 10th IEEE International Conference on Networking, Sensing and Control (ICNSC), Evry, France, 10–12 April 2013.
4. Andrén, F.P.; Strasser, T.; Langthaler, O.; Veichtlbauer, A.; Kasberger, C.; Felbauer, G. Open and interoperable ICT solution for integrating distributed energy resources into smart grids. In Proceedings of the 2016 IEEE

- 21st International Conference on Emerging Technologies and Factory Automation (ETFA), Berlin, Germany, 6–9 September 2016.
5. NIST Framework and Roadmap for Smart Grid Interoperability Standards, Release 2.0. Available online: https://www.nist.gov/sites/default/files/documents/public_affairs/releases/smartgrid_interoperability_final.pdf (accessed on 15 February 2019).
 6. Final Report of the CEN/CENELEC/ETSI Joint Working Group on Standards for Smart Grids. Available online: https://www.etsi.org/images/files/Report_CENCLCETSI_Standards_Smart_Grids.pdf (accessed on 15 February 2019).
 7. Koß, D.; Bytschkow, D.; Gupta, P.K.; Schätz, B.; Sellmayr, F.; Bauereiß, S. Establishing a smart grid node architecture and demonstrator in an office environment using the soa approach. In Proceedings of the 2012 International Workshop on Software Engineering for the Smart Grid (SE4SG), Zurich, Switzerland, 3 June 2012; pp. 8–14.
 8. Vukmirović, S.; Erdeljan, A.; Kulić, F.; Luković, S. Software architecture for smart metering systems with virtual power plant. In Proceedings of the MELECON 2010—2010 15th IEEE Mediterranean Electrotechnical Conference, Valletta, Malta, 26–28 April 2010.
 9. Hackenberg, G.; Irlbeck, M.; Koutsoumpas, V.; Bytschkow, D. Applying formal software engineering techniques to smart grids. In Proceedings of the 2012 International Workshop on Software Engineering for the Smart Grid (SE4SG), Zurich, Switzerland, 3 June 2012; pp. 50–56.
 10. Rad, B.R.; Aliee, F.S. Computational Grid as an Appropriate Infrastructure for Ultra Large Scale Software Intensive Systems. In Proceedings of the 2010 International Conference on Complex, Intelligent and Software Intensive Systems (CISIS), Krakow, Poland, 15–18 February 2010; pp. 469–474.
 11. Anvaari, M.; Cruzes, D.S.; Conradi, R. Smart Grid software applications as an ultra-large-scale system: Challenges for evolution. In Proceedings of the 2012 IEEE PES Innovative Smart Grid Technologies (ISGT), Washington, DC, USA, 16–20 January 2012; pp. 1–6.
 12. Worighi, I.; Maach, A.; Hafid, A. Smart grid architecture and impact analysis of a residential microgrid. In Proceedings of the 2016 4th IEEE International Colloquium on Information Science and Technology (CiSt), Tangier, Morocco, 24–26 October 2016; pp. 854–859.
 13. Ananthavijayan, R.; Karthikeyan, S.P.; Raglend, I.J.; Edward, J.B.; Kumar, K.S. Requirement framework of smart grid software architecture. In Proceedings of the 2017 International Conference on High Voltage Engineering and Power Systems (ICHVEPS), Sanur, Indonesia, 2–5 October 2017.
 14. Pérez, J.; Díaz, J.; Vidal, C.; Rodriguez, D.; Fernández, D. Self-Balancing Distributed Energy in Power Grids: An Architecture Based on Autonomic Computing. In Proceedings of the 2014 47th Hawaii International Conference on System Sciences (HICSS), Waikoloa, HI, USA, 6–9 January 2014.
 15. Strasser, T.; André, F.; Kathan, J.; Cecati, C.; Buccella, C.; Siano, P.; Leitao, P.; Zhabelova, G.; Vyatkin, V.; Vrba, P.; et al. A review of architectures and concepts for intelligence in future electric energy systems. *IEEE Trans. Ind. Electron.* **2015**, *62*, 2424–2438. [[CrossRef](#)]
 16. López, G.; Moreno, J.I.; Sánchez, E.; Martínez, C.; Martín, F. Noise Sources, Effects and Countermeasures in Narrowband Power-Line Communications Networks: A Practical Approach. *Energies* **2017**, *10*, 1238. [[CrossRef](#)]
 17. Wu, F.F.; Varaiya, P.P.; Hui, R.S. Smart grids with intelligent periphery: An architecture for the energy internet. *Engineering* **2015**, *1*, 436–446. [[CrossRef](#)]
 18. Laval, S.; Godwin, B. *Distributed Intelligence Platform (DIP) Reference Architecture Volume 1: Vision Overview*; Duke Energy Duke Energy Corporation: Charlotte, NC, USA, 2015; pp. 1–31.
 19. Bachmann, F.; Bass, L.; Carriere, J.; Clements, P.; Garlan, D.; Ivers, J.; Nord, R.; Little, R. Software Architecture Documentation in Practice: Documenting Architectural Layers. March 2000. Available online: <http://citeseerx.ist.psu.edu/viewdoc/download?doi=10.1.1.465.4046&rep=rep1&type=pdf> (accessed on 15 February 2019).
 20. Villa, D.; Martin, C.; Villanueva, F.J.; Moya, F.; López, J.C. A dynamically reconfigurable architecture for smart grids. *IEEE Trans. Consum. Electron.* **2011**, *57*, 411–419. [[CrossRef](#)]
 21. Tan, S.; Song, W.Z.; Yothment, S.; Yang, J.; Tong, L. ScorePlus: An integrated scalable cyber-physical experiment environment for Smart Grid. In Proceedings of the 2015 12th Annual IEEE International Conference on Sensing, Communication, and Networking (SECON), Seattle, WA, USA, 22–25 June 2015; pp. 381–389.

22. Khamphanchai, W.; Saha, A.; Rathinavel, K.; Kuzlu, M.; Pipattanasomporn, M.; Rahman, S.; Akyol, B.; Haack, J. Conceptual architecture of building energy management open source software (BEMOSS). In Proceedings of the IEEE PES Innovative Smart Grid Technologies, Europe (ISGT-Europe), Istanbul, Turkey, 12–15 October 2014; pp. 1–6.
23. Gorton, I.; Liu, Y.; Yin, J. Grid OPTICS (TM): A design for plug-and-play smart grid software architecture. In Proceedings of the 2012 First International Workshop on Software Engineering for the Smart Grid (SE- SmartGrids), Zurich, Switzerland, 3 June 2012; pp. 38–41.
24. Karady, G.G.; Huang, A.Q.; Baran, M. FREEDM system: An electronic smart distribution grid for the Future. In Proceedings of the Transmission and Distribution Conference and Exposition (T&D), 2012 IEEE PES, Orlando, FL, USA, 7–10 May 2012; pp. 1–6.
25. Huang, A.Q.; Crow, M.L.; Heydt, G.T.; Zheng, J.P.; Dale, S.J. The future renewable electric energy delivery and management (FREEDM) system: The energy internet. *Proc. IEEE* **2011**, *99*, 133–148. [[CrossRef](#)]
26. Bertocco, M.; Tamarin, F. A system architecture for distributed monitoring and control in a Smart Microgrid. In Proceedings of the 2012 IEEE Workshop on Environmental Energy and Structural Monitoring Systems (EESMS), Perugia, Italy, 28 September 2012; pp. 24–31.
27. Bobba, R.; Heine, E.; Khurana, H.; Yardley, T. Exploring a tiered architecture for NASPINet. In Proceedings of the Innovative Smart Grid Technologies (ISGT), Gothenburg, Sweden, 19–21 January 2010; pp. 1–8.
28. Patil, S.; Vyatkin, V.; McMillin, B. Implementation of FREEDM Smart Grid distributed load balancing using IEC 61499 function blocks. In Proceedings of the IECON 2013—39th Annual Conference of the IEEE Industrial Electronics Society, Vienna, Austria, 10–13 November 2013; pp. 8154–8159.
29. Zhabelova, G.; Vyatkin, V. Multiagent smart grid automation architecture based on IEC 61850/61499 intelligent logical nodes. *IEEE Trans. Ind. Electron.* **2012**, *59*, 2351–2361. [[CrossRef](#)]
30. Architecture view. Available online: <http://smartgridstandardsmap.com/> (accessed on 15 February 2019).
31. Alagoz, B.B.; Kaygusuz, A.; Karabiber, A. A user-mode distributed energy management architecture for smart grid applications. *Energy* **2012**, *44*, 167–177. [[CrossRef](#)]
32. Miguel, M.L.F.; Jamhour, E.; Pellenz, M.E.; Penna, M.C. A Power Planning Algorithm Based on RPL for AMI Wireless Sensor Networks. *Sensors* **2017**, *17*, 679. [[CrossRef](#)]
33. Pérez, J.; Díaz, J.; Garbajosa, J.; Yagüe, A.; Gonzalez, E.; Lopez-Perea, M. Towards a reference architecture for large-scale smart grids system of systems. In Proceedings of the 2015 IEEE/ACM 3rd International Workshop on Software Engineering for Systems-of-Systems, Florence, Italy, 17 May 2015.
34. Gjermundrod, H.; Bakken, D.E.; Hauser, C.H.; Bose, A. GridStat: A flexible QoS-managed data dissemination framework for the power grid. *IEEE Trans. Power Deliv.* **2009**, *24*, 136–143. [[CrossRef](#)]
35. Pipattanasomporn, M.; Feroze, H.; Rahman, S. Multi-agent systems in a distributed smart grid: Design and implementation. In Proceedings of the 2009 IEEE/PES Power Systems Conference and Exposition, Seattle, WA, USA, 15–18 March 2009.
36. Grijalva, S.; Tariq, M.U. Prosumer-based smart grid architecture enables a flat, sustainable electricity industry. In Proceedings of the Innovative Smart Grid Technologies (ISGT), 2011 IEEE PES, Anaheim, CA, USA, 17–19 January 2011.
37. Batista, N.C.; Melício, R.; Mendes, V.M.F. Layered Smart Grid architecture approach and field tests by ZigBee technology. *Energy Convers. Manag.* **2014**, *88*, 49–59. [[CrossRef](#)]
38. Li, Z.; Wang, Z.; Tournier, J.C.; Peterson, W.; Li, W.; Wang, Y. A Unified Solution for Advanced Metering Infrastructure Integration with a Distribution Management System. In Proceedings of the 2010 First IEEE International Conference on Smart Grid Communications (SmartGridComm), Gaithersburg, MD, USA, 4–6 October 2010.
39. Petruševski, I.; Rakić, A.; Popović, I. Layered AMI architecture for various grid topologies and communication technologies. *Telfor J.* **2016**, *8*, 38–43. [[CrossRef](#)]
40. Kim, J.; Filali, F.; Ko, Y.-B. Trends and Potentials of the Smart Grid Infrastructure: From ICT Sub-System to SDN-Enabled Smart Grid Architecture. *Appl. Sci.* **2015**, *5*, 706–727. [[CrossRef](#)]
41. Parvez, I.; Sarwat, A.I.; Wei, L.; Sundararajan, A. Securing Metering Infrastructure of Smart Grid: A Machine Learning and Localization Based Key Management Approach. *Energies* **2016**, *9*, 691. [[CrossRef](#)]
42. Park, S.-W.; Son, S.-Y. Cost Analysis for a Hybrid Advanced Metering Infrastructure in Korea. *Energies* **2017**, *10*, 1308. [[CrossRef](#)]

43. Balijepalli, V.M.; Khaparde, S.A.; Gupta, R.P. Towards Indian smart grids. Available online: <http://www.desmartgrid.com/wp-content/uploads/2012/07/Towards-Indian-Smart-Grids-.pdf> (accessed on 15 February 2019).
44. Patti, E.; Pons, E.; Martellacci, D.; Castagnetti, F.B.; Acquaviva, A.; Macii, E. multiflex: Flexible multi-utility, multi-service smart metering architecture for energy vectors with active prosumers. In Proceedings of the 2015 International Conference on Smart Cities and Green ICT Systems (SMARTGREENS), Lisbon, Portugal, 20–22 May 2015.
45. Trefke, J.; Dänekas, C.; Rohjans, S.; Vázquez, J.M. Adaptive architecture development for Smart Grids based on integrated building blocks. In Proceedings of the 2012 3rd IEEE PES International Conference and Exhibition on Innovative Smart Grid Technologies (ISGT Europe), Berlin, Germany, 14–17 October 2012.
46. Program on Technology Innovation Common Needed Attribute of Architecture for an Integrated Grid. 2016. Available online: <http://integratedgrid.com/wp-content/uploads/2016/09/00000003002009240.pdf> (accessed on 15 February 2019).
47. Jararweh, Y.; Al-Ayyoub, M.; Boussehla, A.; Benkhalifa, E. Software Defined based smart grid architecture. In Proceedings of the 2015 IEEE/ACS 12th International Conference of Computer Systems and Applications (AICCSA), Marrakech, Morocco, 17–20 November 2015.
48. Zhou, L.; Rodrigues, J.J. Service-oriented middleware for smart grid: Principle, infrastructure, and application. *IEEE Commun. Mag.* **2013**, *51*, 84–89. [[CrossRef](#)]
49. Kumar, Y.P.; Bhimasingu, R. Key Aspects of Smart Grid Design for Distribution System Automation: Architecture and Responsibilities. *Procedia Technol.* **2015**, *21*, 352–359. [[CrossRef](#)]
50. Albagli, A.N.; Falcão, D.M.; de Rezende, J.F. Smart grid framework co-simulation using HLA architecture. *Electr. Power Syst. Res.* **2016**, *130*, 22–33. [[CrossRef](#)]
51. Vrba, P.; Mařík, V.; Siano, P.; Leitão, P.; Zhabelova, G.; Vyatkin, V.; Strasser, T. A review of agent and service-oriented concepts applied to intelligent energy systems. *IEEE Trans. Ind. Inform.* **2014**, *10*, 1890–1903. [[CrossRef](#)]
52. Xu, Z.; Yang, P.; Zhang, Y.; Zeng, Z.; Zheng, C.; Peng, J. Control devices development of multi-microgrids based on hierarchical structure. *IET Gener. Transm. Distrib.* **2016**, *10*, 4249–4256. [[CrossRef](#)]
53. Sharifi, L.; Freitag, F.; Veiga, L. ARTA: An economic middleware to exchange pervasive energy and computing resources. In Proceedings of the 2016 IEEE International Conference on Smart Grid Communications (Smart Grid Comm), Sydney, NSW, Australia, 6–9 November 2016.
54. Zhabelova, G. Software Architecture and Design Methodology for Distributed Agent-Based Automation of SMART Grid. September 2013. Available online: <https://researchspace.auckland.ac.nz/bitstream/handle/2292/21409/whole.pdf?sequence=2> (accessed on 15 February 2019).
55. Considine, T.; Cox, W.; Cazalet, E.G. Understanding Microgrids as the essential smart energy architecture. 2014. Available online: http://coxsoftwarearchitects.com/Resources/Grid-Interop2012/Understanding_Microgrids_as_the_Essential_Architecture_of_Smart_Energy_20121201_Paper.pdf (accessed on 15 February 2019).
56. Zhabelova, G.; Patil, S.; Yang, C.W.; Vyatkin, V. Smart Grid applications with IEC 61499 reference architecture. In Proceedings of the 2013 11th IEEE International Conference on Industrial Informatics (INDIN), Bochum, Germany, 29–31 July 2013; pp. 458–463.
57. Zhabelova, G.; Vyatkin, V.; Dubinin, V.N. Toward Industrially Usable Agent Technology for Smart Grid Automation. *IEEE Trans. Ind. Electron.* **2015**, *62*, 2629–2641. [[CrossRef](#)]
58. Schmutzler, J.; Gröning, S.; Wietfeld, C. Management of distributed energy resources in IEC 61850 using web services. In Proceedings of the 2011 IEEE International Conference on Smart Grid Communications (Smart Grid Comm), Brussels, Belgium, 17–20 October 2011; pp. 315–320.
59. Bredillet, P.; Lambert, E.; Schultz, E. CIM, 61850, COSEM standards used in a model driven integration approach to build the smart grid service oriented architecture. In Proceedings of the 2010 First IEEE International Conference on Smart Grid Communications (SmartGridComm), Gaithersburg, MD, USA, 4–6 October 2010; pp. 467–471.
60. Adolf, D. Agent Based Architecture for Smart Grids. Available online: <http://citeseerx.ist.psu.edu/viewdoc/download?doi=10.1.1.703.5131&rep=rep1&type=pdf> (accessed on 15 February 2019).

61. Ductor, S.; Gil-Quijano, J.J.; Stefanovitch, N.; Mele, P.R. GRENAD, A modular and generic Smart-Grid framework. In Proceedings of the 2015 Federated Conference on Computer Science and Information Systems (FedCSIS), Lodz, Poland, 13–16 September 2015; pp. 1781–1792.
62. Wang, W.; Xu, Y.; Khanna, M. A survey on the communication architectures in smart grid. *Comput. Netw.* **2011**, *55*, 3604–3629. [[CrossRef](#)]



© 2019 by the authors. Licensee MDPI, Basel, Switzerland. This article is an open access article distributed under the terms and conditions of the Creative Commons Attribution (CC BY) license (<http://creativecommons.org/licenses/by/4.0/>).

Review

Electric Vehicle Charge Stations Location Analysis and Determination—Ankara (Turkey) Case Study

Tohid Harighi ^{1,2}, Sanjeevikumar Padmanaban ^{3,*}, Ramazan Bayindir ^{2,*}, Eklas Hossain ⁴ and Jens Bo Holm-Nielsen ³

¹ Graduate School of Natural and Applied Sciences, Gazi University, 06500 Ankara, Turkey

² Department of Electrical and Electronics Engineering, Faculty of Technology, Gazi University, 06500 Ankara, Turkey

³ Center for Bioenergy and Green Engineering, Department of Energy Technology, Aalborg University, 6700 Esbjerg, Denmark

⁴ Oregon Renewable Energy Center (OREC), Department of Electrical Engineering & Renewable Energy, Oregon Tech, Klamath Falls, OR 97601, USA

* Correspondence: san@et.aau.dk (S.P.); bayindir@gazi.edu.tr (R.B.); Tel.: +45-2097-5179(S.P.)

Received: 4 July 2019; Accepted: 2 September 2019; Published: 9 September 2019

Abstract: Locating electric vehicle charge stations has always been an important problem for electric distributors. Many basic and complex solutions have been provided by algorithms and methods to solve this problem in real and assumed grids. However, the data, which has been used in those algorithms, are not consistent with the diversity of locations, thus, do not meet the expected results. Grid locations are the most important aspects of this issue in the eyes of designers, investors, and the general public. Locating charge stations must be determined by plans which have influenced majority in the society. In some countries, power quality has been increased by storages, which are used in vehicle-to-grid (V2G) and similar operations. In this paper, all of the variables for locating charging stations are explained according to Ankara metropolitan. During the implemented analysis and literature reviews, an algorithm, based on location and grid priorities and infrastructures, are 154 kV and 33 kV, have been designed. Genetic algorithms have been used to demonstrate this method even though other algorithms can also be adopted to meet the priority.

Keywords: electric vehicles; charging station; transformer; Energy PLAN; grid; renewable energy

1. Introduction

Charging stations or other types of energy storages need organization when they are used for special targets. Considering the grid's situation, an organized program should cover the supply and demand needs of the grid. Supply needs, such as low loss operation without side effects, and demand needs, such as abundance in the charge station, low cost, and increased power quality, are required to be fulfilled. All of these needs and similar problems, issues or remodeling methods have created a basis to providing organization for electric vehicles (EV) charge stations. Factors, such as societal, populace, grid infrastructure, and renewable conditions [1], critical power range, and financial analysis of a location, play important roles in determining the grid condition. However, supply/demand power and coordination, and the estimation of equipment is the telling factor, which needs focus to meet the incessant load demand.

The estimation of power, especially on the demand side of the grid, is very difficult [2]. Increasing or decreasing the rate of grid power does not go on determined patents, such as battery open circuit voltage estimation by Extended Kalman Filter (EKF) or similar estimation operations [3]. Supply/demand and coordinating for EVs charge station estimations have a lot in common, so they can contribute to an increase in power quality in the grid, directly when the grid infrastructure is ready. The benefits of

this work are not limited to some factors, such as the decrease in green-house gas (GHG) emissions. Fuel transmission between oil refineries to gas stations consume electric power, especially in gas stations where compressed natural gas (CNG) stations use electric convertors. At present, too many researchers are trying to create and optimize algorithms to harvest fine results, but the methods and algorithms should be fed by trustworthy numerical data. In addition, the experiments are to be simulated using simulation software, such as MATLAB. In one Finnish study, to meet Finland's target of 100% renewable energy usage by 2050's (funded and presented by Ministry of Economy and Employment), the research on Energy PLAN (created by Aalborg University) modelling has focused on energy potential and generation from a perspective of economy, the rate of fuel usage, and CO₂ emission according to decrease in GHG emission policy [4]. The result of this investigation shows that the energy future, based on 100% renewable energy, is entirely possible. In another study focused on Delhi, India's energy sector, the Japanese Society for the Promotion of Science (JSPS) investigated the future of energy and its optimization methods in Delhi. Their study found that integrated-systematic modelling should be used for energy flow in urban energy systems. They have used an optimal energy scenario and found an energy gap between supply and demand. This research paid attention to government energy policy in improving the demand side of their energy sector [5]. However, government policy and social behavior strongly influence the GHG emission in the transportation sector, in many countries, such as Austria [5]. The emission of CO₂ is one of the primary problems in China and the CO₂ condition will be in 2030 with the use of control or uncontrolled EVs, V2G and similar transportation systems. Studies have shown that the application of these transportation systems provide advantages, such as decreasing peak load, which is used for EV charging; generating power from renewable energy sources (RES); and reducing energy generation and EV charging costs [6]. Some of the literature has focused on the distance of charge stations with respect to the most capable grids. A Taiwanese study looked into helping customers receive better service from the grid by creating charge stations at reasonable distances in Taiwan [7]. Therefore, it is possible to determine probable locations for EV charging stations, based on the grid and transportation technology of the time, rather than based on any specific algorithm.

Several algorithm-based research are still used in smart grid and V2G operations for special conditions or purposes which are explained below. One study focused on uncertain situations with respect to V2G operation pricing, using the robust game-theory to treat uncertain issues. This algorithm was named ENTRUST (Energy Trading under Uncertainty in Smart Grid Systems) [8]. This study achieved reliability and cost efficiency in terms of energy management. Another grid lead system is known as multi-agent energy management. In this system, all elements of demand side of the grid (home, building, industries, and vehicles) are connected. It can improve autonomy, connectivity, diversity, and appearance of the systems in the grid. Another study in Great Britain (GB) [9], created a dynamic virtual energy storage systems (VESS) to solve the dynamic frequency response. This model uses V2G and similar technology storages to notify grid whenever it needs emergency energy or whenever the rhythm of the energy flow has been disturbed. This model considered the response capacity of an EVs cluster. Researchers have furthermore developed some algorithms for EV charge stations, including the flow refueling location model (FRLM) [10] maximum covering location problem (MCLP) [11], nonlinear auto-regressive (NAR) [12], Genetic Algorithm (GA) [13], Genetic Algorithm-particle swarm optimization (GA-PSO) [14], and Genetic Algorithm-binary particle swarm optimization (GA-BPSO) [15].

Each research has coordinated points by special parameters, which is the dominant factor in supporting the system objectives. Previously described models, scenarios, and algorithms are the key to managing the grid and to increasing responsibility for EVs, charge stations and interconnected storage. The coordination of EV charging stations at first sight needs these methods to solve some pre-requisites. This paper considers Ankara's metropolitan electric infrastructure and the conditions dependent on Ankara's electricity infrastructure to determine potential locations for the charging stations. In Ankara's case, the grid has not been updated to be smart enough to include online sensors,

which may be used in determined algorithms. This study attempts to determine the location by specifications of the grid infrastructure, categorizing the capacity of transformers and their other parameters. A method, based on the Genetic Algorithm is designed to verify the probability of a location meeting the requirement is shown.

The rest of the paper is organized as follows. Section 2 discusses the case study, particularly considering four locations in Ankara. Section 3 takes grids in Ankara in consideration to nominate them as the station location. Section 4 brings transformers into inspection by delineating several parameters to select transformers capable of matching the EV application. Section 5 presents the corresponding transformer indices and parameters to aid the selection process. Considering this framework, the layout of the estimation algorithm with respect to the Genetic Algorithm is explained in Section 6. Finally, conclusions are drawn in Section 7.

2. Case Study

In this paper, four transformer centers have been considered at the start/end points, which are supplied by A point and finally used by D point. Each point has been analyzed by their maintenance history and current peak load point. Transformer maintenance history and current peak load point can illustrate most of their qualities. This research attempts to create a defined glance to recognize points, which are necessary for determining the location of EV charging stations, that can help to build a connection with the grid plan. In the next sections, the proposed solution for determining the coordination of EV charging stations will be elaborated with examples. Ankara metropolitan electricity grid is one of the real cases to study, indicating important parameters, when the grid should be ready to supply electric vehicle and storages.

As demonstrated in the literature, the categories of charging stations distance can change quality of power, service, cost and EVs technology acceptance ratio between members of society. The range of charging stations were determined by various items, such as the grid infrastructure and existing EVs going around. Additionally if the grid does not use charging stations, some locations should be determined by other specifications. These can be different in each grid and depends on the grid's condition. According to the previously mentioned information and Ankara metropolitan electricity infrastructure, the distance of grid terminals and power capacity are critical points in the coordination of electric vehicle charge station topic. A city's transportation routes are different from the route of the power transmission grid and each location has specific power capacity details. In the first step, designers must select locations like points or places, which have the lowest distance to electricity terminals and are suitable for transportation systems. The goal is to measure energy, and responsibility for supply and demand. For example, two different points in Ankara have been assessed - the A and B transformer centers. Both of them are on main and crowded streets, but the A transformer center's condition makes it more operational than the B transformer center. This is, because the A transformer center is close to downtown where the main transportation terminals, such as buses and trains are localized. Whereas 1~2 km from downtown, metro, terminals and location of transformer A and B have many free spaces, parking, schools, hospitals and ministries. It seems that in this area, a large amount of vehicles are stationary and this can be potentially beneficial. In contrast, the B transformer center does not have those options, and because of this, the B transformer center loses its priority to build a charging station. Figure 1 has given the locations of both transformer centers and a map of Ankara for clarity.

Location EV charge station points should be categorized by reasonable distances such as 30, 35, 40, 45, and 50 km, depending on area and infrastructure condition. In the mentioned case, the grid conditions were analyzed, based on the transformer status, even though there was no pre-defined storage center or organized charge station. This indicates that transformer specifications could provide prospective information to evaluate the likelihood of charging stations.

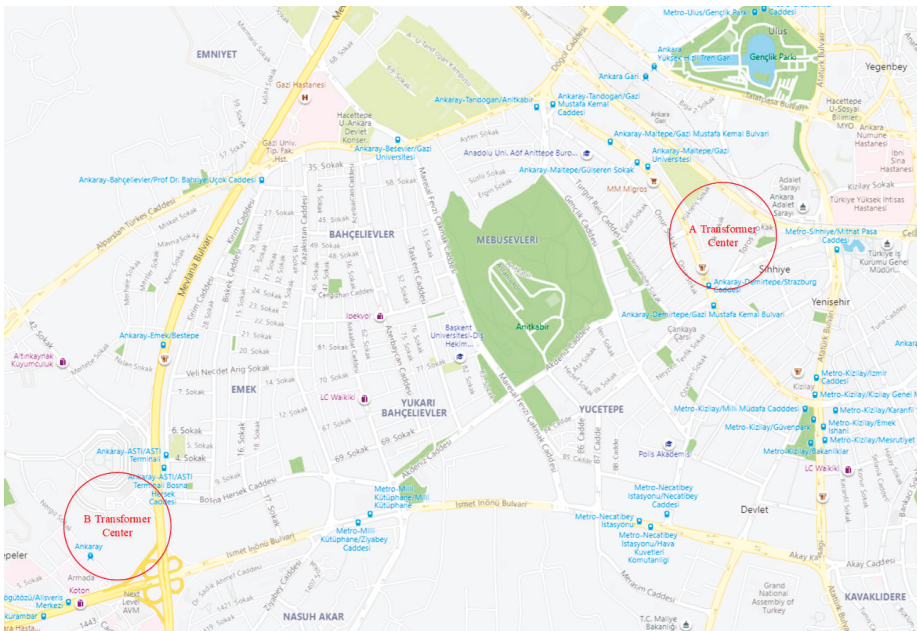


Figure 1. Map of Ankara, and area maps of the A and the B Transformer Centers [16].

3. Grid Conditions in Ankara

One of the important factors in grid stability is its dependency on the grid size and infrastructure revises, but efficiency and responsibility are negotiable. The electricity grid of the provinces of Ankara, Bartın, Çankırı, Karabük, Kastamonu, Kırıkkale, and Zonguldak are controlled by the ENERJISA Company (Hanmeli Avenue No:1 Sıhhiye/ANKARA) [17]. At first, the stability of grid should be examined with respect to power and size. This area has special specifics, which help to stabilize the grid. As the area is located in the middle of Turkey and neighbors the five other grid control areas, Ankara can receive energy from five different electricity areas, which means that this area has enough reserve power from the Turkish National Grid. This area is formed from provinces, which have an energy generation rate more than their consumption rate. Some information about those provinces are shown in Table 1.

Table 1. Some energy consume and generate details of province which are under the control of ankara province [18].

	Power Plants Quantity	Annual Consumed Energy Rate in Turkey	Annual Energy Generation in Turkey
Ankara	69	3.64%	~9.299 GWh
Kırıkkale	9	3.44%	~8.797 GWh
Zonguldak	7	4.10%	~13.332 GWh
Kastamonu	10	0.07%	~188 GWh
Çankırı	3	0.01%	~14 GWh
Karabük	7	0.22%	~575 GWh
Bartın	3	0.02%	~56 GWh

The grid has been shown to be stable at high penetration rate. The energy terminals are in special places, where they can provide high performance in particular aspects such as energy responsibility. However, they cannot exceed an appropriate amount, which are key points in the energy transfer

between grids and storage, thus, both of their accessibilities observe different purposes. Figure 2 illustrates this point clearly. Generally, bi-directional energy transfer has been operated between medium voltage and low voltage range. Bi-directional operation procedures develop in parallel with grid infrastructure and customers.

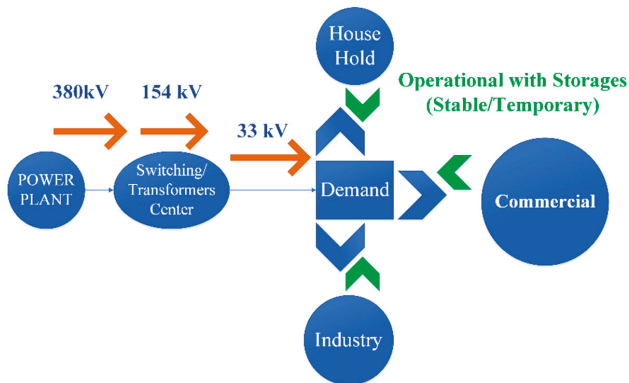


Figure 2. Energy injection side and areas can be operational by storages.

4. Transformer Selection

Transformers are the last operational part of the grid, which directly influence the quality of the grid and charge stations. Generally, all ranges of grid transformers are influenced by storages, such as charging stations or grid independent storages. Low- and mid-range transformers in the grid receive high impact from power electronic equipment, but they need support from high voltage transformers. Some transformer parameters depend on their own operational period, which cannot be determined in routine ways. The capacity of distribution in transformers has the potential to determine the necessary variables in the grid, related to financial problems, aging, health, and their priorities. Hence in this algorithm, the capacity and related problems have a higher priority. Low capacity or overload is the first step in system failure. Overload in electric equipment, like transformers, cause severe faults in the grid. In the second step, it causes a nonlinear increase in the transformers' temperature [19]. One of the regular solutions to solve these problems is by decreasing or changing the load pattern according to different grid specifications [20]. Transformers should be sorted according to their capacity. The flow chart of sorting is shown in Figure 3.

The purpose is to determine high priority transformers in the grid. By changing the timeslot in the Grid Valley filling technology [21], grid demand level, load factor, and transformer aging have been changed at a reasonable scales. It can reduce load about 4~5 GW in a scenario and ambient transformers temperature 1.06~1.64% instead 52~100% in 50 kVA transformers and 200 °C temperature rate. Consequently, transformer aging is influenced with these statistics, where it has changed 17~18 factors, instead of 17~96. Another study has illustrated that EVs generate overload and shape impulses. Such grid problems have been solved through timetable changes and transformer hierarchy, as shown by MATLAB V9.5 software [22,23]. The solving method can change in each location, depending on related problem conditions, therefore, there (There will be various conditions at hand). The smart grid transmission and distribution costs are very important and have been influential in the other side of the grid. The function of transmission and distribution costs has been given in

Equation (1) [24]. Equation (1) has illustrated the importance of grid infrastructure and equipment costs when they have met low/over load. In this equation transformers and lines are the main factors [24].

$$\text{Min } z = \sum_{(i,j) \in \text{Line}} a_{ij}(X_{i,j}) + \sum_{(i,j) \in \text{OverLine}} b_{ij}(X_{i,j}) + \sum_{m \in \text{Over Equip}} c_m(X_m) + \sum_{n \in \text{OutLoad}} d_n(X_n) + \sum_{n \in \text{OutLoad}} e_n(X_n) + \sum_{m \in \text{Ment Equip}} f_m(X_m) + \sum_{k \in \text{Power Equip}} g_k(X_k) + \sum_{m \in \text{Fail Equip}} h_m(X_m) \tag{1}$$

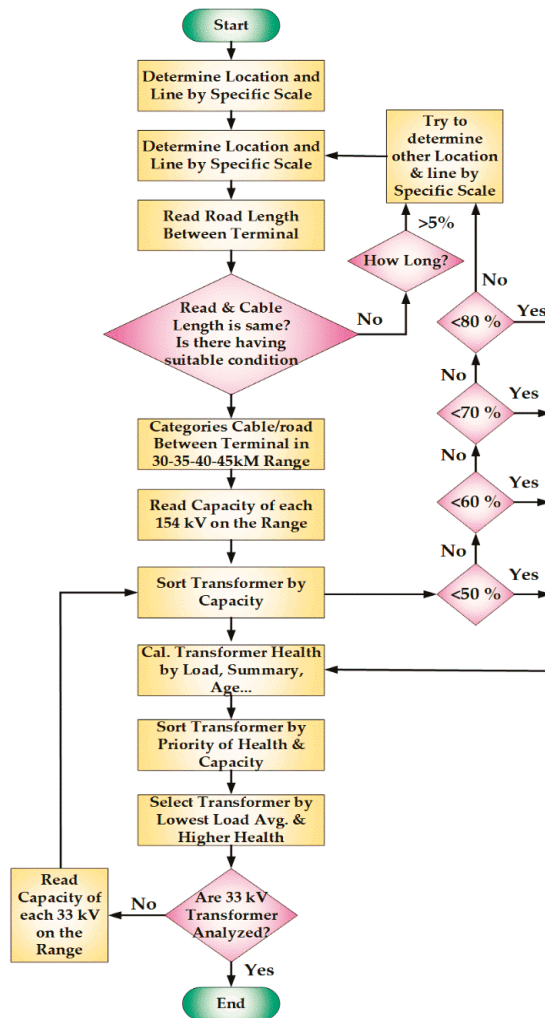


Figure 3. Electric vehicle (EV) charge stations coordination algorithm.

The above equation shows that transmission and distribution costs create a large part of the grid's maintenance cost. The next equations have illustrated aging and the loss of life rate of the transformer for

an average penetration rate of EV [25,26], which completely depends on the transformers' temperature. Through various investigations, EV fast charge stations or similar loads were found to generate an impulse load signal type, consequently, it hides hot-spot temperature points in the transformer, which sensors cannot detect.

$$V = e^{\frac{15000}{110+273} - \frac{15000}{\theta_h+273}} \tag{2}$$

$$L = \int_{t_1}^{t_2} V dt \text{ Or } L \approx \sum_{n=1}^N V_n \times t_n \tag{3}$$

$$D_{TR_PHEV_X} = A \times e^{(B \times T_x - T_r)} \tag{4}$$

$$V_{TR_PHEV_X} = \frac{D_{TR_PHEV_WITHOUT}}{D_{TR_PHEV_X}} \tag{5}$$

$$V_{TR_PHEV_LOW} = A \times T_x - T_r + B \tag{6}$$

$$V_{TR_PHEV_X} = A \times e^{(B \times T_x - T_r)} + C \times e^{(D \times T_x - T_r)} \tag{7}$$

Figure 4 clearly shows the temperature influence on the loss of life (LOL) rate on transformers, which can be proved by Equations from (2) to (7) [25]. The transformers' overall condition is important when transformer temperature exceeds 110 °C, so the LOL rate starts increasing.

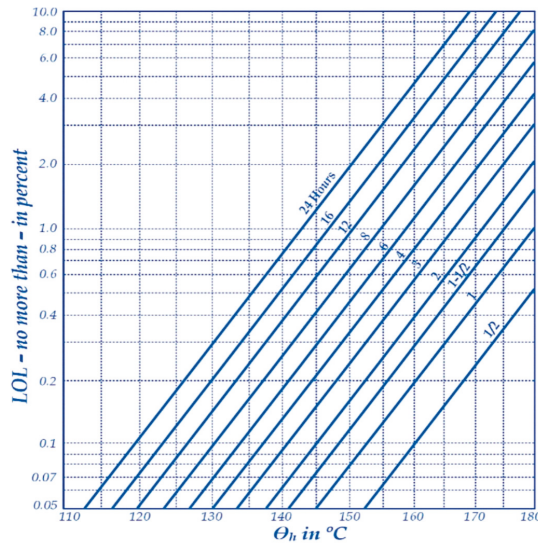


Figure 4. LOL and θ_h in different time [25].

One of the most effective ways to solve this type of problem is to monitor transformer temperatures, which are controlled at SCADA or matched on relay settings [25]. Indisputably, sometimes by assigning more EVs in each grid, some transformers might get overloaded, consequently leading towards faults or interruptions in the grid. The solution to capacity problems depends on the grid communication infrastructure and the grid creation hierarchy. The flow chart of the grid communication infrastructure and the grid creation hierarchy is also represented in Figure 3.

According to the grid condition, there are many factors in the flowchart that can be calculated altogether. For Ankara, we do not have a smart transformer with online monitoring, therefore, we must use tools based on summary data. Table 2 shows information that owner C and D have a high priority to create a charge station on their locations. For example, the data of a grid with air quality sensor results are provided below.

Table 2. A grid transformers' center and their environmental condition.

Transformer Center				Load		
A				649 MW		
Transformer Center	Load	Usage Percentage	Owner	Air Quality PM10	SO ₂	
Transformer No.	A1	33.5	62	A	-	-
	A2	58.5	54	A	-	-
B				Total: 238		
Transformer No.	B1	44	60	B		
	B2	60	55	B	31	7
	B3	69	65	B		
	B4	65	74	B		
C				Total: 210		
Transformer No.	C1	48	66	C	52	15
	C2	32	60	C		
	C3	45	61	C	79	15
	C4	18	58	C		
	C5	52	72	C	14	8
	C6	15	48	D		
D				Total: 109		
Transformer No.	D1	37	55	83	D	41
	D2	7 (15 kV)	61		D	10
	D3	65			C	

In localizing EV charge stations, the regional condition and some of their priorities were more important than the grid infrastructure on their locations. Therefore, they should develop their own location grid infrastructure. In most of the locations parking and public areas provide benefits from the financial and technical side, to create a battery bank and base for an EV charging station. In addition, all of them are explained in the "Selection of High Efficiency and Operational Locations" section of this paper. In this case, the transformers are not smart and the operations group cannot monitor the transformers status, so they do maintenance operations using technical data and by estimation. The transformers are replaced every 30 years and they reach 55~70% capacity during load peak times. These provide some information about the grid, such as transformers work condition. The ANSI/IEEE C57.96-1989 standards [27] recommend transformers be replaced every 20 years, if they have been run under ideal maintenance conditions. The transformers' life expectancy may be calculated by their insulation life equation, as illustrated below:

$$\log_e \text{life} (t) = A_e + \frac{B_e}{T} \quad (8)$$

$$\log_{10} \text{life} (t) = A_{10} + \frac{B_{10}}{T}. \quad (9)$$

Based on Equations (8) and (9), Figures 5 and 6 illustrates the time expectancy curve, used in Equations (8) and (9). It shows that transforms, which age more than 20 years, have been in the best maintenance condition.

Figures 5 and 6 and the related Equations (Equation number 8 and 9) have shown that the transformers have been maintained and are in good condition (the grid has passed "Calculate Transformers Health by Load Summery, Age," term).

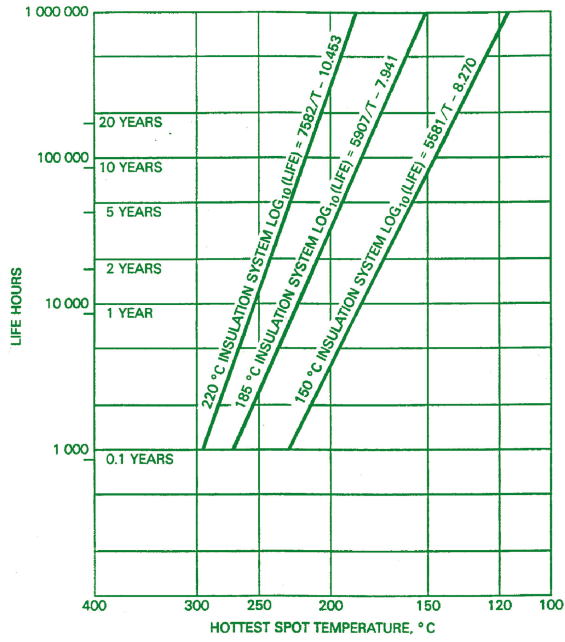


Figure 5. Life hours and hottest spot temperature °C in transformers by LOG₁₀.

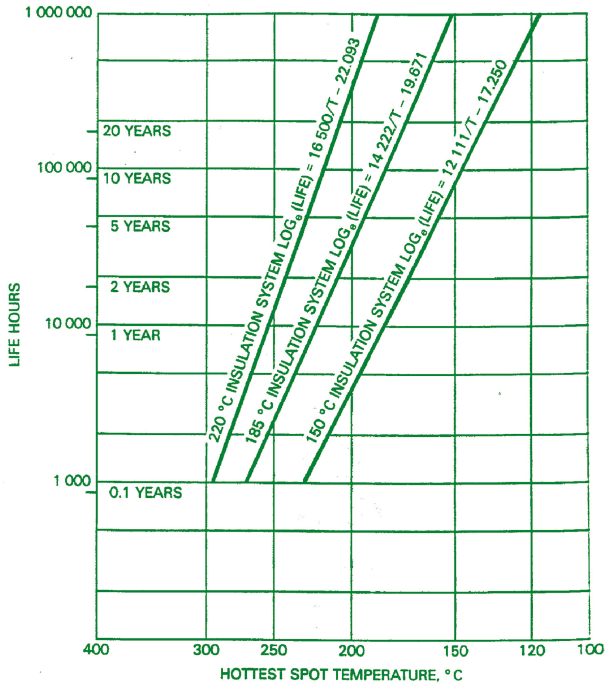


Figure 6. Life hours and hottest spot temperature °C in transformers by LOG₁₀.

5. Assessment of Infrastructure

As a crucial step for assessing the infrastructure, transformers’ heal index should be assessed accurately by some standards and scoring system. Technical condition and their standards should cover their general status [28]. The technical and operational conditions are mentioned below:

- Technical conditions:
 1. Transformer Parallelism Index
 2. Transformer Reserve Index
 3. Transformer Rated Power
- Operational conditions:
 1. Main Health Index (HI_m)
 2. Insulating Paper Health Index (HI_{iso})
 3. DGA Health Index (HI_{CH})
 4. Oil Health Index (HI_{oil})

In this section of the paper, mentioned index is explained briefly.

5.1. Technical Conditions

5.1.1. Transformer Parallelism Index

If transformers are under load and analysis, the Transformer Parallelism Index is determined and shows when it pairs with another transformer, and which part of the grid demand is suitable for this parallelism. This value can change from 0, where parallel transformers cannot work in parallel, or when they are not able to take charge of the connected equipment under the load, to 1, where transformers can respond to the demand. The interval 0 to 1 has illustrated a percentage value in the transformer under the load that can response the maximum load power. This index is accepted from 120% to 140% in Brazil in accordance with the ONS NT 038/2014 standard [29] and is illustrated in Figure 7.

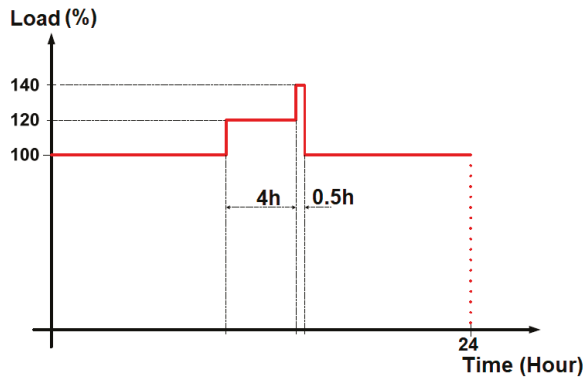


Figure 7. Acceptable Over Load by ONS NT 038/2014.

The Transformer Parallelism Index value is illustrated in Equations (10)–(14);

$$\begin{cases} 1 & \frac{TRP_{Ny}}{TRP_{Nx}} > \frac{f_L}{L_{max}-f_L} \\ \frac{TRP_{Ny}(L_{max}-f_L)}{TRP_{Ny}f_L}; & \frac{TRP_{Ny}}{TRP_{Nx}} \leq \frac{f_L}{L_{max}-f_L} \wedge 0 < f_L \leq L_{max} \\ 0 & f_L > L_{max} \wedge f_L = 0 \end{cases} \quad (10)$$

$$TRP_{Ny} = \sum_{f_L \geq 0} TRP - TRP_{Nx} \tag{11}$$

$$f_L \geq 0 \tag{12}$$

$$TRP_{Ny} \geq 0, \forall y \in N \tag{13}$$

$$TRP_{Nx} \geq 0, \forall x \in N \tag{14}$$

5.1.2. Transformer Reserve Index

The Transformer Reserve Index is an index of transformers that can increase safety and reliability. It is a very important index in identifying whether power equipment can respond to normal failure and random interruption. However, charging stations, specifically fast charging stations, where production increase appears to produce impulse signals in their connected transformers and responses from transformers must be received. An example of this condition from real data has been explained in a study from São Miguel Island. Figure 8 has illustrated this fact in a curve by time and daily load [19].

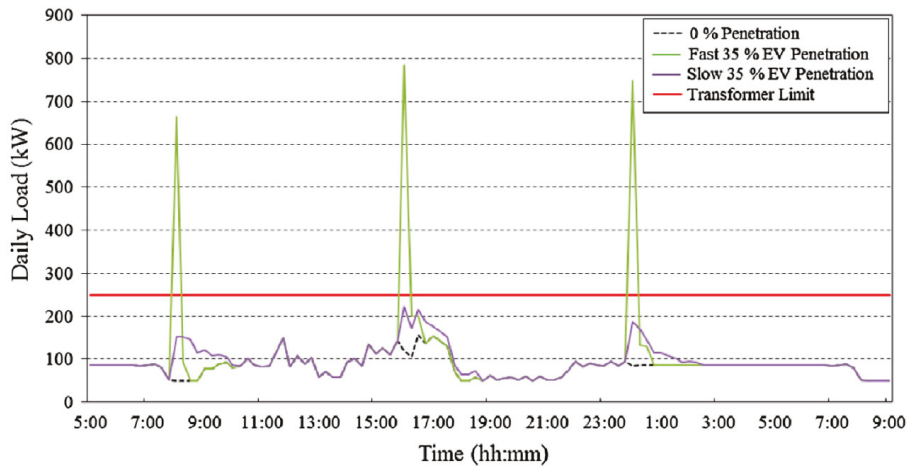


Figure 8. Transformer inputs in a fast and slow charge system by daily load versus time.

This problem can be partially solved by reserve index. To solve the mentioned issue, except transformer reserve, charging stations storage reserve is more sensible. Hence both of the reserves should increase logically.

5.1.3. Transformer Rated Power

The capacity of transformers is one of the important factors in receiving positive feedback from both the supply and demand side of the grid. The temperature in all aspects of the transformers depends on transformer rating. It must be stable in the operational area. As seen in the correlation between the life hour and temperature of transformer in Figure 5, transformer temperature can be a determinant in controlling the transformer conditions.

5.2. Operational Conditions

5.2.1. Transformer’s Main Health Index (HI_m)

The transformer main health index has always been a useful factor in the transformer operational period. This index has been sensitive to temperature fluctuations, which changes in various ratios in the transformer life, so it depends on system summary. Transformers Main Health Index (HI_m) is

determined by the initial main health index reference point, which is named: HI_0 . HI_m is defined by Equations (15) and (16) mentioned below:

$$HI_m = HI_0 \times e^{\beta \times (T_2 - T_1)} \quad (15)$$

$$\beta = \frac{\ln 6.5 - \ln 0.5}{T_2 - T_1}. \quad (16)$$

5.2.2. Transformers' Insulating Paper Health Index (HI_{iso})

Insulation paper in each transformer directly determines the efficiency and life of a transformer. The transformer condition can be illustrated by identifying this index. Transformers Insulating Paper Health Index (HI_{iso}) can be recognized by analyzing some gases, such as carbon monoxide and carbon dioxide, in the transformer which is damaged due to overheating over its lifetime. The Transformers Insulating Paper Health Index (HI_{iso}) is presented in Equation (17):

$$HI_{iso} = \omega_1 HI_{C,O} \times \omega_2 HI_{fur} \quad (17)$$

$$HI_{fur} = 3.344 \times (C_{fur})^{0.413}. \quad (18)$$

From [30], where C_{fur} is content of furfural to determine, HI_{fur} is the index of it, from [28] $C_{fur} = 5$ means that the transformer is deteriorated and it can break down, in this condition $HI_{fur} = 6.5$. On the other hand $C_{fur} = 0.01$ when it is newer and $HI_{fur} = 0.5$. $HI_{C,O}$ is defined by carbon monoxide and carbon dioxide gases analysis.

5.2.3. Transformer's Dissolved Gas Analysis (DGA) Health Index (HI_{CH})

The Transformer's DGA health index (HI_{CH}) is one of the important and regular tests to determine a power transformer's health. In this health index, the values of hydrogen (H_2), methane (CH_4), ethane (C_2H_6), ethylene (C_2H_4), acetylene (C_2H_2), carbon monoxide (CO), and carbon dioxide (CO_2) are analyzed in the transformer to estimate the power transformer's material condition, and consequently, the transformer's physical condition can be elaborated. The DGA health index (HI_{CH}) is illustrated in Equation (19):

$$HI_{CH} = \sum_{i=1}^5 \omega_i \cdot F_{C,H}(i) \quad (19)$$

where, $F_{C,H}$ is the quantity of transformer ageing, hydrocarbon gas factor function, and ω is the weight of presented gases.

5.2.4. Transformer's Oil Health Index (HI_{oil})

The Transformer's Oil Health index can have some errors, such as acid value, high fluctuation of voltage, micro water, and dielectric losses. Also, these factors are the result of the transformer's cooling system and the transformer topology, which is met in transformer oil. This index calculation is given in Equation (20):

$$HI_{oil} = \sum_{i=1}^4 \omega_i F_{oil}(i) \quad (20)$$

where, F_{oil} is the oil factor function, determined the hydrocarbon gas factor function and ω is the weight of presented gases.

6. Results

In this section, we show that there are many factors which influence the distribution of charge stations. Air quality, transformer conditions, change infrastructure location, and local condition have illustrated that there are very important factors to feed the algorithms mentioned in the Introduction section of the paper. For example, the Gaussian distribution method in Equation (15) can give different results, depending on three factors, rather than two factors. Indeed, the factors change the distribution system variance and reference of their changes:

$$f(x) = \frac{1}{\sqrt{2\pi\sigma}} e^{-\frac{1}{2}\left(\frac{x-\mu}{\sigma}\right)^2} - \infty < x < +\infty. \tag{21}$$

In addition, it is one of the distribution systems between different types. Today, most of the distribution systems work by multi-functional operations, based on the same system. The Genetic Algorithm is the most used algorithms for the same goal. However, they can work by different variables and functions. The control of each algorithm has its own special strategy and their responsibility efficiency depends on valid operational information from the location. Figure 9 has illustrated a hierarchy of input data for algorithms. In addition, operations in each algorithm will change if other priorities are used in their hierarchy.

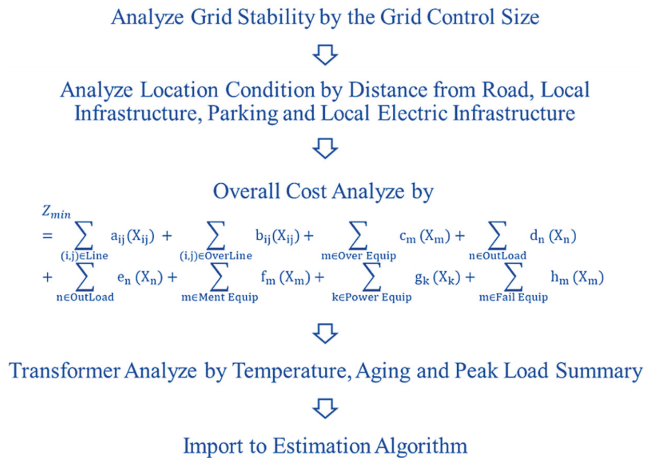


Figure 9. Hierarchy of algorithm input data.

In this case, the result of the “Estimation Algorithm” block depends on Turkish energy policy which involves long-term planning. According to the data mentioned in Table 1, two and location information, the GA is a reasonable method in creating a charging station point. Therefore, there are many drivers, reasons, and information, which can change algorithm targets. The information, which is issued by first data can be changed or improved by the GA algorithm. Figure 10 has mentioned an algorithm that was designed by the hierarchy presented in Figure 9. The algorithm has analyzed and sorted pure data to import on the main estimation algorithm. Firstly, the algorithm achieves location information, however, one of the algorithm targets is the charging station determination near the transportation road to reduce equipment faults during energy transmission. In the next step, the algorithm has been redetermined in each fail loop or unsuccessful operation. In addition, the algorithm sorts each charging stations in some distance, which depends on grid and customers’ needs. In the second step, the condition of the grid infrastructure has played a big role on algorithm output. In first technical command, it selects transformers, which have the highest reservoir capacity, so the transformers can absorb and transfer grid energy, and lacking in quality. The transformer

should be selected by the highest criteria so that the charging stations, especially fast charging stations, behave differently than transformers' norm. In the second step, which contains the analysis of technical condition, the determination of the points have been issued by their previous technical conditions. Transformers' conditions can be calculated by temperature or maintenance information.

According to above-mentioned operations, three points (B, D and C) have been determined to be the locations for building EV fast charging stations in Ankara. There are sufficient reasons to select the mentioned transformer centers, by the time they have some difference between mentioned points. Some local infrastructure and transformer responsibility factors have different factors which can be solved by some location problem using GA.

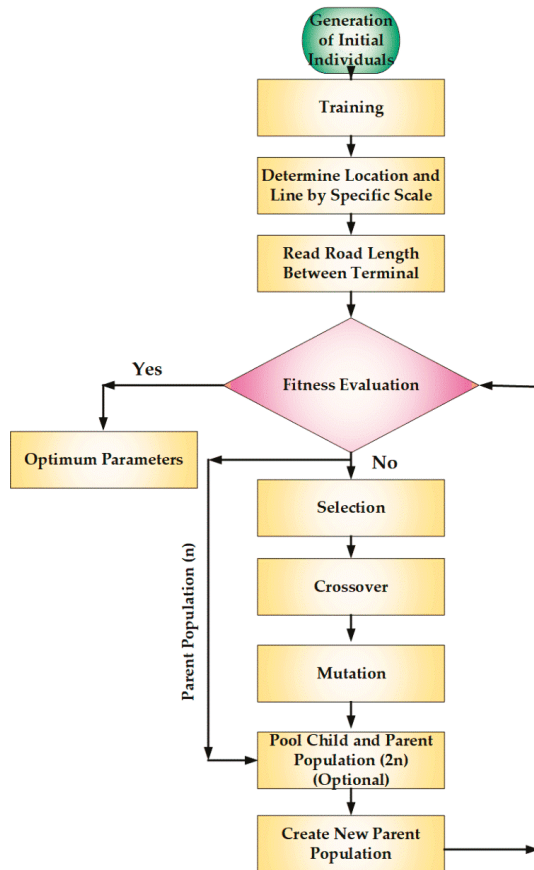


Figure 10. Flow chart of Genetic Algorithm (GA) estimation method.

Using the above-mentioned factors, the designers should give some scores to parameters, in order to determine factors' priorities, then, their data might be ready to input on estimating algorithms. For example, in GA it can be solved by the Genetic Algorithm shown in Figure 10.

According to the above flowchart, the algorithm can adapt in most of the estimating algorithms. For three areas, marked B, C, and D, several sets of locations and electric infrastructure have been arranged as chromosome structures, shown in Table 3. Six chromosome sets are based on the flowchart in Figure 10. The locations are sorted based on distance (a gene), local infrastructure (b gene), parking (c gene), and electric infrastructure (d gene). The generations are derived according to

low loads, ageing, and transformer capacity transformer index of the mentioned areas respectively. A maximum of 30 locations have been considered to satisfy the objective function mentioned as:

$$F_{obj} = a + 2b + 3c + 4d - 30. \tag{22}$$

Table 3. Chromosome structure for aforementioned locations with their corresponding areas (termed as B, C, and D).

	a	b	c	d
	Gen_1	Gen_2	Gen_3	Gen_4
← Chromosome Length ⇒				
Area B				
Location	27	24	27	12
Electric Infrastructure	9	6	15	9
Area C				
Location	6	24	9	27
Electric Infrastructure	18	24	24	21
Area D				
Location	27	15	6	27
Electric Infrastructure	15	21	21	18

Six chromosome have been created by location and infrastructure genes. The calculation of determination of the fittest chromosomes have been illustrated in Table 4.

Table 4. Determination of fitness function and probability for the first generator.

<i>i</i>	Chromosome <i>i</i> [a;b;c;d]	F_obj[i]	Fitness[i] = $\frac{1}{F_{obj[i]}}$ + 1	P[i] = $\frac{Fitness[i]}{Total_Fitness}$	Cumulative Probability, C[i]
1	[27; 24; 27; 12]	$((27 + (2*24) + (3*27) + (4*12) - 30)) = 174$	0.005714285	0.131445255	0.131445255
2	[09; 06; 15; 09]	$((9 + (2*6) + (3*15) + (4*9) - 30)) = 072$	0.013698630	0.315108524	0.446553779
3	[06; 24; 09; 27]	$((6 + (2*24) + (3*9) + (4*27) - 30)) = 159$	0.006250000	0.143768265	0.590322044
4	[18; 24; 24; 21]	$((18 + (2*24) + (3*24) + (4*21) - 30)) = 192$	0.005181347	0.119186123	0.709508167
5	[27; 15; 06; 27]	$((27 + (2*15) + (3*6) + (4*27) - 30)) = 153$	0.006493506	0.149369615	0.85887778
6	[15; 21; 21; 18]	$((15 + (2*21) + (3*21) + (4*18) - 30)) = 162$	0.006134969	0.141122216	0.999999998 ≈ 1.0
			Total_Fitness = 0.043472737		

If the random values ranging from 0–1 are initiated and if $C[1] < R[1] < C[2]$, then chromosome [2] can be set as the new population for the next generation.

$$R = [0.37, 0.08, 0.971, 0.829, 0.735, 0.359]$$

By those random patterns, new chromosomes have listed in below:

Chromosomes 2: [09; 06; 15; 09] as New Chromosome 1

Chromosomes 1: [27; 24; 27; 12] as New Chromosome 2

Chromosomes 6: [15; 21; 21; 18] as New Chromosome 3

Chromosomes 5: [27; 15; 06; 27] as New Chromosome 4

Chromosomes 5: [27; 15; 06; 27] as New Chromosome 5

Chromosomes 2: [09; 06; 15; 09] as New Chromosome 6

Considering a crossover-rate of 25%, if the corresponding value of $R[k]$ is less than the rate, the chromosome will be considered as the parent chromosome. For an array of random number:

$$R = [0.518, 0.224, 0.108, 0.383, 0.071, 0.481]$$

By the new randomization and chromosomes, the parents can be presented as below:

Chromosome 2: [27; 24; 27; 12]

Chromosome 3: [15; 21; 21; 18]

Chromosome 5: [27; 15; 06; 27]

By the random numbers that have given in crossover section, new set of crossovers will be:

Chromosome [2] × chromosome [3]

Chromosome [2] × chromosome [5]

Chromosome [3] × chromosome [5]

Chromosome 2: Chromosome 2 × Chromosome 3 = [27; 24; 27; 12] × [15; 21; 21; 18] = [27; 24; 21; 18]

Chromosome 3: Chromosome 3 × Chromosome 5 = [15; 21; 21; 18] × [27; 15; 06; 27] = [15; 21; 06; 27]

Chromosome 5: Chromosome 5 × Chromosome 2 = [27; 15; 06; 27] × [27; 24; 27; 12] = [27; 15; 27; 12]

New chromosomes after the crossover process have been illustrated below:

Chromosome [1]: [09; 06; 15; 09]

Chromosome [2]: [27; 24; 21; 18]

Chromosome [3]: [15; 21; 06; 27]

Chromosome [4]: [27; 15; 06; 27]

Chromosome [5]: [27; 15; 27; 12]

Chromosome [6]: [09; 06; 15; 09]

For a mutation rate of 10%, as there are 24 genes in total, the number of mutation will be $0.1 \times 24 = 2.4$, which can be equated to 2. Thus, the mutated genes are marked in bold.

Chromosome [1]: [09; **06**; 15; 09]

Chromosome [2]: [27; 24; 21; 18]

Chromosome [3]: [15; 21; **06**; 27]

Chromosome [4]: [27; 15; **06**; 27]

Chromosome [5]: [27; 15; 27; 12]

Chromosome [6]: [09; **06**; 15; 09]

The mutated genes must be replaced by random numbers from 0–30 to obtain the new set of chromosomes to proceed for iterating in the next generation. If the numbers be 10, 15, 20 and 25 respectively, the new chromosomes will be:

Chromosome [1]: [09; **10**; 15; 09]

Chromosome [2]: [27; 24; 21; 18]

Chromosome [3]: [15; 21; **15**; 27]

Chromosome [4]: [27; 15; **20**; 27]

Chromosome [5]: [27; 15; 27; 12]

Chromosome [6]: [09; **25**; 15; 09]

This is the chromosomes of generation one of the algorithm. The process will be iterated until the value of a, b, c, and d meets the optimum value to satisfy the equation. After iterating for 5 generations, the evolution fitness chart will be as represented in Figure 11:

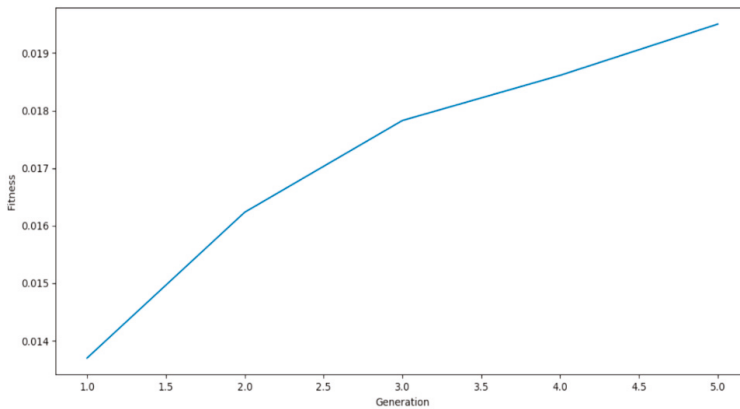


Figure 11. Evolution fitness curve showing gradual increase in fitness value corresponding to the generation.

The algorithm considered three areas, and after selecting several locations according to the aforementioned parameters (Figure 9), sorted the data into four segments. However, by creating six chromosomes, the algorithms mentioned in Figure 10 were followed to obtain the first generation of the chromosome. The aim was to attain the best value for the variables in the objective function, so that the optimum location for the charging station can be determined. Fitness value for each corresponding

generation is calculated, and as it can be seen, fitness increased with each generation, indicating the success of the algorithm. The higher the value of fitness, the better the algorithm. Thus, after several iterations, the optimal locations in these areas were determined in Ankara metropolitan, as the locations illustrated in Figure 12.

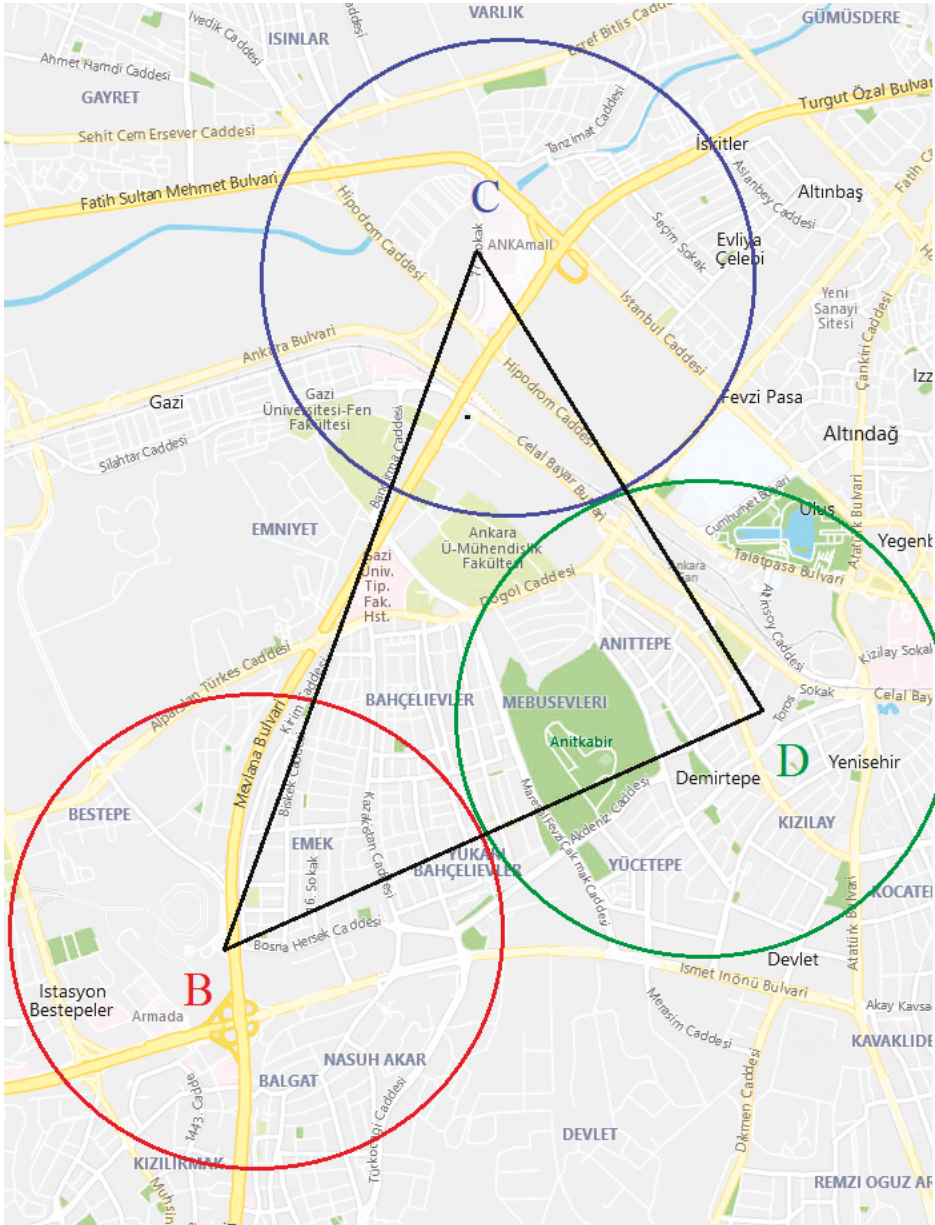


Figure 12. Selected points in Ankara (By Bing map).

7. Conclusions

In this research, an algorithm has been provided, which explains the hierarchy of the way the locations of EV charging stations should be determined by experimental exemplification from some literatures and the Ankara case study. The algorithm has been made up of three sections: Finding a location by specifications of the grid infrastructure, categorizing the capacity of transformers, and transformer analysis. It has been created especially for grid designers who have recently started to determine the points for charging stations in cities. In the Ankara case study, considerations for stability of the grid has been eliminated from the algorithm, because the grid can be considered to be stable for having adequate reserved power from neighboring control areas. The novelty of this research is the assertion that some limited parameters can show grid equipment conditions in the past to solve grid problems. Finally, this research has built a congruency and connection between the algorithm theories, programming languages, and practical strategy for the grid. The research has indicated that the transformers' condition, electric infrastructure, budget, and various other aspects, which are influenced by energy consumption, are important factors in approaching this issue. Furthermore, this research has shown that the maintenance history of the grid equipment and infrastructure are the key points in determining the locations of electric vehicles charge stations. The optimum locations have been determined using a Genetic Algorithm, which has been mathematically interpreted and analyzed. EVs and storage are garnering interests to the People's Republic of China, Europe, Japan, the United States of America, and recently, it has caught India's attention for the purpose of decreasing GHG emission as soon as possible. Science and technology is improving every second. This algorithm can be a stepping stone in the field of technology, which is used for autonomous systems on storages supplied by the grid or DC link.

Author Contributions: All authors contributed equally to the research activities and for its final presentation as a full manuscript.

Funding: No source of funding was attained for this research activity.

Acknowledgments: The authors would like to acknowledge the support and technical expertise received from the center for Bioenergy and Green Engineering, Department of Energy Technology, Aalborg University, Esbjerg, Denmark, which made this publication possible.

Conflicts of Interest: The authors declare no conflict of interest.

Abbreviations

	Description
z	The objective function of transmission and distribution cost
$X_{i,j}$	The transmission power flow from substations
X_m	The electric power flow in apparatus m
X_n	The outage power of load n
$a_{i,j}$	The cost of the transmission and distribution loss during normal operation
$b_{i,j}$	The cost of the transmission and distribution loss during overload operation
c_m	The damage caused by a shortened service life due to overload operation
d_n	The customer's outage cost
e_n	The supplier's outage cost
f_m	The maintenance cost
g_m	The fuel cost of power apparatus
h_m	The repair cost of failed apparatus
<i>Line</i>	The sets of transmission lines
<i>OverLine</i>	The sets of overload lines
<i>OutLoad</i>	The sets of outage loads
<i>MentEquip</i>	The set of apparatus in the transmission and distribution system
<i>FailedEquip</i>	The set of failed apparatus in the transmission and distribution system

<i>PowerEquip</i>	The set of power generation apparatus
<i>V</i>	Relative aging rate
θ_h	Hot-spot temperature
<i>L</i>	Total aging over the time period considered
V_n	Relative aging rate during an interval <i>n</i>
<i>N</i>	Total number of intervals during the time period considered.
$D_{TR_PHEV_X}$	Oil temperature at the bottom of the winding.
<i>A</i>	Top-oil temperature derived as the average of the tank outlet oil temperature and the tank oil pocket temperature.
<i>B</i>	Mixed oil temperature in the tank at the top of the winding (often assumed to be the same temperature as A).
$T_x_T_r$	Initial load rate without PHEV.
<i>C</i>	Temperature of the average oil in the tank (Page)
<i>D</i>	Oil temperature at the bottom of the winding.
$\sum TRP$	Sum of the nominal powers of the transformers in parallel.
TRP_{Nx}	Rated power of the transformer under analysis.
TRP_{Ny}	The nominal power of the transformers in parallel with the transformer being analyzed
f_L	Charge factor of the set of power transformers
L_{max}	Maximum load allowed.
<i>N</i>	Total number of power transformers in parallel
<i>a</i>	Transformation ratio
V_p	Primary voltage;
V_s	Secondary voltage
HI_m	Transformer's Main Health Index
HI_0	Transformer's Main Health Index reference point
T_1, T_2	Temperatures at point 1 and 2 respectively
HI_{iso}	Transformer's Insulating Paper Health Index
β	Coefficient of age of the equipment
C_{fur}	Content of furfural
HI_{fur}	Index of the content of furfural
HI_{CO}	Index from carbon monoxide and carbon dioxide gas analysis
$F_{C,H}$	Hydrocarbon gas factor function
HI_{CH}	Dissolved Gas Analysis health index
ω	Weight of gas
F_{oil}	Oil factor function
H_{oil}	Transformer's Oil Health Index
<i>EKF</i>	Extended Kalman Filter
<i>CNG</i>	Compressed Natural Gas

References

1. Harighi, T.; Bayindir, R.; Padmanaban, S.; Mihet-Popa, L.; Hossain, E. An Overview of Energy Scenarios, Storage Systems and the Infrastructure for Vehicle-to-Grid Technology. *Energies* **2018**, *11*, 2174. [[CrossRef](#)]
2. Harighi, T.; Bayindir, R. Load Estimation Use in Electric Vehicle Charge Station Coordination in Different Node and Definite Area. In Proceedings of the 2018 International Conference on Smart Grid (icSmartGrid), Nagasaki, Japan, 4–6 December 2018.
3. Wang, Q.; Wang, J.; Zhao, P.; Kang, J.; Yana, F.; Dua, C. Correlation between the model accuracy and model-based SOC estimation. *Electrochim. Acta* **2017**, *228*, 146–159. [[CrossRef](#)]
4. Østergaard, P.A. Reviewing EnergyPLAN simulations and performance indicator applications in EnergyPLAN simulations. *Appl. Energy* **2015**, *154*, 921–933. [[CrossRef](#)]
5. Farzaneh, H.; Doll, C.N.; Oliveira, J.A.P.D. An integrated supply-demand model for the optimization of energy flow in the urban system. *J. Clean. Prod.* **2016**, *114*, 269–285. [[CrossRef](#)]
6. Li, Y.; Davis, C.; Lukszo, Z.; Weijnen, M. Electric vehicle charging in China's power system: Energy, economic and environmental trade-offs and policy implications. *Appl. Energy* **2016**, *173*, 535–554. [[CrossRef](#)]

7. Wang, Y.W.; Lin, C.C.; Lee, T.J. Electric vehicle tour planning. *Trans. Res. Part D* **2018**, *63*, 121–136. [[CrossRef](#)]
8. Misra, S.; Bera, S.; Ojha, T.; Mouftah, H.; Anpalagan, A. ENTRUST: Energy trading under uncertainty in smart grid systems. *Comput. Netw.* **2016**, *110*, 232–242. [[CrossRef](#)]
9. Meng, J.; Mu, Y.; Jia, H.; Wu, J.; Yu, X.; Qu, B. Dynamic frequency response from electric vehicles considering travelling behavior in the Great Britain power system. *Appl. Energy* **2016**, *162*, 966–979. [[CrossRef](#)]
10. He, Y.; Kockelman, K.M.; Perrine, K.A. Optimal locations of U.S. fast charging stations for long-distance trip completion by battery electric vehicles. *J. Clean. Prod.* **2019**, *214*, 452–461. [[CrossRef](#)]
11. Zarandi, M.F.; Davari, S.; Sisakht, S.H. The large scale maximal covering location problem. *Sci. Iran.* **2011**, *18*, 1564–1570. [[CrossRef](#)]
12. Heydarian-Forushani, E.; Golshan, M.; Shafie-khah, M. Flexible interaction of plug-in electric vehicle parking lots for efficient wind integration. *Appl. Energy* **2016**, *179*, 338–349. [[CrossRef](#)]
13. Zhou, B.; Yao, F.; Littler, T.; Zhang, H. An electric vehicle dispatch module for demand-side energy participation. *Appl. Energy* **2016**, *177*, 464–474. [[CrossRef](#)]
14. Mozafar, M.R.; Moradi, M.H.; Amini, M.H. A Simultaneous Approach for Optimal Allocation of Renewable Energy Sources and Charging Stations based on Improved GA-PSO Algorithm. *Sustain. Cities Soc.* **2017**, *32*, 627–637. [[CrossRef](#)]
15. Hu, D.; Zhang, J.; Zhang, Q. Optimization design of electric vehicle charging stations based on the forecasting data with service balance consideration. *Appl. Soft Comput. J.* **2019**, *75*, 215–226. [[CrossRef](#)]
16. Bing Map. Available online: <https://www.bing.com/maps> (accessed on 8 April 2019).
17. EnerjiSA. Başkent Elektrik Dağıtım, A.Ş. Available online: <https://www.enerjisa.com.tr/en/about-enerjisa/our-operations/distribution/baskent-edas> (accessed on 5 September 2019).
18. Yilmaz, A. Enerji Atlası. Available online: <https://www.enerjiatlas.com/sehir/ankara/> (accessed on 8 April 2019).
19. Godina, R.; Rodrigues, E.; Paterakis, N.; Erdinc, O.; Catalão, J. Innovative impact assessment of electric vehicles charging loads on distribution transformers using real data. *Energy Convers. Manag.* **2016**, *120*, 206–216. [[CrossRef](#)]
20. Clairand, J.M.; Rodríguez-García, J.; Álvarez-Bel, C. Smart Charging for Electric Vehicle Aggregators considering Users Preferences. *IEEE Trans. J.* **2018**, *6*, 54624–54635. [[CrossRef](#)]
21. Munoz, E.R.; Razeghi, G.; Zhang, L.; Jabbari, F. Electric vehicle charging algorithms for coordination of the grid and distribution transformer levels. *Energy* **2016**, *113*, 930–942. [[CrossRef](#)]
22. Zou, S.; Hiskens, I.; Ma, Z. Consensus-based coordination of electric vehicle charging considering transformer hierarchy. *Control Eng. Pract.* **2018**, *80*, 138–145. [[CrossRef](#)]
23. Shokrzadeh, S.; Ribberink, H.; Rishmawi, I.; Entchev, E. A simplified control algorithm for utilities to utilize plug-in electric vehicles to reduce distribution transformer overloading. *Energy* **2017**, *133*, 1121–1131. [[CrossRef](#)]
24. Hanai, M.; Kojima, H.; Hayakawa, N.; Shinoda, K.; Okubo, H. Integration of Asset Management and Smart Grid with Intelligent Grid Management System. *IEEE Trans. Dielectr. Electr. Insul.* **2013**, *20*, 2195–2202. [[CrossRef](#)]
25. Godina, R.; Rodrigues, E.; Shafie-khah, M.; Matias, J.; Catalão, J. Overloading Analysis of an Industrial Client Distribution Transformer in a Portuguese Island. In *2016 IEEE International Energy Conference (ENERGYCON)*; IEEE: Leuven, Belgium, 2016.
26. Turker, H.; Bacha, S.; Chatroux, D.; Hably, A. Low-Voltage Transformer Loss-of-Life Assessments for a High Penetration of Plug-In Hybrid Electric Vehicles (PHEVs). *IEEE Trans. Power Deliv.* **2012**, *27*, 1323–1331. [[CrossRef](#)]
27. Linsley, K.; White, C.H. *IEEE Guide for Loading Dry-Type Distribution and Power Transformers*; IEEE: New York, NY, USA, 1989.
28. Schmitz, W.I.; Feil, D.L.P.; Canha, L.N.; Abaide, A.R.; Marchesan, T.B.; Carraro, R. Operational vulnerability indicator for prioritization and replacement of power transformers in substation. *Electr. Power Energy Syst.* **2018**, *102*, 60–70. [[CrossRef](#)]

29. Standard, B. *NT ONS 038 2014—Transformadores—Ensaio e Elevação de Temperatura em Sobrecarga*; Operador Nacional do Sistema Elétrico: Rio de Janeiro, Brazil, 2014.
30. En-Wen, L.; Bin, S. Transformer health status evaluation model based on multi-feature factors. In *2014 International Conference on Power System Technology*; IEEE: Chengdu, China, 2014.



© 2019 by the authors. Licensee MDPI, Basel, Switzerland. This article is an open access article distributed under the terms and conditions of the Creative Commons Attribution (CC BY) license (<http://creativecommons.org/licenses/by/4.0/>).

Review

Critical Review of PV Grid-Tied Inverters

B. Kavya Santhoshi ¹, K. Mohana Sundaram ^{1,*}, Sanjeevikumar Padmanaban ²,
Jens Bo Holm-Nielsen ² and Prabhakaran K. K. ³

¹ Department of Electrical and Electronics, Vel Tech Multi Tech, Chennai 600062, Tamil Nadu, India; kavyabe2010@gmail.com

² Center for Bioenergy and Green Engineering, Aalborg University, 6700 Esbjerg, Denmark; san@et.aau.dk (S.P.); jhn@et.aau.dk (J.B.H.-N.)

³ Center for System Design, National Institute of Technology Karnataka, Surathkal 575025, India; k7prabhakaran@gmail.com

* Correspondence: kumohanasundaram@gmail.com; Tel.: +91-960-004-7399

Received: 12 March 2019; Accepted: 15 May 2019; Published: 20 May 2019

Abstract: Solar Photovoltaic (PV) systems have been in use predominantly since the last decade. Inverter fed PV grid topologies are being used prominently to meet power requirements and to insert renewable forms of energy into power grids. At present, coping with growing electricity demands is a major challenge. This paper presents a detailed review of topological advancements in PV-Grid Tied Inverters along with the advantages, disadvantages and main features of each. The different types of inverters used in the literature in this context are presented. Reactive power is one of the ancillary services provided by PV. It is recommended that reactive power from the inverter to grid be injected for reactive power compensation in localized networks. This practice is being implemented in many countries, and researchers have been trying to find an optimal way of injecting reactive power into grids considering grid codes and requirements. Keeping in mind the importance of grid codes and standards, a review of grid integration, the popular configurations available in literature, Synchronization methods and standards is presented, citing the key features of each kind. For successful integration with a grid, coordination between the support devices used for reactive power compensation and their optimal reactive power capacity is important for stability in grid power. Hence, the most important and recommended intelligent algorithms for the optimization and proper coordination are peer reviewed and presented. Thus, an overview of Solar PV energy-fed inverters connected to the grid is presented in this paper, which can serve as a guide for researchers and policymakers.

Keywords: ancillary services; grid; inverter; PV; reactive power; solar; Quasi-Z source inverter (QZSI); Y source inverter (YSI)

1. Introduction

Grid-tied photovoltaic systems are power-generating systems that are connected with grids. Solar PV energy that is generated must be processed with the help of a grid-connected inverter before putting it to use. This inverter is present between the solar PV arrangement and the utility grid; it could be a single unit or a collection of small inverters attached to the individual PV units. Due to the lowered cost of power electronic devices and advancements in renewable energy technology, there is significant encouragement for the power industry to utilize PV solar energy and to attach it to a medium or low voltage distribution grid. The renewable electrical energy market has experienced an extraordinary increase in scope in recent years. Its main catalyst in 2016 was solar photovoltaics, which are boosting the capacity of renewables all over the world. Due to reductions in costs, solar and wind energy are playing an increasingly important role and are proving to be competitive with fossil fuels in many

countries. Two-thirds of overall electricity additions in 2016 were from renewable sources of energy [1]. According to the International Energy Agency, solar is leading in additions compared to wind and hydropower. The statistics of net additions and retirements in electricity capacity are shown in Figure 1.

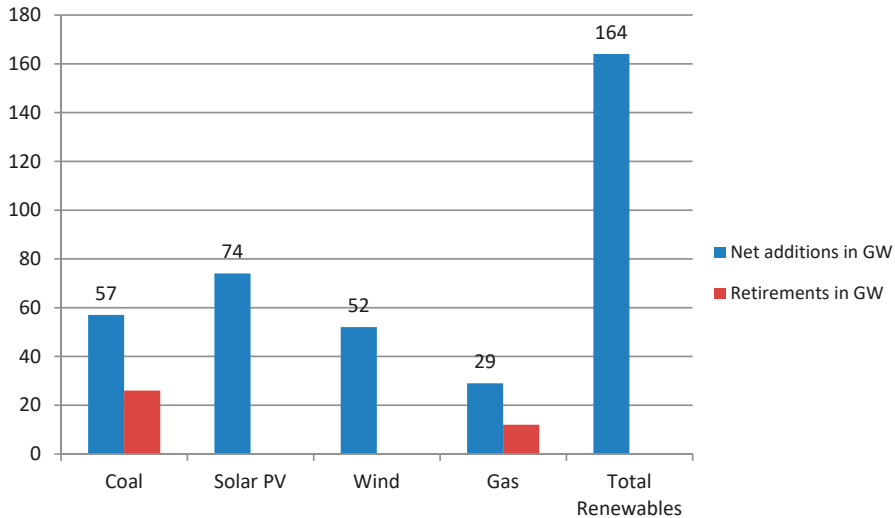


Figure 1. Net additions and retirements of Electricity capacity in 2016. Reproduced from [1], International Energy Agency: 2017.

From [2], it is noted that Solar PV has dominated all other forms of electricity production. Its capacity comprises almost 600 Giga Watt (GW) more than all other forms of energy combined. Thus, with this increasing trend in use of Solar PVs, it becomes even more important to study the obstacles faced in extracting energy from solar PV systems and then exporting it or integrating it with the grid. The primary factors to be borne in mind while integrating PV solar energy with the grid are:

1. Reducing the cost during power conversion stage
2. Improving the reliability of the converter in use
3. Reducing the harmonics in the output current obtained
4. Reducing the number of switches/components used in grid integration
5. Ensuring continuity in supply by providing back up power for PVs.
6. Controlling the real and reactive power
7. Maintaining a constant direct current (DC) link voltage via a suitable control scheme
8. Detecting the maximum power point of PV panel using Maximum Power Point Tracking (MPPT) techniques.

Henceforth, a detailed review is done, keeping in mind the current trend and effectiveness of energy produced, and the simplicity of its integration with the grid. This paper is organized as follows:

Section 2: Ancillary services in electric market

Section 3: PV-grid inverters—A summary of different topologies

Section 4: A Review on Intelligent Algorithms and Optimization Techniques

Section 5: Conclusion & future scope

Section 6: References

2. Ancillary Services in Electric Market

2.1. Definitions of Ancillary Service

In this section, a brief introduction to ancillary services has been given with standard definitions from the literature. An insight to Reactive Power (Q) being an ancillary service is provided. In order to understand the concept of ancillary services, a few definitions from the literature have been listed here.

- * As per International Electro technical Commission (IEC) 60050-617, ancillary services are “services necessary for the operation of an electric power system provided by the system operator and/or by power system users” [3].
- * According to the Union of Electric Industry EURELECTRIC: “Ancillary Services are those services provided by generation, transmission and control equipment which are necessary to support the transmission of electric power from producer to purchaser. These services are required to ensure that the System Operator meets its responsibilities in relation to the safe, secure and reliable operation of the interconnected power system. The services include both mandatory services and services subject to competition” [3].
- * Federal Energy Regulatory Commission (FERC) defined ancillary services as those “necessary to support the transmission of electric power from seller to purchaser given the obligations of control areas and transmitting utilities within those control areas to maintain reliable operations of the interconnected transmission system” [4].

2.2. Popular Ancillary Services in Electric Power Market

Figure 2 shows some popular ancillary services in electric power market. They are:

1. Q Management: Q Management is a service that is unbundled to both suppliers and consumers. A system operator can control this service but the control is limited to local control area. Q management is the same ancillary service as voltage control. Voltage control is done to balance voltages in accordance with the prescribed limits during different time slots of power transmission. Q injection and absorption leads to system stability and yields protection against unforeseen events that may cause voltage breakdown. Hence, reactive-power must be made available to meet the expected demand and serve as a reserve margin during emergencies.
2. Real power (P) loss replacement: P loss is the variation in P generated and delivered. Due to resistance in each active and passive element in the transmission line, loss is unavoidable. International Organization for Standardization (ISO) should generate power online in order to cope up with P losses although suppliers also make up for the losses.
3. Supplemental operating reserve: Supplemental-operating reserve includes generating units, which must supply power within ten minutes and must be completely available within thirty minutes.
4. Reliability reserve: Reliability reserve includes generating units and spinning reserves, which must be made available completely within ten minutes.
5. Operating reserve: Operating reserve ancillary service is used to balance the power generation to the load because of unexpected outages.
6. Load following: Load-following ancillary service includes two functions performed by the control area (interconnection frequency maintenance and load balance) and two more functions performed by customer (monitoring fluctuations in load and keeping in track of long-term changes). Thus, there are four different components in load following ancillary service.
7. Scheduling and dispatch: Scheduling is a separate ancillary service and not connected to dispatch, but they are lumped together since they are less expensive and coordinated by ISO. Scheduling is to anticipate load requirement and assign generating units accordingly. Dispatch is the actual control of generation units and transmission units, which are available in order to satisfy the load demand. Scheduling, as well as dispatch, are quite inexpensive.

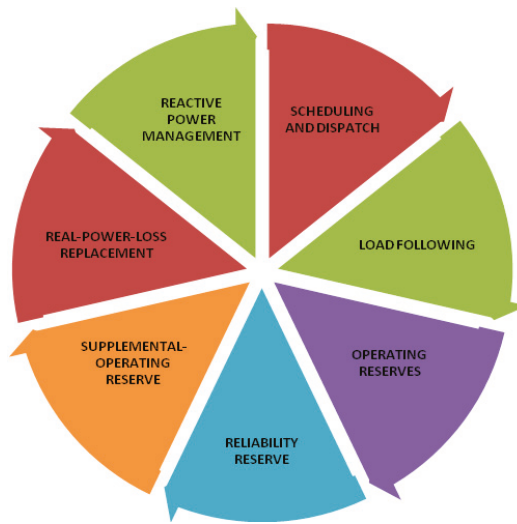


Figure 2. Popular ancillary services in electric power market suggested by FERC.

2.3. Additional Services in Electric Power Market

Figure 3 shows additional services in electric power market suggested by FERC. They are:

1. Black start capability: Under certain conditions in which the system collapses, drawing power from the grid becomes an impossible event. Thus, some special generating units called black start units are used to restart devoid of taking power from grid.
2. Time correction: Generally, most of the electrical clocks work by means of counting the cycles in the frequency of power. Although this frequency is kept constant, there will be an error of 0.01 Hz. If time correction were not done, there would be an error of roughly 10 s a day considering 50 Hz cycle.
3. Standby Service: Standby service serves as a generating capacity, which is kept at reserve to supply energy when emergencies occur. Standby capacity is used in circumstances in which a customer's power is interrupted due to an outage or when the generating unit is under scheduled maintenance or when a customer's power demand exceeds the actual contracted one.
4. Planning Reserve: It serves as a planned generating unit based on customer requirement. Hence, it is a customized one and cannot be the same for all customers.
5. Redispatch: Due to transmission losses and constraints, least cost power dispatch is not possible. This is known as congestion. In order to avoid congestion, redispatch is done to adjust the power that is input to the transmission line. This method is applied within control areas.
6. Transmission Services:
 - Transmission system monitoring and control
 - Transmission reserves
 - Repair and maintenance of the transmission network
 - Metering, billing and communications.
7. Power Quality: Power quality means provision of uninterrupted power which is purely sinusoidal to customers
8. Planning, Engineering & Accounting Services:
 - a. Planning services:

- Load forecasting
 - Scheduling
 - Coordination of the maintenance of generating units
 - Coordination of power transmission maintenance and power outages.
- b. Engineering services:
- Black-start studies
 - Load-flow analysis
 - Planning for bulk-power system expansion.
- c. Accounting services:
- Scheduling
 - Billing
 - Contract administration
 - Reporting to several regulatory bodies.

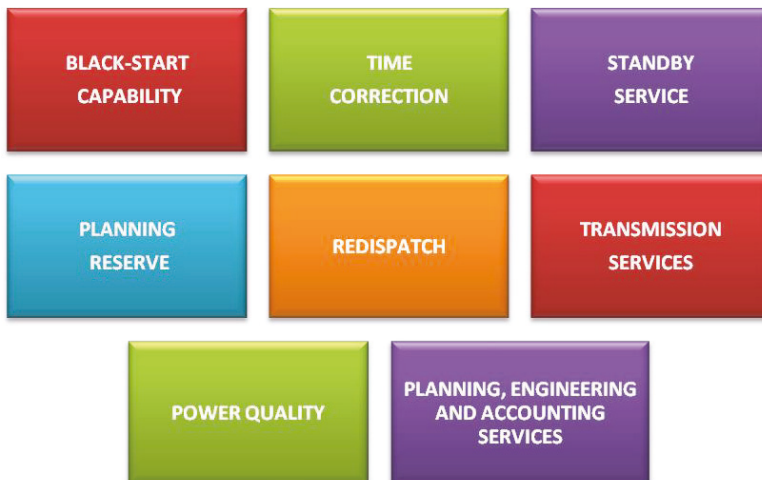


Figure 3. Additional services in electric power market suggested by FERC.

2.4. Q Injection to Grid

One of the primary ancillary services that is necessary for a power system operator is Q injection to grid [5]. In Figure 4, the red curve indicates the capability of the PV inverter to provide Q. Furthermore, based on the voltage at point of common coupling (PCC), freedom of having higher current distortion is permissible. Several countries have added Reactive power injection to grid into the countries' standard grid code (GC) requirements. In general, if a country follows standard GC, power generation by PVs is required to cease immediately when there is a fault occurring in the grid. However, because of high level of penetration of PVs into grid, a sudden and quick power interruption due to a fault in the grid would cause severe problems. For to this reason, many countries like Spain, Italy, Germany and Japan have modified their GCs [6–9].

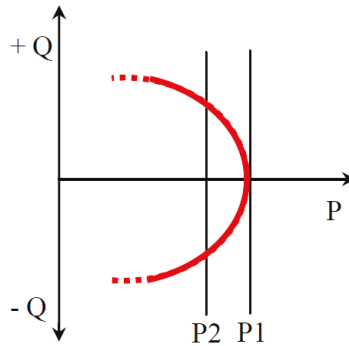


Figure 4. PV inverter reactive power capability based on current limits.

There are numerous services that can be extracted with the use of PVs. Figure 5 shows some of the important ancillary services involving solar PVs. It can be noted that ancillary services provided by PV systems open an important pathway in electric power market and Q injection to grid has been area of research for the last three decades [10–22].

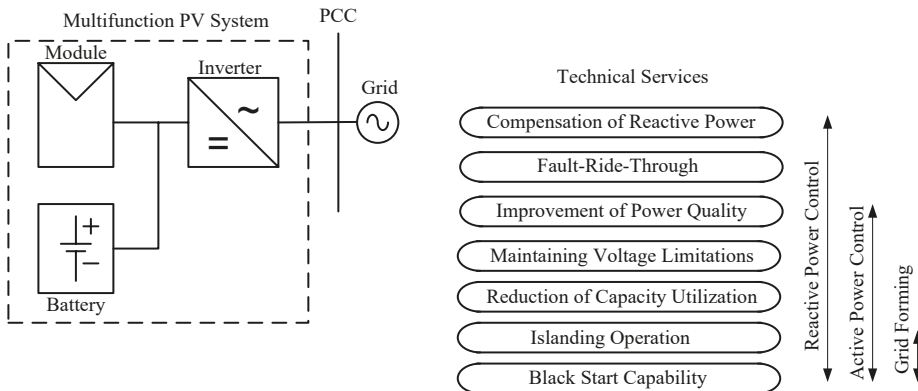


Figure 5. Services provided by PV systems.

Solar-PV panels do not possess Q, since they provide electric power by using PV effect. The power conversion from DC of solar panels to AC injected to grid takes place due to inverter circuitry. This inverter has the capability of providing Q support in fault/normal conditions. Inverters could provide various other ancillary services. Some of these such as lowvoltage ride-through (LVRT) and MPPT have become necessary. Although, Q support has not been made mandatory for grid connected PV systems, the higher penetration levels of PVs indicate more accessibility to control of P and Q. Hence, it would become a code included in GCs of all countries using more renewable form of power conversion. In general, for PV-grid topologies, the inverter converts the DC of PV panels to alternating current (AC) that is to be supplied to grid. Figure 6 shows a single-phase PV-grid system that can be used for requirements up to 7 kW. There are many types of inverters that are used in a PV-grid scenario. In the following section, a brief summary of inverter topologies for use in grid-connected systems is provided.

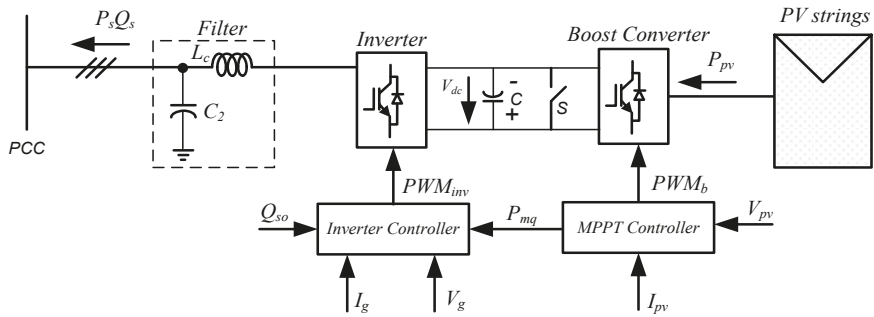


Figure 6. A sketch of single-phase PV-grid system.

3. PV-Grid Inverters—A Summary of Different Topologies

Numerous works have been proposed in literature to illustrate various topologies of inverters including state-of-art review [23]. Traditional inverters such as voltage source inverter (VSI) and current source inverter (CSI) have a major drawback, i.e., voltage buck and boost actions cannot take place simultaneously. In order that buck and boost actions take place collectively, an additional converter has to be added in the circuitry, making the whole system more expensive. Popular impedance source inverters (ZSIs) have been discussed in the literature; they have the ability to overcome the major disadvantage of involving a two-stage topology in power conversion. Both boosting and bucking actions are possible with this topology. ZSI is a combination of VSI and CSI. Boosting of voltage takes place at the DC link with the help of a unique technique called shoot-through [24,25]. In recent years, an interesting inverter topology namely admittance source inverter (YSI) was introduced. The following section gives an overview on different inverter topologies available in literature.

3.1. Traditional Inverters Vs Multilevel Inverters

One of the traditional configurations of inverters that is connected to power grid is VSI (shown in Figure 7). In VSIs, the output voltage is always lesser than the input voltage. VSIs have the ability to introduce currents with low harmonics into the grid. When a CSI (shown in Figure 8) is used instead of VSI, current injection to grid can take place without the need of an additional converter. The output from a VSI and CSI comprises of two unique levels of voltage, but it suffers from higher switching losses. The rate of change of voltage (dv/dt) is higher for traditional two-level inverters. The frequency of switching is also high. They are most suited for low voltage applications.

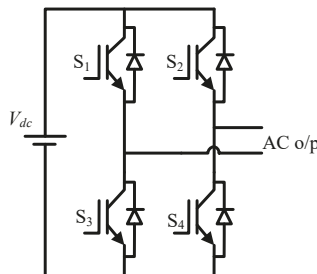


Figure 7. Voltage source inverter.

Multilevel inverters (MLIs) were introduced to overcome the drawbacks of traditional inverters. The classification of MLIs is given in Figure 9. Switching losses are a main factor of concern in two level inverters. Using MLIs, they can be minimized. MLIs aid to reduce switching losses and harmonics.

They can be used for high voltage applications. The rate of change of voltage (dv/dt) is lesser for MLIs. The levels of voltage could be increased to greater than two. Hence, a pure sinusoidal waveform is obtained as the output of the inverter. The harmonics in the output are mitigated and losses could be reduced largely. With the introduction of multilevel topology in CSI (shown in Figure 10), low harmonic currents are obtained. The frequency at which the switching action takes place is reduced with the introduction of a multilevel topology for a current source inverter. A brief comparison between traditional inverters and multilevel inverters is presented in Table 1. Table 2 summarizes the state of art PV grid inverter topologies of MLIs.

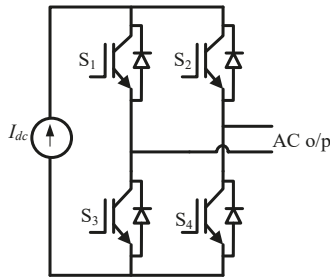


Figure 8. Current source inverter.

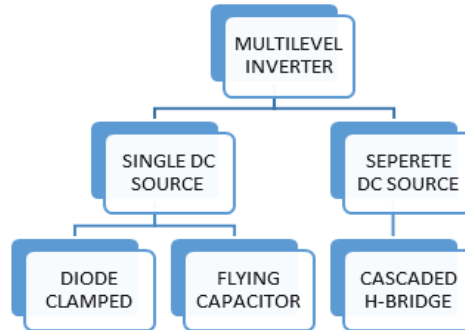


Figure 9. Classification of multilevel inverter topologies.

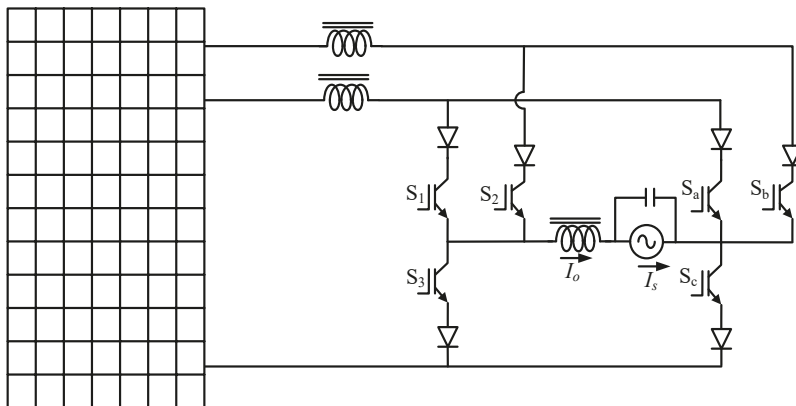


Figure 10. A multilevel CSI topology.

Table 1. Traditional two-level inverters Vs MLI.

Factor under Consideration	Two Level Inverter	Multilevel Inverter
Switching loss	High	Low
dv/dt	High	Low
Voltage stress on switches	More	Less
Switching frequency	High	Low
Levels of voltage in output	Two	more than two
Harmonics	More	Less

Table 2. State of art PV grid inverter topologies of MLIs.

Network Structure	Advantages	Disadvantages
Diode-Clamped	<ul style="list-style-type: none"> Control of Reactive power flow is possible. High efficiency. Filters are not essential to reduce harmonics. 	<ul style="list-style-type: none"> For high levels of diode-clamped structure, the number of diodes required is more. Control of Real power flow for individual converter is tedious.
Flying Capacitors	<ul style="list-style-type: none"> Extra ride through capability during power outage. It gives proper switching combination to balance different voltage levels. Real and reactive power flow can be controlled No need of filters to reduce harmonics. 	<ul style="list-style-type: none"> The number of capacitors required is high for high level. For real power transmission, losses and switching frequency are high
Cascade Multilevel Inverter With Separate DC Sources	<ul style="list-style-type: none"> Because of same structure, it allows the scalable, modularized circuit layout and packaging. Less number of components is needed for getting same number of voltage level. No need of extra diodes and capacitors. 	<ul style="list-style-type: none"> Separate DC sources are required for the real power conversion.

3.2. Concept of Z Source and Its Application in Solar Industry

Even though multilevel inverters have shown better performance than traditional inverters, they still have drawbacks. The number of switches is quite high in an MLI. Although the switches required need smaller rating, the number of required switches is high, thus making the circuit complex and costly. Thus, ZSIs with several advantages over the aforementioned inverters were introduced. Figure 11 shows a voltage fed ZSI.

A ZSI is a combination of inductors and capacitors. A ZSI would operate as a VSI or CSI depending on the application. The output voltage ranges from zero to infinity. Many researchers have adapted impedance source topologies and many advances in the topologies have been listed in literature like YSIs and their advancements [26,27] and ZSIs and their advancements [28–65]. Figure 12a–c give an overall classification of topologies of impedance source networks. A summary of these topologies, as presented in different literature works, is presented in the following section.

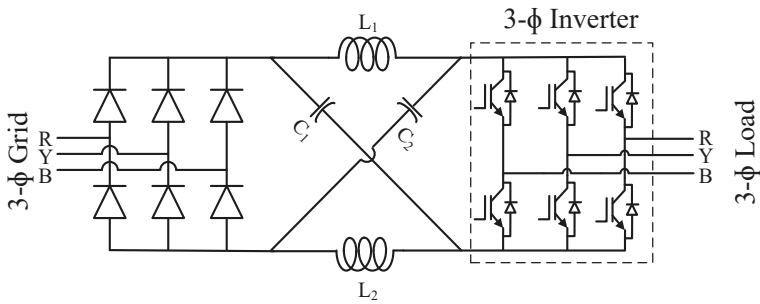


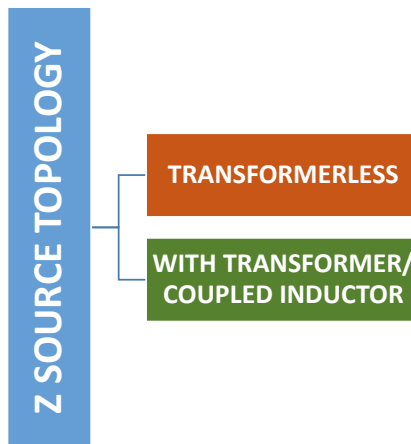
Figure 11. A voltage fed ZSI.

Solar modules are widely preferred in both residential and commercial applications. PV cells are connected in parallel and series in order to form one module. Many such modules in combination is a panel. To develop economical and efficient PV systems, MPPT algorithms are used. Generally, the inverter portion of the PV-inverter-grid structure comprises of a boost circuit and a filter. MPPT algorithms may or may not be used depending upon the application. In PV systems, in order to obtain dc-ac conversion, ZSI is an intelligent choice [66]. ZSIs can boost the voltage levels with a very compact structure. For a 10 kilowatt (kW) PV system, 20 kW inverter is required with a traditional inverter but by using ZSIs, a 10 kW inverter is enough for a 10 kW PV system with same kilo volt-ampere (KVA) maintained. Traditional inverters pose challenges in their control and modulation mechanisms. These issues are eradicated using ZSIs.

The boost factor for a simple boost control method can be obtained from Equations (1) and (2) where M is the modulation index, and B is the Boost factor, T is the total time-period, which is one complete cycle. T0 is the time-period for which the output waveform is obtained.

$$B = 1/(2M - 1) \tag{1}$$

$$1 - M = T0/T \tag{2}$$



(a)

Figure 12. Cont.

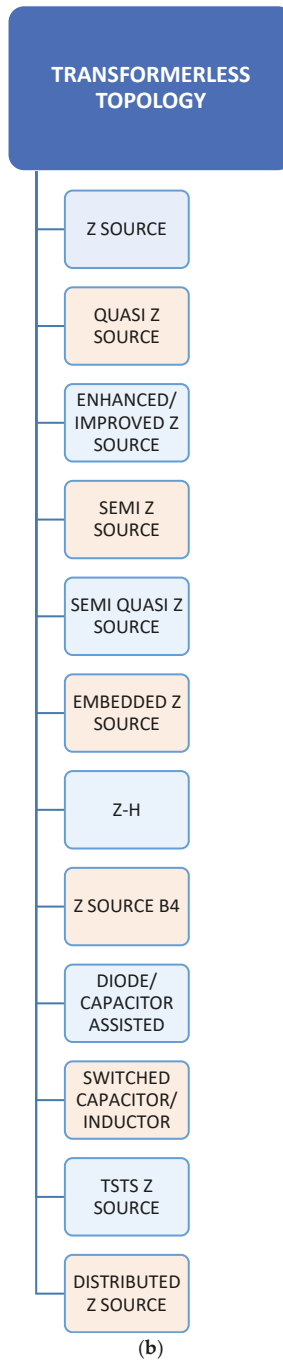


Figure 12. Cont.

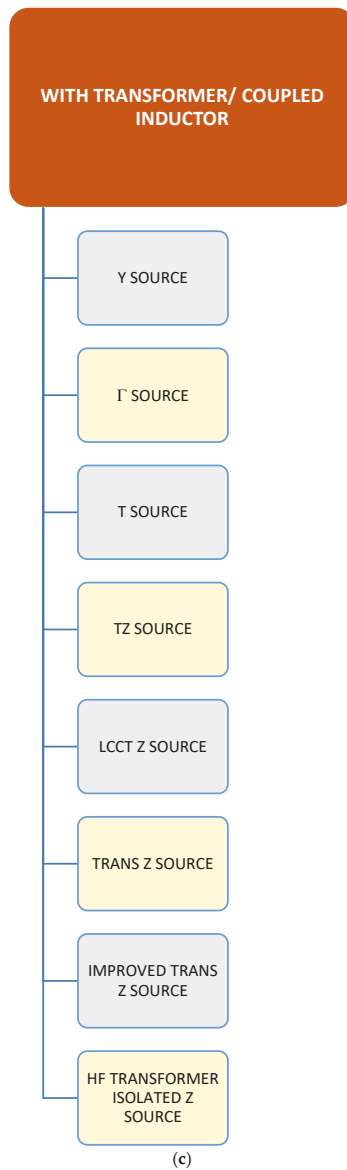


Figure 12. (a) Broad classification of Z source network topologies. (b) Classification of Z source transformerless topologies. (c) Classification of Z source topologies with transformer/coupled inductor.

Summaries of state of the art PV-grid inverter topologies of Z source networks without transformer and with transformer/coupled inductor are presented in Tables 3 and 4 respectively. The features of each structure with components used, including passive elements and semiconductor devices peer reviewed from different literature works are listed. Detailed topological figures can be obtained from the respective reference papers cited for each structure listed in the tables.

Table 3. State of art PV grid inverter topologies of transformer less Z source networks.

Network Structure	NOS	NOC	NOL	Features
Z-Source [67]	1 Diode	2	2	<ul style="list-style-type: none"> The first introduced, basic circuit to overcome conceptual and theoretical barriers of VSI and CSI. The inductor of current-fed ZSI must sustain high currents. Many topologies are derived from this topology. Discontinuous input current and higher voltage stress on capacitors.
Quasi Z-Source [68]	1 Diode	2	2	<ul style="list-style-type: none"> The very first change of Z-source network. Continuous input current. Reduced passive component ratings. Reduced component count.
Improved Z-Source [31,32]	1 Diode	2	2	<ul style="list-style-type: none"> Reduced capacitor voltage stress. Limit inrush current at start up.
Semi Z-Source, Semi Quasi Z-source [33–35]	2 switches	2	2	<ul style="list-style-type: none"> Higher voltage stress across switches compared to ZSI/qZSI. Reduced count of active components. Lower cost. Eliminates leakage currents Most suitable for grid-connected PV system.
Embedded Z-Source [36–38,48]	1 Diode	2	2	<ul style="list-style-type: none"> Extracts smooth current from the source without adding additional components or passive filter
Z-H Converter [39]	4 switches	2	2	<ul style="list-style-type: none"> Shoot through state is not required for voltage boosting. Diode at front-end is eliminated.
Z-Source B4 [43]	1 Diode	2	2	<ul style="list-style-type: none"> Reduced number of active semiconductors. Simplify the control and gating circuitries.
Diode/Capacitor assisted [41,51]	3 diodes 2 diodes	3 4	3 3	<ul style="list-style-type: none"> Higher voltage boost and lower voltage stress across the capacitor compared to ZSI/QZSI Number of components increases based on number of stages
Switched capacitor/inductor [17,50]	7 diodes	2	4	<ul style="list-style-type: none"> Higher voltage boost capability. Component count increases based on corresponding size and cost Lower voltage stress across the capacitor compared to ZSI/QZSI
TSTS Z source [45,55]	3 switches	2	3	<ul style="list-style-type: none"> Reduced number of active semiconductors Common ground. Lower device stress. It has Buck-boost capability. High power density
Distributed Z source [60]		Distributed Z		<ul style="list-style-type: none"> Removes discrete passive and active components for Z source design. Eliminates parasitic effect. High frequency operation and better efficiency

Table 4. State of art PV grid inverter topologies of Z source networks with transformer/coupled inductor.

Network Structure	NOS	NOC	NOL	Features
Y SOURCE [27]	1 diode	1	Integrated three windings	<ul style="list-style-type: none"> • Better utilization of input voltage • THD is reduced • Versatile • More degrees of freedom for choice of gain of converter • Higher voltage boost and higher modulation index could be achieved • Very high gain could be achieved with small duty cycle
Γ SOURCE [45,53,65]	1 diode	2	One inductor and one two-winding coupled inductor	<ul style="list-style-type: none"> • Higher gain could be achieved by reducing the turns ratio of the coupled inductor • Better spectral performance at the inverter output
T SOURCE [59,61]	1 diode	1	Integrated two windings	<ul style="list-style-type: none"> • Increased voltage gain compared to ZSI and QZSI. • Reduced component stress • Fewer reactive components compared to ZSI and QZSI • Common ground with load
TZ SOURCE [62]	1 diode	2	Two integrated two windings	<ul style="list-style-type: none"> • Produces higher voltage boost with N
LCCT Z SOURCE [54,64]	1 diode	2	One inductor and one two-winding coupled inductor	<ul style="list-style-type: none"> • Continuous input current despite light load condition • Capable of filtering high frequency ripple from input current
TRANS Z SOURCE [46,49,52,58]	1 diode	1	Integrated two windings	<ul style="list-style-type: none"> • Reduced component stress • Increased voltage gain compared to ZSI and QZSI. • Fewer reactive components compared to ZSI and QZSI • Common ground with load
IMPROVED TRANS Z SOURCE [56]	1 diode	2	1 inductor and 1 transformer	<ul style="list-style-type: none"> • Higher boost factor compared to LCCT-ZSIs, QZSI with input LC filter and trans ZSIs • Resonant current suppression is achieved
HF TRANSFORMER ISOLATED Z SOURCE [57]	1 diode 1 switch	4	Two integrated two windings	<ul style="list-style-type: none"> • Input-output isolation • Lower component stress

In Tables 3 and 4, the following abbreviations were used

- NOS—Number of semiconductor devices
- NOC—Number of capacitors
- NOL—Number of inductors

3.3. Grid Integration Configurations, Synchronization & Standards

Grid-integrated PV systems could be of various power levels and sizes. They are designed for specific applications and needs, with a scope ranging from one PV module to over 100 MW [69]. Hence, a generic PV-inverter-grid structure, as shown in Figure 13, could vary for each plant.

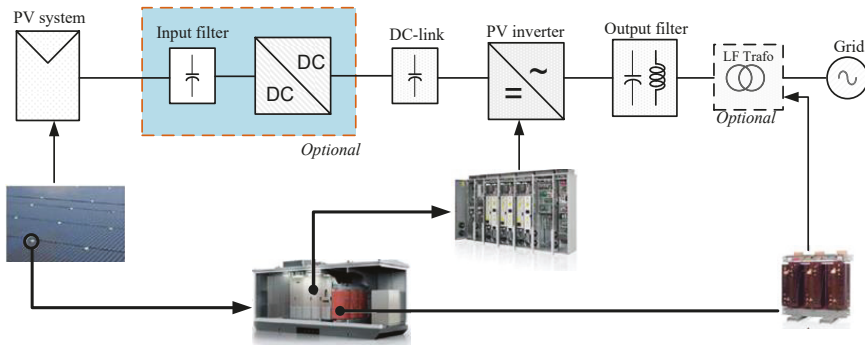


Figure 13. A generic structure of a PV-inverter-grid structure (Picture courtesy of ASEA Brown Boveri).

In order to make things seem less complex, PV-grid systems are divided based on power rating into

- Small scale (a few Ws a few tens of kW)
- Medium scale (a few tens of kW to a few hundreds of kW) and
- Large scale (a few hundredkW to several hundreds of MW).

Table 5 gives a summary of PV-grid-inverter configurations along with pros and cons of each configuration to provide a clear-cut guidance in choosing the type of system depending upon the requirements.

Table 5. PV grid inverter configurations—An Overview.

Comparative index	Small Scale	Medium Scale	Large Scale
Power range	<350 W	<10 kW	<850 kW
Configuration	AC module	String	Central
Power semiconductor device(PSD)	MOSFET	MOSFET, IGBT	IGBT
Inverter efficiency	Lowest	High	Highest
Pros	<ul style="list-style-type: none"> • Flexible/modular • Highest MPPT efficiency • Easy installation 	<ul style="list-style-type: none"> • Good MPPT efficiency • Reduced dc wiring • Transformerless (most common) 	<ul style="list-style-type: none"> • Simple structure • Highest inverter efficiency • Reliable
Cons	<ul style="list-style-type: none"> • Higher losses • Higher cost per watt • Two stage is mandatory 	<ul style="list-style-type: none"> • High component count • One string, one inverter 	<ul style="list-style-type: none"> • Needs blocking diodes (for array) • Not flexible

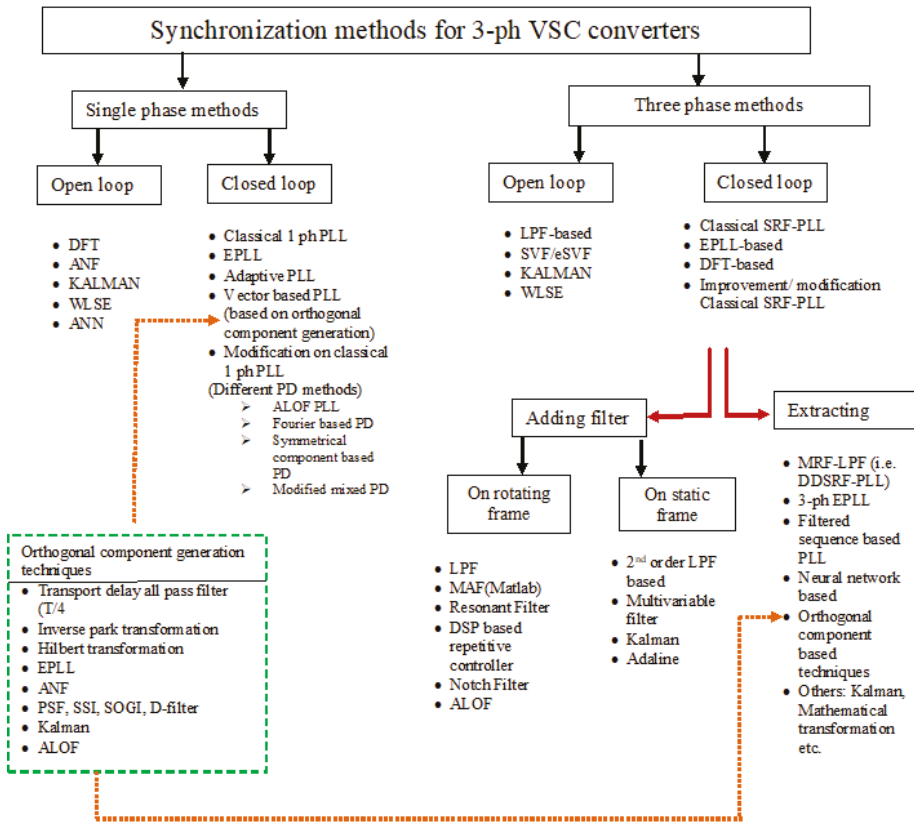


Figure 14. PV-Grid Synchronization methods. Reproduced from [70], 14th European Conference on Power Electronics and Applications (EPE): 2011.

Synchronization of the inverter with the grid is a major challenge in grid integration. Typically, inverters operate like current sources that inject the current in phase with grid voltage [71]. Therefore, pf needs to be maintained at unity or near to unity while the grid is connected to an inverter system. The most important thing is the synchronization of the inverter with the grid voltage. The rule of thumb for synchronization is that the total real power of the grid must be equal to the voltage of the grid and current of the inverter summed. Based on the synchronization rule, the Equation (3) is derived.

$$P(\text{grid}) = V(\text{grid}) + I(\text{inverter}) \tag{3}$$

Several methodologies can be studied from literature for synchronization of grid and PV inverter. Figure 14 gives a brief of literature works surveyed in this regard. Grid integration and the injection of current into the grid play a critical role in the operation of a grid connected PV system. Different works have highlighted current injection into the grid in accordance with recommended standards [72–87].

Due to the increase in PV-grid applications, many standards and GCs are proposed in order to have secure transmission of power into grid. Some of the well-known bodies that develop the standards are Institute of Electrical and Electronic Engineers (IEEE) of USA, IEC of Switzerland and Deutsche Kommission Elektrotechnik (DKE) of Germany. A summary of these standards and GCs is given in Table 6.

Table 6. A Summary of International codes for PV applications.

Category	Codes	Area of Implication
Grid connected	IEC 61727, IEC 60364-7-712	Installations of buildings.
	IEC 61683, IEC 62093, IEC 62116	Utility interface Measuring efficiency.
	UL 1741, IEC 62446	Interconnected PV inverters, system documentation & commissioning tests Useful in independent power systems
EMI	EN61000	European Union EMC directive for residential, private sectors, light industrial and commercial facilities.
	FCC Part 15	U.S. EMC directive for residential, commercial, light industrial, and industrial facilities
Low voltage ride through (LVRT)	IEC 61727	$V < 50\%$ at 0.1s $50\% \leq V < 85\%$ at 2.0 s
Anti-islanding	IEEE 1547/UL 1741 IEC 62116	Island detection
	VDE 0126-1-1	Impedance measurement
Monitoring	IEC 61850-7, IEC 60870, IEC 61724,	Transmission grids and systems for power service automation Distributed energy resources and logical nodes Measurement, data exchange, and analysis
Off grid	IEC 62509, IEC 61194, IEC 61702	Battery charge controllers
	IEEE Standard 1526, IEC/PAS 62111	Stand-alone systems
	IEC 62124	Rating of direct-coupled pumping systems Specifications for rural decentralized electrification.
Rural systems	IEC/TS 62257	Medium-scale renewable energy and hybrid systems. Safeguard from electrical hazards. Choice to select generator sets and batteries. Micro power systems and microgrids.

4. A Summary of Intelligent Algorithms & Optimization Techniques in Grid-Tied Inverters

Due to a rapid increase in complexity, optimization has become necessary in the design of every system. When PVs are involved, it means that there is going to be intermittency in the output power. In order that the load is fed without any fluctuation, optimization techniques must be incorporated to get smoother and better output. In order to understand modern intelligent algorithms and optimization techniques, one must have an understanding on the computational intelligence, which is used along with optimization techniques. Figure 15 lists the computational intelligence platforms that are discussed briefly in the following section.

1. Artificial Neural Network (ANN): The ANN was originally introduced by Rosenblatt [85]; it is a replica of human brain, and is useful for forecasting the availability of renewable energy [86].
2. Fuzzy Logic (FL): FL is used in decision making. The theory behind its application pertaining to current area of study can be found in [87], and the methodology for practical application in Renewable energy systems can be inferred from [88].
3. Multiagent system (MAS): Every component in the system is represented as an agent with unique objectives. A detailed review on the subject can be studied in [89].

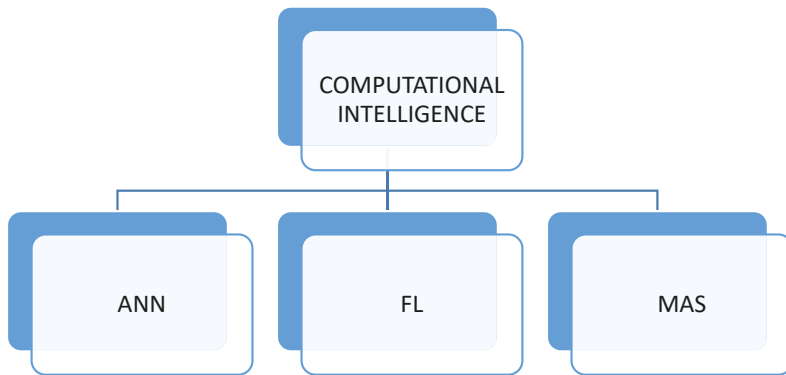
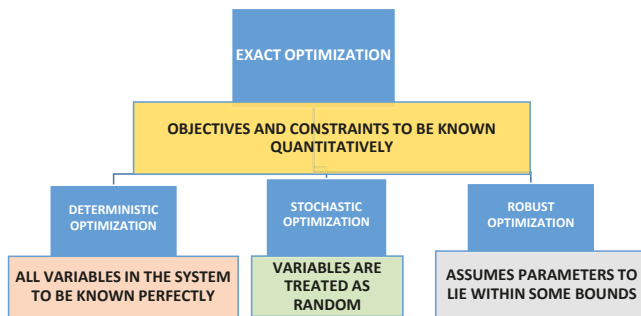
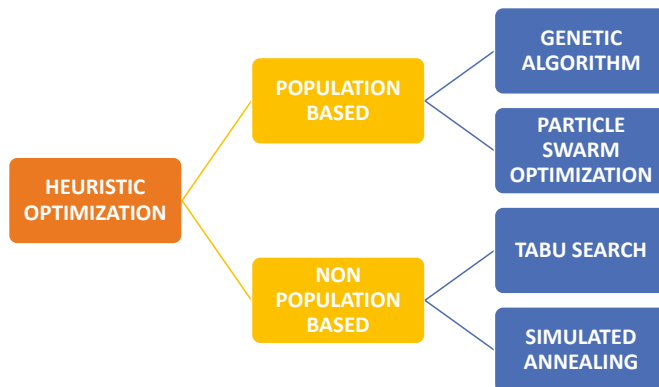


Figure 15. Computational intelligence techniques.

Figure 16a shows the classification of exact optimization depending on treatment of uncertainties. Figure 16b shows the classification of heuristic optimization. Table 7 lists the optimization techniques used in transmission and distribution systems with Q as one of the control variables. Table 8 summarizes various Q control techniques applied to the different sets of surveyed configurations.



(a)



(b)

Figure 16. (a) Classification of exact optimization depending on treatment of uncertainties. (b) Classification of Heuristic optimization.

Table 7. A summary of literature works surveyed related to optimization.

Objective Function	Optimization Tool	Control Variables	System Type
Minimize P loss [90]	SO (SOCP)	Q of PV, subject to stochastic P of PV	Distribution
Minimize total cost of a distribution system [91]	PSO	Q of PV, Q of EV	Distribution
Minimize P loss [92]	ES	Generator bus voltages, tap positions of transformer, Q of capacitor banks	Transmission
Minimize P loss [93]	Ant colony optimization (ACO)	Generator bus voltages, tap positions of transformer, Q of capacitor banks	Transmission
Minimize P loss [94]	PSO	Q of PV, P and Q of Battery Energy storage system (BESS), CL, tap positions of transformer	Distribution

Table 8. A summary of control techniques surveyed.

Configuration	Features/Control Scheme Employed
AC stacked PV inverter architecture [87]	<ul style="list-style-type: none"> No need for communications between inverters Combined Constant Peak Current Control and Constant Active Power Control Grid inductor is very small (50 micro Henry)
8 bus radial test feeder used for sensitivity analysis [95]	<ul style="list-style-type: none"> $\cos\phi(P,U)$ and $Q(U)$ methods employed pf control in terms of injected active power and local grid-voltage dependent reactive power is illustrated.
Distributed PV Generators [86]	<ul style="list-style-type: none"> Decentralized method for Q flow control is adapted Inverter Q is produced as a function of P [Q(P)] German GC is followed
16 bus and 81 bus distribution systems [96]	<ul style="list-style-type: none"> A Q planning model is proposed Provides extra VAR capacity Short-term planning and decision Uses APL and UC for control
1 main feeder and 6 laterals. 4 loads connected to main feeder at different points. 10 loads are derived from 6 laterals [76].	<ul style="list-style-type: none"> Auto-adaptive controller is used. During daylight, PV generates P; Q injection is reduced. During the absence of sunlight, Q equal to rated power is injected into the grid. Sensitivity theory and Lyapunov theorem are used.
Cigré 32 bus system [63,78]	<ul style="list-style-type: none"> GAMS/MINOS5 solver is used for solving Non-linear programming (NLP) Emphasis is laid on design of a competitive market for Q ancillary service from generator.
7 level QZSI with TSC and TSR [97,98]	<ul style="list-style-type: none"> A unique master-slave controller is proposed This topological advancement saves 42 percent of inverter rating.

5. Conclusions and Future Scope

Grid-tied inverter topologies are important components for the interface between the RER and the utility grid. Now, single-phase, transformerless configurations of range 1–10 kW are gaining interest. When compared to transformer-based configurations, the main advantages of transformerless configurations are:

- Less complexity
- Lower cost
- Higher efficiency
- Lighter weight
- Smaller volume

Thanks to the technological advancements in the area of power electronics, numerous transformerless inverters derived from conventional H-bridge topology have been developed. These inverters offer high efficiency and reliability. They also have lower electromagnetic interference, since transformers or coupled inductors are not involved in the design. In recent times, low-efficiency PV arrays have been widely used. In order to achieve maximal efficiency, the materials involved in fabrication of PV panels need to be carefully investigated and used. In this paper, a critical review of grid connected PV systems was performed. The definition of ancillary services and the reactive power market with reactive power as an ancillary service was examined. A review of the different topologies of inverters with special reference to state of art topologies such as γ source inverter derivatives was presented. Unique aspects of each topology in terms of structure and functional merits/demerits were presented in detail. In the coming era, a basic understanding of power converters becomes necessary for the successful integration of PVs with grid. Fulfilling the GC requirements also becomes a major challenge. Hence, in this paper, the synchronization between the inverter and the grid was examined, with the aim of outlining important concepts in grid synchronization and standards. Finally, intelligent algorithms and optimization techniques surveyed from different literature works were listed. A summary of different works available in the literature has been presented with the aim of providing researchers with an overview of grid-connected architectures. With the advent of Perovskite material used in solar cells, solar technology has seen tremendous advances. Future work may focus on the manufacturing side of solar cells, since this is currently an area of great discussion.

Author Contributions: All authors contributed equally in this research activities for its final presentation as full research article.

Funding: This research received no external funding.

Conflicts of Interest: The authors declare no conflict of interest.

Nomenclature

Acronyms

AC	Alternating current
ACO	Ant colony optimization
ANN	Artificial neural network
BESS	Battery Energy storage system
CSI	Current source inverter
DC	Direct Current
DO	Deterministic Optimization
DVR	Dynamic voltage restorer
DKE	Deutsche Kommission Elektrotechnik
EA	Evolutionary algorithm
EMF	Electromotive force
EMI	Electromagnetic interference
ESS	Energy storage system
FACTS	Flexible AC transmission system
FERC	Federal Energy Regulatory Commission
FL	Fuzzy logic
FRT	Fault ride-through
GA	Genetic algorithm
GC	Grid code
GW	Giga Watt
HF	High frequency
HVRT	High voltage ride-through
IEC	International Electro technical Commission

IEEE	Institute of Electrical and Electronic Engineers
IGBT	Insulated gate bipolar transistor
ISO	International Organization for Standardization
KVA	Kilo volt ampere
Kw	Kilo watt
LCCT	inductor–capacitor–capacitor–transformer
LVRT	Low voltage ride-through
MAS	Multiagent System
MFAPSO	Multi-function agent based particle swarm optimization
MLI	Multilevel inverter
MOSFET	Metal oxide semiconductor field effect transistor
MPC	Model predictive control
MPPT	Maximum power point tracking
NER	National electricity rules
NLP	Non-linear programming
NSGA	Non-dominated sorting GA
OLTC	On-load tap changer
OPF	Optimal power-flow
PCC	Point of common coupling
PEC	Power electronic converter
PLL	Phase Locked loop
PSD	Power semiconductor device
PSO	Particle swarm optimization
PV	Photovoltaic
PWM	Pulse-width modulation
RO	Robust Optimization
SA	Simulated annealing
SO	Stochastic Optimization
THD	Total Harmonic Distortion
TS	Tabu search
TSC	Thyristor switched capacitor
QZSI	Quasi impedance Source Inverter
VSI	Voltage source inverter
YSI	Admittance source inverter
ZSI	Impedance source inverter
Variables	
X	Reactance
δ	Angle between stator voltage and internal emf
ϕ	Angle between voltage and current
S	Apparent power
P	Real power
Q	Reactive power
V	Voltage
I	Current
E	Electromotive force
D	Duty cycle
T	Time period
m	Modulation index
W	Watt
kW	Kilowatt
MW	Megawatt

References

1. International Energy Agency. Renewables 2017: Analysis and Forecasts to 2022. Available online: <https://www.iea.org/renewables/> (accessed on 31 October 2018).
2. International Energy Agency. Renewables 2018: Analysis and Forecasts to 2023. Available online: <https://webstore.iea.org/market-report-series-renewables-2018> (accessed on 1 November 2018).
3. Pierno, A.; di Noia, L.P.; Rubino, L. Ancillary services provided by PV power plants. *Leonardo Electron. J. Pract. Technol.* **2016**, *28*, 57–76.
4. Hirst, E.; Kirby, B. *Electric-Power Ancillary Services*; ORNL/CON-426; Oak Ridge National Laboratory: Oak Ridge, TN, USA, 1996.
5. Xavier, L.S.; Cupertino, A.F.; Pereira, H.A. Ancillary services provided by photovoltaic inverters: Single and three phase control strategies. *Comput. Electr. Eng.* **2018**, *70*, 102–121. [[CrossRef](#)]
6. Yang, Y.; Blaabjerg, F.; Wang, H. Low-voltage ride-through of single-phase transformerless photovoltaic inverters. *IEEE Trans. Ind. Appl.* **2014**, *50*, 1942–1952. [[CrossRef](#)]
7. Comitato Elettrotecnico Italiano. *Reference Technical Rules for Connecting Users to the Active and Passive LV Distribution Companies of Electricity*; CEI: Milan, Italy, 2011.
8. Stetz, T.; Marten, F.; Braun, M. Improved low voltage grid-integration of photovoltaic systems in Germany. *IEEE Trans. Sustain. Energy* **2013**, *4*, 534–542. [[CrossRef](#)]
9. Miyamoto, Y. Technology for high penetration residential PV systems. In Proceedings of the 5th International Conference on Integration of Renewable and Distributed Energy Resources, Berlin, Germany, 4–6 December 2012.
10. Patel, U.N.; Patel, H.H. An Effective Power Management Strategy for Photovoltaic based Distributed Generation. In Proceedings of the 2016 IEEE 16th International Conference on Environment and Electrical Engineering (EEEIC), Florence, Italy, 7–10 June 2016.
11. Xiao, W.; Edwin, F.; Spagnuolo, G.; Jatskevich, J. Efficient Approaches for Modeling and Simulating Photovoltaic Power Systems. *IEEE J. Photovolt.* **2013**, *3*, 500–508. [[CrossRef](#)]
12. Trabelsi, M.; Abu-Rub, H.; Ge, B. 1-MW Quasi-Z-Source based Multilevel PV Energy Conversion System. In Proceedings of the 2016 IEEE International Conference on Industrial Technology (ICIT), Taipei, Taiwan, 14–17 March 2016.
13. Meraj, M.; Rahman, S.; Iqbal, A.; Ben-Brahim, L.; Alammari, R.; Abu-Rub, H. A Hybrid Active and Reactive Power Control with Quasi Z-Source Inverter in Single-Phase Grid-Connected PV systems. In Proceedings of the IECON 2016—42nd Annual Conference of the IEEE Industrial Electronics Society, Florence, Italy, 23–26 October 2016.
14. Sarkar, M.N.I.; Meegapola, L.G.; Datta, M. Reactive Power Management in Renewable Rich Power Grids: A Review of Grid-Codes, Renewable Generators, Support Devices, Control Strategies and Optimization Algorithms. *IEEE Access* **2018**, *6*, 41458–41489. [[CrossRef](#)]
15. Liu, L.; Li, H.; Zhao, Y.; He, X.; Shen, Z.J. 1MHz cascaded Z-source inverters for scalable grid-interactive photovoltaic (PV) applications using GaN device. In Proceedings of the 2011 IEEE Energy Conversion Congress and Exposition, Phoenix, AZ, USA, 17–22 September 2011; pp. 2738–2745.
16. Jabr, R.A. Linear decision rules for control of reactive power by distributed photovoltaic generators. *IEEE Trans. Power Syst.* **2017**, *33*, 2165–2174. [[CrossRef](#)]
17. Jafarian, H.; Enslin, J.; Parkhideh, B. On Reactive Power Injection Control of Distributed Grid-tied AC-stacked PV Inverter Architecture. In Proceedings of the 2016 IEEE Energy Conversion Congress and Exposition (ECCE), Milwaukee, WI, USA, 18–22 September 2016.
18. Yang, Y.; Wang, H.; Blaabjerg, F. Reactive power injection strategies for single-phase photovoltaic systems considering grid requirements. *IEEE Trans. Ind. Appl.* **2014**, *50*, 4065–4076. [[CrossRef](#)]
19. Ouldamrouche, S.; Bouchakour, S.; Arab, H.; Abdeladim, K.; Cherfa, F.; Kerkouche, K. Reactive Power issues in Grid Connected Photovoltaic Systems. In Proceedings of the International Conference on Nuclear and Renewable Energy Resources, Antalya, Turkey, 26–29 October 2014.
20. Gandhi, O.; Rodríguez-Gallegos, C.D.; Brahmendra, N.; Bieri, M.; Reindl, T.; Srinivasan, D. Reactive Power Cost from PV Inverters Considering Inverter Lifetime Assessment. *IEEE Trans. Sustain. Energy* **2018**, *10*, 738–747. [[CrossRef](#)]

21. Solanki, N.; Patel, J. Photovoltaic Solar Farms Operating in VAR Mode: A Review. *J. Power Electron. Power Syst.* **2016**, *6*, 73–85.
22. Pvpvs, I. *Task 14: Transition from Uni-Directional to Bi-Directional Distribution Grids*; International Energy Agency: Paris, France, 2014.
23. Gupta, A.K.; Samuel, P.; Kumar, D. A state of art review and challenges with impedance networks topologies. In Proceedings of the 2016 IEEE 7th Power India International Conference (PIICON), Bikaner, India, 25–27 November 2016; pp. 1–6. [[CrossRef](#)]
24. Kavya Santhoshi, B.; Kuppusamy, M.; Sivasubramanian, M.; Akila, S. A Novel Multiport Bidirectional Dual Active Bridge Dc-dc Converter for Renewable Power Generation Systems. *Indian J. Sci. Technol.* **2016**, *9*. [[CrossRef](#)]
25. Santhoshi, B.K.; Divya, S.; Kumar, M.S. Selective harmonic elimination for a PV based Quasi—Z Source Inverter for drive systems. In Proceedings of the 2014 IEEE National Conference on Emerging Trends in New & Renewable Energy Sources and Energy Management (NCET NRES EM), Chennai, India, 16–17 December 2014; pp. 143–147.
26. Siwakoti, Y.P.; Blaabjerg, F.; Loh, P.C. Quasi-Y-source inverter. In Proceedings of the 2015 Australasian Universities Power Engineering Conference (AUPEC), Wollongong, Australia, 27–30 September 2015; pp. 1–5. [[CrossRef](#)]
27. Siwakoti, Y.P.; Loh, P.C.; Blaabjerg, F.; Town, G. Y-source impedance network. *IEEE Trans. Power Electron.* **2014**, *29*, 3250–3254. [[CrossRef](#)]
28. Abdelhakim, A.; Davari, P.; Blaabjerg, F.; Mattavelli, P. Analysis and Design of the Quasi-Z-Source Inverter for Wide Range of Operation. In Proceedings of the 2018 IEEE 19th Workshop on Control and Modeling for Power Electronics (COMPEL), Padova, Italy, 25–28 June 2018.
29. Li, Y.; Anderson, J.; Peng, F.Z.; Liu, D. Quasi Z-source inverter for photovoltaic power generation systems. In Proceedings of the 2009 Twenty-Fourth Annual IEEE Applied Power Electronics Conference and Exposition, Washington, DC, USA, 15–19 February 2009; pp. 918–924.
30. Ge, B.; Abu-Rub, H.; Peng, F.Z.; Lei, Q.; de Almeida, A.T.; Ferreira, F.J.T.E.; Sun, D.; Liu, Y. An energy stored quasi-Z-source inverter for application to photovoltaic power system. *IEEE Trans. Ind. Electron.* **2013**, *60*, 4468–4481. [[CrossRef](#)]
31. Tang, Y.; Xie, S.; Zhang, C. An improved Z-source inverter. *IEEE Trans. Power Electron.* **2011**, *26*, 3865–3868. [[CrossRef](#)]
32. Tang, Y.; Xie, S.; Zhang, C.; Xu, Z. Improved Z-source inverter with reduced Z-source capacitor voltage stress and soft-start capability. *IEEE Trans. Power Electron.* **2009**, *24*, 409–415. [[CrossRef](#)]
33. Cao, D.; Jiang, S.; Yu, X.; Peng, F.Z. Low cost single-phase semi-Z source inverter. In Proceedings of the 2011 Twenty-Sixth Annual IEEE Applied Power Electronics Conference and Exposition (APEC), Fort Worth, TX, USA, 6–11 March 2011; pp. 429–436.
34. Cao, D.; Jiang, S.; Yu, X.; Peng, F.Z. Low-cost semi-Z-source inverter for single-phase photovoltaic systems. *IEEE Trans. Power Electron.* **2011**, *26*, 3514–3523. [[CrossRef](#)]
35. Haimovich, H.; Middleton, R.H.; de Nicola, L. Large-signal stability conditions for semi-quasi-Z-source inverters: Switched and averaged models. In Proceedings of the 52nd IEEE Conference on Decision and Control, Florence, Italy, 10–13 December 2013.
36. Loh, P.C.; Gao, F.; Blaabjerg, F. Embedded EZ-source inverter. *IEEE Trans. Ind. Appl.* **2010**, *46*, 256–267.
37. Gao, F.; Loh, P.C.; Li, D.; Blaabjerg, F. Asymmetrical and symmetrical embedded Z-source inverters. *IET Power Electron.* **2011**, *4*, 181–193. [[CrossRef](#)]
38. Gao, F.; Loh, P.C.; Blaabjerg, F.; Gajanayake, C.J. Operational analysis and comparative evaluation of embedded Z-source inverters. In Proceedings of the 2008 IEEE Power Electronics Specialists Conference, Rhodes, Greece, 15–19 June 2008; pp. 2757–2763.
39. Zhang, F.; Peng, F.Z.; Qian, Z. Z-H converter. In Proceedings of the 2008 IEEE Power Electronics Specialists Conference, Rhodes, Greece, 15–19 June 2008; pp. 1004–1007.
40. Nguyen, M.K.; Lim, Y.C.; Cho, G.B. Switched-inductor quasi-Zsource inverter. *IEEE Trans. Power Electron.* **2011**, *26*, 3183–3191. [[CrossRef](#)]
41. Gajanayake, C.J.; Luo, F.L.; Gooi, H.B.; So, P.L.; Siow, L.K. Extended-boost Z-source inverters. *IEEE Trans. Power Electron.* **2010**, *25*, 2642–2652. [[CrossRef](#)]

42. Loh, P.C.; Blaabjerg, F. Magnetically coupled impedance-source inverters. *IEEE Trans. Power Electron.* **2013**, *49*, 2177–2187. [[CrossRef](#)]
43. Loh, P.C.; Duan, N.; Liang, C.; Gao, F.; Blaabjerg, F. Z-source B4 inverter. In Proceedings of the 2007 IEEE Power Electronics Specialists Conference, Orlando, FL, USA, 17–21 June 2007; pp. 1363–1369.
44. Nguyen, M.K.; Lim, Y.C.; Choi, J.H. Two switched-inductor quasi-Z-source inverters. *IET Power Electron.* **2012**, *5*, 1017–1025. [[CrossRef](#)]
45. Loh, P.C.; Li, D.; Blaabjerg, F. Current-type flipped- Γ -source inverters. In Proceedings of the 7th International in Power Electronics and Motion Control Conference, Harbin, China, 2–5 June 2012; pp. 594–598.
46. Li, D.; Loh, P.C.; Zhu, M.; Gao, F.; Blaabjerg, F. Cascaded multicell trans-Z-source inverters. *IEEE Trans. Power Electron.* **2013**, *28*, 826–836.
47. Zhu, M.; Yu, K.; Luo, F.L. Switched inductor Z-source inverter. *IEEE Trans. Power Electron.* **2010**, *25*, 2150–2158.
48. Itozakura, H.; Koizumi, H. Embedded Z-source inverter with switched inductor. In Proceedings of the IECON 2011—37th Annual Conference of the IEEE Industrial Electronics Society, Melbourne, Australia, 7–10 November 2011; pp. 1342–1347.
49. Qian, W.; Peng, F.Z.; Cha, H. Trans-Z-source inverters. *IEEE Trans. Power Electron.* **2011**, *26*, 3453–3463. [[CrossRef](#)]
50. Li, D.; Loh, P.C.; Zhu, M.; Gao, F.; Blaabjerg, F. Generalized multicell switched-inductor and switched-capacitor Z-source inverters. *IEEE Trans. Power Electron.* **2013**, *28*, 837–848. [[CrossRef](#)]
51. Gajanayake, C.J.; Gooi, H.B.; Luo, F.L.; So, P.L.; Siow, L.K.; Vo, Q.N. Simple modulation and control method for new extended boost quasi Z-source. In Proceedings of the TENCON 2009—2009 IEEE Region 10 Conference, Singapore, 23–26 January 2009; pp. 1–6.
52. Shin, D.; Cha, H.; Lee, J.P.; Yoo, D.W.; Peng, F.Z.; Kim, H.G. Parallel operation of trans-Z-source inverter. In Proceedings of the 8th International Conference on Power Electronics—ECCE Asia, Jeju, Korea, 30 May–3 June 2011; pp. 744–748.
53. Loh, P.C.; Li, D.; Blaabjerg, F. Γ -Z-source inverters. *IEEE Trans. Power Electron.* **2013**, *28*, 4880–4884. [[CrossRef](#)]
54. Adamowicz, M.; Strzelecki, R.; Peng, F.Z.; Guzinski, J.; Rub, H.A. New type LCCT-Z-source inverters. In Proceedings of the 2011 14th European Conference on Power Electronics and Applications, Birmingham, UK, 30 August–1 September 2011; pp. 1–10.
55. Huang, L.; Zhang, M.; Hang, L.; Yao, W.; Lu, Z. A family of three switch three-state single-phase Z-source inverters. *IEEE Trans. Power Electron.* **2013**, *28*, 2317–2329. [[CrossRef](#)]
56. Nguyen, M.K.; Lim, Y.C.; Park, S.J. Improved trans-Z-source inverter with continuous input current and boost inversion capability. *IEEE Trans. Power Electron.* **2013**, *28*, 4500–4510. [[CrossRef](#)]
57. Jiang, S.; Cao, D.; Peng, F.Z. High frequency transformer isolated Z-source inverters. In Proceedings of the 2011 Twenty-Sixth Annual IEEE Applied Power Electronics Conference and Exposition (APEC), Fort Worth, TX, USA, 6–11 March 2011; pp. 442–449.
58. Jiang, S.; Peng, F.Z. Modular single-phase trans-Z-source inverter for multi-input renewable energy system. In Proceedings of the 2012 Twenty-Seventh Annual IEEE Applied Power Electronics Conference and Exposition (APEC), Orlando, FL, USA, 5–9 February 2012; pp. 2107–2114.
59. Kumar, S.P.; Shailaja, P. T-shaped Z-source inverter. *Int. J. Eng. Res. Technol.* **2012**, *1*, 1–6.
60. Peng, F.Z. Z-source network for power conversion. In Proceedings of the 2008 Twenty-Third Annual IEEE Applied Power Electronics Conference and Exposition, Austin, TX, USA, 24–28 February 2008; pp. 1258–1265.
61. Strzelecki, R.; Adamowicz, M.; Strzelecka, N.; Bury, W. New type T-source inverter. In Proceedings of the 2009 Compatibility and Power Electronics, Badajoz, Spain, 20–22 May 2009; pp. 191–195.
62. Nguyen, M.K.; Lim, Y.C.; Kim, Y.G. TZ-source inverters. *IEEE Trans. Ind. Electron.* **2013**, *60*, 5686–5695. [[CrossRef](#)]
63. Bhattacharya, K.; Zhong, J. Reactive power as an ancillary service. *IEEE Trans. Power Syst.* **2001**, *16*, 294–300. [[CrossRef](#)]
64. Adamowicz, M.; Strzelecki, R.; Peng, F.Z.; Guzinski, J.; Rub, H.A. High step-up continuous input current LCCT-Z-source inverters for fuel cells. In Proceedings of the 2011 IEEE Energy Conversion Congress and Exposition, Phoenix, AZ, USA, 17–22 September 2011; pp. 2276–2282.
65. Mo, W.; Loh, P.C.; Blaabjerg, F. Asymmetrical Γ -source inverters. *IEEE Trans. Ind. Electron.* **2014**, *61*, 637–647. [[CrossRef](#)]

66. Kavya Santhoshi, B.; Mohana Sundaram, K. Hybrid Converter with Simultaneous AC and DC Output for Nano-Grid Applications with Residential System. *J. Eng. Appl. Sci.* **2018**, *13*, 3289–3293.
67. Peng, F.Z. Z-source inverter. *IEEE Trans. Ind. Appl.* **2003**, *39*, 504–510. [CrossRef]
68. Anderson, J.; Peng, F.Z. Four quasi-Z-source inverters. In Proceedings of the 2008 IEEE Power Electronics Specialists Conference, Rhodes, Greece, 15–19 June 2008; pp. 2743–2749.
69. First Solar Sarnia PV Power Plant, Ontario, Canada. Available online: <http://www.firstsolar.com/en/Projects/Sarnia-Solar-Project> (accessed on 19 December 2013).
70. Boyra, M.; Thomas, J.-L. A review on synchronization methods for grid-connected three phase VSC under unbalanced and distorted conditions. In Proceedings of the 2011-14th European Conference on Power Electronics and Applications (EPE), Birmingham, UK, 30 August–1 September 2011; pp. 1–10.
71. Mohana Sundaram, K.; Anandhraj, P.; Vimalraj Ambeth, V. PV-Fed Eleven-Level Capacitor Switching Multi-Level Inverter for Grid Integration. In *Advances in Smart Grid and Renewable Energy*; Sen Gupta, S., Zobaa, A., Sherpa, K., Bhoi, A., Eds.; Lecture Notes in Electrical Engineering; Springer: Singapore, 2018; Volume 435.
72. IEEE 929-2000. *IEEE Recommended Practice for Utility Interface of Photovoltaic (PV) Systems*; IEEE: Piscataway, NJ, USA, 2000.
73. Committee EL-042. *AS 4777.2—2005. Grid Connection of Energy Systems via Inverters. Part 2: Inverter Requirements*; Australian Standard: Sydney, Australia, 2005.
74. Oliva, A.; Chiacchiarini, H.; Aymonino, A.; Mandolesi, P. Reduction of Total Harmonic Distortion in Power Inverters. *Lat. Am. Appl. Res.* **2005**, *35*, 89–93.
75. Çelebi, A.; Çolak, M. The effects of harmonics produced by Grid connected photovoltaic systems on electrical networks. Available online: http://www.emo.org.tr/ekler/0172ea66506f59c_ek.pdf (accessed on 25 November 2018).
76. Watson, N.R.; Miller, A. Power Quality Indices: A Review. In Proceedings of the EEA Conference & Exhibition, Wellington, Newzealand, 24–26 June 2015.
77. IEEE Standard 519-2014. *IEEE Recommended Practices and Requirements for Harmonic Control in Electric Power Systems*; IEEE Power and Energy Society: Piscataway, NJ, USA, 2014.
78. Dartawan, K.; Austria, R.; Le, H.; Suehiro, M. Harmonic issues that limit solar photovoltaic generation on distribution circuits. In Proceedings of the World Renewable Energy Forum, Denver, CO, USA, 13–17 May 2012.
79. Abdurrahman, A.; Zakary, A.; A shazly, A. Simulation and Implementation of Grid-connected Inverters. *Int. J. Comput. Appl.* **2012**, *60*, 41–49.
80. Romero-Caravel, E.; Spagnuolo, G.; Tranquillo, L.G.; Ramos-Puja, C.A.; Santino, T.; Xiao, W.M. Grid-Connected Photovoltaic Generation Plants: Components and Operation. *IEEE Ind. Electron. Mag.* **2013**, *7*, 6–20. [CrossRef]
81. Koura, S.; Leon, J.I.; Vinnikov, D.; Tranquillo, L.G. Grid-Connected Photovoltaic Systems: An Overview of Recent Research and Emerging PV Converter Technology. *IEEE Ind. Electron. Mag.* **2015**, *9*, 47–61. [CrossRef]
82. Cagnano, A.; Torelli, F.; Alfonzetti, F.; de Tuglie, E. Can PV plants provide a reactive power ancillary service? A treat offered by an on-line controller. *Renew. Energy* **2011**, *36*, 1047–1052. [CrossRef]
83. Sousa, J.L.; Brito, C.J.; Fernao Pires, V. Impact of Photovoltaic Systems with ancillary services in low voltage grids. In Proceedings of the 15th Biennial Baltic Electronics Conference (BEC2016) Tallinn, Estonia, 3–5 October 2016.
84. Zhong, J.; Bhattacharya, K. Toward a Competitive Market for Reactive Power. *IEEE Trans. Power Syst.* **2002**, *17*, 1206–1215. [CrossRef]
85. Rosenblatt, F. The perceptron: A probabilistic model for information storage and organization in the brain. *Psychol. Rev.* **1958**, *65*, 386–408. [CrossRef]
86. Yuce, B.; Li, H.; Rezgui, Y.; Petri, I.; Jayan, B.; Yang, C. Utilizing artificial neural network to predict energy consumption and thermal comfort level: An indoor swimming pool case study. *Energy Build.* **2014**, *80*, 45–56. [CrossRef]
87. Kovacic, Z.; Bogdan, S. *Fuzzy Controller Design: Theory and Applications, Volume 19 of Automation and Control Engineering*; CRC Press: Boca Raton, FL, USA, 2006.
88. Radhakrishnan, B.M.; Srinivasan, D. A multi-agent based distributed energy management scheme for smart grid applications. *Energy* **2016**, *103*, 192–204. [CrossRef]

89. Khare, A.R.; Kumar, B.Y. Multiagent structures in hybrid renewable power system: A review. *J. Renew. Sustain. Energy* **2015**, *7*, 063101. [[CrossRef](#)]
90. Kekatos, V.; Wang, G.; Conejo, A.J.; Giannakis, G.B. Stochastic Reactive Power Management in Microgrids With Renewables. *IEEE Trans. Power Syst.* **2014**, *30*, 3386–3395. [[CrossRef](#)]
91. Gandhi, O.; Zhang, W.; Rodríguez-Gallegos, C.D.; Srinivasan, D.; Reindl, T. Continuous optimization of reactive power from PV and EV in distribution system. In Proceedings of the 2016 IEEE Innovative Smart Grid Technologies—Asia (ISGT-Asia), Melbourne, Australia, 28 November–1 December 2016; pp. 281–287. [[CrossRef](#)]
92. Kumar, D.S.; Srinivasan, D.; Reindl, T. Optimal power scheduling of distributed resources in Smart Grid. In Proceedings of the 2013 IEEE Innovative Smart Grid Technologies-Asia (ISGT Asia), Bangalore, India, 10–13 November 2013; Volume 9, pp. 1–6.
93. Abbasy, A.; Hosseini, S. Ant Colony Optimization-Based Approach to Optimal Reactive Power Dispatch: A Comparison of Various Ant Systems. In Proceedings of the 2007 IEEE Power Engineering Society Conference and Exposition in Africa—Power Africa, Johannesburg, South Africa, 16–20 July 2007; pp. 16–20.
94. Ziadi, Z.; Taira, S.; Oshiro, M.; Funabashi, T. Optimal power scheduling for smart grids considering controllable loads and high penetration of photovoltaic generation. *IEEE Trans. Smart Grid* **2014**, *5*, 2350–2359. [[CrossRef](#)]
95. Demirok, E.; Gonzalez, P.C.; Frederiksen, K.H.B.; Sera, D.; Rodriguez, P.; Teodorescu, R. Local Reactive Power Control Methods for Overvoltage Prevention of Distributed Solar Inverters in Low-Voltage Grids. *IEEE J. Photovolt.* **2011**, *1*, 174–182. [[CrossRef](#)]
96. Alkaabi, S.; Zeineldin, H.; Khadkikar, V. Short-Term Reactive Power Planning to Minimize Cost of Energy Losses Considering PV Systems. *IEEE Trans. Smart Grid* **2018**, *10*, 2923–2935.
97. Rahman, S.; Meraj, M.; Iqbal, A.; Ben-Brahim, L.; Alammari, R. Thyristor based SVC and multilevel qZSI for Active and Reactive power management in solar PV system. In Proceedings of the 2017 11th IEEE International Conference on Compatibility, Power Electronics and Power Engineering (CPE-POWERENG), Cadiz, Spain, 4–6 April 2017; pp. 528–533. [[CrossRef](#)]
98. Wang, T.; O'Neill, D.; Kamath, H. Dynamic Control and Optimization of Distributed Energy Resources in a Microgrid. *IEEE Trans. Smart Grid* **2015**, *6*, 2884–2894. [[CrossRef](#)]



© 2019 by the authors. Licensee MDPI, Basel, Switzerland. This article is an open access article distributed under the terms and conditions of the Creative Commons Attribution (CC BY) license (<http://creativecommons.org/licenses/by/4.0/>).

Review

Nature-Inspired MPPT Algorithms for Partially Shaded PV Systems: A Comparative Study

Somashree Pathy ¹, C. Subramani ^{1,*}, R. Sridhar ¹, T. M. Thamizh Thentral ¹ and Sanjeevikumar Padmanaban ²

¹ Department of Electrical and Electronics Engineering, SRM Institute of Science and Technology, Chennai, Tamil Nadu 603203, India; p.soma92@gmail.com (S.P.); sridharmanly@gmail.com (R.S.); thentral2kuna@gmail.com (T.M.T.T.)

² Department of Energy Technology, Aalborg University, 6700 Esbjerg, Denmark; san@et.aau.dk

* Correspondence: csmsrm@gmail.com; Tel.: +91-960-001-3988

Received: 22 January 2019; Accepted: 8 April 2019; Published: 16 April 2019

Abstract: PV generating sources are one of the most promising power generation systems in today's power scenario. The inherent potential barrier that PV possesses with respect to irradiation and temperature is its nonlinear power output characteristics. An intelligent power tracking scheme, e.g., maximum power point tracking (MPPT), is mandatorily employed to increase the power delivery of a PV system. The MPPT schemes experiences severe setbacks when the PV is even shaded partially as PV exhibits multiple power peaks. Therefore, the search mechanism gets deceived and gets stuck with the local maxima. Hence, a rational search mechanism should be developed, which will find the global maxima for a partially shaded PV. The conventional techniques like fractional open circuit voltage (FOCV), hill climbing (HC) method, perturb and observe (P&O), etc., even in their modified versions, are not competent enough to track the global MPP (GMPP). Nature-inspired and bio-inspired MPPT techniques have been proposed by the researchers to optimize the power output of a PV system during partially shaded conditions (PSCs). This paper reviews, compares, and analyzes them. This article renders firsthand information to those in the field of research, who seek interest in the performance enhancement of PV system during inhomogeneous irradiation. Each algorithm has its own advantages and disadvantages in terms of convergence speed, coding complexity, hardware compatibility, stability, etc. Overall, the authors have presented the logic of each global search MPPT algorithms and its comparisons, and also have reviewed the performance enhancement of these techniques when these algorithms are hybridized.

Keywords: photovoltaic systems; MPPT technique; partial shading; global MPP (GMPP); nature-inspired algorithms

1. Introduction

The increasing load demand on one side and the depletion of fossil fuels on the other side forces the world to look for alternative energy resources. Also, the concern regarding pollution through the greenhouse effect and other environmental issues associated with the conventional energy sources make renewable energy resources (RES) more attractive [1]. Among various non-conventional sources, solar energy is more widely used because of the abundant availability of solar irradiation on the earth's surface [2]. The photovoltaic (PV) cells convert direct sunlight into electricity, but as the solar irradiance and temperature are fluctuating in nature, as a result, it reduces the PV panel efficiency. The main drawbacks of the PV system are its highly intermittent nature, lower conversion efficiency, lower rating, high implementation cost, and maintenance issues. PV panels also get affected due to partial shading because of clouds, tree branches, birds, etc. These factors make it essential to deploy a dc–dc converter with an MPPT technique for tracking the maximum power point from the PV panel under all operating

conditions. The MPPT control algorithm is employed along with the dc–dc converter, where the control algorithm adjusts the duty cycle according to the variation in solar irradiation and temperature, which will boost the lower voltage output of the PV system. A PV cell has very low power rating [3–6], and these cells can be connected in series or parallel according to the required current and voltage rating. The series and parallel combination constitute a PV module and the modules are connected together to form a PV array [7]. This makes power electronic interfaces indispensable in any PV system for ensuring the system voltage compatible with a load or grid [8]. PV panels can be implemented as a rooftop setup and it can also operate in standalone mode and grid-connected mode [9].

For a PV system, the output voltage depends on the temperature of the panel and the current value of the irradiance level. The PV system gives the optimum output under the standard test condition (STC-irradiance = 1000 W/m², temperature = 25 °C, 1.5 air mass) [3,10]. MPPT trackers embody a control algorithm and converter to ensure that PV panels operate at MPP to render maximum possible power. This tracking scheme becomes futile when PV panels are partially shaded. In the research arena, there was a paradigm shift in MPPT algorithms as a host of research articles are being published every year on global search algorithms [8,9]. Many studies have been done toward developing an efficient and reliable MPPT algorithm to extract the maximum operating power point from the PV panel [11–13]. Both conventional and computational intelligence algorithms are used for MPPT [14,15]. Most of the conventional algorithms perform effectively under uniform solar irradiation and temperature but fail to track the true maximum operating point during varying weather or partial shading conditions [16,17].

The efficient nature-inspired algorithms based on MPPT techniques are the particle swarm optimization (P&O) algorithm, ant colony optimization (ACO) algorithm, artificial bee colony (ABC) algorithm, differential evolution (DE), etc. These algorithms are used for global search problems and can operate effectively under uniform solar irradiation and temperature, as well as partial shading and rapidly changing environmental conditions. Hybridization of these algorithms also has been done for enhancing the performance and reliability of these algorithms. In Reference [18], the authors have proposed a swarm chasing MPPT algorithm for module integrated converters and the performance is also compared with conventional P&O method. Here, the swarm-chasing technique is found to be more superior. Comparative study on well-entrenched global peak tracking algorithms is archived in a research forum [15,19]. Some researchers paid due credit to the conventional algorithms and examined whether the algorithms could be sustained during partial shading. In Reference [19], conventional and computational intelligence MPPT techniques were presented, which describes the working of each algorithm with their merits and demerits. The quest toward proposing new algorithms has not dwindled as one can witness recent research articles on global search MPPT [8,9,13,15].

In this paper, a review has been done for five evolutionary algorithms that are reliable and more pragmatic for practical deployment. This paper has been framed in such a manner that it gives a clear understanding of PV characteristics, partial shading, and MPP search mechanisms. The paper is organized in such a way that Section 2 presents PV modeling and PV characteristics analysis during both uniform irradiation condition and PSCs. Section 3 discusses the soft computing algorithms reviewed in this paper, whereas Section 4 follows a brief discussion about the reviewed algorithms. The concluding part is given in Section 5.

2. PV Modeling and Its Characteristic Curves

Figure 1 depicts a general block diagram of a PV generating system. In the given diagram, a PV panel connected with a dc–dc converter and the duty cycle of the converter is controlled by the MPPT algorithm. The MPPT algorithm will sense the required parameters from the solar system, and accordingly, it modifies the converter duty cycle. Hence, under all conditions, maximum output power is obtained from the panel. Then the converter output can be directly connected to the dc load or it can also be given to ac loads by connecting them through an inverter.

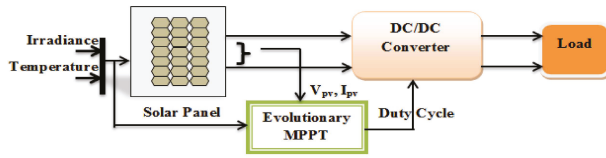


Figure 1. Diagram of PV connected to a load.

A PV module consists of many solar cells that are generally made up of silicon material. When the light energy falls on the solar cell, then the electrons start to move and current flows. Solar cells are considered current sources. There are many types of solar cell models, among which, the single diode model is well established and a simple structure [10,20]. In this paper, a single diode model solar cell is shown in Figure 2. It is basically a diode connected in parallel with a current source along with one shunt and one series resistor. In the figure, I_{pv} is the current generated by light, I_D is the current across diode, whereas I_{sh} represents the current flowing through a shunt resistance R_{sh} , and I is the output current. For the mathematical modeling of the PV system, the basic equations are given below.

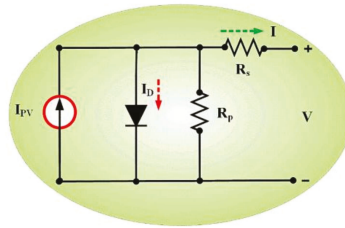


Figure 2. Circuit for the modelling of a single diode PV cell.

$$I = I_{pv} - I_0 \left[\exp \left[\frac{V + IR_s}{aV_T} \right] - 1 \right] - \frac{V + IR_s}{R_{sh}} \tag{1}$$

where V_T is the PV array thermal voltage = kT/q . I_p represents the photocurrent, I_0 represents reverse saturation current, and R_s and R_{sh} represent the series and shunt resistance respectively, a is the diode ideality factor, q is the charge of the electron i.e., 1.6×10^{-19} C, k represents Boltzmann’s constant ($1.3806503 \times 10^{-23}$ J/K), and T is the temperature.

$$I_0 = I_{o_STC} \left[\frac{T_{STC}}{T} \right]^3 \exp \left[\frac{qE_g}{ak} \left[\frac{1}{T_{STC}} - \frac{1}{T} \right] \right] \tag{2}$$

In the above equation E_g represents band gap energy of the semi-conductor material and I_{o_STC} denotes the nominal saturation current at STC, T_{STC} is the temperature under STC (25 °C).

In simplified form, I_0 can be written as

$$I_0 = \frac{(I_{sc_STC} + K_I \Delta T)}{\exp \left[\frac{V_{oc_STC} + K_V \Delta T}{aV_T} \right] - 1} \tag{3}$$

here K_I is the coefficient of the short circuit current, K_V is the open circuit voltage coefficient, I_{sc_STC} is the short circuit current under STC, V_{oc_STC} is the open circuit voltage under STC, and $\Delta T = T - T_{STC}$.

In Figure 3a,b the I-V graph and P-V graph for different irradiation levels are shown. The I-V graph shown in Figure 3a shows that according to the temperature and irradiance, the voltage and current value also varies. Here, the current value depends on the irradiance, i.e., directly proportional, and the voltage depends on the temperature [20]. Hence, the PV operating point does not stay at the maximum operating value and it varies with the environmental conditions, which in turn, reduces the

power. Therefore, it is preferable to install more PGS than the required demand, but simultaneously, it increases the cost [21]. Therefore, the dc–dc converter with an effective MPPT technique is deployed for the PV systems to modify the converter duty cycle according to the environmental conditions and thereby tracks the maximum power point for all operating conditions. During uniform irradiance, the P–V graph shows only one peak power point, which gives the corresponding maximum voltage and current. Hence, the conventional MPPT techniques would suffice to track the true MPP and is found to be reliable.

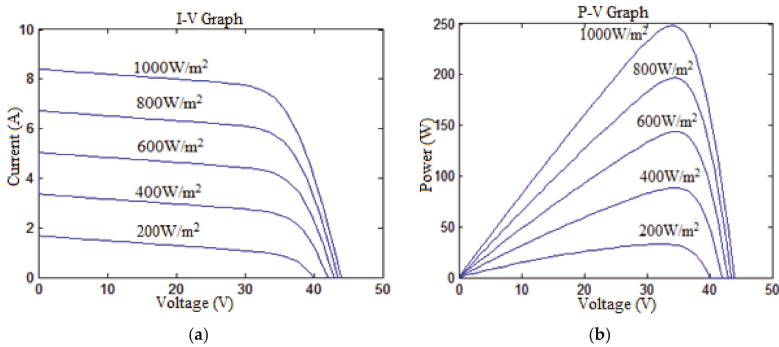


Figure 3. P–V characteristics graph for different irradiation levels. (a) shows the current versus voltage graph for different irradiation levels; (b) shows the power versus voltage graph for different irradiation levels.

However, when some of the PV panels in an array receive non-uniform irradiance and temperature, i.e., they are shaded, then the power production of the shaded panel decreases relative to an unshaded one. The shaded panels absorb a large amount of current from the unshaded panels in order to operate. This condition is called hot spot formation and this damages the PV panel [22,23]. To avoid this condition, a bypass diode is connected in parallel across each panel, as shown in Figure 4a,b, which provides another way for conduction during the occurrence of partial shading [24]. As shown in Figure 4c,d, during the partial shading condition, there exist multiple peak points in the P–V characteristics graph, among which only one point is the true maximum power point. These multiple peak points are considered the local maximum power points (LMPPs), and among all the LMPPs, the true MPP is called the global maximum power point (GMPP). Most of the conventional MPPT techniques fail to identify the GMPP among all the LMPP. For this purpose, many researchers have proposed various stochastic, evolutionary, and swarm-based algorithms and hybridization of these algorithms has also been done for more reliable and effective MPP tracking.

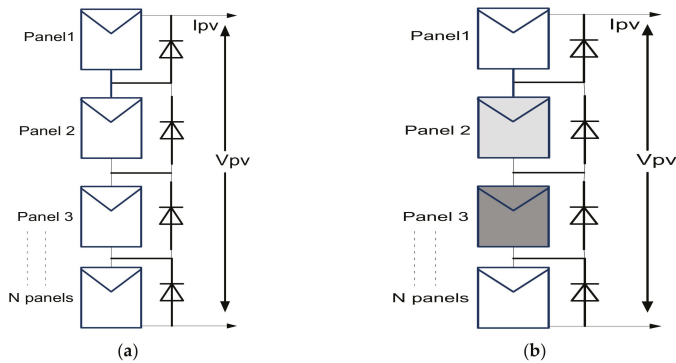


Figure 4. Cont.

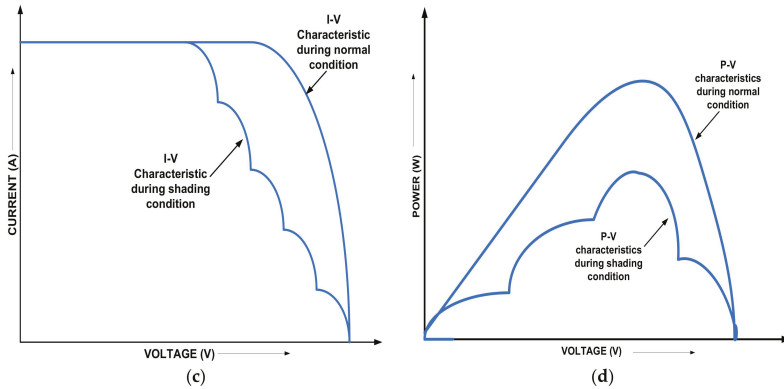


Figure 4. PV panels operation during partial shading conditions: (a) PV panels under normal operation, (b) PV panels under a shading condition, (c) I–V characteristic of PGS during partial shading, and (d) P–V characteristic of PGS during partial shading.

3. Intelligent Nature Inspired Algorithms: An Overview

The specific evolutionary algorithms discussed are

- particle swarm optimization (PSO) algorithm
- differential evolution (DE) algorithm
- ant colony optimization (ACO) algorithm
- artificial bee colony (ABC) optimization algorithm
- bacteria foraging optimization algorithm (BFOA).

The analysis of these algorithms has been done with respect to the convergence speed, execution, and reliability.

3.1. Particle Swarm Optimization (PSO)

PSO is the most widely used algorithm used for the MPPT technique. This algorithm was discovered in 1995 by Eberhart and Kennedy. PSO is widely accepted by researchers due to its simple and easy to implementation characteristics. This algorithm is motivated by the communal activity of the crowding of birds and schooling activity of fish. PSO is a global optimization algorithm that finds the best solution in a multi-dimensional path. Therefore, it is able to track the GMPP from all local MPPs even when the PV panel is under a partial shading condition or the PV panel possesses multiple peak points. PSO uses many operating agents that share information about their respective search behavior, where all agents are termed as a particle. Here, a number of particles move in the search space in order to get the best solution. Each particle adjusts its movement by following the best solution and mean while searches for new solutions will be in progress [25]. The particle referred here can be voltage or duty cycle. For finding the optimal solution, the particle must follow the best position of its own or the best position of its neighbor. The mathematical representation of the PSO algorithm is given in the following equations [26,27]:

$$u_i(k + 1) = qu_i(k) + c_1r_1(p_{best,i} - g_i(k)) + c_2r_2(g_{best,i} - g_i(k)) \tag{4}$$

$$g_i(k + 1) = g_i(k) + u_i(k + 1) \tag{5}$$

where $i = 1, 2, 3, \dots, N$.

u_i —velocity of the particle

g_i —particle position

- k—number of iterations
- q—inertia weight
- r_1, r_2 —random variables which are distributed uniformly between [0,1]
- c_1, c_2 —cognitive and social co-efficient respectively
- p_{best} —individual particle’s best position
- g_{best} —best position between all the particle’s individual best position

PSO finds the global maxima voltage point according to the maximum power in the P–V graph. For this, we need to specify PSO parameters such as power and voltage value, size of the swarm, and number of iterations. PSO stores the best value as p_{best} and continues to update until it finds the g_{best} point or it satisfies the objective function [15,27,28]:

$$P_{best,i} = g_i(k) \tag{6}$$

$$f(g_i(k)) > f(g_i(k + 1)) \tag{7}$$

where the function “f” is the PV panel operating power. During partial shading, the particles are re-initialized to find g_{best} and it must satisfy the below condition. A flowchart of the PSO algorithm is given in Figure 5.

$$\left| \frac{P(g_{i+1}) - P(g_i)}{P(g_i)} \right| > \Delta P \tag{8}$$

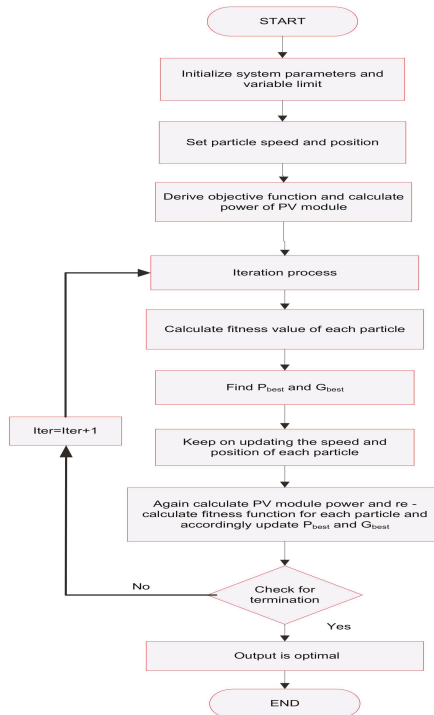


Figure 5. PSO algorithm.

In Reference [24], a cost-effective PSO algorithm is presented, which uses one single pair of sensors for controlling multiple PV arrays. The algorithm is also compared with many conventional techniques, from which, the proposed algorithm is found to be more effective and it also tracks the MPP even

during partial shading conditions. The authors in Reference [9] have presented a PSO algorithm integrated with an overall distribution (OD) algorithm. The OD technique is used to efficiently track the MPP during any shading conditions and is again integrated with PSO to improve the accuracy of the MPPT technique. A novel two-stage PSO MPPT is proposed in Reference [29]. Here, for partial shading conditions and to achieve improved convergence speed, a shuffled frog leaf algorithm (SFLA) with an adaptive speed factor is implemented with PSO. For partially shaded PV power systems, a modified PSO is presented in Reference [30] whose effectiveness is shown in the paper. Many studies have been done using PSO as an MPPT technique for both uniform irradiation and partially shaded conditions. However, the standard PSO performance is enhanced and modified by using hybridization and modification in the algorithm [25,28,31–35], which increases the system efficiency and is found to be more reliable.

3.2. Differential Evolution (DE)

This algorithm was suggested by Price and Storn in 1995. DE is a randomly varying population-based algorithm and it finds its application in global optimization problems [36]. This algorithm is well-suited for non-linear, non-differentiable, multi-dimensional problems [37]. Therefore, this algorithm can be implemented for PV panel maximum power extraction as the PV characteristics possesses a highly non-linear graph as they are intermittent in nature [16,20]. Furthermore, even during partial shading conditions, it can track the global optimum power point [38,39]. In the DE algorithm, the complexity reduces as it requires much fewer parameters (particles) to tune. This tuning of particles makes sure that in every iteration, the particles converge toward the best solution in the search space. DE algorithm follows various steps for optimization and those are initialization, mutation, recombination/crossover, and selection [40]. The DE algorithm flowchart is shown in Figure 6.

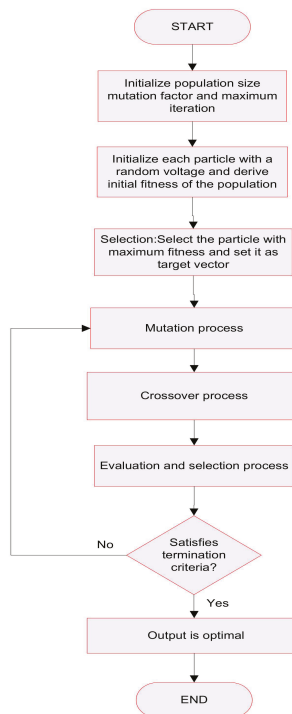


Figure 6. DE algorithm.

3.2.1. Initialization

DE optimizes the problem by using different formulas for creating new particles and also by maintaining the population size at the same time. In the search space, out of the existing particles and newly updated particles, the best fitness value particles only remain and others having the least fitness value are replaced. In DE optimization, various control processes are carried out step by step as discussed below. For optimization using DE, at first, initial parameters, population, and number of generations must be initialized [37,41,42].

If a function with “P” real parameters must be optimized, then the population size is taken as “N”, where the “N” value should not be less than 4.

Hence, the parameter vectors can be written as:

$$x_{i,G} = [x_{1,i,G}, x_{2,i,G}, x_{3,i,G}, \dots, x_{P,i,G}] \tag{9}$$

In the above equation $i = 1, 2, \dots, N$; and G is the number of generations.

During initialization process, the user sets a predefined upper and lower boundary value for each particle:

$$x_j^L \leq x_{j,i,1} \leq x_j^U \tag{10}$$

The initial values are chosen randomly for each particle but in uniform intervals between the upper and lower interval of the particle.

3.2.2. Mutation

Here, each individual becomes a target vector. Mutation is performed for all N particles in the search space and hence it expands the search space. For a particular particle $x_{i,G}$, three random vectors are taken such as $x_{r1,G}$, $x_{r2,G}$, and $x_{r3,G}$ in such a manner that all the indices i , $r1$, $r2$, and $r3$ are distinct from each other.

For finding out the donor vector (the new particle formed from the mutation process), add the weighted difference of two vectors with the third vector:

$$u_{i,G+1} = x_{r1,G} + F(x_{r2,G} - x_{r3,G}) \tag{11}$$

where F is the mutation factor, which lies between $[0,2]$; $u_{i,G+1}$ is the donor vector.

3.2.3. Crossover

Here, the next generation is formed from the parent particles. Therefore, recombination is performed between the target and mutant vector to get the next generation vector, which is a trial vector. In other words, the trial vector $u_{i,G+1}$ is formed by considering the elements of the target vector $x_{i,G}$ and also from the elements of the mutant vector/donor vector $u_{i,G+1}$.

Crossover may be reached on the D variables when an arbitrarily chosen number between 0 to 1 lies in the range of the CR value, where CR is a constant value and is used for controlling DE parameters. The condition is given as:

$$u_{j,i,G+1} = \begin{cases} u_{j,i,G+1} & \text{if } \text{rand}_{j,i} \leq \text{CR and } j = I_{\text{rand}} \\ x_{j,i,G} & \text{if } \text{rand}_{j,i} > \text{CR and } j \neq I_{\text{rand}} \end{cases} \tag{12}$$

where

$$i = 1, 2, \dots, N$$

$$j = 1, 2, \dots, D$$

$\text{rand}_{j,i}$ is any value randomly chosen within $[0,1]$

I_{rand} is a random integer whose value lies within $(1, 2, \dots, D)$. This value makes sure that $u_{i,G+1} \neq x_{i,G}$.

3.2.4. Selection

In DE optimization, the population size is kept constant throughout the generation process. Therefore, a selection criterion provides the best parameter for the next generation. In this process, both parent vector/target vector and the trial vector are compared, and if the trial vector is able to give a better fitness value compared to that of the target vector, then the target vector, i.e., the parent vector, is replaced by the trial vector and the generation gets updated.

DE has its wide acceptance in global search problems. The authors in reference [38] have proposed a DE-based MPPT technique that works with the boost converter for a partially shaded PV system. In the above work, performance of DE algorithm is compared with a conventional algorithm and its efficiency is verified. A detail survey about DE algorithm use in various fields with its advantages and disadvantages is given in reference [43]. The fundamentals of DE, its application to various multi-objective optimization problems, such as constrained, uncertain optimization problems are reviewed in reference [44]. A modified DE with a mutation process being modified, i.e., instead of choosing the parents randomly for mutation, each individual is assigned with a probability of selection, which is inversely proportional to the distance from the mutated individual, is presented in Reference [45]. This modified DE can be applied for solving various optimization problems with some small changes according to the requirement of the optimization problem. A modified DE algorithm for finding the PV model parameters during varying weather conditions and partial shading is given in Reference [46], and the algorithm presented here uses only the PV datasheet information. The original DE and the modified one, and also hybridization of the DE algorithm with various computational techniques or with conventional methods, have been proposed by many researchers [47,48]. The DE algorithm possesses many advantages, but PSO is superior to it in many aspects, such as less coding complexity and parameter tuning.

3.3. Ant Colony Optimization (ACO)

This technique was first proposed by Colorni, Dorigo, and Maniezzo [49]. This is a probability-based algorithm used for a computational problem-solving purpose. This algorithm is inspired by real ants' behavior for searching the shortest path from their colony to an available food source. The ants will follow the shortest distance between their nest and food [15]. Initially, when the ants search for food, they leave a pheromone trail for other ants to follow the same path. This pheromone trail is a chemical material to which members of the same species respond [50]. The thickness of the pheromone trail increases when it is followed by more ants. These ants may also follow the same path while returning to their nest, thereby making the pheromone trail thicker. Hence, the same path is followed by most of the ants till they find any other shortest path by exchanging information about the pheromone. If the path for the food is not the shortest one, then eventually the pheromone disappears [15,27,51].

ACO in MPPT

For implementing ACO in MPPT, most of the ants' behavior is considered. Here, ants are initialized first and the objective function is set by considering the irradiation and temperature exposure of each panel. The procedure followed in the ACO algorithm for optimization is given below [50]:

- Step 1: Initialize all ants and evaluate K random solutions.
- Step 2: Rank solutions according to their fitness value.
- Step 3: Perform a new solution.
- Step 4: Observe the ant that has the global best position (solution).
- Step 5: Upgrade the pheromone trail.
- Step 6: Check for termination criteria.
- Step 7: If satisfied, then the existing solution is the global best value, else go to Step 3.
- Step 8: End.

For finding the pheromone concentration, the formula is given as:

$$T_{ij} = \rho T_{ij}(t-1) + \Delta T_{ij} \quad (13)$$

In the above equation

$t = 1, 2, 3, \dots, T$

T_{ij} is the revised concentration of the pheromone

ΔT_{ij} is the change in pheromone concentration

ρ is the pheromone concentration rate.

The main function of ACO is to track the global peak power operating point at which the PV system operates.

$$\text{Fitness function} = \text{Panel 1}(V_1 \times (I(S_1, T_1))) + \text{Panel 2}(V_2 \times (I(S_2, T_2))) + \text{Panel 3}(V_3 \times (I(S_3, T_3))) + \dots + \text{Panel N}(V_N \times (I(S_N, T_N))) \quad (14)$$

where V_1 , S_1 , and T_1 represent the panel 1 voltage, irradiance, and temperature, respectively, and so on for the other panels.

In references [42,52], the authors have used an ACO algorithm to improve the PV system efficiency for a partial shading condition. Apart from the MPPT techniques, the ACO has wide application such as optimization in hydro-electric generation scheduling, optimal reactive power dispatch for line loss reduction, microwave corrugated filter design, etc. [53–55]. For further improving the ACO performance, i.e., its convergence speed and ease of operation, it can also be combined with various evolutionary and conventional algorithms. The ACO algorithm performs excellently for partially shaded PV modules with improved system performance [56,57]. In reference [58], an ACO-PSO-based MPPT technique is given for a partially shaded PV system. The proposed hybrid algorithm is implemented with an inter-leaved boost converter, which improves the output power and provides a constant voltage to the load. The authors in reference [59] have proposed a hybrid algorithm by considering the simplest conventional and widely used P&O (perturb and observe) with ACO. P&O fails during partial shading and falls on local MPP, hence in the hybrid algorithm, ACO helps the algorithm converge towards the GMPP. This hybrid algorithm improves the system performance and reliability.

3.4. Artificial Bee Colony (ABC)

This swarm technology-based meta-heuristic algorithm is used to solve multi-dimensional and multi-modal problems. The algorithm was proposed by Karaboga [60]. It is inspired by various behaviors of honeybees such as foraging, learning, memorizing, and sharing of information for optimization [61–63]. For the ABC algorithm, food locations are considered as effective solutions and the amount of nectar it produces defines the quality of the food source (i.e., fitness of the food source) [64]. Here, the bees are classified into three categories (first one is called employed bees, second one is onlooker bees, and the third one is scout bees), and the three types of bees perform mostly three types of foraging behavior, which are first searching the food source, then employing the employed bees for getting the food from the food source, and lastly, discarding the food source due to its lack of nectar quality [15,27]. The employed bees search for food or find the food location. The bee that makes decision regarding the food source is called the onlooker bee. The food sources discovered by the employed bees that cannot be improved are discarded, and the employed bees that found them become scout bees. Here, the number of bees is equal to the number of employed scout bees and onlooker bees. Flowchart of ABC algorithm is given in Figure 7.

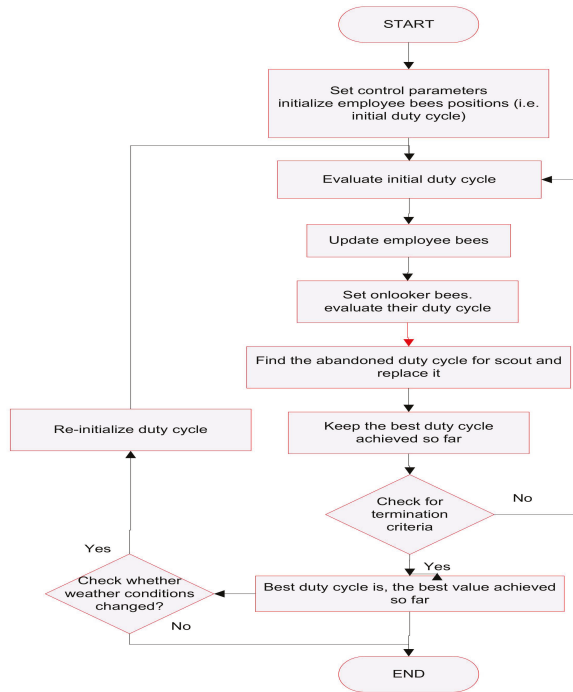


Figure 7. ABC algorithm.

ABC as the MPPT

For analyzing the MPPT technique based on the ABC algorithm, every candidate solution is considered as duty cycle “d” of the dc–dc converter. Hence, here the optimization function has only one parameter “d” to be optimized. Let us consider a D-dimensional problem having N_p food sources has to be optimized, where N_p is the number of number of bees in the search space. Hence, by assuming that each food source has one employed bee, then the i th food source location for the t th iteration is given by

$$X_i^t = [x_{i1}^t, x_{i2}^t, x_{i3}^t, \dots, x_{id}^t, \dots, x_{iD}^t]^T \tag{15}$$

Randomly generate the food source as:

$$x_{id} = L_d + r(U_d - L_d) \tag{16}$$

where U_d and L_d are upper and lower limit for the d th dimension problem, and r is a random number whose value is chosen between $[0,1]$.

In the next step, the employed bees search for a new food source V_i near to X_i along with a randomly selected dimension d :

$$v_{id} = x_{id} + \beta(x_{id} - x_{jd}) \tag{17}$$

where v_{id} is the new food source; j is a randomly chosen vector where $i \neq j \in (1, 2, 3, \dots, N_p)$ and β is a randomly chosen value between $[1, -1]$.

In the above condition, if it is found that the new food source is better than that of the old one, then the new food source gets updated, whereas the old one is discarded; else, the old food source remains in the next iteration [15].

Again, the available food source information is shared with onlooker bees and the food source is selected by the onlooker bees based on a probability criteria:

$$P_i = \frac{\text{fitness}_i}{\sum_{n=1}^{N_p} \text{fitness}_n} \quad (18)$$

In this step, the employed bees also get updated with the help of a greedy selection process. In the next step, after the prescribed number of iterations or when the limit values for the new food source quality have not improved, then the food source gets abandoned and goes for termination. The bees associated with the abandoned food sources become scout bees and search for new available food sources and checks for termination criteria. If the available solutions are acceptable and maximum iterations are reached, then the process terminates; otherwise, it continues the search.

The performance analysis of the ABC algorithm is given in reference [65]. Here, the performance of the algorithm is compared with PSO, DE, and other evolutionary algorithms for multi-modal and multi-functional problems where ABC is found to be giving better result compared to others. ABC has successfully been implemented for leaf-constrained minimum spanning problems too [66]. In reference [67], the authors have done a comparative study of the ABC algorithm for a large set of numerical optimization problems and the results obtained are compared with population-based algorithms. It was found that the results obtained by ABC are superior, and in some cases, same as the population-based algorithms where ABC has the advantage of having less control parameters than others. ABC-based MPPT techniques for PV system are given in Reference [68] and the results are compared with the P&O algorithm where the ABC-based MPPT gives a better performance. From various researchers, the effectiveness of the ABC algorithm as an MPPT technique for both uniform and partial shading conditions are shown and found to be better than the existing techniques [69–71]. A modified ABC algorithm (MABC) is presented in reference [72] whose performance is compared with the genetic algorithm (GA), PSO, and ABC, and was found to be more suitable for reducing the power loss of PV modules during a partial shading condition.

3.5. Bacteria Foraging Optimization Algorithm (BFOA)

This is a nature-inspired algorithm that is inspired by various foraging behaviors of *Escherichia Coli* (*E. Coli*). The *E. Coli* bacteria present inside the intestine of humans and animals possesses various multi-functional foraging behaviors so as to maximize the consumption of energy per unit time for one particular foraging process. When the foraging process occurs due to the environmental conditions, the bacterium with a high fitness value or those that are able to withstand the environmental changes continue to survive and the others get eliminated [73]. These bacteria follows four basic steps for getting to a nutrient-rich location, i.e., for foraging. These four steps are chemotaxis, swarming, reproduction, and elimination-dispersal [74].

3.5.1. Chemotaxis

The *E. coli* bacteria moves inside the human intestine searching for a nutrient-rich location with the help of locomotory organelles called flagella. This search of the bacteria for nutrients is called chemotaxis. With the help of flagella, the bacterium can swim or tumble, and these are the basic functions performed by the bacterium during the chemotaxis process [75]. In the swimming case, the bacterium moves continuously in some direction, but in the tumble case, it changes its direction randomly. The chemotactic method in terms of a mathematical equation is given as:

$$\theta^i(j+1, k, l) = \theta^i(j, k, l) + C(i) \frac{\Delta(i)}{\sqrt{\Delta^T(i) \cdot \Delta(i)}} \quad (19)$$

where

$\theta^i(j+1, k, l)$ is the i th bacterium at j th chemotactic for k th reproductive and l th elimination dispersal step

$C(i)$ is the unit step size of the bacterium taken in a random direction

$\Delta(i)$ represents a vector that lies in an arbitrary direction and its elements lie within $[-1, 1]$.

3.5.2. Swarming

The *E. Coli* and *Salmonella typhimurium* (*S. typhimurium*) bacteria show group behavior in which stable spatiotemporal swarms are formed in a semisolid nutrient medium. The group of *E. Coli* bacteria surrounded by a semisolid matrix with a single chemo-effector place themselves in the travelling ring, thereby moving up the nutrient gradient. The cells will release an attractant aspartate when it gets simulated by a high level of succinate, and with the help of this, the bacteria will form into groups and will move as concentric patterns of swarms with a high bacterial density.

3.5.3. Reproduction

In this step, the bacteria with a lower fitness value or the non-healthy bacteria are eliminated, which covers half of the bacteria population. Then, the healthier bacteria, i.e., the bacteria with higher fitness value, will asexually split into two bacteria. In this process, reproduction occurs and the population of the search space remains constant.

$$J_{\text{health}}^i = \sum_{j=1}^{N_c+1} J^i(j, k, l) \quad (20)$$

where N_c is the number of chemotactic steps; J_{health}^i is the health of the i th bacterium.

3.5.4. Elimination and Dispersal

A sudden change in the environment where the bacteria lives might occur due to various reasons and this phenomenon is called elimination and dispersal. The bacteria may be living at a better nutrient gradient environment, but due to environmental changes, some of the bacteria may get killed or dispersed to a new location. Due to this, many bacteria are spread all over the environment from the human intestine to hot springs and also to the underground environment. For implementing these phenomena of the bacteria in BFOA, some of the bacteria are randomly liquidated with a much lower probability, whereas the new replacements are initialized over the search space randomly. These events have the possibility of destroying the chemotaxis process, or they may assist the chemotaxis process because the dispersal of the bacterium may place it in a new good food location.

The above explained BFOA finds its application in various fields. In reference [73], a hybrid least square fuzzy-based BFOA is proposed for the harmonic estimation in power system voltage and current waveforms. Due to its capability of handling non-linear optimization, the phase estimation is done by BFOA and the linear least square method is used for amplitude estimation of the harmonic component. In reference [76], the authors have analyzed the chemotaxis process of BFOA from the classical gradient descent point of view. In this method the convergence speed of the BFOA algorithm has been enhanced. BFOA has also been implemented for active noise cancellation systems successfully [77]. Authors in reference [78] presented a grid-tied PV system based on an active shunt power filter (ASPF) technique. As controlling a dc-link voltage using PI controller is difficult due to the existence of varying loads, in this paper BFOA is used to optimize the PI controller parameters. A PSO-guided BFOA algorithm is considered for PV parameter estimation in reference [79]. Here, the optimization problem is solved using PSO, BFOA, and PSO-guided BFOA in an LDK PV test module and it is found that the later provides best fitness value. In [80], both conventional and computational techniques with hybridization of the algorithms are used for maximum PV power extraction and the performance of the algorithms is compared. Here P&O, fuzzy-based P&O, and

fuzzy P&O with parameters tuned by BPSO (i.e., BFOA-PSO) have been considered for PV systems, among which, the later BPSO tuned fuzzy P&O was found to be the best one. BFOA has been used as an efficient parameter extraction technique for PV cells. It shows more accurate results compared to the classical Newton–Raphson method, PSO, and enhanced simulated annealing for different PV modules with different test conditions [81]. From the literature, it is seen that BFOA can be applied to various global search problems for finding out the best solution.

4. Critical Evaluation of MPPT Algorithms

While selecting an algorithm for optimization problem, various aspects need to be considered and those are reliability, implementation cost, convergence speed, complexity of the algorithm, etc. The evolutionary algorithms play an important role while considering the partial shading condition of PV panels. From the literature, it is seen that there are many MPPT techniques available with different control techniques, and there is still a lot to explore. The deep analysis of the algorithms gives clear knowledge about the recent advancement in the said area. It shows the various factors affecting achieving the optimization goal and also shows the limitations. Among the five important MPPT algorithms discussed, here PSO is found to be the most used one. Basic PSO has a simple coding structure and is quite effective at tracking GMPP but sometimes due to rapidly changing weather conditions, it may reduce its convergence speed and start oscillating near the GMPP. Hence, in the literature it is found that many researchers' have implemented hybrid PSO or modified PSO to achieve the optimization goal. It is seen that PSO with DE, PSO with P&O, PSO with genetic algorithm, etc., has been used, which gives a better convergence speed and less oscillation. The swarm intelligent algorithms like ACO and ABC involve simple and cost-effective implementation, and perform better than the standard PSO algorithm. However, at some period of time, these fall on local maxima. The performance of those algorithms can be further improved by combining them with conventional, artificial intelligence techniques or using soft computing techniques. This will reduce the convergence time and will track the GMPP. The DE algorithm is quite similar to the swarm intelligent algorithms but in some cases, it fails to track the GMPP as the parameters have no direction. Hence, it may follow a wrong direction. This algorithm can be improved by hybridizing with the soft computing techniques. BFOA based on bacteria foraging behavior provides a large search space and simple calculations, and the limitations of the algorithm can be overcome by modifying the parameter selection process or by combining it with other optimization techniques. The advantages and disadvantages of these five algorithms are listed in Table 1.

In Table 2, the use of nature-inspired algorithms as MPPT techniques for various PV models are analyzed. These techniques can be further improved by narrowing the search space, limiting the number of optimization parameters, and also by selecting suitable control parameters. This, in turn, can increase the speed of convergence and can also find the best fitness value. Both the conventional and soft computing algorithms can be integrated such that the limitations of both the algorithms can be reduced and the resulting hybrid algorithm may improve the performance of the PV system. However, this might increase the implementation cost and complexity of the system. From this review of the literature, it is noted that most of these algorithms are similar and vary with a narrow border. Therefore, selection of the algorithms solely depend on the researcher's optimization criteria, which may be a cost function, a simple and easy to implement technique, etc. Therefore, an efficient, robust, economical, and simple algorithm has to be developed that, in turn, can increase the use of a PV system to its optimum.

Table 1. Advantages and disadvantages of reported algorithms.

Sl. No	Algorithm Name	Advantage	Disadvantage
1	PSO	<ul style="list-style-type: none"> Fast convergence and tracks true MPPT during partial shading conditions. High efficiency 	<ul style="list-style-type: none"> High implement cost Complex calculation Oscillates during rapidly changing conditions
2	ACO	<ul style="list-style-type: none"> Possesses a simple and cost-effective technique for practical implementation Good convergence speed and efficient for PSC 	<ul style="list-style-type: none"> Optimization process is lengthy and complex calculation as more parameters need to be optimized.
3	ABC	<ul style="list-style-type: none"> It does not depend on the system's initial condition Simple structure Easy to implement 	<ul style="list-style-type: none"> During some period of time it fails to track the true GMPP
4	DE	<ul style="list-style-type: none"> Independent of initial parameters for finding true GMPP Fast convergence Have fewer control parameters 	<ul style="list-style-type: none"> The particles have no direction during convergence Particles need to be modified to converge towards the best solution
5	BFOA	<ul style="list-style-type: none"> It does not get affected more by the system size and non-linearity Ability to handle more objective function Fast convergence 	<ul style="list-style-type: none"> After some period of time it falls on local maxima Complex calculation

Table 2. Comparison of various algorithms used in the literature.

Ref. No	Method Used	Year of Publication	System Under Consideration	Observed Condition	Converter Used	Advantages
[25]	PSO combined with P&O	2015	Stand alone	PSC	dc-dc	<ul style="list-style-type: none"> Faster convergence, reduced oscillation, better performance than standard PSO
[31]	Dormant PSO and INC	2015	Stand alone	PSC	dc-dc	<ul style="list-style-type: none"> Improved efficiency Reduced global search time Output voltage fluctuation reduced
[35]	PSO	2015	Grid-Tied	PSC	dc-dc	<ul style="list-style-type: none"> Increased system efficiency
[32]	Enhanced Leader PSO (EL-PSO)	2017	Stand alone	PSC	dc-dc	<ul style="list-style-type: none"> Faster than classical PSO Performs better than PSO and P&O
[82]	PSO and INC	2017	Rooftop PV	PSC	dc-dc	<ul style="list-style-type: none"> Reduced implementation cost Improved system efficiency
[26]	Combination of HL and SAPSO (HSAPSO)	2018	Stand alone	PSC	dc-dc	<ul style="list-style-type: none"> Reduced search area Algorithm complexity reduced Improved performance
[38]	DE	2010	Stand alone	PSC	dc-dc boost converter	<ul style="list-style-type: none"> Very fast response and accurate results

Table 2. Cont.

Ref. No	Method Used	Year of Publication	System Under Consideration	Observed Condition	Converter Used	Advantages
[47]	DE	2012	Stand alone	PSC	dc–dc boost converter	<ul style="list-style-type: none"> • More accurate results • Fast convergence • Eliminates steady state oscillation after MPP is tracked
[37]	DE with modified mutation direction	2014	Stand alone	PSC	dc–dc	<ul style="list-style-type: none"> • Performs well during varying load and irradiation • Improved efficiency than P&O • Easy to implement
[48]	Improved DE	2018	Stand alone	PSC with varying load condition	dc–dc sepic converter	<ul style="list-style-type: none"> • High efficiency >99% • Faster response
[59]	Improved ACO based P&O	2016	Stand alone	PSC	dc–dc	<ul style="list-style-type: none"> • Improved static and dynamic convergence
[50]	ACO	2016	Stand alone	PSC	dc–dc	<ul style="list-style-type: none"> • Performs better than conventional MPPT
[56]	ACO	2013	Stand alone	PSC	dc–dc	<ul style="list-style-type: none"> • Reduced cost • Simple structure • Finds the GMPP effectively
[57]	ACO-New Pheromone Update Strategy (ACO-NPU)	2017	Stand alone	PSC	dc–dc	<ul style="list-style-type: none"> • Reduced computation time
[69]	ABC	2015	Stand alone	PSC	dc–dc	<ul style="list-style-type: none"> • Requires less control parameters • Convergence is independent of system initial condition • Better tracking of GMPP than PSO
[70]	ABC	2015	Stand alone	PSC	dc–dc	<ul style="list-style-type: none"> • Faster tracking of GMPP • Reduced output power oscillation • Energy saving improves • Increased revenue generation
[72]	MABC	2015	Stand alone	PSC	dc–dc	<ul style="list-style-type: none"> • Optimizes the power loss constraint • Mitigates shading effects
[78]	BFOA tuned PI	2016	Grid-Tied	Varying load conditions	-	<ul style="list-style-type: none"> • Reduced harmonics • Meets the load demand • Robust system
[80]	BPSO Fuzzy P&O	2017	Stand alone	-	dc–dc	<ul style="list-style-type: none"> • More effective than conventional techniques • Improved system performance

5. Conclusions

In this paper, five evolutionary algorithms—PSO, DE, ABC, ACO, and BFOA—were analyzed and reviewed. The discussed evolutionary algorithms are competent enough to obtain global peak power even in rapidly varying atmospheric conditions and also during shading. The operating principle of the said algorithms varies along with their choice of operating parameters. The review paper also discussed the use of those MPPT techniques by hybridizing them along with other MPPT techniques. This method improves the performance as compared to the standard versions. Each algorithm has its own merits and demerits, which are discussed in the review article, which gives a brief idea regarding selecting one MPPT technique for partially shaded PVs. The practical implementation of these algorithms still remains quite complex due to their effectiveness, reliability, cost for implementation,

nature of coding involved, etc., in multi-objective functions. The advent of advanced processors and simulation compatible hardware tools has made the process effective. Potential tools like hardware in loop (HIL), dSPACE, etc., facilitates the pragmatic hardware realization of a real-time scenario. Taking into account the necessity of MPPT for partially shaded PV, there is a wide scope of research for finding new efficient MPPT techniques. This paper has summarized five important global search algorithms that can kindle the interest among the researchers to either modify the five discussed algorithms or propose a new algorithm.

Author Contributions: Investigation, writing—original draft, methodology, S.P.; project administration, supervision, writing—review and editing, C.S.; validation, R.S.; resources, T.M.T.T.; software, S.P.

Funding: This research received no external funding.

Conflicts of Interest: The authors declare no conflict of interest.

References

1. Singh, B.; Shahani, D.T.; Verma, A.K. Neural network controlled grid interfaced solar photovoltaic power generation. *IET Power Electron.* **2014**, *7*, 614–626. [[CrossRef](#)]
2. Eltawil, M.A.; Zhao, Z. Grid-connected photovoltaic power systems: Technical and potential problems—A review. *Renew. Sustain. Energy Rev.* **2010**, *14*, 112–129. [[CrossRef](#)]
3. Dolara, A.; Faranda, R.; Leva, S. Energy comparison of seven MPPT techniques for PV systems. *J. Electromagn. Anal. Appl.* **2009**, *1*, 152. [[CrossRef](#)]
4. Alqarni, M.; Darwish, M.K. Maximum power point tracking for photovoltaic system: modified perturb and observe algorithm. In Proceedings of the 2012 47th International Universities Power Engineering Conference (UPEC), London, UK, 4–7 September 2012.
5. Ishaque, K.; Salam, Z.; Amjad, M.; Mekhilef, S. An improved particle swarm optimization (PSO)—Based MPPT for PV with reduced steady-state oscillation. *IEEE Trans. Power Electron.* **2012**, *27*, 3627–3638. [[CrossRef](#)]
6. Tyagi, V.V.; Rahim, N.A.; Rahim, N.A.; Jeyraj, A.; Selvaraj, L. Progress in solar PV technology: Research and achievement. *Renew. Sustain. Energy Rev.* **2013**, *20*, 443–461. [[CrossRef](#)]
7. Kroposki, B.; Sen, P.K.; Malmedal, K. Optimum Sizing and Placement of Distributed and Renewable Energy Sources in Electric Power Distribution Systems. *IEEE Trans. Ind. Appl.* **2013**, *49*, 2741–2752. [[CrossRef](#)]
8. Chao, R.M.; Ko, S.H.; Lin, H.K.; Wang, I.K. Evaluation of a Distributed Photovoltaic System in Grid-Connected and Standalone Applications by Different MPPT Algorithms. *Energies* **2018**, *11*, 1484. [[CrossRef](#)]
9. Li, H.; Yang, D.; Su, W.; Lü, J.; Yu, X. An overall distribution particle swarm optimization MPPT algorithm for photovoltaic system under partial shading. *IEEE Trans. Ind. Electron.* **2019**, *66*, 265–275. [[CrossRef](#)]
10. Celik, A.N.; Acikgoz, N. Modelling and experimental verification of the operating current of mono-crystalline photovoltaic modules using four-and five-parameter models. *Appl. Energy* **2007**, *84*, 1–15. [[CrossRef](#)]
11. ESRAM, T.; Chapman, P.L. Comparison of photovoltaic array maximum power point tracking techniques. *IEEE Trans. Energy Convers.* **2007**, *22*, 439–449. [[CrossRef](#)]
12. Belkaid, A.; Colak, U.; Kayisli, K. A comprehensive study of different photovoltaic peak power tracking methods. In Proceedings of the 2017 IEEE 6th International Conference on Renewable Energy Research and Applications (ICRERA), San Diego, CA, USA, 5–8 November 2017; pp. 1073–1079.
13. Priyadarshi, N.; Sharma, A.K.; Priyam, S. Practical Realization of an Improved Photovoltaic Grid Integration with MPPT. *Int. J. Renew. Energy Res.* **2017**, *7*, 1880–1891.
14. Remy, G.; Bethoux, O.; Marchand, C.; Dogan, H. *Review of MPPT Techniques for Photovoltaic Systems*; Laboratoire de Génie Electrique de Paris (LGEPE)/SPEE-Labs, Université Pierre et Marie Curie P6: Paris, France, 2009.
15. Jiang, L.L.; Srivatsan, R.; Maskell, D.L. Computational intelligence techniques for maximum power point tracking in PV systems: A review. *Renew. Sustain. Energy Rev.* **2018**, *85*, 14–45. [[CrossRef](#)]
16. Sridhar, R.; Jeevananthan, S.; Dash, S.S.; Vishnuram, P. A new maximum power tracking in PV system during partially shaded conditions based on shuffled frog leap algorithm. *J. Exp. Theor. Artif. Intell.* **2017**, *29*, 481–493. [[CrossRef](#)]
17. Miyatake, M.; Veerachary, M.; Toriumi, F.; Fujii, N.; Ko, H. Maximum power point tracking of multiple photovoltaic arrays: A PSO approach. *IEEE Trans. Aerosp. Electron. Syst.* **2011**, *47*, 367–380. [[CrossRef](#)]

18. Chen, L.R.; Tsai, C.H.; Lin, Y.L.; Lai, Y.S. A biological swarm chasing algorithm for tracking the PV maximum power point. *IEEE Trans. Energy Convers.* **2010**, *25*, 484–493. [[CrossRef](#)]
19. Kamarzaman, N.A.; Tan, C.W. A comprehensive review of maximum power point tracking algorithms for photovoltaic systems. *Renew. Sustain. Energy Rev.* **2014**, *37*, 585–598. [[CrossRef](#)]
20. Villalva, M.G.; Gazoli, J.R.; Ruppert Filho, E. Comprehensive approach to modeling and simulation of photovoltaic arrays. *IEEE Trans. Power Electron.* **2009**, *24*, 1198–1208. [[CrossRef](#)]
21. Onat, N. Recent developments in maximum power point tracking technologies for photovoltaic systems. *Int. J. Photoenergy* **2010**, *2010*, 245316. [[CrossRef](#)]
22. Karatepe, E.; Hiyama, T. Artificial neural network-polar coordinated fuzzy controller based maximum power point tracking control under partially shaded conditions. *IET Renew. Power Gener.* **2009**, *3*, 239–253.
23. Ramaprabha, R.; Mathur, B.L. Genetic algorithm based maximum power point tracking for partially shaded solar photovoltaic array. *Int. J. Res. Rev. Inf. Sci. (IJRRIS)* **2012**, *2*, 161–163.
24. Liu, Y.H.; Huang, S.C.; Huang, J.W.; Liang, W.C. A particle swarm optimization-based maximum power point tracking algorithm for PV systems operating under partially shaded conditions. *IEEE Trans. Energy Convers.* **2012**, *27*, 1027–1035. [[CrossRef](#)]
25. Sundareswaran, K.; Palani, S. Application of a combined particle swarm optimization and perturb and observe method for MPPT in PV systems under partial shading conditions. *Renew. Energy* **2015**, *75*, 308–317. [[CrossRef](#)]
26. Koad, R.B.A.; Zobia, A.F. Comparison between the Conventional Methods and PSO Based MPPT Algorithm for Photovoltaic Systems. *Int. J. Electr. Robot. Electron. Commun. Eng.* **2014**, *8*, 673–678.
27. Li, G.; Jin, Y.; Akram, M.W.; Chen, X.; Ji, J. Application of bio-inspired algorithms in maximum power point tracking for PV systems under partial shading conditions—A review. *Renew. Sustain. Energy Rev.* **2018**, *81*, 840–873. [[CrossRef](#)]
28. Chaieb, H.; Sakly, A. A novel MPPT method for photovoltaic application under partial shaded conditions. *Sol. Energy* **2018**, *159*, 291–299. [[CrossRef](#)]
29. Mao, M.; Duan, Q.; Zhang, L.; Chen, H.; Hu, B.; Duan, P. Maximum Power Point Tracking for Cascaded PV-Converter Modules Using Two-Stage Particle Swarm Optimization. *Sci. Rep.* **2017**, *7*, 9381. [[CrossRef](#)] [[PubMed](#)]
30. Dileep, G.; Singh, S.N. An improved particle swarm optimization based maximum power point tracking algorithm for PV system operating under partial shading conditions. *Sol. Energy* **2017**, *158*, 1006–1015. [[CrossRef](#)]
31. Shi, J.; Zhang, W.; Zhang, Y.; Xue, F.; Yang, T. MPPT for PV systems based on a dormant PSO algorithm. *Electr. Power Syst. Res.* **2015**, *123*, 100–107. [[CrossRef](#)]
32. Gavhane, P.S.; Krishnamurthy, S.; Dixit, R.; Ram, J.P.; Rajasekar, N. EL-PSO based MPPT for Solar PV under Partial Shaded Condition. *Energy Procedia* **2017**, *117*, 1047–1053. [[CrossRef](#)]
33. Da Silva, S.A.; Sampaio, L.P.; de Oliveira, F.M.; Durand, F.R. Feed-forward DC-bus control loop applied to a single-phase grid-connected PV system operating with PSO-based MPPT technique and active power-line conditioning. *IET Renew. Power Gener.* **2016**, *11*, 183–193. [[CrossRef](#)]
34. Renaudineau, H.; Donatantonio, F.; Fontchastagner, J.; Petrone, G.; Spagnuolo, G.; Martin, J.P.; Pierfederici, S. A PSO-based global MPPT technique for distributed PV power generation. *IEEE Trans. Ind. Electron.* **2015**, *62*, 1047–1058. [[CrossRef](#)]
35. De Oliveira, F.M.; da Silva, S.A.; Durand, F.R.; Sampaio, L.P.; Bacon, V.D.; Campanhol, L.B. Grid-tied photovoltaic system based on PSO MPPT technique with active power line conditioning. *IET Power Electron.* **2016**, *9*, 1180–1191. [[CrossRef](#)]
36. Storn, R.M.; Price, K.V. Differential evolution—a simple and efficient adaptive scheme for global optimization over continuous spaces. *J. Glob. Optim.* **1995**, *3*, 1–15.
37. Tey, K.S.; Mekhilef, S.; Yang, H.T.; Chuang, M.K. A differential evolution based MPPT method for photovoltaic modules under partial shading conditions. *Int. J. Photoenergy* **2014**, *2014*, 945906. [[CrossRef](#)]
38. Taheri, H.; Salam, Z.; Ishaque, K. A novel maximum power point tracking control of photovoltaic system under partial and rapidly fluctuating shadow conditions using differential evolution. In Proceedings of the 2010 IEEE Symposium on Industrial Electronics & Applications (ISIEA), Penang, Malaysia, 3–5 October 2010; pp. 82–87.

39. Tajuddin, M.F.N.; Ayob, S.M.; Salam, Z.; Saad, M.S. Evolutionary based maximum power point tracking technique using differential evolution algorithm. *Energy Build.* **2013**, *67*, 245–252. [[CrossRef](#)]
40. Price, K.V.; Storn, R.M.; Lampinen, J.A. *Differential Evolution: A Practical Approach to Global Optimization*; Springer Science & Business Media: Berlin/Heidelberg, Germany, 2006.
41. Sheraz, M.; Abido, M.A. An efficient MPPT controller using differential evolution and neural network. In Proceedings of the 2012 IEEE International Conference on Power and Energy (PECon), Kota Kinabalu, Malaysia, 2–5 December 2012; pp. 378–383.
42. Kumar, N.; Hussain, I.; Singh, B.; Panigrahi, B.K. Rapid MPPT for uniformly and partial shaded PV system by using JayaDE algorithm in highly fluctuating atmospheric conditions. *IEEE Trans. Ind. Inform.* **2017**, *13*, 2406–2416. [[CrossRef](#)]
43. Neri, F.; Tirronen, V. Recent advances in differential evolution: A survey and experimental analysis. *Artif. Intell. Rev.* **2010**, *33*, 61–106. [[CrossRef](#)]
44. Das, S.; Suganthan, P.N. Differential evolution: A survey of the state-of-the-art. *IEEE Trans. Evol. Comput.* **2011**, *15*, 4–31. [[CrossRef](#)]
45. Epitropakis, M.G.; Tasoulis, D.K.; Pavlidis, N.G.; Plagianakos, V.P.; Vrahatis, M.N. Enhancing differential evolution utilizing proximity-based mutation operators. *IEEE Trans. Evol. Comput.* **2011**, *15*, 99–119. [[CrossRef](#)]
46. Ishaque, K.; Salam, Z. An improved modeling method to determine the model parameters of photovoltaic (PV) modules using differential evolution (DE). *Sol. Energy* **2011**, *85*, 2349–2359. [[CrossRef](#)]
47. Tajuddin, M.F.; Ayob, S.M.; Salam, Z. Tracking of maximum power point in partial shading condition using differential evolution (DE). In Proceedings of the 2012 IEEE International Conference on Power and Energy (PECon), Kota Kinabalu, Malaysia, 2–5 December 2012; pp. 384–389.
48. Tey, K.S.; Mekhilef, S.; Seyedmahmoudian, M.; Horan, B.; Oo, A.M.T.; Stojcevski, A. Improved Differential Evolution-based MPPT Algorithm using SEPIC for PV Systems under Partial Shading Conditions and Load Variation. *IEEE Trans. Ind. Inform.* **2018**, *14*, 4322–4333. [[CrossRef](#)]
49. Dorigo, M.; Maniezzo, V.; Colnori, A. Ant system: Optimization by a colony of cooperating agents. *IEEE Trans. Syst. Man Cybern. Part B (Cybern.)* **1996**, *26*, 29–41. [[CrossRef](#)]
50. Sridhar, R.; Jeevananthan, S.; Dash, S.S.; Selvan, N.T. Unified MPPT controller for partially shaded panels in a photovoltaic array. *Int. J. Autom. Comput.* **2014**, *11*, 536–542. [[CrossRef](#)]
51. Liu, L.; Dai, Y.; Gao, J. Ant colony optimization algorithm for continuous domains based on position distribution model of ant colony foraging. *Sci. World J.* **2014**, *2014*, 428539. [[CrossRef](#)] [[PubMed](#)]
52. Jiang, L.L.; Maskell, D.L. A uniform implementation scheme for evolutionary optimization algorithms and the experimental implementation of an ACO based MPPT for PV systems under partial shading. In Proceedings of the 2014 IEEE Symposium on Computational Intelligence Applications in Smart Grid (CIASG), Orlando, FL, USA, 9–12 December 2014.
53. Huang, S.-J. Enhancement of hydroelectric generation scheduling using ant colony system based optimization approaches. *IEEE Trans. Energy Convers.* **2011**, *16*, 296–301. [[CrossRef](#)]
54. El-Ela, A.A.; Kinawy, A.M.; El-Sehiemy, R.A.; Mouwafi, M.T. Optimal reactive power dispatch using ant colony optimization algorithm. *Electr. Eng.* **2011**, *93*, 103–116. [[CrossRef](#)]
55. Mantilla-Gaviria, I.A.; Díaz-Morcillo, A.; Balbastre-Tejedor, J.V. An ant colony optimization algorithm for microwave corrugated filters design. *J. Comput. Eng.* **2013**, *2013*, 942126. [[CrossRef](#)]
56. Jiang, L.L.; Maskell, D.L.; Patra, J.C. A novel ant colony optimization-based maximum power point tracking for photovoltaic systems under partially shaded conditions. *Energy Build.* **2013**, *58*, 227–236. [[CrossRef](#)]
57. Titri, S.; Larbes, C.; Toumi, K.Y.; Benatchba, K. A new MPPT controller based on the Ant colony optimization algorithm for Photovoltaic systems under partial shading conditions. *Appl. Soft Comput.* **2017**, *58*, 465–479. [[CrossRef](#)]
58. Nivetha, V.; Gowri, G.V. Maximum power point tracking of photovoltaic system using ant colony and particle swarm optimization algorithms. In Proceedings of the 2015 2nd International Conference on Electronics and Communication Systems (ICECS), Coimbatore, India, 26–27 February 2015; pp. 948–952.
59. Sundareswaran, K.; Vigneshkumar, V.; Sankar, P.; Simon, S.P.; Nayak, P.S.R.; Palani, S. Development of an improved P&O algorithm assisted through a colony of foraging ants for MPPT in PV system. *IEEE Trans. Ind. Inform.* **2016**, *12*, 187–200.

60. Karaboga, D. *An Idea Based on Honey Bee Swarm for Numerical Optimization [Technical Report-TR06]*; Erciyes University, Engineering Faculty, Computer Engineering Department: Kayseri, Turkey, 2005.
61. Tereshko, V. Reaction-diffusion model of a honeybee colony's foraging behavior. In *Proceedings of the 6th International Conference on Parallel Problem Solving from Nature*; Springer: London, UK, 2000; pp. 807–816.
62. Tereshko, V.; Lee, T. How information mapping patterns determine foraging behaviour of a honeybee colony. *Open Syst. Inf. Dyn.* **2002**, *9*, 181–193. [[CrossRef](#)]
63. Tereshko, V.; Loengarov, A. Collective decision-making in honeybee foraging dynamics. *Comput. Inf. Syst. J.* **2005**, *9*, 1–7.
64. Hassan, S.; Abdelmajid, B.; Mourad, Z.; Aicha, S.; Abdenaceur, B. An Advanced MPPT Based on Artificial Bee Colony Algorithm for MPPT Photovoltaic System under Partial Shading Condition. *Int. J. Power Electron. Drive Syst.* **2017**, *8*, 647–653. [[CrossRef](#)]
65. Karaboga, D.; Basturk, B. On the performance of artificial bee colony (ABC) algorithm. *Appl. Soft Comput.* **2008**, *8*, 687–697. [[CrossRef](#)]
66. Singh, A. An artificial bee colony algorithm for the leaf-constrained minimum spanning tree problem. *Appl. Soft Comput.* **2009**, *9*, 625–631. [[CrossRef](#)]
67. Karaboga, D.; Akay, B. A comparative study of artificial bee colony algorithm. *Appl. Math. Comput.* **2009**, *214*, 108–132. [[CrossRef](#)]
68. Bilal, B. Implementation of artificial bee colony algorithm on maximum power point tracking for PV modules. In *Proceedings of the 2013 8th International Symposium on Advanced Topics in Electrical Engineering (ATEE)*, Bucharest, Romania, 23–25 May 2013.
69. Benyoucef, A.S.; Chouder, A.; Kara, K.; Silvestre, S.; Ait Sahed, O. Artificial bee colony based algorithm for maximum power point tracking (MPPT) for PV systems operating under partial shaded conditions. *Appl. Soft Comput.* **2015**, *32*, 38–48. [[CrossRef](#)]
70. Sundareswaran, K.; Sankar, P.; Nayak, P.S.; Simon, S.P.; Palani, S. Enhanced energy output from a PV system under partial shaded conditions through artificial bee colony. *IEEE Trans. Sustain. Energy* **2015**, *6*, 198–209. [[CrossRef](#)]
71. Sawant, P.T.; Lbhatar, P.C.; Bhattar, C.L. Enhancement of PV system based on artificial bee colony algorithm under dynamic conditions. In *Proceedings of the IEEE International Conference on Recent Trends in Electronics, Information & Communication Technology (RTEICT)*, Bangalore, India, 20–21 May 2016; pp. 1251–1255.
72. Fathy, A. Reliable and efficient approach for mitigating the shading effect on photovoltaic module based on Modified Artificial Bee Colony algorithm. *Renew. Energy* **2015**, *81*, 78–88. [[CrossRef](#)]
73. Mishra, S. A hybrid least square-fuzzy bacterial foraging strategy for harmonic estimation. *IEEE Trans. Evol. Comput.* **2005**, *9*, 61–73. [[CrossRef](#)]
74. Passino, K.M. Biomimicry of bacterial foraging for distributed optimization and control. *IEEE Control Syst.* **2002**, *22*, 52–67.
75. Biswas, A.; Dasgupta, S.; Das, S.; Abraham, A. A synergy of differential evolution and bacterial foraging optimization for global optimization. *Neural Netw. World* **2007**, *17*, 607.
76. Dasgupta, S.; Das, S.; Abraham, A.; Biswas, A. Adaptive computational chemotaxis in bacterial foraging optimization: An analysis. *IEEE Trans. Evol. Comput.* **2009**, *13*, 919–941. [[CrossRef](#)]
77. Gholami-Boroujeni, S.; Eshghi, M. Non-linear active noise cancellation using a bacterial foraging optimisation algorithm. *IET Signal Process.* **2012**, *6*, 364–373. [[CrossRef](#)]
78. Kumar, A.; Gupta, N.; Gupta, V. A synchronization of PV source by using bacterial foraging optimization based PI controller to reduce day-time grid dependency. In *Proceedings of the 2017 IEEE International Conference on Intelligent Techniques in Control, Optimization and Signal Processing (INCOS)*, Srivilliputhur, India, 23–25 March 2017.
79. Awadallah, M.A.; Venkatesh, B. Bacterial foraging algorithm guided by particle swarm optimization for parameter identification of photovoltaic modules. *Can. J. Electr. Comput. Eng.* **2016**, *39*, 150–157. [[CrossRef](#)]
80. Dabra, V.; Paliwal, K.K.; Sharma, P.; Kumar, N. Optimization of photovoltaic power system: A comparative study. *Prot. Control Mod. Power Syst.* **2017**, *2*, 3. [[CrossRef](#)]

81. Subudhi, B.; Pradhan, R. Bacterial Foraging Optimization Approach to Parameter Extraction of a Photovoltaic Module. *IEEE Trans. Sustain. Energy* **2018**, *9*, 381–389. [[CrossRef](#)]
82. Liu, J.; Li, J.; Wu, J.; Zhou, W. Global MPPT algorithm with coordinated control of PSO and INC for rooftop PV array. *J. Eng.* **2017**, *2017*, 778–782. [[CrossRef](#)]



© 2019 by the authors. Licensee MDPI, Basel, Switzerland. This article is an open access article distributed under the terms and conditions of the Creative Commons Attribution (CC BY) license (<http://creativecommons.org/licenses/by/4.0/>).

MDPI
St. Alban-Anlage 66
4052 Basel
Switzerland
Tel. +41 61 683 77 34
Fax +41 61 302 89 18
www.mdpi.com

Energies Editorial Office
E-mail: energies@mdpi.com
www.mdpi.com/journal/energies



MDPI
St. Alban-Anlage 66
4052 Basel
Switzerland

Tel: +41 61 683 77 34
Fax: +41 61 302 89 18

www.mdpi.com



ISBN 978-3-03936-187-8